



Kent Academic Repository

Zona, Stefania (2013) *Quantum dot-labelled antibody to quantify expression of the EGF family of receptors and ligands in breast cancer specimens.* Doctor of Philosophy (PhD) thesis, University of Kent.

Downloaded from

<https://kar.kent.ac.uk/94146/> The University of Kent's Academic Repository KAR

The version of record is available from

<https://doi.org/10.22024/UniKent/01.02.94146>

This document version

UNSPECIFIED

DOI for this version

Licence for this version

CC BY-NC-ND (Attribution-NonCommercial-NoDerivatives)

Additional information

This thesis has been digitised by EThOS, the British Library digitisation service, for purposes of preservation and dissemination. It was uploaded to KAR on 25 April 2022 in order to hold its content and record within University of Kent systems. It is available Open Access using a Creative Commons Attribution, Non-commercial, No Derivatives (<https://creativecommons.org/licenses/by-nc-nd/4.0/>) licence so that the thesis and its author, can benefit from opportunities for increased readership and citation. This was done in line with University of Kent policies (<https://www.kent.ac.uk/is/strategy/docs/Kent%20Open%20Access%20policy.pdf>). If you ...

Versions of research works

Versions of Record

If this version is the version of record, it is the same as the published version available on the publisher's web site. Cite as the published version.

Author Accepted Manuscripts

If this document is identified as the Author Accepted Manuscript it is the version after peer review but before type setting, copy editing or publisher branding. Cite as Surname, Initial. (Year) 'Title of article'. To be published in *Title of Journal*, Volume and issue numbers [peer-reviewed accepted version]. Available at: DOI or URL (Accessed: date).

Enquiries

If you have questions about this document contact ResearchSupport@kent.ac.uk. Please include the URL of the record in KAR. If you believe that your, or a third party's rights have been compromised through this document please see our [Take Down policy](https://www.kent.ac.uk/guides/kar-the-kent-academic-repository#policies) (available from <https://www.kent.ac.uk/guides/kar-the-kent-academic-repository#policies>).

UNIVERSITY OF KENT

**QUANTUM DOT-LABELLED
ANTIBODY TO QUANTIFY
EXPRESSION OF THE EGF FAMILY OF
RECEPTORS AND LIGANDS IN
BREAST CANCER SPECIMENS**

THESIS SUBMITTED TO THE UNIVERSITY OF KENT FOR THE
DEGREE OF DOCTOR OF PHILOSOPHY

Stefania Zona

2013



F226085

DECLARATION

I declare that the work presented in this thesis is my own original research work except where otherwise stated.

This work has not been already accepted or concurrently submitted in candidature for any other degree or qualification.

Signed: Stephanie Zane

Date: 07/06/2013

ACKNOWLEDGEMENT

I would like to express my appreciation and thank my supervisor Professor Bill Gullick whose guidance, help, patience and support have been fundamental, and without which this project would have not been possible.

I would also like to address my sincere thanks to all the past and present members of the "Gullick lab", in particular to Edith, Ming and Mariana, for their encouragement, help, moral support and friendship throughout this time. I am also grateful to Ian Brown for his help with the confocal microscope and to many other people whose help has contributed to the realisation of this work.

I would like to thank Emmet McIntyre for his love, help, support and advices throughout these years.

I would like to express my deepest gratitude to my family whose love, patience and support has made possible the completion of this work and for which I'll never forget.

Finally I would like to acknowledge the Breast Cancer Campaign for providing fund to support this research.

ABSTRACT

The epidermal growth factor receptors (ErbB1, ErbB2, ErbB3 and ErbB4) have become an attractive target for drug development. In particular ErbB2 is one of the most important biomarkers routinely used to predict breast cancer patients' response to Herceptin, an effective drug for the treatment of breast cancers expressing high levels of ErbB2. The current techniques in clinical use for the assessment of ErbB2 are immunohistochemistry (IHC) and fluorescence in situ hybridization (FISH); however both IHC and FISH have several limitations which may result in patient misclassification. Using Quantum dots (Qdot) labelled antibodies, laser scanning confocal microscopy and image segmentation techniques, we have developed a new system which provides a more linear and scalable quantification of ErbB2 expression in formalin fixed paraffin embedded breast cancers. We first demonstrated that the Qdot system could reliably detect ErbB2 expression in IHC 3+ and 2+ cases on a tissue microarray containing 60 samples of formalin fixed paraffin embedded breast cancer sections. We then apply the system to quantify ErbB2 expression in 145 primary breast cancers treated with Herceptin, all previously classified as 3+ or 2+ by IHC or FISH positive. A comparison of immunofluorescent staining with conventional immunohistochemistry showed that the Qdot system gives more linear and scalable measurements of receptor levels. In both breast tumour sets the system detected very different levels of ErbB2 expression extending over a sixty fold range. We have evaluated the correlation between ErbB2 receptor levels, measured by Qdots, and patient's response to Herceptin. These preliminary data showed better survival in the high ErbB2 expressing cases which is consistent with the hypothesis that Herceptin has a greater benefit in patients with high ErbB2 levels.

CONTENTS

DECLARATION	ii
ACKNOWLEDGEMENT	iii
FIGURES.....	xi
TABLES.....	xv
ABBREVIATIONS.....	xvi

1 - INTRODUCTION

1.1 CELL SIGNALLING	1
1.2. THE SUPERFAMILY OF RECEPTOR TYROSINE KINASES.....	2
1.3. THE EPIDERMAL GROWTH FACTOR FAMILY OF RECEPTOR AND LIGANDS	4
1.4. ErbB RECEPTOR STRUCTURE	6
1.5. ErbB LIGANDS.....	11
1.6. RECEPTOR DIMERISATION	12
1.7. ErbB NETWORK	15
1.9. ErbB INTRACELLULAR TRAFFIKING AND ENDOCYTOSIS.....	18
1.10. ErbB FAMILY OF RECEPTORS AND LIGANDS IN NORMAL DEVELOPMENT	21
1.11. THE ErbB RECEPTORS AND LIGANDS IN HUMAN CANCER.....	22
1.12. CANCER TREATMENTS: ERBB TARGETED THERAPIES	25
1.13. BREAST CANCER	28
1.13.1. OVERVIEW OF BREAST DEVELOPMENT AND ANATOMY	28
1.13.2. COMMON HISTOLOGICAL TYPES OF BREAST CANCER	30
1.13.3. COMMON MOLECULAR TYPES OF BREAST CANCER	31
1.13.4. ERBB2 IN BREAST CANCER	33
1.13.5. THE GOOD AND THE BAD ABOUT HERCEPTIN	35
1.13.5.ROLE OF ERBB FAMILY IN BREAST CANCER	39
1.13.6. ERBB TARGETED FOR THERAPIES IN BREAST CANCER.....	41
1.14. PATIENTS SELECTION	43
1.14.1. IMMUNOHISTOCHEMISTRY AND FLUORESCENCE IN SITU HYBRIDISATION.....	44
1.14.2. OTHER TECHNOLOGIES FOR ERBB2 TESTING.....	49

1.15. QUANTUM DOT NANOTECHNOLOGY	50
1.16. AIMS.....	52

2 - MATERIAL AND METHODS

2.1. CELL CULTURE	53
2.1.1 CELL LINES UTILISED IN THIS STUDY	53
2.1.2 RECOVERING CELL LINES FROM FROZEN STOCKS	53
2.1.3 GROWTH AND MAINTENANCE OF CELL LINES	54
2.1.4 CRYOPRESERVATION OF CELL LINES	54
2.2 ANTIBODIES USED IN THIS STUDY	55
2.2.1 PRIMARY ANTIBODIES.....	55
2.2.2 SECONDARY ANTIBODIES.....	56
2.3 CELL IMMUNOFLUORESCENCE	56
2.4 TRANSFORMATION OF E.COLI WITH PLASMID DNA	57
2.5 TRANSIENT TRANSFECTION	59
2.6 WESTERN BLOTTING	59
2.6.1 CELL LYSIS.....	59
2.6.2 SDS-PAGE GEL ELECTROPHORESIS	60
2.6.3 PROTEIN ELECTRO BLOTTING.....	62
2.6.4 IMMUNODETECTION AND DEVELOPING	62
2.7 TISSUES USED FOR IMMUNOHISTOCHEMICAL AND IMMUNOFLUORESCENT STUDIES	63
2.7.1 TISSUES SOURCES	63
2.7.2 PREPARATION OF FFPE SECTIONS OF RAT PANCREAS	64
2.8 IMMUNOHISTOCHEMICAL STUDY	65
2.8.1 STAINING PROCESS.....	65
2.8.2 SCORING SYSTEM.....	65
2.9 IMMUNOFLUORESCENT STAINING OF FFPE TISSUES.....	66
2.9.1 FFPE TISSUE IMMUNOFLUORESCENCE OF RAT PANCREAS.....	66
2.9.2 OPTIMISATION OF QDOT IMMUNOFLUORESCENT PROTOCOL	66
2.9.3 QDOT IMMUNOFLUORESCENT STAINING OF BREAST CANCER TISSUE ARRAYS	67

2.10	MICROSCOPY.....	67
2.10.1	LIGHT MICROSCOPY	67
2.10.2	FLUORESCENCE MICROSCOPY.....	67
2.10.3	CONFOCAL MICROSCOPY	67
2.11	AUTOFLUORESCENCE.....	68
2.11.1	METHOD TO REDUCE AUTOFLUORESCENCE.....	68
2.11.2	DETERMINATION OF AUTOFLUORESCENCE PROFILE.....	68
2.12	QUANTUM DOT STUDIES.....	69
2.12.1.	DETERMINATION OF QDOT SPECTRA PROFILE	69
2.13	PROCEDURE FOR IMAGE ACQUISITION	70
2.13.1	TESTING CONFOCAL CALIBRATION	70
2.13.2	DETERMINATION OF PARAMETERS FOR IMAGE ACQUISITION.....	70
2.13.2	IMAGES ACQUISITION.....	71
2.14.	IMAGE QUANTIFICATION ANALYSIS	72
2.15	STATISTICAL ANALYSIS	73

3 - DETECTION OF ERBB RECEPTORS EXPRESSION

3.1.	INTRODUCTION.....	74
3.2.	AIMS.....	75
3.3.	RESULTS.....	76
3.3.1.	IMMUNOFLUORESCENCE STUDY.....	76
3.3.1.1	DETERMINATION OF PRIMARY ANTIBODY SPECIFICITY	76
3.3.1.2.	DETECTION OF ERBB RECEPTORS BY QDOT.....	78
3.3.1.3.	DOUBLE LABELLING OF ERBB2 AND ERBB3 WITH QDOT.....	82
3.3.2.1.	DETECTION OF ERBB RECEPTORS IN CELL LINES	85
3.3.2.2.	DETECTION OF ERBB RECEPTORS IN TRANSFECTED CELLS	87
3.3.3.1.	IMMUNOHISTOCHEMICAL STAINING OF FOUR RECEPTORS IN BREAST CANCER TISSUE.....	90
3.3.3.2.	CORRELATION BETWEEN ERBB2 EXPRESSION AND ERBB3 EXPRESSION IN BREAST CANCER	94

3.4	DISCUSSION	
3.4.1.	ANTIBODY SPECIFICITY.....	95
3.4.2.	CELL IMMUNOFLUORESCENCE WITH QDOTS	99
3.4.3.	DOUBLE IMMUNOFLUORESCENCE USING QDOTS	100
3.4.3.	IMMUNOHISTOCHEMICAL STUDIES.....	101

4 - APPLICATION OF QDOT TECHNOLOGY ON FORMALIN FIXED PARAFFIN EMBEDDED TISSUES

4.1	INTRODUCTION.....	105
4.2	AIMS.....	106
4.3	RESULTS	107
4.3.1.	DETECTION OF α -CELLS ON RAT PANCREAS.....	107
4.3.2.	ESTABLISHING STANDARD PROTOCOL FOR QDOT LABELLING	109
4.3.3.	DETECTION OF ERBB2 EXPRESSION IN A BREAST CANCER TISSUE ARRAY CONTROL	112
4.3.4.	AUTOFLUORESCENCE STUDIES IN FFPE TISSUES.....	117
4.3.4.1.	REDUCTION OF AUTOFLUORESCENCE BY PHOTBLEACHING	117
4.3.4.2.	STUDY OF AUTOFLUORESCENCE SPECTRA PROFILE IN RAT PANCREAS AND BREAST CANCER TISSUES	119
4.3.4.2.	QDOT 525 AND QDOT585 SPECTRA PROFILE AND REDUCTION OF AUTOFLUORESCENCE	123
4.4.	DISCUSSION.....	124
4.4.1.	DEVELOPMENT OF QDOT STANDARD PROTOCOL.....	124
4.4.2.	APPLICATION OF QDOT TECHNOLOGY TO FFPE BREAST CANCER TISSUES.....	125
4.4.3.	AUTOFLUORESCENCE STUDIES.....	127

5 - QUANTIFICATION OF ERBB2 EXPRESSION IN BREAST CANCER TUMOURS BASED ON QDOT IMMUNOFLUORESCENCE IMAGING

5.1	INTRODUCTION	130
5.2.	AIMS.....	131
5.3.	RESULTS.....	132
5.3.1.	IMAGES ACQUISITION	132

5.3.1.1. ESTABLISHING STANDARD PARAMETERS FOR THE IMAGES ACQUISITION.....	133
5.3.1.2. MAINTAINING CONSISTENCY OF THE CONFOCAL MICROSCOPE	142
5.3.2. QUANTIFICATION ANALYSIS	146
5.3.2.1. QUANTIFICATION OF ERBB2 IN BREAST CANCER TISSUES.....	151
5.3.2.2. VALIDATION OF QDOT QUANTIFICATION SYSTEM VERSUS THE IHC SYSTEM....	155
5.4. DISCUSSION.....	156
5.4.1. IMAGES COLLECTION	156
5.4.2. INSTRUMENT CONSISTENCY	159
5.4.3. QUANTIFICATION ANALYSIS	160

6 - QUANTIFICATION OF PRIMARY BREAST CANCER TREATED WITH HERCEPTIN

6.1 INTRODUCTION.....	164
6.2 AIMS.....	165
6.3. RESULTS.....	166
6.3.1. QUANTIFICATION OF ERBB2 IN A SERIES OF BREAST CANCERS TREATED WITH HERCEPTIN.....	166
6.3.2 STATISTICAL ANALYSIS	170
6.4. DISCUSSION.....	175
6.4.1. ASSESSMENT OF ERBB2 STATUS BY QDOT.....	175
6.4.2 CORRELATION BETWEEN QDOT QUANTIFICATION AND PATIENTS RESPONSE TO HERCEPTIN.....	177

7 - QUANTIFICATION OF ErbB3

7.1. INTRODUCTION.....	179
7.2. AIMS	180
7.3. RESULTS.....	181
7.3.1. TESTING THE 49.3 POLYCLONAL ANTIBODY IN IMMUNOFLUORESCENCE AND IMMUNOHISTOCHEMICAL STAINING.....	181
7.3.2. DETECTION OF ERBB3 BY QDOTS IN BREAST CANCER TISSUES.....	183
7.4. DISCUSSION.....	185

8 - GENERAL DISCUSSION

8.1. DISCUSSION.....187

8.1.1. CONCLUSION.....197

REFERENCES.....199

FIGURES

Figure 1.1	Domain organisation of the RTKs families.....	3
Figure 1.2	Domain organisation of several NRTKS.....	4
Figure 1.3	Evolution of ErbB network.....	5
Figure 1.4	General structure of ErbB receptors.....	7
Figure 1.5	Structure of CR2 domain.....	8
Figure 1.6	Crystal Structure of the extracellular domain of all the ErbB receptors.....	10
Figure 1.7	Structure of EGF-like motif.....	11
Figure 1.8	Schematic representation of ligand-induced EGF receptor dimerisation.....	13
Figure 1.9	Model of interaction between receptor domains.....	14
Figure 1.10	ErbB network.....	26
Figure 1.11	Crosstalk between the ErbB family and other systems.....	18
Figure 1.12	ErbB receptor trafficking.....	19
Figure 1.13	Effect on tumour growth of ErbB receptors alone and in combinations.....	24
Figure 1.14	Schematic illustration of receptor targeted therapies.....	26
Figure 1.15	Schematic structure of an adult female breast.....	29
Figure 1.16	Schematic representation of a normal breast duct and two types of breast cancer.....	30
Figure 1.17	Summary of different Herceptin antitumor mechanisms.....	36
Figure 1.18	Representation of different resistance mechanisms of Herceptin.....	38
Figure 1.19	Example of the IHC test for ErbB2.....	45
Figure 1.20	ASCO/CAP guideline for the interpretation of ErbB2 IHC test.....	145
Figure 1.21	ASCO/CAP guidelines for the interpretation of the ErbB2 FISH test.....	48
Figure 1.22	Schematic structure of Qdot.....	51
Figure 3.1	Detection of ErbB receptors with AlexaFluor 546.....	77
Figure 3.2	Immunofluorescent staining of SKBR3 cells.....	78
Figure 3.3	Evaluation of immunofluorescent staining with anti-mouse Qdot 525 secondary antibody.....	79

Figure 3.4	Immunofluorescent staining with anti-mouse Qdot 525 and antirabbit Qdot 585.....	81
Figure 3.5	Double labelling of MDA-MB453 cells.....	83
Figure 3.6	Lambda stacks.....	84
Figure 3.7	Emission Spectrum of Qdot 525 and Qdot 585.....	85
Figure 3.8	Evaluation of antibody specificity by Western blotting.....	86
Figure 3.9	Western blot analysis for antibody cross-reactivity.....	88
Figure 3.10	Different IHC methods.....	90
Figure 3.11	Immunohistochemical staining of ErbB1 in breast cancer tissues.....	91
Figure 3.12	Immunohistochemical staining of ErbB2 in breast cancer tissues.....	92
Figure 3.13	Immunohistochemical staining of ErbB3 in breast cancer tissues.....	93
Figure 3.14	Immunohistochemical staining of ErbB4 in breast cancer tissues.....	93
Figure 3.15	Percentage of breast cancer samples.....	94
Figure 3.16	Comparison between AlexaFluor and Qdot spectra profiles.....	100
Figure 4.1	Immunohistochemical staining of rat pancreas tissues.....	107
Figure 4.2	Immunofluorescent staining of rat pancreas tissue with AlexaFluor 546 anti-mouse secondary antibody.....	108
Figure 4.3	Immunofluorescent staining of rat pancreas tissue with anti-glucagon primary antibody and anti-mouse Qdot 525 secondary antibody.....	108
Figure 4.4	Optimisation of incubation time of Qdot 525 anti-mouse secondary antibody....	110
Figure 4.5	Optimisation of Qdot 525 anti-mouse secondary antibody concentration.....	115
Figure 4.6	Immunohistochemistry test performed on a control microarray slide.....	112
Figure 4.7	Breast cancer ErbB2 control array stained with CB11 mouse primary antibody and Qdot 525 anti-mouse secondary antibody.....	113
Figure 4.8	Spectral separation of Qdot 525 fluorescent signal and autofluorescent signal....	115
Figure 4.9	Merged two-colour images of the green and red channel after spectral reassignment.....	116
Figure 4.10	Photobleaching method to reduce the autofluorescence.....	118
Figure 4.11	Photobleaching effect on the autofluorescence.....	118
Figure 4.12	Autofluorescence in a FFPE rat pancreas tissue.....	119
Figure 4.13	Variation of the autofluorescence between two different FFPE breast cancer tissues.....	120

Figure 4.14 Autofluorescence emission spectra profiles from the tissue areas shown in Figure 4.13 first row.....	121
Figure 4.15 Autofluorescence spectra profile of the tissue areas shown in Figure 4.13 second row.....	122
Figure 4.16 Emission profile of Qdot 525 when excited with 405nm laser light.....	123
Figure 4.17 Emission spectra of Qdot 585.....	124
Figure 4.18 Spectral Dye Separation of Qdot 525 specific signal and autofluorescence.....	127
Figure 5.1 Wavelength scan of Qdot 585.....	135
Figure 5.2 Reduction of noise by using the frame averaging method.....	136
Figure 5.3 Application of “look up table” tool.....	137
Figure 5.4 Breast cancer tissues expressing ErbB2.....	138
Figure 5.5 Channels used for the image acquisition.....	139
Figure 5.6 Images showing the autofluorescence of breast cancer tissues expressing ErbB2.....	140
Figure 5.7 Merges of two colour images of the green (485nm-505nm) and red (575nm-595nm) channel.....	141
Figure 5.8 The histogram shows the mean intensities of the images in Figure 5.8.....	142
Figure 5.9 Vascular bundles from Lily of the Valley (<i>Convallaria majalis</i>).....	143
Figure 5.10 Comparison of the mean intensities from the control images shown in Figure 5.9.....	144
Figure 5.11 Comparison of images of ErbB2 3+ breast cancer tissue acquired simultaneously in two channels on different days.....	145
Figure 5.12 The histograms show the mean intensities of the images in Figure 5.11.....	145
Figure 5.13 Example of segmented images.....	147
Figure 5.14 Histogram of the pixel intensities of the image collected in the red channel within the three region of interest ROI 1-2-3 corresponding to the tumour areas	148
Figure 5.15 Histogram of the pixel intensities of the image collected in the red channel.....	150
Figure 5.16 Qdot 585-Immunofluorescent staining of the control microarray slide with four cores of breast cancer tissues.....	150
Figure 5.17 Qdot-immunofluorescent staining of breast cancer tissues scored as 3+ by IHC.....	152
Figure 5.18 Qdot-immunofluorescent staining of breast cancer tissues scored as 2+ by IHC.....	153

Figure 5.19	The two histograms show Qdot 585 signal quantification.....	154
Figure 5.20	Validation of the Qdot quantification system versus the IHC test.....	155
Figure 5.21	Breast cancer tissues expressing ErbB 2.....	157
Figure 5.22	The histogram shows the mean intensities obtained from the images of the control section acquired in the red channel using the same setting.....	159
Figure 5.23	Quantification of Qdot 585 signal with the contribution of the autofluorescence and the autofluorescence only.....	161
Figure 5.24	Two examples of three different tumour areas within the same section.....	162
Figure 6.1	Qdot-immunofluorescent staining of primary breast cancer tissues scored as 3+ by IHC.....	167
Figure 6.2	Qdot-immunofluorescent staining of primary breast cancer tissues scored as 2+ by IHC.....	168
Figure 6.3	The histogram summarises the Qdot quantification results of 123 breast cancers over expressing ErbB2 at 2+ and 3+ levels.....	169
Figure 6.4	Validation of Qdot quantification values of 123 primary breast cancers over expressing ErbB2 versus IHC score.....	170
Figure 6.5	Median values of Qdot measurement.....	171
Figure 6.6	A median level was chosen as cut-off point to divide patients into two groups, one group with high Qdot score, and the other group with low Qdots score.....	172
Figure 6.7	Kaplan Meier survival analysis of the whole population.....	174
Figure 6.8	Kaplan Meier survival analyses in node positive patients.....	174
Figure 7.1	Immunofluorescence of HEK293-ErbB3 cells.....	181
Figure 7.2	Immunohistochemical staining of ErbB3 in FFPE breast cancer tissues.....	182
Figure 7.3	ErbB3 expression in a set of human breast cancer tissues.....	183
Figure 7.4	Qdot 585 immunofluorescent staining of FFPE breast cancer tissues.....	184

TABLES

Table 1.1 Common molecular subtypes of breast cancer. Table adapted from Alizart et al 2010 and Weigelt et al 2010	33
Table 3.1 ErbB receptor expression in a set of breast cancer samples.....	94
Table 3.1 Summary of the disease status in 115 breast cancer patients treated with Herceptin.....	171

ABBREVIATIONS

ABC	Avidin-Biotin Complex
ADAM	A disintegrin and metalloprotease
AOTF	Acousto Optical Tunable Filter
APS	ammonium persulfate
AR	amphiregulin
ASCO/CAP	American Society of Clinical Oncology/College of American Pathologist
AS MDW	Application Solution Multidimensional Workstation
ATP	Adenosine Tri-Phosphate
BSA	bovine serum albumin
BTC	betacellulin
CISH	chromogenic in situ hybridisation
CR	cysteine-rich domain
DAB	3,3' diaminobenzidine tetrachloride
DCIS	ductal carcinoma <i>in situ</i>
DMEM	Dulbecco's modified Eagle's medium
DMSO	dimethyl sulfoxide
DNA	deoxyribonucleic acid
ECD	extracellular domain
ECL	enhanced chemiluminescence
EDTA	ethylene diamine tetra acetic acid
EGF	epidermal growth factor
EGFR	epidermal growth factor receptor
EGTA	ethylene glycol tetraacetic acid
ELISA	enzyme linked immune-sorbent assay

EM-CDD	electron multiplier charge couple device
EPR	epiregulin
ER	oestrogen receptor
FBS	foetal bovine serum
FCS	foetal calf serum
FDA	Food and Drug Administration
FFPE	formalin fixed paraffin embedded
FISH	fluorescence in situ hybridisation
GH	growth hormone
GPCR	G-protein coupled receptors
Grb2	growth-factor-receptor bound-2
HB-EGF	heparin-binding EGF
HRG	heregulin
HRP	horse radish peroxidase
IDC	invasive ductal carcinoma
ILC	invasive lobular carcinoma
IF	immunofluorescence
Ig	immunoglobulin
IGF1R	insulin-like growth factor 1 receptor
IHC	immunohistochemistry
Jak	Janus tyrosine kinase
kDa	kilo Dalton
L1-L2	ligand binding domain 1-2
LB	Luria-Bertani
LCIS	lobular carcinoma in situ
LSCM	laser scanning confocal microscope
LUT	look up table

MAPK	mitogen-activated protein kinase
mAb	monoclonal antibody
MBC	metastatic breast cancer
ml	millilitre
MMP	metalloproteinase
mRNA	messenger ribonucleic acid
MUC4	mucin 4
nm	nanometer
nM	nanomolar
NRG	neuregulin
NRTK	non receptor tyrosine kinase
NSCLC	non-small-cell lung cancer
PAGE	polyacrylamide gel electrophoresis
PDGF	platelet-derived growth factor
PBS	phosphate buffered saline
PCR	polymerase chain reaction
PI3K	phosphatidylinositol 3-kinase
PMT	photo multiplier tube
PR	progesterone receptor
PRL	prolactin
PTB	phosphotyrosine binding domain
PTK	protein tyrosine kinase
Qdot	quantum dot
QE	quantum efficiency
qRT-PCR	quantitative real time polymerase chain reaction
RNA	ribonucleic acid
ROI	region of interest

RTK	receptor tyrosine kinase
SDS	sodium dodecyl sulphate
SH2	Src homology 2
SISH	silver in situ hybridisation
Shc	Src-homology-2-containing
SP	spectral prism
T-DM1	Trastuzumab-derivate maytanasine 1
TEMED	N,N,N,N'-Tetra-methyl-ethylenediamine
TGF- α	transforming growth factor- α
TK	tyrosine kinase
TKD	tyrosine kinase domain
TKI	tyrosine kinase inhibitor
TMA	tissue microarray
TMPS	triple membrane passing signalling
Trp	tryptophan
V	voltage
VEGF	vascular endothelial growth factor
WB	western blot

1-INTRODUCTION

1.1 CELL SIGNALLING

The existence of living organisms depends on ability of the cells to correctly perceive, interpret and respond to a continuous flow of information from the external and internal environment. All cellular organisms possess a sophisticated communication network that coordinates the biological activity of the cells and the physiology of the organism as a whole. Cells can transmit information to each other in several ways, such as paracrine, endocrine or autocrine signalling, producing appropriate responses. The cellular communication system is composed of a class of proteins called cellular receptors and a class of molecules known as ligands or extracellular signalling molecules. The interaction between cellular receptors and their specific ligands triggers, within the cell, a wide number of processes that modify cell behaviour allowing normal cellular development and growth. The extracellular messengers (which comprise hormones, neurotransmitters and growth factors) contain the information from the cell and the receptors are capable of binding these ligands with high affinity thereby mediating the activation of many signal transduction pathways. Receptors can be intracellular, both cytoplasmic and nuclear; these receptors respond to hydrophobic signalling molecules able to cross the membrane. Cell surface receptors are targets for hydrophilic signalling molecules. Moreover, these proteins have different modes of action: the intracellular receptors, following ligand binding, generally attach directly to specific DNA target sequences and alter gene expression, promoting the synthesis of new proteins; the cell surface receptors are transmembrane proteins that upon ligand binding act on existing target molecules initiating intracellular signal transduction. Several types of cell surface receptors have been identified: cell-adhesion molecules, ionotropic, G protein coupled, guanylyl cyclase, cytokine and tyrosine kinase receptors; each class of these proteins can be also divided in many subclasses.

Furthermore, all these systems are finely regulated so that the cells can respond to variations in their environment. The human ErbB receptor family and its ligands represent an elaborate network able to generate a high level of signalling diversity.

Errors that occur in this system can cause deregulated cell growth and differentiation that is crucial for malignant transformation.

1.2. THE SUPERFAMILY OF RECEPTOR TYROSINE KINASES

Protein tyrosine kinases (PTK) are key elements in the cell communication network and are involved in sending, receiving and elaborating messages responsible for the cellular responses. Human PTKs comprises 58 receptor tyrosine kinases (RTKs) divided in 20 subfamilies (Lemmon and Schlessinger) (Fig. 1.1) and 32 cellular tyrosine kinases, also called non receptor tyrosine kinases (NRTKs), divided into 10 subfamilies (Fig.1.2) (Robinson et al., 2000). While the RTKs mediate a signal carried by a ligand and initiate downstream signalling pathways, the NRTKs are essential components of the signalling cascades. Examples of RTK families include receptors for insulin and many growth factors, such as epidermal growth factor (EGF), platelet-derived growth factor (PDGF), fibroblast growth factor (FGF), and vascular endothelial growth factor (VEGF) and nerve growth factor (NGF) (Fig. 1.1). The main NRTKs families comprise Src, Janus kinase (Jak), Focal Adhesion Kinase (Fak) and Abl, among others (Hubbard and Till, 2000) (Fig. 1.2). All RTKs have a similar domain organisation: an extracellular domain for ligand-binding, a transmembrane region, followed by a cytoplasmic tyrosine kinase (TK) portion which has catalytic activity and finally a C-terminal tail. While the structure of the juxtamembrane domain and TK domain are similar across all RTKs subfamilies, the structure of the extracellular domains is very different. Typically the extracellular domains can exhibit immunoglobulin (Ig)-like domains, one or two cysteine-rich domains, fibronectin type III-like domains and EGF-like domains (Hubbard, 1999). All RTKs are located on the cell surface and are monomers in their inactive state. Ligand binding to the extracellular domain of the RTKs induces conformational changes and promotes receptor dimerisation. Activated receptor dimers catalyse autophosphorylation on tyrosine residues on the tyrosine kinase domain (TKD) creating docking sites for adaptor and scaffolding proteins that contain Src homology-2 (SH2) and phosphotyrosine-binding (PTB) domains (Cohen et al., 1995; Schlessinger, 2000). These proteins then use a variety of specific motifs to target other cytoplasmic proteins to activate specific signalling cascades. Through these complex mechanisms,

RTKs can transmit a signal from the cell surface to the nucleus, which can generate the appropriate response.

Activation and deactivation of these mechanisms are tightly controlled to guarantee normal cell growth, differentiation and survival. To date it has been well established that PTKs play a role in cancer development often as consequence of mutations in different domains of the RTKs resulting in constitutive receptor activation, and/or over expression of normal receptors. Mutations may also occur in NRTKs producing a constitutive activation of different signalling pathways (Kolibaba and Druker, 1997; Porter and Vaillancourt, 1998). An increasing knowledge of the PTKs structure, activation mechanisms, signalling pathways and regulation, will assist in the further development of targeted drug therapies (Bennasroune et al., 2004).

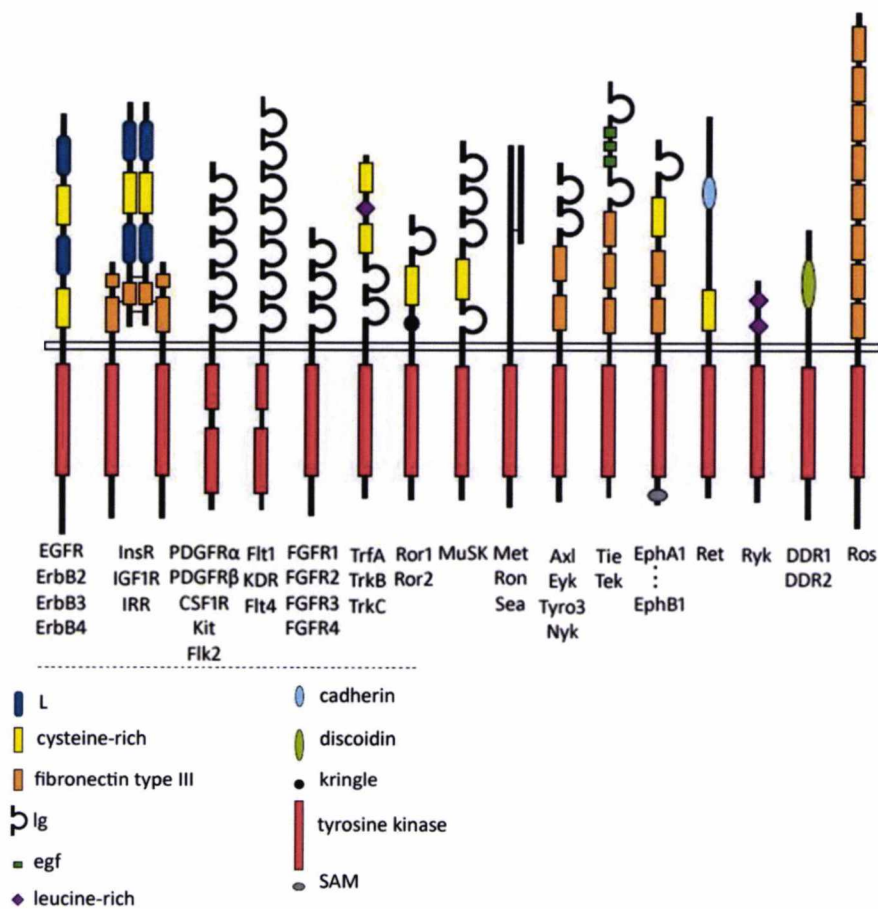


Figure 1.1 Domain organisation of the RTKs families. RTKs are transmembrane protein with a cytoplasmic, TM membrane and extracellular portion. As shown, all the RTKs families share a similar TK domain; however the extracellular domain varies greatly across the different families. (Images adapted from Hubbard and Till, 2000).

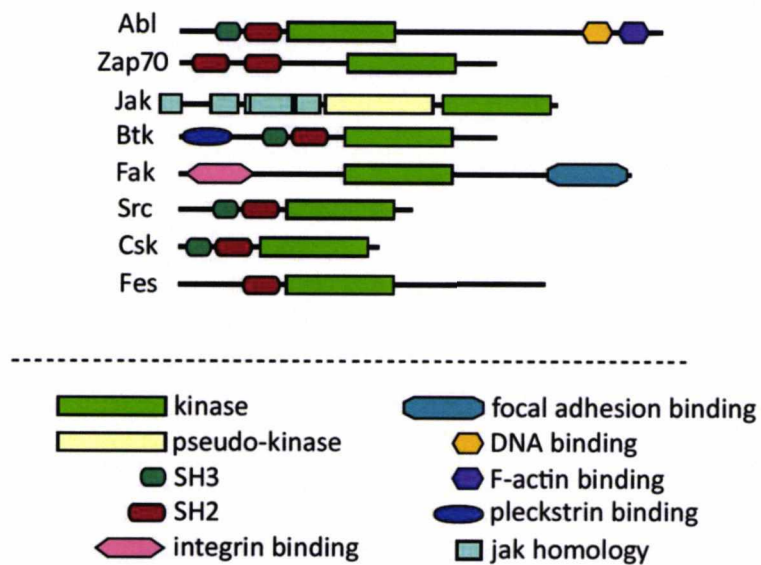


Figure 1.2 Domain organisation of several NRTKS (Hubbard and Till, 2000).

1.3. THE EPIDERMAL GROWTH FACTOR FAMILY OF RECEPTOR AND LIGANDS

The human ErbB receptor family and its ligands represent an elaborate network able to generate a high level of signalling diversity. It is evolved from a simpler system, for instance in the nematode *Caenorhabditis elegans* a single gene has been identified namely LET-23, homologous to EGFR and one ligand called LIN-3 (Fig. 1.3 A) and in the fruitfly *Drosophila melanogaster* there are five ligands and one receptor called DER (Fig. 1.3 B) (Stein and Staros, 2000; Citri and Yarden, 2006). This simple network has evolved, in vertebrates, to four receptors and eleven ligands as results of an evolutionary process to enhance signalling diversity and regulation in more complex organisms (Amit et al., 2007).

The ErbB receptors are located on the cell membrane and include four receptors ErbB1, ErbB2, ErbB3 and ErbB4. ErbB4 also exists in four isoforms, generated by alternative splicing of the full length form of ErbB4; it has also been shown that these ErbB4 isoforms are tissue specific (Elenius et al., 1997; Elenius et al., 1999). In the

literature it is possible to find different names attributed to each one of the ErbB receptor: ErbB1 is also called HER1 or EGFR, ErbB2 is called Neu or HER2, ErbB3 is called HER3 and ErbB4 may also be referred to as HER4. In this document, we will refer to the receptors using ErbB1, ErbB2, ErbB3 and ErbB4. To date, eleven ligands for ErbB1, ErbB2 and ErbB3 receptors have been identified: epidermal growth factor (EGF), amphiregulin (AR), transforming growth factor- α (TGF α), epigen (EPI), betacellulin (BTC), heparin binding EGF (HB-EGF) and epiregulin (EPR) and the neuregulins 1-4 (NGR 1-4) (Gullick, 2001; Sweeney and Carraway, 2000). Interestingly, no direct ligand for ErbB2 has been found, suggesting that has evolved to operate only as a heterodimerization partner (Stein and Staros, 2000) (Fig.1.3 C).

Genetic studies on *Caenorhabditis elegans*, *Drosophila melanogaster* and mice, have revealed that members of epidermal growth factor receptor family are involved in a wide number of physiological events such as embryonic and adult development, cellular proliferation, differentiation, survival and motility (Olayioye et al., 2000; Casalini et al., 2004).

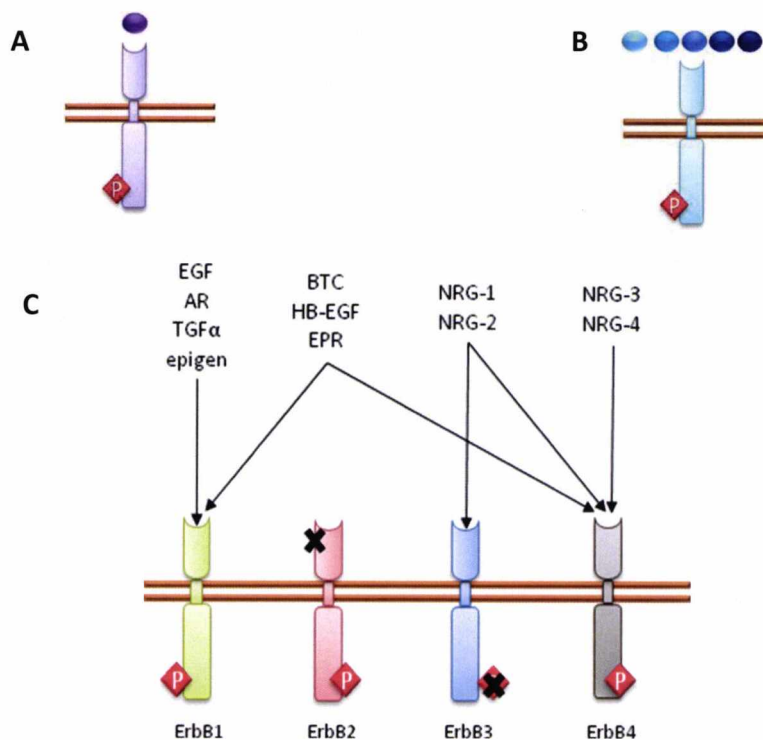


Figure 1.3 Evolution of ErbB network. In (A), the nematode *Caenorhabditis elegans* which expresses a single ErbB receptor and one ligand; in (B), the fruitfly *Drosophila melanogaster* with one receptor and five ligands; (C) the complex ErbB network in vertebrates with four receptors and eleven ligands (Citri and Yarden, 2006).

1.4. ErbB RECEPTOR STRUCTURE

All receptor proteins that belong to the ErbB family share a common basic structure. The first receptor to be discovered and studied was the epidermal growth factor receptor (EGFR) (Bazley and Gullick, 2005). Its structure can be taken as prototype for this class of proteins.

A typical ErbB structure consists in three functional domains: one extracellular, one transmembrane and one cytoplasmic, each of which can be divided into further subdomains. The extracellular portion is heavily glycosylated and comprises two ligand-binding domains (L1 and L2) and two cysteine-rich domains (CR1 and CR2) arranged in the following order: L1-CR1-L2-CR2 (Fig. 1.4). The transmembrane region is made up by hydrophobic residues that form a α -helix and anchors the receptor to the membrane (Gullick et al., 1992). The cytoplasmic domain consists of three subdomains: a juxtamembrane region (Jura et al., 2009a), that seems to be responsible for many protein interactions involved in several regulatory functions such as internalisation and recruitment of numerous factors implicated in downstream signalling; a tyrosine kinase domain with enzymatic activity, and C-terminal tail that has six tyrosine residues which, following receptor activation, are phosphorylated generating docking sites for SH2 domain containing proteins (Martin-Fernandez et al., 2002).

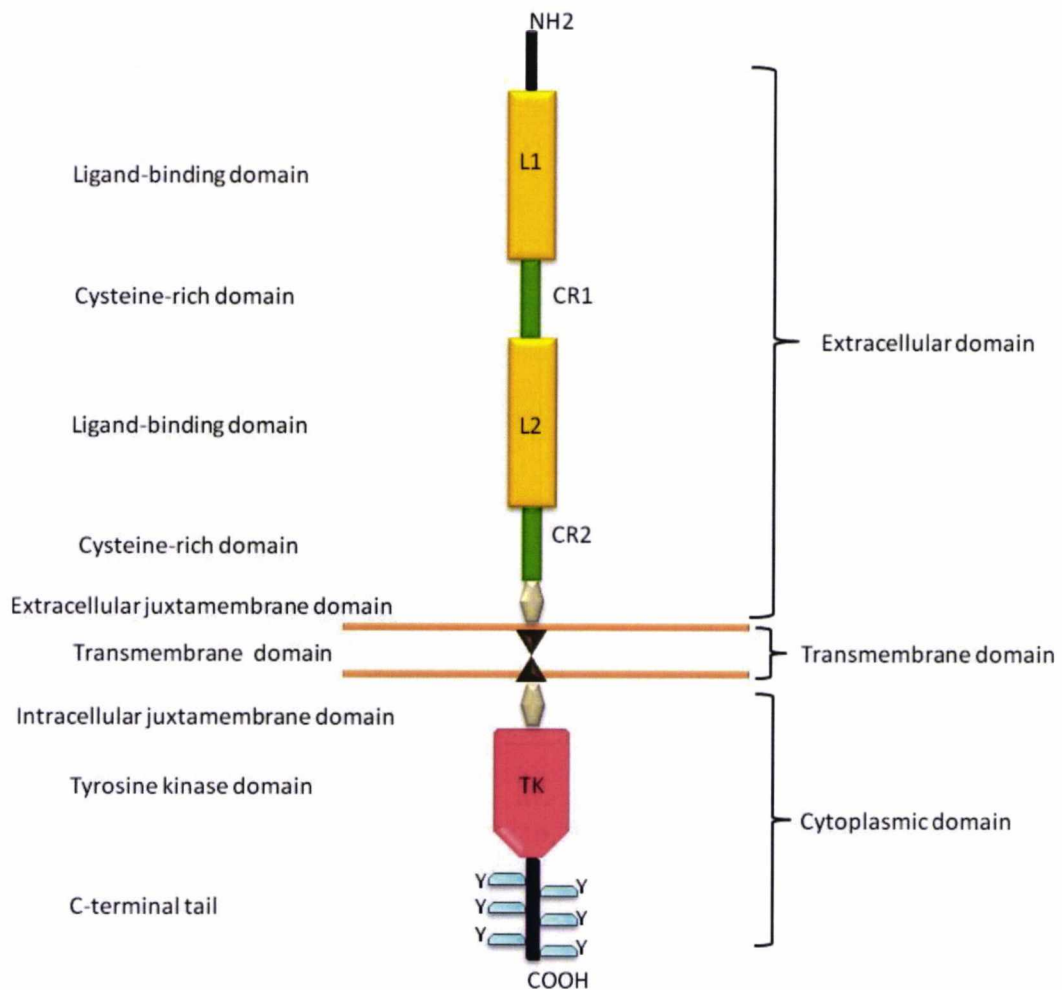


Figure 1.4 General structure of ErbB receptors. ErbB structure can be divided into three main domains: extracellular, transmembrane and intracellular. The extracellular portion comprises the ligand-binding domains (L1 and L2), the cysteine-rich domains (CR1 and CR2) and the extracellular juxtamembrane domain. The cytoplasmic portion comprises the intracellular juxtmembrane region, the tyrosine kinase domain and a C-terminal tail. (Image adapted from Bazley and Gullick, 2005)

X-ray crystallography has been used to determine the three dimensional structure of the various domains of the ErbB1 protein. In the extracellular region L1 and L2 assume a solenoidal structure formed by six right-handed β -helix turns which together form the ligand binding pocket in which the ligand makes contact with both L1 domain and L2. CR1 and CR2 are structurally associated with L1 and L2 through a tryptophan (Trp) residue at position 176- between L1 and CR1- and Trp492 between L2 and CR2- that

establish hydrogen bonds between the peptide chains (Jorissen et al., 2000; Garrett et al., 2002; Jorissen et al., 2003). CR1 and CR2 are cysteine rich regions containing two types of disulphide-bonded modules termed C1 and C2. C1 is characterised by a single bond between Cys1 and Cys3, while C2 contains two bonds, the first one between Cys1 and Cys3 and the other between Cys2 and Cys4, the other one between Cys2 and Cys4. In the CR1 domain there are 8 modules in the order C2-C2-C2-C1-C1-C1-C1-C1 while CR2 domain contains 7 modules in the order C2-C1-C1-C2-C1-C1-C2, as shown in figure 1.5

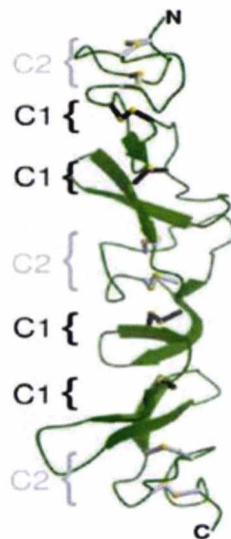


Figure 1.5 Structure of CR2 domain. The image shows the cysteine rich regions containing 7 disulphide-bonded molecules in order C2-C1-C1-C2-C1-C1-C2. (Image from Burgess et al., 2003).

In addition to describing the general and molecular structure of the receptors, it is important to consider how they are organised and orientated in space. The first C2 module of both CR domains establishes contacts with its preceding L domain which appears to stabilise the orientation of the L domain (Burgess et al., 2003; Jorissen et al., 2000; Ward et al., 2001). In addition the CR1 and CR2 loops are essential for stabilisation of the ligand-binding site, receptor dimerisation with another ErbB protein and activation of the intracellular TK domain (Burgess et al., 2003). The structure of extracellular domain of unliganded ErbB3 and ErbB4 is very similar to those reported for inactive forms of ErbB1 and all assume a tethered conformation (Fig.1.6). This

conformation is determined by the presence of molecular contact points between CR1 and CR2 domains. Three residues, Tyr/Asp/Lys/, are conserved in all vertebrate orthologs of ErbB1, ErbB3 and ErbB4, but not in ErbB2, and are essential for the formation of the ligand binding site (Jorissen et al., 2000; Cho and Leahy, 2002; Bouyain et al., 2005).

In relation to the structure of ErbB1, ErbB2 shows unique characteristics. As mentioned above it is the only member of the family that does not bind any ligand and its main biological function is to act as a co-receptor for the other ErbB proteins forming heterodimeric complexes. It is possible to explain this property by observing its molecular structure: this appears quite similar to others ErbB receptors except for the extracellular domain. ErbB2 adopts a compact bi-lobed structure where the L1 and L2 domains are close together creating a structure in which the binding site is not accessible for the ligand. This structure confers to ErbB2 a conformation comparable with ErbB1 and ErbB3 in the activated state (Fig 1.6). These data suggest that ErbB2 due to its unique conformation is ready to interact with different ErbB receptors in the absence of bound ligand (Burgess et al., 2003; Garrett et al., 2003).

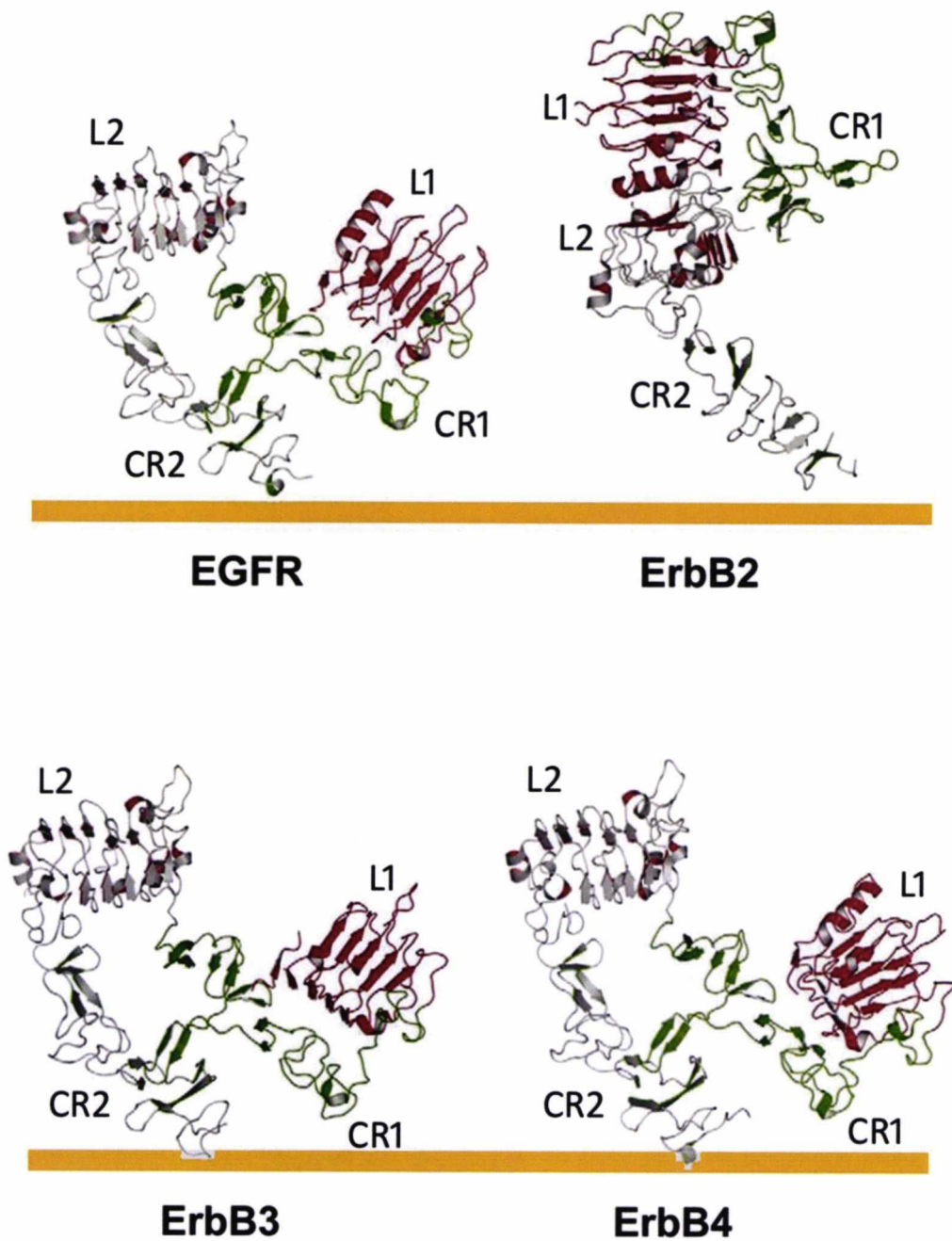


Figure 1.6 Crystal Structure of the extracellular domain of all the ErbB receptors. ErbB1, ErbB3 and ErbB4 exist on the membrane in a tethered conformation in absence of ligand. ErbB2 is the only receptor which has a tethered conformation with domains L1 and L2 closed together and CR2 exposed resembling the activated conformation of the other receptors. (Image adapted from Lemmon, 2009).

1.5. ErbB LIGANDS

All ligands of the EGF family are characterised by the presence of a related conserved element of 50 amino acids that form the epidermal growth factor like (EGF-like) motif. This motif contains a distinct pattern of six cysteine residues, which form three disulphide bonds, and these stabilise its conformation which is essential for binding to the ErbB receptors (Fig. 1.7) (Abe et al., 1998; Burgess et al., 2003).

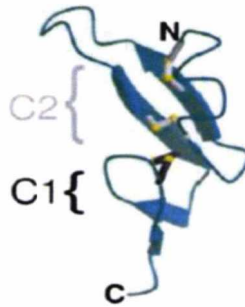


Figure 1.7 Structure of EGF-like motif. EGF has six cysteines forming three disulphide bonds corresponding to C2 module and C1 module. (Image from Burgess et al., 2003).

As mentioned earlier, there are 11 genes that encode for EGF ligands. On the basis of their ligand-binding specificity it is possible to divide the ligands in four categories: ligands that bind ErbB1 alone are EGF, AR and TGF- α , ligands that bind both ErbB1 and ErbB4 comprise BTC, HB-EGF and EPR, NGR 1 and 2 bind to ErbB3 and ErbB4 and NRG 3 and 4 bind ErbB4 alone (Fig 1.3 C) (Gullick, 2001; Sweeney and Carraway, 2000). Furthermore, NRG 1 has been found to be expressed as 15 alternative isoforms, produced by alternative splicing of the mRNA encoding for NRG 1 (Falls, 2003). Most of the ligands, with the exception of some NRG isoforms are initially expressed as precursor proteins anchored to the membrane, from where they are released as soluble forms following a proteolytic cleavage by metalloproteinases (Falls, 2003; Kinugasa et al., 2004). Alternative names of the NRG ligands are divergent neuregulin 1 (Don-1) (Busfield et al., 1997) or neural- and thymus-derived activator for ErbB kinases (NTAK) (Higashiyama et al., 1997), as they were found mainly expressed in the brain and in the cerebellum. Another potential ErbB ligand that was discovered more recently is epigen. While epigen binds ErbB1 with lower affinity than EGF or TGF- α , it

can induce a similar cellular growth to that observed with TGF- α (Strachan et al., 2001).

1.6. RECEPTOR DIMERISATION

Structural studies of epidermal growth factor receptors have shown that ErbB receptors, with the exception of ErbB2, reside on the cell surface in an inactive or auto-inhibited state (Garrett et al., 2002; Burgess et al., 2003). In this tethered conformation, the close interaction between CR1 and CR2 domains constrain L1 and L2 domains in an orientation such that the dimerisation arm, located within domain CR1, is not available to interact with a second receptor, thus preventing dimerisation (Schlessinger, 2002). The absence of this mechanism in ErbB2 contributes to its increased oncogenicity when over expressed in cells (Bazley and Gullick, 2005).

Ligand binding promotes various conformational rearrangements that drive receptor dimerisation. It is likely that ErbB proteins are present on the membrane in a dynamic equilibrium between different conformational states both as monomers and inactive dimers or tetramers, rather than in a rigid structure (Clayton et al., 2005). Ligand-binding occurs with a monomeric receptor that has an extended shape in which the L1 and L2 domains are disposed with the right orientation in space. As shown in the diagram below (Fig. 1.8) ligand then traps the receptor in a dimerisation competent state (Ferguson et al., 2003). The ligand-receptor (1:1) interacts with a second monomeric complex forming a dimeric complex (2:2). The ligand establishes various bonds with domains L1 and L2 of a monomeric receptor (Lemmon et al., 1997; Ogiso et al., 2002) affecting indirectly the CR1 and CR2 domains involved in the auto-inhibition such that the dimerisation arm becomes exposed and is available to interact with the dimerisation loop of a second receptor (Ferguson et al., 2003; Lemmon, 2009). Moreover, domain CR2 could function as an additional site that optimises the contact across the dimer interface stabilising the dimeric complex allowing higher dimerisation resulting in the formation of tetrameric structures (Fig. 1.8) (Schlessinger, 2002; Dawson et al., 2005).

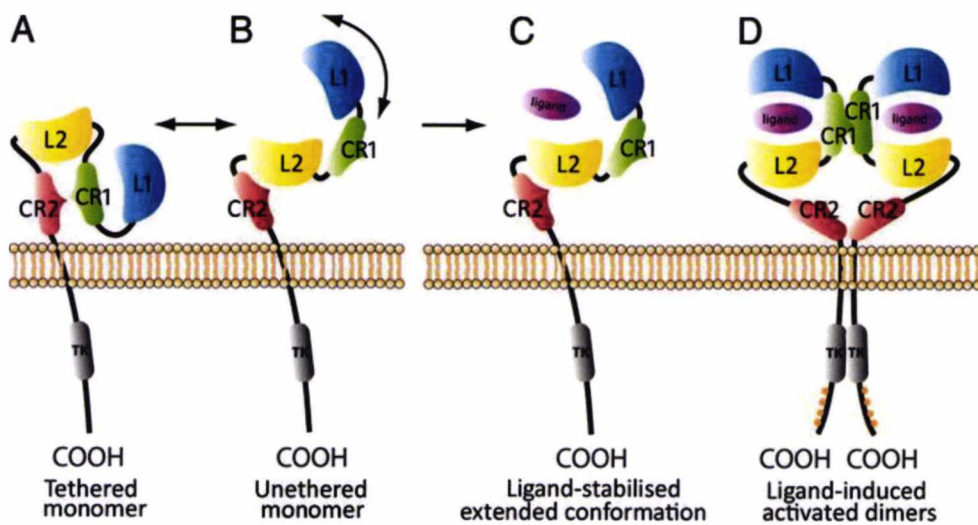


Figure 1.8 Schematic representation of ligand-induced EGF receptor dimerisation. Receptors are present on the membrane in different conformations as tethered monomers (A) and untethered monomers (B). The ligand binds the receptor between domain L1 and L2 and traps the receptor in a extended conformation (C) where the dimerisation arm CR1, is exposed and therefore able to interact with another liganded receptor forming the dimer-complex (D). In the dimer the tyrosine kinase domain of one receptor phpsphorylates tyrosine residues in the c-terminal tail of the other receptor. (Image adapted from Lammerts van Bueren et al. 2008).

The dimerisation of the extracellular region induces allosteric interactions between the intracellular portions of the receptors resulting in the formation of asymmetric kinase domain dimers where one kinase domain acts as activator of the other (called the receiver) (Zhang et al., 2006). The tyrosine kinase domain has a bi-lobed fold which is composed of an NH₂-terminal domain and COOH-terminal domain. Between the two lobes is a cleft where ATP binds. In this spatial disposition the C-terminal lobe of the activator is juxtaposed to the N-terminal lobe of the receiver and the juxtamembrane segment of the receiver engages the C-terminal lobe of the activator, stabilising the asymmetric dimer (Fig. 1.9) (Zhang et al., 2006; Bose and Zhang, 2009; Jura et al., 2009a). Therefore the C-terminal lobe of one molecule makes contact with the N-terminal lobe forming a salt bridge (Hubbard, 2006; Zhang et al., 2006). It is this arrangement that permits the tyrosine kinase domains to trans-phosphorylate one another. The phosphorylation occurs on the tyrosine residues on the C-terminal

domain but unlike most other families of receptor tyrosine kinases there is no phosphorylation in the activation loop (Stamos et al., 2002). Therefore, autophosphorylation represents a pivotal mechanism through which the receptors can transduce signals. Unlike all the other ErbB receptors, the ErbB3-TKD has shown interestingly characteristics. Studies on ErbB3-TKD domain concluded that the ErbB3 receptor is kinase-defective and can function only as an activator of the other members of the family but not as receiver (Sierke et al., 1997; Jura et al., 2009b). However, recently it has been reported by (Shi et al., 2009) and colleagues, that ErbB3 possesses a weak kinase activity, about 1000 fold lower than EGFR-TKD, but still sufficient for trans-autophosphorylation within ErbB dimer complexes.

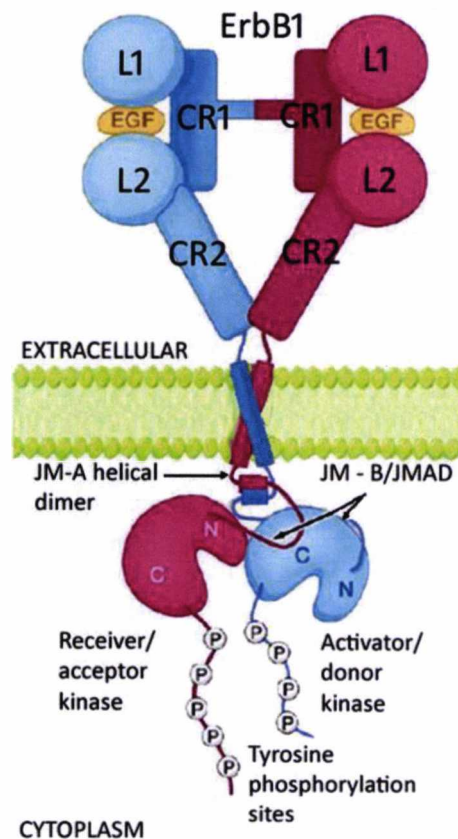


Figure 1.9 Model of interaction between receptor domains. The image shows the interaction between the extracellular domain of two ErbB1 molecules in the active conformation, the transmembrane domains that interact through their dimerisation motif, the JM-A segments that form an antiparallel dimer and the TK domains. (Image adapted from Hubbard, 2006).

1.7. ErbB NETWORK

So far I have been described the ligand- binding, receptor dimerisation processes and the activation of the kinase domain. All these represent the initial steps involved in the transduction of the signal. As receptors are able to initiate multiple signalling cascades, it is natural to wonder what can determine signal diversification and the specificity of the cellular response. To this end it is important to consider the selective action carried out by the ligand: each growth factor is able to activate some ErbB receptors rather than others as well as induce different homo and heterodimer combinations (Gullick, 2001). This may provoke different conformations of the receptor within the dimeric complex that results in the use of distinct phosphorylation sites which initiate specific intracellular signal cascades depending on the ligand in question (Beerli and Hynes, 1996; Sweeney and Carraway, 2000; Hynes et al., 2001). Indeed, the phosphotyrosines (pTyr) associated with the tail of each ErbB receptors, represent the second determinant, after the ligands, for signal specificity. Through pTyr, each ErbB receptor recruits several signal transducers. These intracellular proteins contain SH2 homology domains or PTB domains which associate with the pTyr on the receptor activating various pathways. Many second messengers also contain the SH3 domain, through which they promote the recruitment of specific cytoplasmatic proteins, for example the Sos protein and their translocation to the cellular membrane (Schlessinger and Lemmon, 2003). Some contain intrinsic enzymatic activity, for example Src kinase, protein tyrosine phosphatase (PTP) or phospholipase C (PLCy), or can act like adaptors such as Shc, Grb2, Gab1, that posses binding sites for the recruitment of many others effectors and/or transducers (Schlessinger, 2000; Olayioye et al., 2000; Jorissen et al., 2003; Bazley and Gullick, 2005; Schlessinger and Lemmon, 2006; Normanno et al., 2006). Thus, even if receptors can share some pathways, specificity and potency of downstream signalling depends on different sets of signalling proteins that each receptor can recruit on its docking sites and directly activate. For instance ErbB3 and one of the ErbB4 isoforms can directly and efficiently activate the PI3K pathway using the p85 subunit (Elenius et al., 1999), on the other hand ErbB1 and ErbB2 cannot, as these receptors don't have the site through which they can bind PI3K (Fedi et al.,

1994); however ErbB1 and ErbB2 can still activate PI3K through adaptors (e.g. Gab1, p120^{cb1}), or through the Ras-MAPK pathway (Fig. 1.10) (Soltoff, 1995; Prenzel et. al. 2001; Citri and Yarden, 2006).

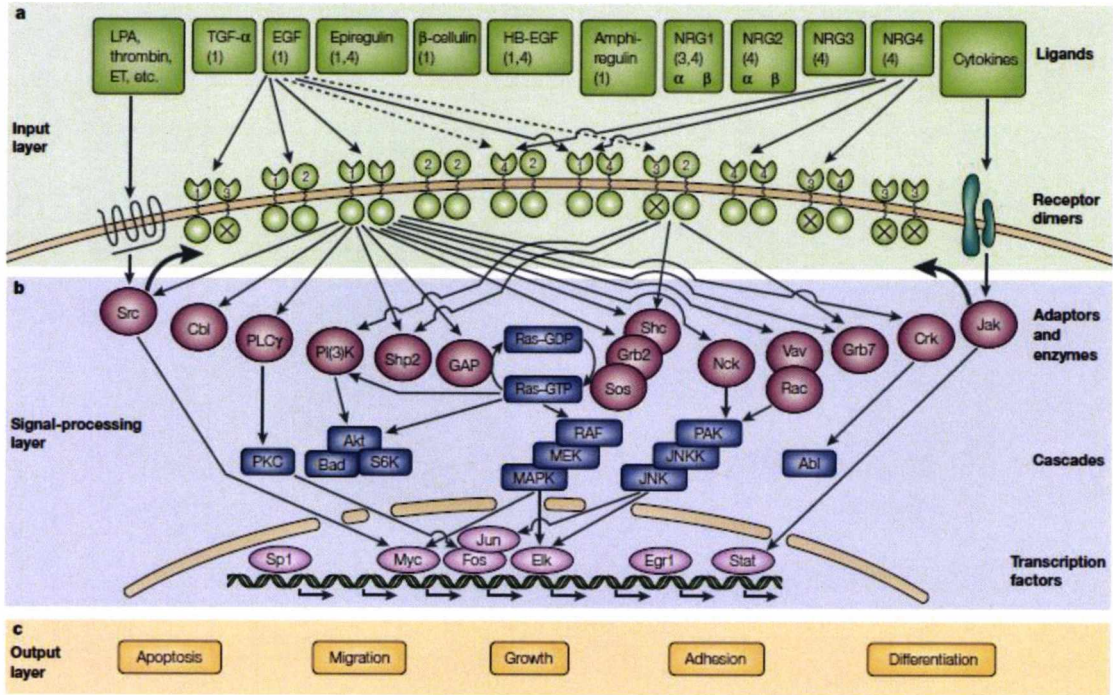


Figure 1.10 ErbB network. (a), (b) and (c) show three different steps for the transmission of the signal: the first step corresponds to the input layer (a) where a ligand binds the specific receptor which, once activated, forms hetero- or homo-dimers with another member of the ErbB family. (b) The second step corresponds to the signal-processing layer: activated receptors can recruit NRTKs proteins and initiate many signalling pathways that transmit the message to the nucleus. (c) The last step, the output layer, shows several cell responses. The specificity of the output depends on the ligand and the receptor that have initiated a specific pathway. (Image from Yarden and Sliwkowski, 2001).

1.8. SIGNALLING CROSSTALK AND RECEPTOR TRANSACTIVATION

Ligand-binding is not the only mechanism through which ErbB receptors can be activated. ErbB receptors can be phosphorylated by heterologous receptors or other molecules through a mechanism known as transactivation. The most characterised mechanism of the ErbB transactivation step involves activation of G-protein coupled receptors (GPCRs) by agonists such as lysophosphatidic acid (LPA), carbachol and

thrombin (Daub et al., 1997). GPCRs can trans-activate ErbB receptors mainly through two mechanisms. In the first mechanism, known as triple-membrane-passing signalling (TMPS), the activation of GPCRs by an agonist, stimulates intracellular metalloproteinases (MMPs) such as a disintegrin and metalloproteinase (ADAM), which promote the cleavage of transmembrane ErbB ligands precursors including HB-EGF, TGF α , betacellulin and epiregulin; thereby the released ligand can bind and activate the ErbB receptor (Wetzker and Bohmer, 2003; Luttrell and Luttrell, 2004). In the second mechanism GPCRs trans-activates ErbB family through c-Src kinases, either indirectly, via PyK2, or directly through the formation of a β -arrestin/Src complex (Carpenter, 1999; Wetzker and Bohmer, 2003; Luttrell and Luttrell, 2004). Activated Src kinases can either stimulate ErbB receptors indirectly by activating MMPs or through a direct phosphorylation of Tyr845 on the EGFR/ErbB1 receptor (Biscardi et al., 1999). Steroid hormones, such as estrogen receptor (ER), are also implicated in trans-activation of the ErbB1-Erk signalling pathway in breast cancer. Indeed ER induces ErbB1 phosphorylation via the GPCR, GPR30. GPR30 activates Src kinases through the G β _v subunit; thus Src kinases can activate the MMPs which can release HB-EGF (Filardo et al., 2000; Filardo, 2002). Another class of proteins able to trans-activate ErbB receptors is the cytokine receptor superfamily. For instance, it has been demonstrated that in prostate carcinoma, interleukin-6 can induce the phosphorylation of ErbB2 and ErbB3, increasing catalytic activity of ErbB2 (Qiu et al., 1998) and in breast cancer promote MAP kinase activity co-operating with ErbB1 (Hynes et al., 2001). Two different groups, Yamauchi et al., and Huang et al., have also demonstrated that the growth hormone (GH) induces tyrosine phosphorylation of ErbB1 (Yamauchi et al., 1997; Yamauchi et al. 1998; Huang et al., 2003) and that autocrine secretion of prolactin (PRL) stimulates tyrosine phosphorylation of ErbB2 in human breast cancer (Yamauchi et al., 2000). It has also been shown that cross-talk between the cytokine receptor superfamily and the ErbB family occurs via Janus tyrosine kinase 2 (Jak2) which phosphorylates specific tyrosines on ErbB1 and ErbB2 creating docking sites for Grb2 and initiates the Ras-MAP signalling cascade which may result in uncontrolled cell proliferation.

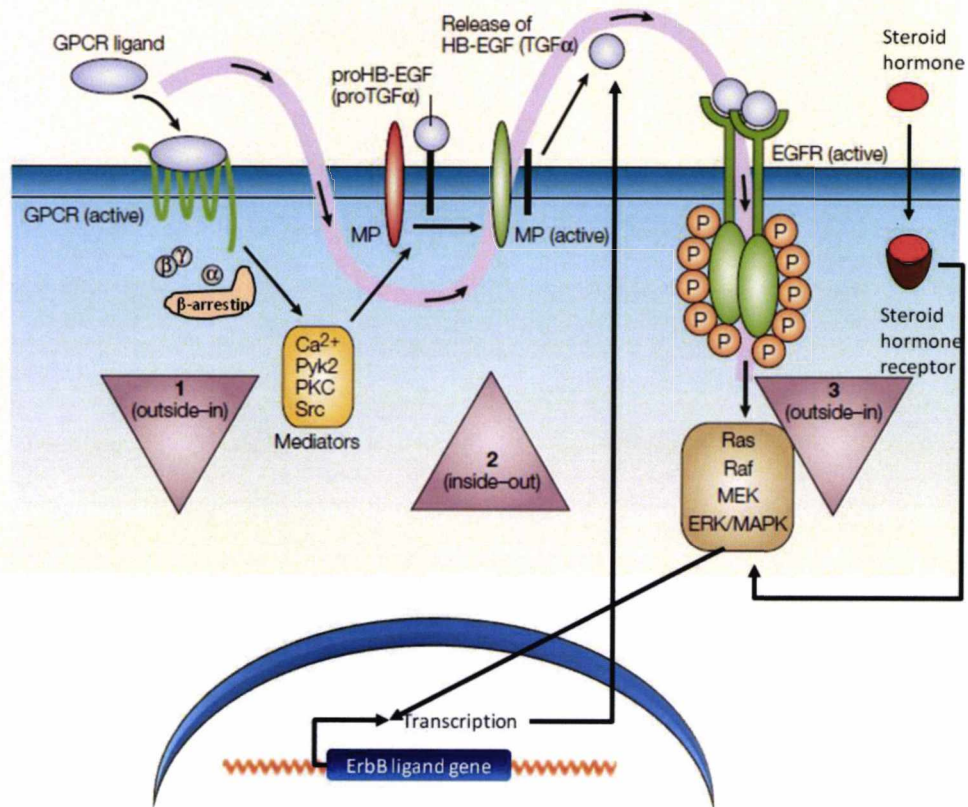


Figure 1.11 Crosstalk between the ErbB family and other systems. G-protein coupled receptor (GPCR) ligands acting through the GPCR complex (containing β , γ and α subunit, and β -arrestin) can stimulate ErbB signalling through mediators or directly by activating metalloproteinases (MMPs) which cleave and release from the membrane ErbB ligands which can bind ErbBs. The activated receptors can subsequently stimulate different signalling cascades. Also steroid hormones can induce ErbB receptor phosphorylation stimulating transcription of genes encoding for ErbB ligands and activating MMPs through a GPR30 dependent mechanism. (Image adapted from (Burgess et al., 2003; Wetzker and Bohmer, 2003).

1.9. ErbB INTRACELLULAR TRAFFICKING AND ENDOCYTOSIS

So far we have explained how ligands and receptors together can induce downstream signalling pathways, and how this complex network is able to discriminate among different signalling cascades. Another feature of this network can be found in its ability to either enhance (positive feedback) or attenuate (negative feedback) the amplitude

and duration of the signals. In general, while the amplitude depends upon the number of ligand and receptor molecules available, the duration depends on mechanisms and molecules engaged in the termination of the signal. A key role in the regulation of ErbB signalling resides in the receptors endocytic trafficking. In general 80-90% of the receptors are present on the plasma membrane available for ligand binding due to a slow internalisation rate compared with the rapid recycling rate (Fry et al., 2009; Sorkin and Goh, 2008). However following the ligand binding this turnover changes dramatically (Burke et al., 2001).

ErbB1, in contrast with the other members of the ErbB receptor family, is the only receptor where the ligand stimulation induces internalisation. Under physiological conditions, receptor internalisation is mediated by mechanisms called clathrin-mediated endocytosis. Clathrin-coated pits give rise to endocytic vesicles which are released from the membrane into the cytoplasmic compartment; here they form early endosomes from where receptors can be recycled back to the plasma membrane or entered into the degradation pathway. In this case the early endosomes form multivesicular bodies and receptors are targeted to lysosomes (Fig. 1.12) (Carpenter, 2000; Wiley and Burke, 2001; Wiley, 2003). Whether the receptor activated by the ligand will enter either the recycling pathway or the degradation pathway depends on the stability of the interaction between the ligand and the receptor. For example, the interaction between EGF and ErbB1 is stable and it is not affected by the acidic environment present in the endosomes, resulting in the lysosomal degradation of both. In contrast, the interaction between TGF α and the receptor is pH sensitive, therefore at the endosomal pH, the ligand dissociates from the receptor which is recycled to the cell membrane (Wiley, 2003; Roepstorff et al., 2008).

In contrast to ErbB1, ErbB2, ErbB3 and ErbB4 have a slow constitutive internalisation rate, are more efficiently recycled to the cell surface (Baulida et al., 1996) and their down-regulation is not induced by ligand binding. Interestingly, they can transfer their properties to ErbB1 forming heterodimeric complexes which can intensify the signal and increase its duration (Sorkin and Goh, 2008). The molecular mechanisms behind receptor down-regulation are still not clearly understood. It has been proposed that

the carboxyl-terminal domain of ErbB2 either lacks recruiting sites for those molecular signals which induce receptor internalisation, or contains signals which retain the receptor on the cell membrane (Sorkin and Goh, 2008). This theory is sustained by a study that showed that ErbB2 endocytosis and degradation increases considerably upon proteolytic cleavage of its carboxyl-terminal domain induced by geldanamycin (Lerdrup et al., 2007). While ErbB1 down-regulation is ligand dependent and it is mediated by Cbl which determines receptor ubiquitination at the endosomal compartment (Sweeney and Carraway, 2004), ErbB3 and ErbB4 down-regulation is ligand-independent and it is mediated by Nrdp1 (neuregulin receptor degradation protein) and Itch proteins respectively, that also induce receptors ubiquitination (Roepstorff et al., 2008).

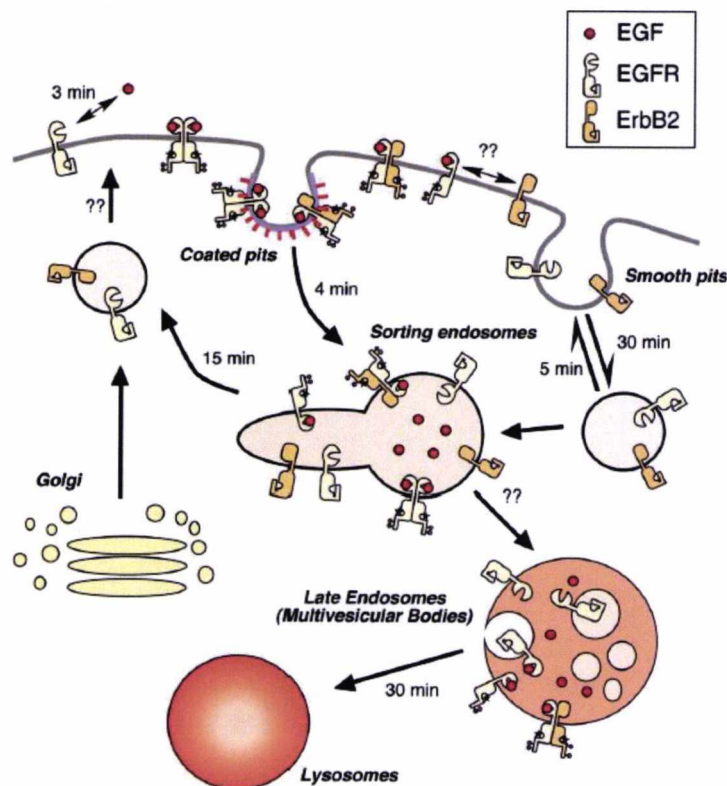


Figure 1.12 ErbB receptor trafficking. Ligand binding induces receptor internalisation. From the early endosomes receptor can be recycled back to the membrane or targeted to the lysosomal compartment and degraded. (Image from Wiley, 2003).

1.10. ErbB FAMILY OF RECEPTORS AND LIGANDS IN NORMAL DEVELOPMENT

The important role of the ErbB receptors and ligands play in mammalian development has been demonstrated with *in vivo* experiments in knockout mice. Mice deficient for ErbB1 or ErbB2, ErbB3, ErbB4 or NRG were either embryonic or postnatal lethal, showing that ErbB receptors are fundamental during embryo development (Iwamoto et al., 2003; Iwamoto and Mekada, 2006). In particular those ErbB1 null mice that survived up to 20 days after birth showed (Threadgill et al., 1995; Miettinen et al., 1995; Sibilias et al., 1998) severe abnormalities in different organs, such as skin, lung, gastrointestinal tract and also in the brain leading to neurodegeneration (Miettinen et al., 1995; Threadgill et al., 1995; Sibilias et al., 1998). Null mutation in genes that encode for ErbB2 ErbB4 and NRG provided genetic evidences that ErbB signalling is essential for the development and function of the heart and the cranial neural crest. Indeed it has been shown that mutant mice died during embryogenesis due to severe abnormalities in the formation of myocardial trabeculation and neuronal structures (Gassmann et al., 1995; Leu et al., 2003; Negro et al., 2004). In the case of mice ErbB3 deficient, the embryos survived slightly longer. Absence of ErbB3 affected the formation of cardiac valves caused anomalies in the development of the neural crest due to defects in the Schwann cells and subsequent motoneuron degeneration (Erickson et al., 1997; Tidcombe et al., 2003). Other groups also demonstrated in null mice that HB-EGF and/or ErbB1 are essential during valvulogenesis and that adult mice lacking of either HB-EGF and/or ErbB1 had severe heart dysfunctions and lung immaturity (Iwamoto et al., 2003; Jackson et al., 2003). Mouse models with null mutations of single ErbB1 ligands or a combination of these displayed multiple abnormalities in several tissues. For instance mice lacking of EGF, TGF- α and/or AR showed defects in the hair follicle, eyelid closure and bone formation, but they were all viable (Schneider and Wolf, 2009).

The specific role of the ErbB proteins in adults has been also analysed and supported by studies with genetically modified mice. The expression of ErbB2, ErbB4 and HB-EGF

is essential for the normal heart function in adults, indeed their absence caused heart failure in mutant mice (Iwamoto et al., 2003; Iwamoto and Mekada, 2006).

Expression of different sets of receptors is also required in adult organisms for the development of the mammary gland. While ErbB1, ErbB2 and ErbB3 signalling are essential for ductal morphogenesis and branching outgrowth in the pubescent gland (Sebastian et al., 1998), ErbB3 and ErbB4 receptors together with ErbB1 are required for lobulo-alveolar development and maturation in later stages during pregnancy and lactation (Tidcombe et al., 2003). As for the ErbB receptors, the specific role of the ErbB ligands in mammary development has been determined with knockout mice. In particular, specific loss of AR resulted in impaired ductal outgrowth during puberty but did not affect lobulo-alveolar maturation, in contrast triple null EGF, AR and TGF- α mice showed poorly differentiated and organised alveoli supporting the hypothesis that expression of EGF and TGF- α are crucial during pregnancy and lactation (Plaut, 1993; Luetkeke et al., 1999).

1.11. THE ErbB RECEPTORS AND LIGANDS IN HUMAN CANCER

It is more than twenty years ago that it was discovered that EGFR is directly linked to neoplasia: the oncogene v-erbB as a mutant EGFR lacking the ligand binding domain which could induce avian erythroblastosis (Downward et al., 1984). It is now clearly proven that the aberrant activation of ErbB receptors facilitate all those processes that drive excessive cellular growth, angiogenesis, metastasis and inhibition of apoptosis (Baselga, 2002; Roskoski, 2004). The three main mechanisms that contribute to the aberrant activation of ErbB proteins include gene amplification, mutation and autocrine stimulation by growth factor molecules. The first mechanism results in receptor over expression, the second event results in constitutive activation of the kinase domain of the receptor and the third generates an excess of ligands (Salomon et al., 1995); all these mechanisms leading at the end to uncontrolled cell growth.

To better understand the involvement of this family of proteins in cancer development, in this section we will provide a brief overview of receptor expression

and co-expression, then ligand expression and co-expression, in many different cancer types.

Over expression of ErbB1 has been observed in 40% of glioblastomas, in head and neck cancer (Wong et al., 1992; Irish and Bernstein, 1993), in kidney, ovarian, bladder, pancreatic prostate and non small cell lung cancer (NSCLC) (Zwick et al., 2001; Shigematsu and Gazdar, 2006). Furthermore, mutations in the extra and intracellular domain have been described in gliomas, breast, ovarian and NSCLC (Nishikawa et al., 1994; Pedersen et al., 2001; Prenzel et al., 2001).

A crucial event in malignant transformation is determined by ErbB2. This gene was isolated and identified as an oncogene in rat neuroblastoma cells where a point mutation in the transmembrane region produces a permanently activated kinase (Zwick et al., 2001; Penuel et al., 2002; Mosesson and Yarden, 2004). Subsequently gene amplification resulting in ErbB2 over expression was found in 25%-30% of patients with breast cancer (Slamon et al., 1987; Slamon et al., 1989). ErbB2 transforming ability and evidence that ErbB2 over expression is sufficient to promote mammary tumorigenesis were confirmed in several studies using transgenic mouse models (Guy et al., 1996; Muller et al., 1988). In addition, while mutations in the TK domain of ErbB2 have been found in lung, gastric, colorectal and breast cancer, (Shigematsu et al., 2005; Lee et al., 2006; Shigematsu and Gazdar, 2006; Wang et al., 2006), these are rare and gene amplification remains the main mechanism by which ErbB2 induces malignant transformation.

The ErbB3 receptor is abundantly expressed in numerous carcinomas such as brain, prostate, colon, pancreas, stomach, ovary and many others (Lyne et al., 1997; Sithanandam and Anderson, 2008). Perhaps because it is kinase defective, ErbB3 expression in cancer is often linked to over expression of another ErbB receptor suggesting its use as a heterodimeric partner. In support of this it has been shown that ErbB3 is an indispensable partner for ErbB2 to promote cell proliferation (Holbro et al., 2003). The formation of ErbB2/ErbB3 dimers is also stimulated by NRG and results in activation of PI3K pathway (Friess et al., 1995; Sithanandam and Anderson, 2008).

In contrast with the other member of the ErbB family, ErbB4 expression in breast cancer was found to be associated with a better outcome and better differentiated histological phenotype (Kew et al., 2000; Srinivasan et al., 2000). Srinivasan et al studied ErbB4 expression in several solid tumours and they demonstrated that ErbB4 was under expressed in all these tumours (Srinivasan et al., 1998). A recent study has reported a somatic mutation in ErbB4 which results in less ability of the receptor to activate specific pathways and it has been suggested that this might favour cell proliferation and survival (Tvorogov et al., 2009). As the most recently discovered member of the family and due to its alternative isoforms, studies on ErbB4 are controversial and what its role is in cancer is still unclear.

Even more interesting has been the discovery that the receptor oncogenicity is considerably enhanced when they are co-expressed (Holbro et al., 2003; Yarden and Sliwkowski, 2001). *In vivo* experiments with transgenic mice have shown that different combinations of ErbB receptors promote tumour growth and also that the level of tumourigenicity depends on the specific type of ErbB receptors expressed. As shown in Figure 1.13 the expression of different sets of receptors determines a faster tumour growth therefore more aggressive phenotype (Alaoui-Jamali et al., 2003).

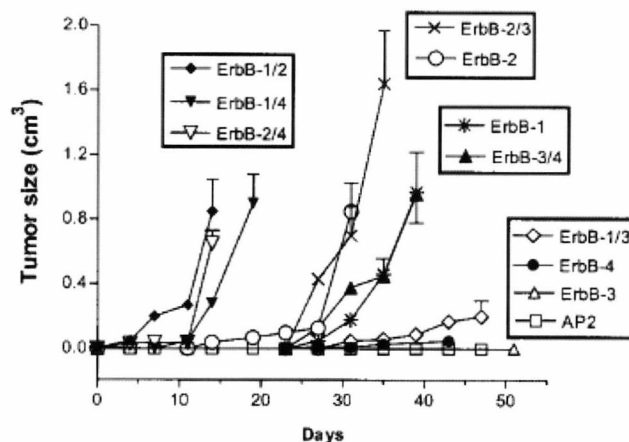


Figure 1.13 Effect on tumour growth of ErbB receptors alone and in combination. (Image from Alaoui-Jamali et al., 2003).

Like ErbB receptors, ErbB ligands also possess different abilities to induce malignant transformation as demonstrated by several studies in transgenic mice (Normanno et al., 2001; Normanno et al., 2006). Expression of EGF-like growth factors has been showed in many human carcinomas. The ability of TGF- α to induce tumour growth has been studied with transgenic mouse models. These studies have shown that over expression of TGF- α facilitates cell proliferation and development of neoplasia (Humphreys et al., 2000). TGF- α also is the growth factor with the greatest transforming power, indeed its expression occurs in the majority of human cancers and it is associated with less differentiated phenotype (Salomon et al., 1995; Normanno et al., 2001) . In contrast, over expression of AR was correlated to more differentiated phenotype (Saeki et al., 1992). Its expression was found mainly in colon, ovarian and breast cancer (Qi et al., 1994; D'Antonio et al., 2002). The involvement of HB-EGF expression in breast carcinoma has been demonstrated by a study that showed that HB-EGF was over expressed in 71.8% of breast cancers and its expression was inversely related to tumour aggressivity, concluding that HB-EGF is probably associated with early phases of the breast cancer (Ito et al., 2001). Expression of NRG1 gene was found mainly in breast and ovarian carcinoma (Normanno et al., 1995; Huang 2004; Gullick, 2009;).

As for the receptors, co-expression of ligands, , has also been found in many tumours. Co-expression of TGF- α , AR and/or NRG was shown by Normanno et al in colon, breast, ovarian, lung and gastric cancers (Normanno et al., 2001) . Also co-expression of NRG1, 2, 3 and 4 were shown to occur in many breast cancers (Dunn et al., 2004). In summary therefore, it is now becoming well established that the ErbB family plays a key role in cancer development and for this reason they are also an attractive target for the development of targeted treatments.

1.12. CANCER TREATMENTS: ErbB TARGETED THERAPIES

In the last few years a large part of oncologic, biomolecular and pharmacologic research has been focused on the development of new anti-neoplastic agents (Fig. 1.14). The ErbB proteins represent an excellent molecular target to generate new

drugs which have the advantage of resulting in greater efficacy and reduced toxic effects for the patient compared to traditional chemotherapy. Based on the knowledge gained during the last twenty years on the ErbB family, many ErbB-targeted therapeutic treatments have been introduced into clinical practise (Salomon and Gullick, 2001; Mendelsohn and Baselga, 2003; Mosesson and Yarden, 2004). The major intervention strategies, extensively studied and already approved for patient treatment, are monoclonal antibodies (mAbs) and small molecule tyrosine kinase inhibitors (TKIs). Both these strategies, through different mechanisms, lead to the inhibition of the PIK3-AKT and MAPK signalling pathways, reducing cell proliferation and survival.

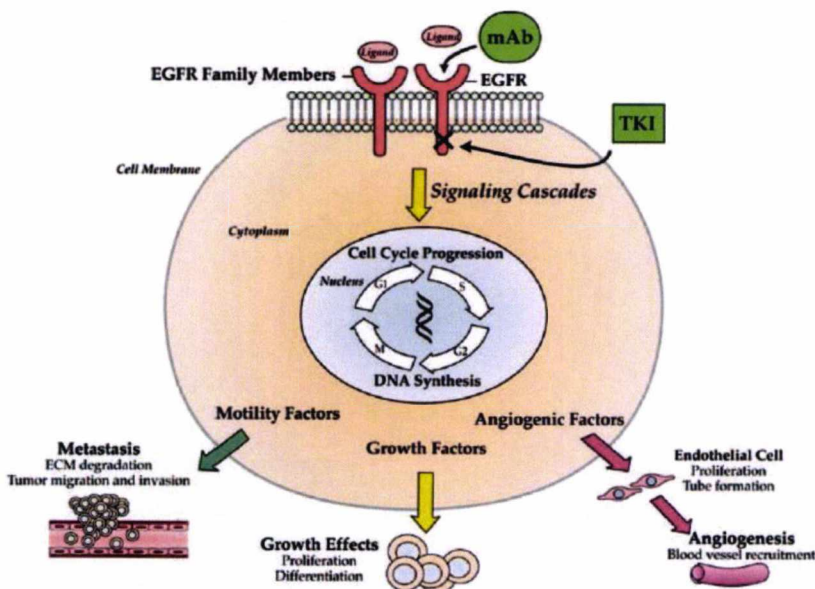


Figure 1.14 Schematic illustration of receptor targeted therapies. (Image from Harari et al 2004).

The mAbs block receptor activation and signal transduction by targeting the extracellular domain of the receptor, in some cases inhibiting ligand-binding; thereby receptors are down-regulated through internalisation and degradation pathways. The two main anti-ErbB mAbs are Cetuximab, which targets ErbB1, and Trastuzumab (Herceptin), which targets ErbB2.

Cetuximab was approved by the Food and Drug Administration (FDA) in February 2004 for the treatment of advanced colorectal cancer and later for the treatment of head and neck cancer. It is a chimeric (human-murine) monoclonal antibody that binds ErbB1 with higher affinity than ErbB1 ligands. As the complex cetuximab:receptor is very stable, it will be internalised and directed to the lysosomal compartment (Kim et al., 2001; Li et al., 2005; Harding and Burtness, 2005). It has been shown that Cetuximab can also arrest the cell cycle, having antiproliferative effects, and can induce apoptosis (Baselga, 2001; de Bono and Rowinsky, 2002; Mendelsohn and Baselga, 2003; Rowinsky, 2004). Another monoclonal antibody direct against ErbB1 is panitumumab, which has been also approved for the treatment of metastatic colorectal cancer (Wu et al., 2008).

Herceptin (Trastuzumab) was approved by the FDA in 1998 for the treatment of breast cancers with over expression of ErbB2. Trastuzumab binds to the extracellular domain of ErbB2, but the mechanism by which inhibits tumour cells proliferation is not well understood. Later in this chapter (see section 1.14), Trastuzumab will be examined in more details. Another monoclonal antibody against ErbB2 is Pertuzumab (Genentech). This monoclonal antibody, approved by the FDA in June 2012 for the treatment of breast cancer in combination with Herceptin, (<http://www.fda.gov/Drugs/Information-OnDrugs/ApprovedDrugs/ucm307592.htm>) inhibits dimerisation of ErbB2 (Franklin et al., 2004). This monoclonal antibody is currently being tested also for the treatment of ovarian cancer and NSCLC.

The second strategy for targeting excessive signalling by RTKs in the treatment of cancer is based on the use of small molecules tyrosine kinase inhibitors. These compounds compete with the ATP and bind to the catalytic pocket of the tyrosine kinase domain blocking receptor phosphorylation and activation of downstream signalling pathways. The TKIs can be divided in reversible and irreversible. TKI are irreversible if they bind covalently the TKD of the targeted receptor. Examples of reversible TKIs are erlotinib (Tarceva, OSI Pharmaceutical/Genethec/Roche) and gefitinib (Iressa, Astra Zeneca) which target ErbB1. These have been approved for the treatment of NSCLC. It has been shown that erlotinib and gefinitib have

antiproliferative activity and induce apoptosis (Arora and Scholar, 2005). There are also tyrosine kinase inhibitors (called dual or pan-ErbB) able to target multiple receptors simultaneously. Two of these dual TKIs are Canertinib (irreversible TKI) and Lapatinib (reversible TKI) which inhibit both ErbB1 and ErbB2 receptors simultaneously (Arkin and Moasser, 2008; Roy and Perez, 2009). Preclinical studies have suggested that multi-target agents can be more effective than therapies directed against a single marker.

1.13. BREAST CANCER

1.13.1. OVERVIEW OF BREAST DEVELOPMENT AND ANATOMY

According to the “Oxford Text Book of Pathology”, the breast is a complex sweat gland that, in both male and female, develops as buds from the same embryological tissue (the milk lines also called ventral epidermal ridges). The primary buds give rise to secondary buds that elongate to form the lactiferous ducts and their branches. Development and maturation of the breast occurs in females at puberty in response to ovarian oestrogen synthesis. During this phase the breast becomes more prominent and the oestrogens determine a rapid growth and branching of the ducts. The terminal ducts end in globular structures called buds which continue to form other lobules of alveolar buds. The complete morphologic maturation and functional activity of the breast is reached during the pregnancy. In this phase a series of hormones, including oestrogen, progesterone and prolactin, cause a further growth of the ducts, lobules and alveolar buds. Furthermore the alveoli under the influence of these hormones and others such as growth factor, insulin and cortisol, become secretory cells. After lactation the secretory function is lost and the secretory cells of the alveoli are removed by apoptosis. A progressive involution of the breast occurs during the menopause. In this third phase the lobular components collapse and the breast epithelial structures regress with loss of stromal cells and collagen fibres.

The adult human female breast (Fig. 1.15) has conical shape with the base situated on the pectoralis major and minor muscles on the chest wall, between the second and the sixth rib. The apex, at the opposite, side is represented by the nipple-areola complex. From the nipple to the base, the mammary gland appears as a ramifying structure. The major milk ducts, between 5 and 10, emerge from the nipple and branch out into lobes; the lobes subdivide into lobules that are formed by clusters of acini also called terminal ductules. These represent the secretory unit. The terminal duct and its lobules form the terminal duct lobular unit (TDLU) that is the functional unit of the breast. All these structure are surrounded by stromal tissue and adipose tissue that have the function to support and protect them. Around the breast an extensive lymphatic system that leads to the axillary lymph nodes. This system plays an important role in breast cancer where tumour cells can invade lymphatic vessels and use the lymphatic system to spread through the body.

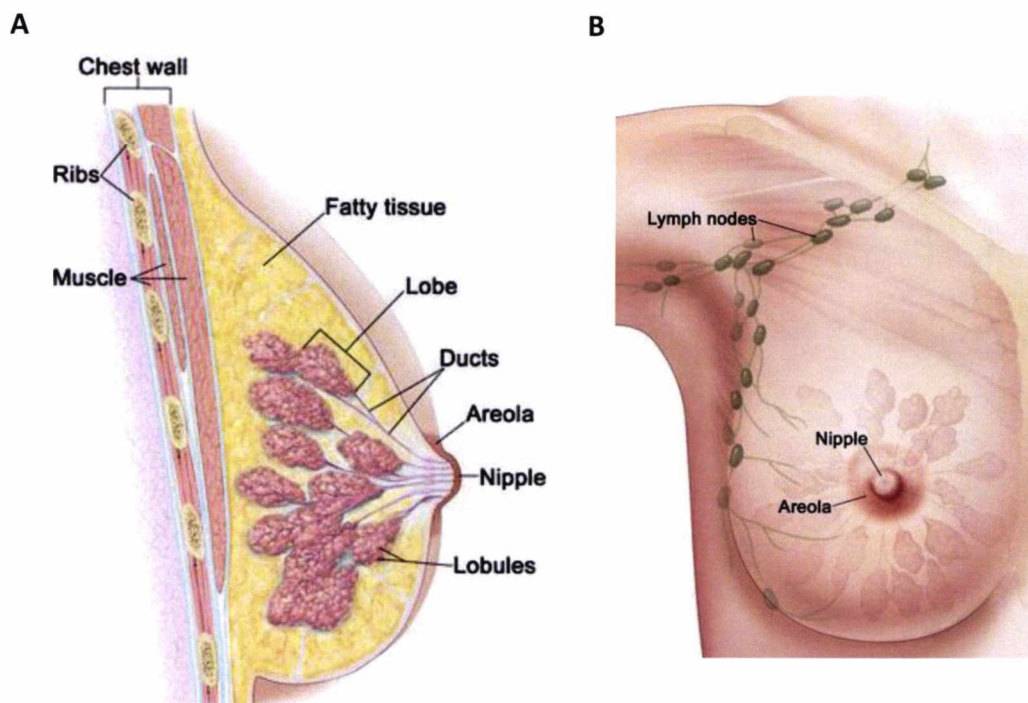


Figure 1.15 Schematic structure of an adult female breast (A); representation of the lymphatic system around the breast (B). (Images adapted from <http://www.healthlinkbc.ca/kb//content/nci/ncicdr0000062970.html>).

1.13.2. COMMON HISTOLOGICAL TYPES OF BREAST CANCER

Breast cancer represents the most common type of cancer in women in the western world. This disease shows a considerable heterogeneity resulting in a large variety of morphological types among which the most frequent are the ductal and lobular neoplasia. A normal duct consists of two cellular layers, an inner layer of epithelial cells lined by a layer of myoepithelial cells. These two layers are enclosed by a basement membrane (Fig. 1.16 A). According to "The Cancer Handbook", breast cancers can be divided into two main categories: non-invasive (in situ) (Fig. 1.16B) and invasive (Fig.1.16 C). In the non-invasive type the tumour is confined within the ducts and/or lobules, in the invasive types the malignant cells spread outside the basement membrane and invade the surrounding tissues.

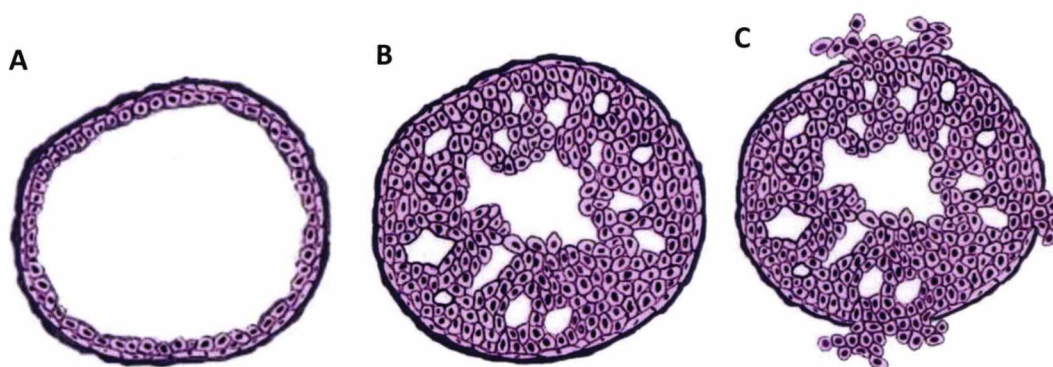


Figure 1.16 Schematic representation of a normal breast duct and two types of breast cancer. (A) Breast duct histology: from outside is shown the basement membrane, myoepithelial cells and mammary ductal cells; (B) Non-invasive ductal carcinoma; (C) invasive ductal carcinoma. (Images adapted from <http://www.breastcancer.org/symptoms/diagnosis/invasive.jsp>).

The main types of non-invasive breast cancer include the ductal carcinoma in situ (DCIS) and lobular carcinoma in situ (LCIS). DCIS is characterised by the presence of tumour cells that have proliferated and filled the lumen of the duct so that the ducts appear more distended and enlarged. Furthermore in this type of tumour, necrotic foci that calcify are often present in the duct. If DCIS is not treated it can progress and become invasive cancer (Brown and Pinder, 2012).

In LCIS the epithelial tumour cells proliferate within the lobules and they appear uniform, pleomorphism is usually absent. One of the main characteristics of LCIS is multifocality. This means that the probability of finding it diffused throughout the breast is high. Furthermore women with LCIS have higher risk of developing invasive disease during their lifetime.

The invasive breast carcinomas can be divided into two main types: invasive ductal carcinoma (IDC) and invasive lobular carcinoma (ILC).

IDC represents the most common type of invasive breast cancer (70-80%). The malignant cells break through the basement membrane and invade the fibrous and adipose tissue around the ducts. Here the tumour cells stimulate the stromal cells to proliferate. This confers to the tumour mass a firm consistency that can be detected by breast palpation. The cytological features of the tumour cells can vary among IDCs; cells can show different histological grade from low (well differentiated) to high (poorly differentiated). These features play an important role in the prognosis of breast cancer as less the cell are differentiated the more aggressive the tumour is and therefore worse is the prognosis(Rakha et al., 2010).

ILC, although having lower incidence than IDC, is the second most common type of breast cancer representing approximately 10% of invasive breast cancers. It is multifocal and has typical pattern of infiltration where the invading cells form strands which are often called "Indian files". The cells are usually regular, small and rounded and with little pleomorphism (Alison et al., 2002).

1.13.3. COMMON MOLECULAR TYPES OF BREAST CANCER

To date, much progress has been made in understanding the disparate genetic causes which underlie breast cancer: for example mutation of the breast cancer type 1 and type 2 genes (BCRA1 and BCRA2), PTEN, TP53 and many other have been associated with development of breast cancer. Since each molecular type has different responsiveness to treatment, the biomolecular characterisation of various groups and subgroups of breast tumour is of importance. To date, the existence of four molecular

subtypes have been identified. These molecular are luminal, basal-like, ErbB2 over expressing and “normal breast-like”(Perou et al., 2000; Weigelt et al., 2005). While luminal tumours are ER positive, the basal-like, ErbB2 and “normal breast-like” tumours are all ER negative. The luminal subtype is comprised of two subcategories, luminal A and luminal B. Luminal A has higher incidence (67% of the tumours) and is characterised by high expression of ER, low proliferation rate and low histological grade. Luminal B has lower levels of ER, higher histological grade and higher proliferation rate. Furthermore, a portion of luminal B tumours also show expression of ErbB2. Therefore luminal B breast cancers have poorer prognosis than luminal A tumours (Zepeda-Castilla et al., 2008; Alizart et al., 2012).

The basal-like subtype is so called because the malignant cells express a pattern of genes typical of the breast basal and myoepithelial cells (Perou et al., 2000). This molecular subtype is also known as “triple negative” as it does not express ER, PR or ErbB2. Characteristically this subtype of breast cancer is positive for ErbB1 expression. The basal-like tumour type has also been associated with those breast tumours that carry the BCRA1 mutation and/or the p53 mutation. This tumour tends to have high histological grade, high proliferation rate and poor prognosis (Zepeda-Castilla et al., 2008; Weigelt et al. 2010).

The normal-like carcinoma shows expression of genes typical of the basal epithelial cells and adipose cells (Perou et al., 2000). This subtype of tumour also shows expression of ErbB1 and low histological grade (Weigelt et al., 2010).

The ErbB2 subtype is characterised by negative or low ER expression, high histological grade and aggressive biological behaviour. Moreover a high proportion of the ErbB2 subtype has been shown to have p53 mutation (Zepeda-Castilla et al., 2008). In the following section I will discuss this subtype of tumour in greater detail.

Molecular subtypes	ER/PR/ErbB2	Additional features
Luminal	A	ER+ and/or PR+ ErbB2-
	B	ER+ and or PR+ ErbB2- (+)
Basal-like	ER- PR- ErbB2-	High histological grade (2 or 3) BCRA1 mutation p53 mutation ErbB1+
Normal-like	ER-/ + PR unknown ErbB2-	High histological grade (3) p53 mutation ErbB1+
ErbB2	ER- PR- ErbB2+	High histological grade (2 or 3) p53 mutation

Table 1.1 Common molecular subtypes of breast cancer. (Table adapted from Weigelt et al., 2010 ; Alizart et al., 2012).

1.13.4. ErbB2 IN BREAST CANCER

The importance of ErbB2 in breast cancer was first established when it was discovered that ErbB2 gene amplification (Slamon et al., 1987) and over expression (Venter et al., 1987) in approximately 25-30% of breast and ovarian cancers and that this alteration conferred to the tumour worse biological behaviour. To date, this finding has been supported by a substantial number of studies and a large body of evidence. It has been shown that breast cancers with ErbB2 amplification can have up to 25 to 100 copies of the ErbB2 gene copies per cell. This means that expression of ErbB2 is increased 40-100 fold resulting in roughly 2 million receptors per cell expressed on the cell surface (Kallioniemi et al., 1992; Moasser, 2007). It is important to emphasize that ErbB2 amplification is an early event in human breast tumorigenesis (Nik-Zainal et al., 2012) unlike for example gastric cancer and ErbB2 status is maintained during cancer progression to invasive and metastatic disease (Perou et al., 2000; Weigelt et al., 2005). Therefore ErbB2 gene amplification does not represent a stage of breast cancer

but it defines a molecular subtype that has a unique signature of gene expression or mutation. It is maintained during all the stages of the breast tumour including metastases and it is with higher probability of progression and poor prognosis (Perou et al., 2000; Weigelt et al., 2005). Other features that characterise ErbB2 amplified breast cancers include low levels of ER and PR, resistance to hormonal chemotherapies, increased sensitivity to some cytotoxic agents, propensity to metastasise to the brain and high histological and nuclear grade (Gutierrez and Schiff, 2011).

To date several mechanisms through which ErbB2 induces cell transformation and tumorigenesis have been identified. Here I will review the most likely and common mechanisms and pathways underlying ErbB2 transforming function.

One of the mechanisms that contributes to ErbB2 tumorigenesis is associated with its ability of potentiate and prolong downstream signalling. Over expression of ErbB2 increases the probability of formation of hetero-dimers with other members of the ErbB family. This interferes with other receptor activity and regulation. As mentioned earlier (see section 1.9) hetero-dimers containing ErbB2 and ErbB1 have a slower internalisation rate and they escape endocytotic degradation in favour of the recycling pathway (Baulida et al., 1996). This enhances the expression of ErbB1 on the cell membrane and its activity resulting in extended duration of signalling pathways. For instance prolonged activation of MAPK and c-jun signalling, initiated by ErbB1 or ErbB3, was observed in cells over expressing ErbB2 (Karunagaran et al., 1996).

As mentioned earlier, ErbB3 is the ErbB2 preferred partner. ErbB2, through the formation of hetero-dimers with ErbB3, activates one of the most oncogenic signalling pathways studied, which is the PI3K/Akt module. Akt is the nodal point of many signalling pathways that control different cellular functions such as proliferation, survival, angiogenesis and glucose metabolism (<http://www.cellsignal.com/pathways/aktsignaling.jsp?gclid=CLOa26Dp0rECFRlKtAodoVQAOQ>). Activation of this pathway, through members of the epidermal growth factor family, occurs specifically through ErbB3 phosphorylation. ErbB3 has seven consensus binding sites for the p85 α subunit

of PIK3, whereas ErbB2 lacks docking sites for the p85 α (Prigent and Gullick, 1994; Soltoff and Cantley, 1996). For instance, ErbB2 through activation of Atk deregulates the cell cycle in favour of cell survival and proliferation by inhibiting p27^{kip1} (Moasser, 2007), p27^{kip1} a kinase inhibitor that arrests cell cycle progression. Furthermore when ErbB2 dimerises with ErbB1, ErbB2 can down-regulate p27^{kip1} by mediating its degradation through the activation of the MAPK pathway (Lenferink et al., 1998). Low levels of p27^{kip1} have been found in breast cancers over-expressing ErbB2 (Moasser, 2007).

There are also other mechanisms, although apparently less central, through which ErbB2 increases its transforming function. It has been suggested that ErbB2 can act in the nucleus as a transcription factor. So far the inducible prostaglandin synthetase cyclooxygenase-2 (COX-2), the chemokine receptor CXCR4 and the E-Twenty-Six (ETS) have been reported as ErbB2 genomic targets (Moasser, 2007).

1.13.5. THE GOOD AND THE BAD ABOUT HERCEPTIN

The first successful targeted therapy directed to the extracellular domain of ErbB2 developed was Herceptin. This is a recombinant humanised monoclonal antibody also called Trastuzumab and produced by Genentech. Herceptin was first approved by the FDA in 1998 for the treatment of metastatic breast cancers (MBC) and later in 2006 for the treatment of lymph node positive breast cancer in the adjuvant setting and early breast cancer and more recently in 2008 also for the treatment of lymph node negative breast cancer in the adjuvant setting (<http://www.fda.gov/NewsEvents/Newsroom/PressAnnouncements/2006/ucm108788.htm>, (Ross et al., 2009). In 2010 the use of Herceptin has been expanded also to the treatment of ErbB2-overexpressing gastric or gastroesophageal (GE) junction adenocarcinoma (<http://www.cancer.gov/cancertopics/druginfo/fda-trastuzumab>).

Antitumor effects.

Herceptin antitumour effects apparently induce several molecular mechanisms. Here I will illustrate the most important (Fig. 1.17)

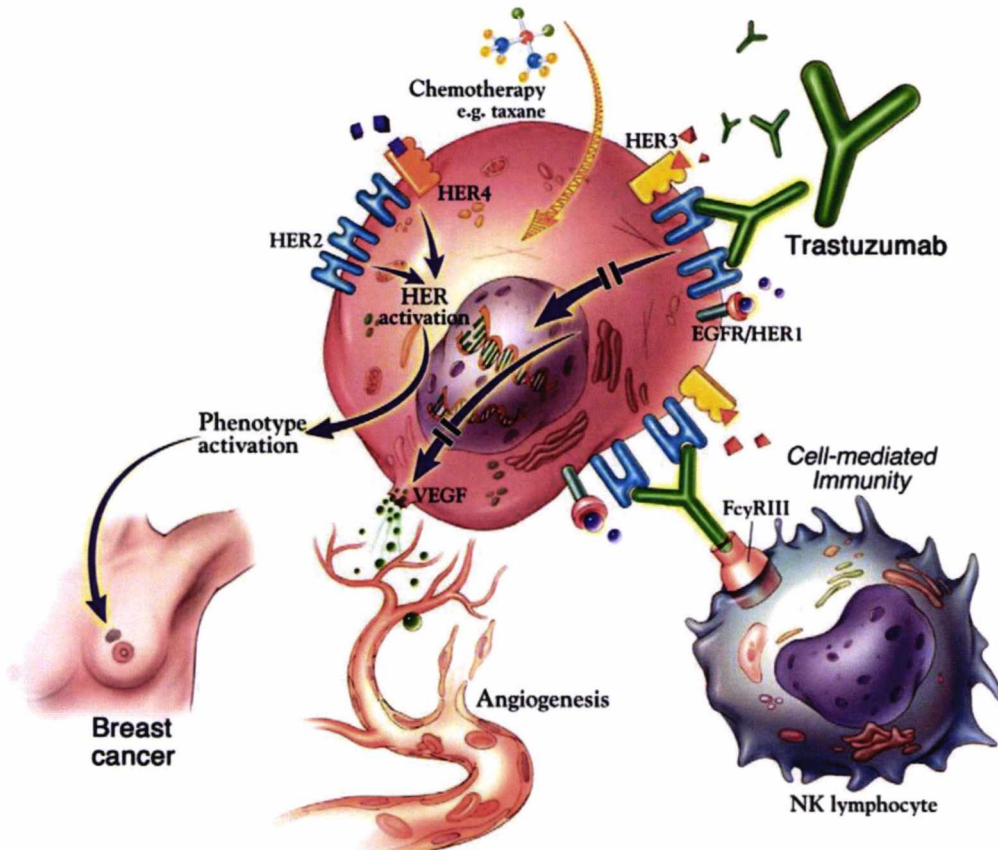


Figure 1.17 Summary of different Herceptin antitumor mechanisms. (Image taken from Nahta and Esteva, 2006).

First, Herceptin reduces cell proliferation by diminishing the activity of intracellular signalling pathways such as PI3K/Akt and MAPK. The reduced activation of these pathways results in increased levels of $p27^{kip1}$ and reduced expression of cyclin dependent kinase (cdk) proteins that sequester $p27^{kip1}$, therefore $p27^{kip1}$ is free to translocate to the nucleus and promote cell cycle arrest and apoptosis. The mechanisms by which Herceptin decreases the ErbB2-mediated signalling are not completely understood (Nahta and Esteva, 2006). It was suggested that Herceptin induced down-regulation of ErbB2 through internalisation and degradation (Harari and Yarden, 2000). However as different studies have reported contradictory evidence this hypothesis has not been confirmed. Another mechanism by which Herceptin inhibits the PI3K pathway has been proposed. Herceptin dissociates the interaction between ErbB2 and Src, therefore Src becomes inactivated. As a consequence, the phosphatase

and tensin homolog (PTEN) is dephosphorylated (activated) and can inhibit the PI3K/Akt pathway. As a result, cell proliferation is inhibited

Another antitumor effect of Herceptin is due to its cytotoxic action mediated by an immune response. Specifically Herceptin induces antibody-dependent cellular cytotoxicity (ADCC). The Fc fragment of the IgG1 of the antibody binds the Fcγ receptor expressed on natural killer cells, which become activated and can mediate cell lysis (Moasser, 2007).

Increased level of angiogenesis and vascular endothelial growth factor (VEGF) was reported in breast cancers with over expression of ErbB2. It has been shown that Herceptin inhibits angiogenesis causing a reduction of microvessel density *in vivo* and endothelial cell migration *in vitro*, a decreased expression of pro-angiogenic factors and increased expression of anti-angiogenic factors (Nahta and Esteva, 2006).

Herceptin also contributes towards reducing the transforming potential of ErbB2 by inhibiting the proteolytic cleavage of the receptor by metalloproteinases. This has two effects: it stops the extracellular fragment of the ErbB2 from being released into the blood stream and stops the formation of p95 ErbB2 membrane-bound fragment. This truncated form of ErbB2 has been associated with more invasive morphology and poorer prognosis. Furthermore the truncated fragment p95 anchored to the membrane has been shown to have increased kinase activity (Fizman and Jasnis, 2011).

Herceptin Resistance

Drug resistance is one of the major reasons why patients fail to respond to treatments. There are two types of resistance. The first is intrinsic resistance and it refers to a pre-existent resistance for which do not respond to drug therapies; the second is acquired resistance and it is induced by the drug, in this case patients become refractory only after they were treated with the drug (Ellis and Hicklin, 2009). Here I will describe the acquired resistance to Herceptin treatment. Despite the fact that patients treated with Herceptin gain an initial benefit from the drug, particularly when it is used in combination with or following chemotherapies, they develop resistance within one

year. To date several mechanisms of resistance have been proposed, here I will to discuss the most relevant (Fig. 1.18)

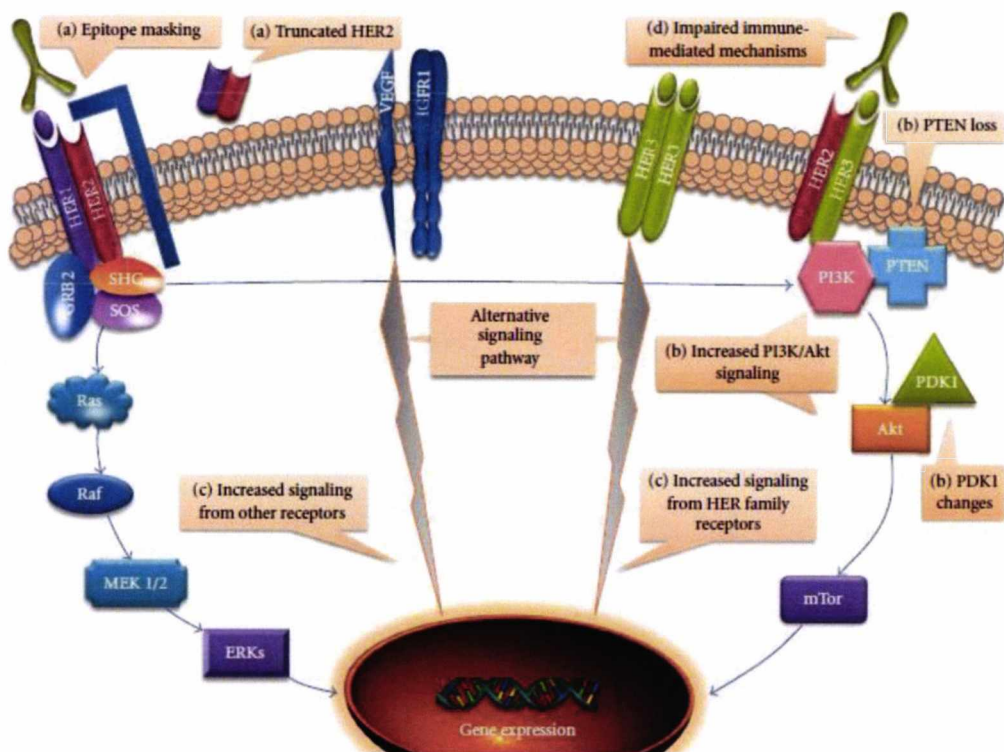


Figure 1.18 Representation of different resistance mechanisms of Herceptin. (Image taken from Fizman and Jasnis, 2011).

It has been shown that over expression of Mucin-4 cell surface associated (MUC4), an heavily glycosylated protein, potentially determines Herceptin resistance and cancer progression. MUC4 binds ErbB2 preventing Herceptin from binding the receptor, furthermore MUC4 binding increases phosphorylation of ErbB2 enhancing its transforming ability. MUC4 also forms a barrier around the cells impeding cancer cells from being recognised by the immune system, therefore it contributes to tumour progression, metastasis and suppression of apoptosis (Fizman and Jasnis).

It has been suggested that presence of truncated forms of ErbB2 may contribute to Herceptin resistance. As mentioned above the p95 ErbB2 form lacks the extracellular portion and therefore Herceptin is not able to bind the receptor. Furthermore, the presence of the extracellular domain (ECD) fragment in the serum may compete away

the drug from binding the ErbB2 full-length protein on the cell. However the studies on the role of the ECD are conflicting and not conclusive.

Other mechanisms of resistance to Herceptin are linked to increased activation of compensatory signalling pathways initiated from other members of the ErbB family and/or from other receptor types. For instance MAPK and PI3K signalling can be activated by ErbB1/ErbB1 or ErbB1/ErbB2 dimers; also formation of ErbB1/ErbB2 and ErbB3/ErbB2 dimers is not hindered by Herceptin. In addition there is evidence that over expression of Insulin-Like Growth Factor-I Receptor (IGF-IR) in ErbB2 positive breast cancers, mediates Herceptin resistance by stimulating MAPK and PI3K/Atk pathways and causes down regulation of p27^{kip1}. The over expression of the VEGF stimulates angiogenesis reducing Herceptin effect (Knuefermann et al., 2003).

Up-regulation or constitutive activation of downstream signalling pathways caused by mutations have been associated with Herceptin resistance. For instance, loss or decreased expression of PTEN and PI3K mutations has been found in breast cancers to confer resistance to Herceptin.

1.13.5. ROLE OF ErbB FAMILY IN BREAST CANCER

The individual members of the ErbB family have been examined to greatly different degrees in breast tumours. The level of expression of ErbB1 has been studied in many cases. ErbB1 positivity was reported in 48% of 5232 breast cancers in 40 different studies (Klijn et al., 1992). Despite ErbB1 over expression being correlated with decreased survival, its value as a prognostic factor still remains to be clarified (Chan et al., 2006). Interestingly, almost all the studies consistently have reported an inverse relationship between ErbB1 and ER showing that ErbB1 expression is twice as high in ER or PR negative tumours, than in ER or PR positive tumours (Klijn et al., 1992). Furthermore, it has been determined that the expression of ErbB1 contributes to resistance to hormonal therapy (Tsutsui et al., 2002; Chan et al., 2006).

Over expression of ErbB3 has been reported in 20-30% of invasive and in one third of breast carcinomas in situ (Lemoine et al., 1992; Badra et al., 2006). To date, different

studies have reported conflicting results with regard to the prognostic role of ErbB3 in breast cancer (Travis et al., 1996). In some of these studies its over expression was associated with worse prognosis, reduced survival and shorter relapse free survival (Hamburger, 2008). In other studies its over expression was associated with lower histological grade, longer disease free survival and longer overall survival (Koutras et al., 2010).

In contrast to the other members of the ErbB receptor family, over expression of ErbB4 in breast cancer was associated with favourable prognosis, low histological grade and reduced cell proliferation rates and ER positivity (Sundvall et al., 2008). On the other hand under expression of ErbB4 was correlated with higher histological grade and poorer clinical outcome (Kew et al., 2000).

In order to better understand the role and the clinical significance of the ErbB proteins in breast cancer it is of fundamental importance to consider the ErbB family as a whole. As mentioned earlier receptors and ligands act synergistically, therefore it is likely that their co-expression plays a more significant role in breast tumour than their individual expression. For instance, through several studies it has emerged that ErbB2 over expression alone is insufficient to drive cellular transformation and dimerisation and ErbB3 is required to induce breast tumour cell proliferation (Holbro et al., 2003). The ErbB2 and ErbB3 complex has been shown to be the most mitogenic dimer of ErbB receptors (Citri et al., 2003) and it seems that ErbB3 has a crucial role in breast cancer tumorigenesis and in the development of resistance to hormone therapies and tyrosine kinase inhibitors (Hamburger, 2008; Koutras et al., 2010). ErbB2-ErbB3 dimers are activated by NRGs that initiate potent mitogenic pathways. Therefore the role of NRGs in breast cancer is also of interest. It has been shown that up-regulation of NRG induces malignant transformation of breast epithelial cells transformation in an autocrine manner (Li et al., 2004). Furthermore Tsai et al have demonstrated that NRG, can induce breast cancer and that it is associated with invasive behaviour and metastasis. They have shown in vitro that the blockage of HRG decreases ErbB activation which results in the regression of both the tumour and the aggressive behaviour (Tsai et al., 2003). However, the role of NRGs is even more complex.

Different NRG ligands can activate ErbB3 and/or and the ErbB4 receptor (see section 1.3). Depending on the activated receptor, NRGs may mediate opposite cell responses, for instance through activation of ErbB3 they promote cell proliferation and through the activation of ErbB4 they induce apoptosis, cell differentiation and inhibition of angiogenesis (Breuleux, 2007). Indeed, as mentioned above breast tumour that over express ErbB4 were associated with favourable prognosis. Furthermore patients with breast cancers co-expressing ErbB2 and ErbB4 have better outcome than patients with breast cancer with over expression of ErbB2 only (Sundvall et al., 2008). A study published by Wiseman et al demonstrated that co-expression of two or more ErbB receptors, ErbB1-2 and 3 but not ErbB4, is associated with a significant decreased disease specific survival and overall survival compared to individual receptor expression or no expression (Wiseman et al., 2005). Another study, recently published, has determined, by immunohistochemical staining, the expression of the entire ErbB family of receptors and ligands in hundreds cases of breast cancer. From this study it has emerged the existence of a strong association between any member of the family and all other members. Furthermore, consistently with other studies, it has shown that the expression of different receptors and ligands was associated with either favourable or worse clinical outcome (McIntyre et al., 2010). Taken together, these results suggest that a more accurate determination of the expression of the ErbB proteins in breast cancer can have an important implication in determining prognosis and therapeutic treatments.

1.13.6. ERBB TARGETED FOR THERAPIES IN BREAST CANCER

As I have previously overviewed (see section 1.11) different therapeutic strategies directed to the ErbB family members, in this section I will focus on novel therapeutic approaches for the treatment of breast cancer.

One of the newest intervention strategies that seeks to overcome Herceptin resistance and improve patients response in ErbB2 over expressing breast tumours is represented by the use of antibody-drug conjugates (ADCs) such as Trastuzumab-emtansine (T-DM1) which was developed by Genentech. The monoclonal antibody Trastuzumab (Herceptin) was conjugated to a cytotoxic agent named “derivative of maytansine 1”

(DM1). Maytansine, an antibiotic isolated from the Maytenus plant, is a potent inhibitor of cell division acting as a cytotoxic microtubule inhibitor. Maytansine binds to the tubulin and obstructs the polymerisation process preventing the formation of microtubules causing cell death (Barok et al., 2011). T-DM1 binds the ErbB2 protein and it is internalised by endocytosis into the cancer cell; here, following lysosomal degradation, the DM1 is released in the tumour cells to accomplish its cytotoxic effect. The novelty of this drug resides in its capacity of releasing the DM1 only after the T-DM1 has been internalised in the tumour cells. This property represented important progress as the major problem encountered with the ADCs was related to their high toxicity caused by a premature release (before internalisation) of the cytotoxic agent (Hurvitz and Kakkar). Safety and efficacy of T-DM1 is being currently evaluated in several randomised phase III clinical studies. To date, T-DM1 has been demonstrated to have potent antitumor effects in both sensitive and resistant breast tumours and is well tolerated with no cardiotoxic effects reported so far (Hurvitz and Kakkar; Tsang and Finn, 2012).

Alternative therapeutic interventions are based on the use of monoclonal antibodies or TKIs that can inhibit multiple receptors. Pertuzumab is a recombinant humanised monoclonal antibody that binds to the dimerisation domain (domain CR1) of ErbB2. As this is a different binding region from the Herceptin binding site, pertuzumab can be used in combination with Herceptin. By steric hindrance pertuzumab blocks ErbB2 dimerisation with other ErbB family receptors inhibiting signalling pathways from ErbB heterodimers (Nahta and Esteva, 2006; Reid et al., 2007). Herceptin and pertuzumab have a complementary activity as while the first suppresses ErbB2 activity (see section 1.12.5), the second inhibits multiple ErbBs signalling, particularly from ErbB2-ErbB3 heterodimers which provide an escape mechanism from Herceptin. The use of these two antibodies with docetaxel is currently being evaluated in phase III clinical study (CLEOPATRA) in patients with advanced disease (Baselga and Swain, 2009). Recent results from this clinical trial have demonstrated statistically significant and clinically meaningful improvement in progression free survival (PFS) in patients with MBC. Patients treated with Herceptin plus pertuzumab and docetaxel resulted in an

increase of 6.1 months in PFS compared to those patients that received Herceptin plus placebo and docetaxel. Ongoing studies are also evaluating the overall survival between the two treatment arms. Furthermore, no major adverse events and no increase in cardiac toxicity has been reported so far (Baselga et al., 2012).

The intervention strategies based on the use of TKIs include Lapatinib and Neratinib. Lapatinib is a highly selective reversible small molecule inhibitor of both ErbB1 and ErbB2. Despite, Lapatinib having demonstrated promising results in preclinical studies, phase I and II studies have shown a modest efficacy as single-agent in refractory ErbB2 positive breast cancer previously treated with Herceptin (Reid et al., 2007). However Lapatinib has demonstrated more encouraging results when was evaluated in combination with a chemotherapeutic agent (Capecitabine) in an open-label randomised phase III trial (Capri et al., 2009; Sutherland et al., 2010). Neratinib is an irreversible TKI of ErbB1, ErbB2 and ErbB4. It is currently under evaluation in combination with chemotherapy. However, in phase II clinical studies Neratinib has already demonstrated its efficacy as a single agent with an overall response rate of 26% in patients previously treated with Herceptin and of 56% in patients not treated with Herceptin (Baselga, 2010).

A different approach in the treatment of ErbB2 positive breast cancer consists of using an anti-neoplastic antibiotic (e.g Tanespimycin) that inhibits the molecular chaperone hsp90 to prevent proteolytic and stabilises various proteins including ErbB2. The Hps90 inhibitors have shown antitumor effect in patients with ErbB2 MBC and they are currently being evaluated in early –phase clinical trial (Tsang and Finn, 2012).

1.14. PATIENTS SELECTION

The development of more effective therapies directed against specific molecular targets has made the identification of predictive factors clinically relevant allowing clinicians to choose the most appropriate and specific treatments for individual patients. The three most important predictive biomarkers routinely used for molecular profiling of breast cancers are the oestrogen receptor and the progesterone receptor,

which predicts response to hormonal therapy, and ErbB2 receptor which predicts response to Herceptin and Lapatinib.

In the following sections I will discuss the two most commonly used assays in clinical practice to determine ErbB2 status together with other less established ErbB2-testing methods.

1.14.1. IMMUNOHISTOCHEMISTRY AND FLUORESCENCE IN SITU HYBRIDISATION

It has been shown that patients with breast cancers which over express ErbB2 are less responsive to standard chemotherapy such as tamoxifen and more responsive to anthracycline-based chemotherapy (Pegram et al., 1998; Shah and Chen, 2011). Since it has been shown that patients with tumours expressing ErbB2 at levels of 3+ scored by immunohistochemistry (IHC) or with ErbB2 gene amplification determined by fluorescence in situ hybridisation (FISH) (Cobleigh et al., 1999; Slamon et al., 2001; Vogel et al., 2002) respond to Herceptin, the assessment of HER2 status has become crucial to identify those patients who most benefit from this drug. Currently the two techniques internationally recommended by the American Society of Clinical Oncology/College of American Pathologist (ASCO/CAP) panel are IHC and FISH (Wolff et al., 2007). IHC is the diagnostic test mainly used to measure over expression of ErbB2 protein, while FISH is used to measure ErbB2 gene copy number for breast cancer samples which give “equivocal” (2+) results by IHC. In the following two paragraphs I will discuss in more detail these two methods.

IHC assay. The IHC technique was developed about 70 years ago (Coons and Kaplan, 1950) for detecting cellular antigens in tissue sections. Since then IHC has become a very useful tool both in research and in clinical diagnosis. This assay is widely applied by the health service to stratify patients for different treatments on the basis of the molecular nature of this breast cancer. As mentioned above the presence of ER, PR or ErbB2 can predict tumour response to different therapies. The IHC test permits the levels of ErbB2 expression to be determined based on the colour intensity of the staining on the membrane (for more details about the technique see section 3.1.1). This scoring system was standardised, using a series of cell lines, by determining the

1- INTRODUCTION

number of receptors present on the cell's surface first and then by determining the relationship between the number of receptors counted and the stain intensity and distribution: the presence of less than 20,000 receptor on the cell's surface corresponded to a score of 0 (no staining), the presence of 100,000 receptors per cell in more than 10% of the cells displaying partial membrane staining and complete membrane staining corresponded to 1+, the presence of 500,000 receptors per cell in more than 10% of the cells with moderate membrane staining corresponded to 2+ and last the presence of 2,300,000 receptor per cells in more than 10% of the cells showing complete membrane staining corresponded to 3+ (Ross et al., 2009) (Fig. 1.19)

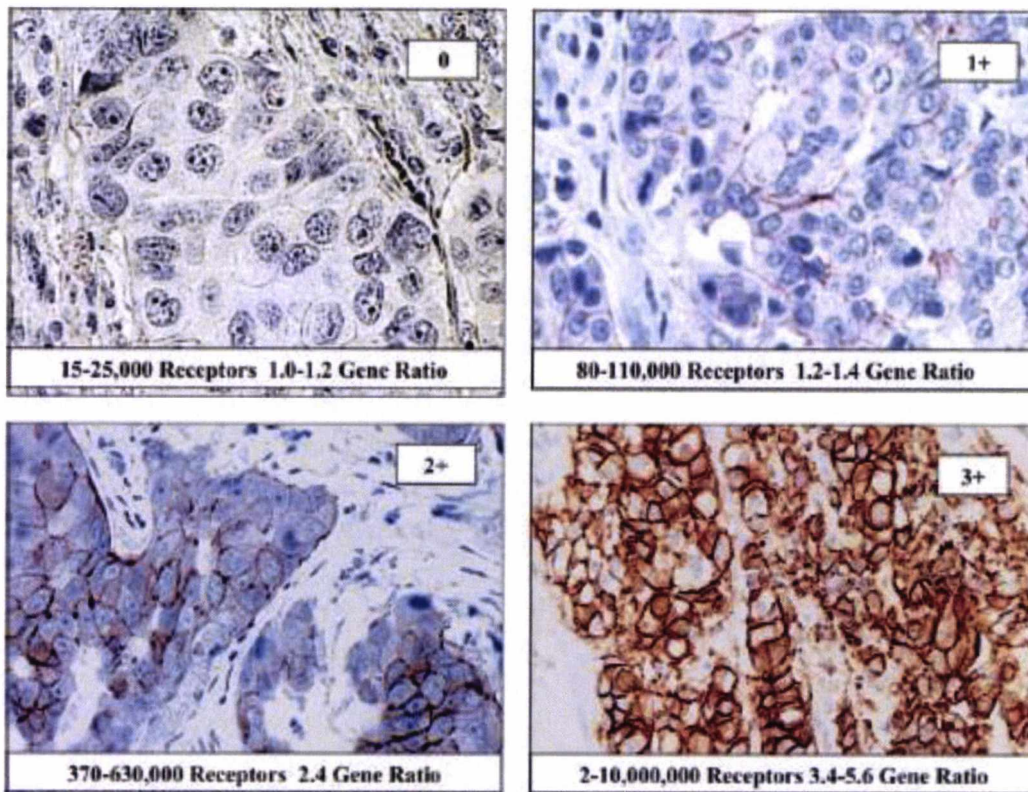


Figure 1.19 Example of the IHC test for ErbB2. (Image taken from Ross et al., 2009).

IHC assay was used in the first phase III trial for the approval of the use of Herceptin for the treatment of metastatic breast cancer (MBC) over expressing ErbB2. The patients were eligible for the study only if the tumour was showing ErbB2 over expression at 2+ or 3+ levels (Slamon et al., 2001).

IHC analysis offers several advantages that can explain the reasons why it has found widespread use: this test is widely available, easy to perform, is relatively inexpensive, stained tissue slides can be easily stored and it employs the use of a simple light microscope. Nonetheless this assay is affected by a series of factors that can influence the test results which can be grouped in three categories: pre-analytic, analytic and post-analytic. The pre-analytic factors include tissue processing and storage; for instance pre-analytic factors are the duration and type of tissue fixation, the embedding material used and the duration of storage of embedded tissues. The analytic factors comprise all those steps and reagents involved in the staining procedure such as type and intensity of antigen retrieval, type of antibody (crucial to this are clonality, specificity and sensitivity of the antibody), antibody concentration used, duration of the antibody incubation time, washing step to remove unbound antibody and reagents used to develop a colour reaction to visualise the antigen-antibody reaction. This reaction is based on an enzyme reaction and therefore it can be affected by temperature, pH and substrate concentration. Post-analytic factors are associated with the use of a validated cut-off point to determine positive scoring vs. negative scoring. They are also related to subjectivity of the scoring system which results in inter-observer variability. Also results can only be scored semi quantitatively dividing the population into quartiles (Meric et al., 2002; Gown, 2008; Shah and Chen, 2011). These factors limit the reproducibility of the test and they make it non-linear. Therefore ErbB2 measurements by IHC are imprecise and lacking in detail.

FISH assay. The FISH assay assesses amplification of the ErbB2 gene by using fluorescently-labelled probes. FISH is recognised as the “gold standard” test as it is a highly sensitive technique, more accurate and reproducible than IHC. Furthermore it allows the simultaneous evaluation of tissue morphology and gene amplification, in this way the gene amplification can be assessed only in invasive cancer cells. The advantage of the FISH test is also that can be scored quantitatively rather than qualitatively. However it is expensive, technically demanding and time-consuming. In addition, gene amplification is only indirectly related to the quantity of HER2 expressed on the cell surface (Allison, 2010).

In order to address all the issues of ErbB2 test accuracy related to tissue processing and assay methodology the ASCO/CAP panel has published specific guidelines seeking to standardise these procedure on a global scale (Bilous et al., 2003). Among all the commercially available antibodies to ErbB2, kits and reagent to perform IHC or FISH, only those that have been approved by the FDA can be legitimately employed for ErbB2 testing. There are two approved IHC kits, the HercepTest™ (DAKO) and PATHWAY™ (Ventana) and three approved FISH assays, PathVysion (Abbott), INFORM (Ventana) and PharmDx™ (DAKO). The ASCO/CAP panel has also realised algorithms for interpreting the ErbB2 status by IHC (Fig. 1.20) and FISH (Fig. 1.21). Based on the ASCO/CAP recommendations the ErbB2 test is considered:

- negative if IHC results are 0 or 1+ (no staining or weak incomplete membrane staining) and if FISH shows ErbB2/CEP17 ratio less than 1.8 or an average of ErbB2 gene copies per nucleus less than 4;
- equivocal if IHC staining has been scored as 2+ (complete circumferential membrane staining that are weak or not uniform in at least 10% of the cells) and if FISH ErbB2/CEP17 ratio is between 1.8 and 2.2 or average gene copy number is between 4 and 6;
- positive if the IHC result is 3+ (more than 30% of invasive breast cancer cells shows dark, homogeneous, circumferential membrane staining in a “chicken wire” pattern) or if ErbB2/CEP17 ratio is more than 2.2 or the average of ErbB2 gene copies per nucleus is more than 6.

Note that the FISH assay is generally applied only to confirm ErbB2 positivity in equivocal cases scored as 2+ by IHC.

Despite all the efforts that have been made to improve the accuracy of these tests, the variation obtained still represents a major problem to the extent that ASCO/CAP has found that 20% of ErbB2 assays performed were inaccurate (Wolff et al., 2007; Brunelli et al., 2008; Sauter et al., 2009).

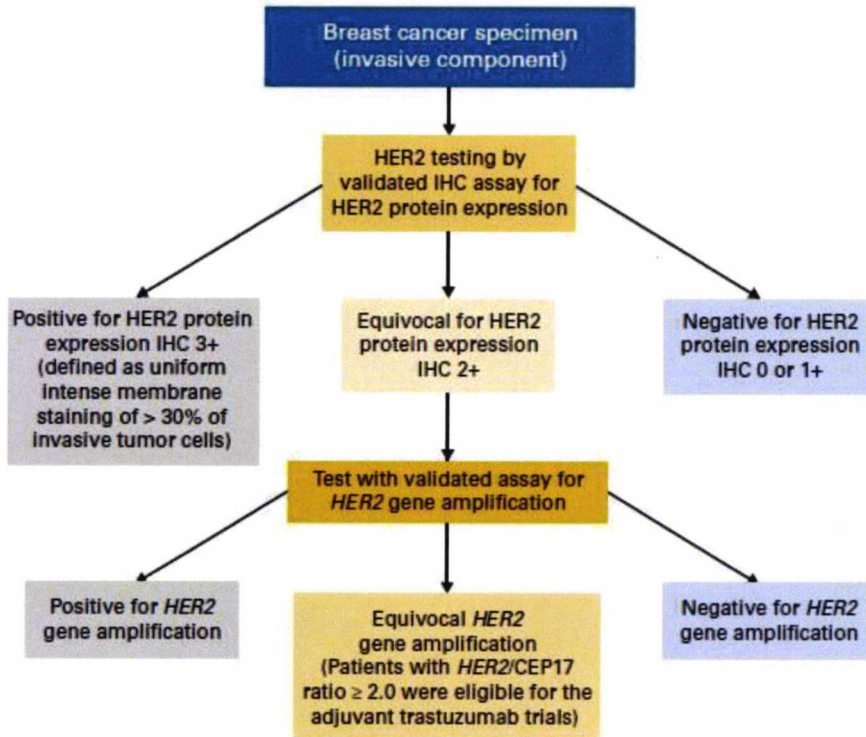


Figure 1.20 ASCO/CAP guideline for the interpretation of ErbB2 IHC test. (Image taken from Wolff et al., 2007).

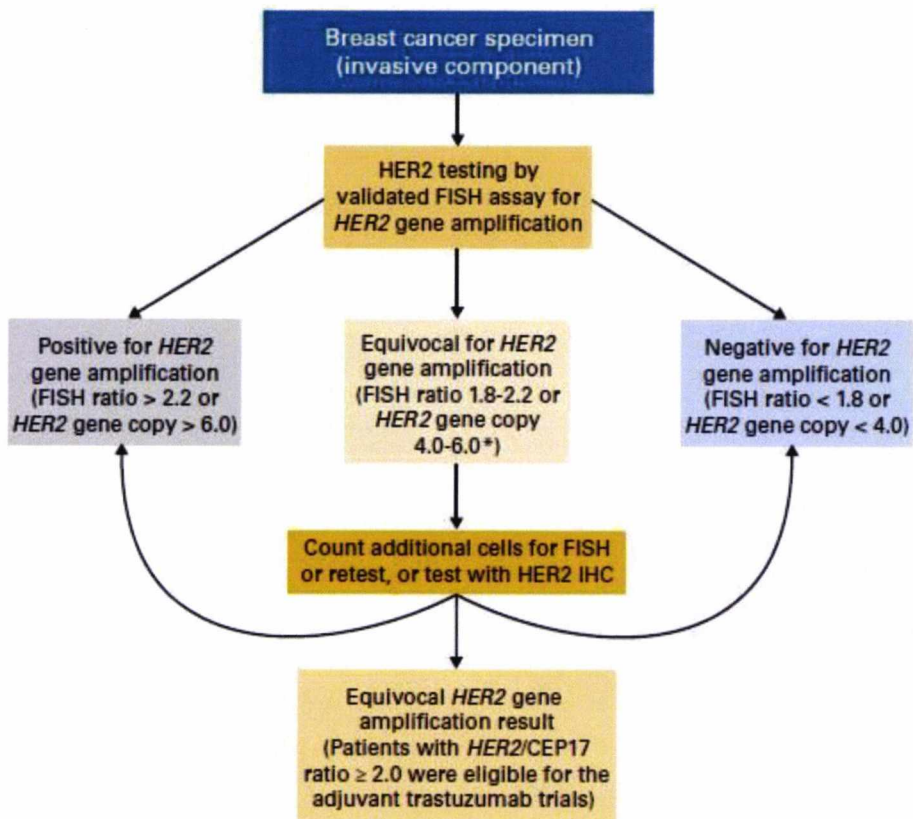


Figure 1.21 ASCO/CAP guidelines for the interpretation of the ErbB2 FISH test. (Image taken from Wolff et al., 2007).

1.14.2. OTHER TECHNOLOGIES FOR ErbB2 TESTING

Beside the IHC and FISH FDA approved assays, there are other assays not yet approved that can measure the amount of ErbB2 at the protein, RNA and DNA levels.

Protein over expression can be measured by using the Enzyme linked immune-sorbent assay (ELISA). In particular this technique has been used to measure the amount of a truncated product of ErbB2 corresponding to the extracellular domain (ECD) which is released into the blood following metalloproteinase cleavage. Elevated levels of ErbB2 ECD product in the serum have been associated with greater response to Herceptin. However high levels of ErbB2 ECD are not present all ErbB2 positive breast cancers and they can be also found in ErbB2-negative breast tumours, therefore the evaluation of ErbB2 ECD levels for clinical purposes has not been recommended (Leyland-Jones and Smith, 2011). The ELISA assay can also be performed on homogenised tissue made straight from tumours biopsies. In theory this would avoid the issues related to fixation, embedding and storage. However the preparation of tissue blocks permits their storage for examination and re-evaluation for research purposes. In addition this technique required the use of a relative large amount of sample that would be lost (Rampaul et al., 2002).

A novel assay called HERmark (Monogram Biosciences) has been recently developed and approved by the FDA. This assay measures total ErbB2 expression and ErbB2 homodimers in FFPE breast cancer tissue. The assay is based on VeraTagTM technology. This assay consists of two different antibodies conjugated to biotin, each directed to a different epitope in the intracellular domain of ErbB2. One of the antibodies is also conjugated to a VeraTag reporter which is released following a chemical reaction. The released VeraTag reporter is then quantified by capillary electrophoresis (Huang et al., 2010; Larson et al., 2010).

Other methods for the assessment of ErbB2 are based on the quantification of RNA levels. This can be achieved by using quantitative real-time polymerase chain reaction (qRT-PCR). Although problems related to the quality of nucleic acid extracted from FFPE tissues and mRNA degradation can be overcome by newer techniques and kits,

the main limitation of qRT-PCR resides in the loss of cellularity, in the mixture of RNA extracts from tumour cells with extracts from normal epithelial cells and inflammatory cells. This causes dilution of the real amount of the RNA being quantified and therefore results in an underestimation of the real mRNA level (Barberis et al., 2008; Jarzab et al., 2008).

As an alternative to FISH there are other assays that can measure gene copy number. These assays include chromogenic in situ hybridisation (CISH) and silver in situ hybridisation (SISH). The first has been approved by the FDA in 2008 and uses an immunoperoxidase reaction to visualise the ErbB2 genes but differently from FISH is mono probe meaning that it does not also probe the centromere 17 as a control for polysomy. A newer CISH kit that can probe ErbB2 gene and CEP 17 copy number has been developed recently. The SISH technique, not yet approved, is based on a horseradish peroxidase reaction that reduces the silver acetate used in the kit and produces a black signal. It can be used to stain CEP17 and the ratio can be calculated by using newly developed software (Ventana Image Analysis System). Detection of DNA by PCR can also be performed, however these techniques suffer the same problems present in the mRNA assay: loss of tissue morphology, large sample size and contamination with DNA from ductal carcinoma in situ or other normal tissue cells (Shah and Chen, 2011) (Moelans et al., 2011).

1.15. QUANTUM DOT NANOTECHNOLOGY

Quantum dots (Qdots) are a new class of fluorochromes. They are formed by a core of a semiconductor material such as CdSe and covered with a shell of ZnS. The core and the shell are encased by a polymer coating substance which make the conjugation with a wide range of biomolecules easier (Fig.1.21).

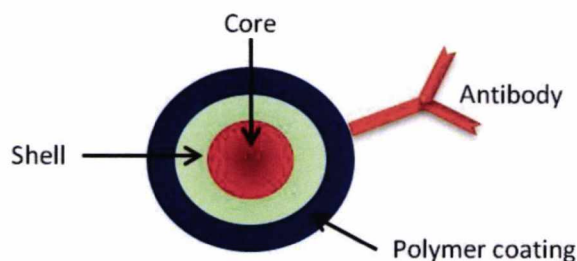


Figure 1.22 Schematic structure of Qdot. Image adapted from www.invitrogen.com

Qdots have shown to have superior properties compared to the organic fluorophores, for instance they are brighter than the Alexa Fluor dyes and more resistant to photobleaching (Monton et al., 2009). Furthermore, the Qdots wavelength emissions vary according to their size and therefore they can be tuned by changing the size of the particles (Zhou and Ghosh, 2007). Qdots are also characterised by a broad excitation spectra and narrow emission spectral profiles that minimises the spectra overlapping area; for all these features Qdots have become the best choice for *in vitro* studies based on immunofluorescence and bio-imaging detection. In addition, Qdots antibodies-conjugate seems to be tailored for simultaneous detection and quantification of multiple biomolecules (True and Gao, 2007). In order to demonstrate the applicability of Qdots in immunofluorescence, they were first used in mouse fibroblast to detect actin filaments. Afterwards they have been successfully employed for many disparate purposes in different biologic techniques both *in vivo* and *in vitro* (Pinaud et al., 2006; Xing and Rao, 2008). For instance Qdots have been used in flow cytometry, in situ hybridisation and immunofluorescence on FFPE tissues (Tholouli et al., 2008). The use of Qdots has found a large application in molecular pathology and represents an innovative and promising technique for determining the diagnosis and prognosis of human cancers. For instance they can be used to detect and quantify biomarkers in primary tumours such as ovarian, breast, prostate and pancreatic cancers by using different techniques prevalently immunolabelling of fixed cell and/or FFPE tissues. Qdots have also been used to detect metastasis of hepatocellular carcinoma both *in vivo* and *in vitro* and to track sentinel lymph nodes (Smith et al., 2006) Peng and Li, 2010). This innovative tool, along with the progress made in cancer research in identifying prognostic and predictive biomarkers, could represent the way

forward to improve cancer diagnosis and in assisting patients screening for personalised medicine.

1.16. AIMS

This project aims to

- I. Develop a system that generates a more linear and scalable measurement of ErbB2 receptor in formalin fixed paraffin embedded (FFPE) breast cancer tissues using quantum dot nanotechnology.

In order to develop the system we

- ◆ Confirmed the specificity of the primary antibodies to detect ErbB receptors.
 - ◆ Tested the performance of the antibodies to detect by immunohistochemistry different levels of ErbB receptors in a series of unselected FFPE breast cancer tissues.
 - ◆ Evaluated the optical properties of Qdots and explored their performance in both cells and FFPE tissues.
 - ◆ Determined a standard protocol for the Qdot immunofluorescence staining of FFPE tissues
 - ◆ Explored different methods to reduce tissue autofluorescence and improve the signal to noise ratio.
 - ◆ Set up a standard method for image acquisition.
 - ◆ Defined the criteria for the quantification analysis.
- II. Apply the new system to measure ErbB2 levels in a series of breast cancers treated with Herceptin to see if we can identify whether those with the highest expression are those who gain most benefit from the drug.
 - III. Explore the applicability of the new system for the detection and measurement of other ErbB receptor family members.

2 – MATERIAL AND METHODS

2.1. CELL CULTURE

2.1.1 CELL LINES UTILISED IN THIS STUDY

The cell lines used in this study were A431, SKBR3, MDA-MB-453 and MDA-MB-361 obtained from ICRF (Imperial Cancer Research Fund); HEK293-HER3 and NIH3T3-HER4, the first obtained Dr Greg Plowman (California, USA), and the second obtained from Dr Bruce Cohen (Bristol Myers Squib, USA), are stable transfected cell lines; COS7 cells were obtained from laboratory stock.

Cell line	Morphology	Source	Disease
A431	Epithelial	Skin; epidermis	Epidermoid carcinoma
SKBR3	Epithelial	Mammary gland; breast	Adenocarcinoma
MDA-MB453	Epithelial	Mammary gland; breast	Metastatic carcinoma
NIH 3T3	(Mouse embryonic) fibroblast	Embryo/NIH Swiss mice	
HEK 293	Epithelial	Embryonic kidney	
COS7	Fibroblast	kidney, SV40 transformed T antigen	

2.1.2 RECOVERING CELL LINES FROM FROZEN STOCKS

The vial of cells was removed from liquid nitrogen and placed in a 37°C water bath until the cells were thawed. To avoid contamination, the outside of the vial was treated and wiped with 70% Industrial Methylated Spirit (IMS) and transferred in a laminar flow tissue culture hood. The following operations were also carried out in the hood. 1ml of the cell suspension was transferred to a 15 ml falcon tube containing 4ml of pre-warmed medium and then centrifuged at 1000 rpm for 5min. The supernatant was aspirated and the cells were suspended in 5ml of fresh medium. The mix was transferred in a 25 cm² tissue culture flask (Sarstedt Inc., USA) and the cells were incubated at 37°C in an atmosphere of 95% air and 5% CO₂. After 24h cells were examined under a microscope to confirm the presence of attached cells to the flask

surface. To remove residual DMSO, debris and unhealthy cells, the medium was gently removed and replaced with 5ml of fresh medium. If the cells were not confluent, the incubation was continued until cells had reached 70% confluence or more. At this point, the cells were subcultured.

2.1.3 GROWTH AND MAINTENANCE OF CELL LINES

All cell lines used in this study were grown following standard procedures for culturing adherent mammalian cells. Cells were grown and routinely maintained in Dulbecco's modified Eagle's medium (DMEM) supplemented with 10% Fetal Bovine Serum (FBS), L-Glutamine (1%) and penicillin-streptomycin (1%) (all from Invitrogen, UK). Cells were grown in a humidified incubator at 37°C in 95% air and under 5% CO₂ using 25cm² tissue culture flasks until a confluent monolayer was formed. At this point cells were ready to be plated out for experiments. After the medium was removed and discarded, the cells were briefly washed with 1ml of pre-warmed Trypsin-Ethylene diamine tetra acetic acid (Trypsin-EDTA) (0.05% trypsin, 0.53mM sodium EDTA) from Invitrogen, UK, which then was removed and replaced with 0.5ml of new trypsin-EDTA. Flasks were gently rocked, to allow the trypsin-EDTA to completely cover the cell monolayer, and incubated at 37°C in 95% air and 5% CO₂ from 5 to 10mins depending on the cell line. During this time, cell dissociation was checked every 2min under a microscope, when the majority of the cells were detached, 5ml of pre-warmed medium was added to the trypsinised cells. The resuspended cells were aliquoted into flasks or dishes according to the experiments undertaken. In general for routine maintenance of cell lines from 0.3ml up to 0.8ml of cells, depending on the cell line, were diluted in 5ml medium in a 25 cm² tissue culture flask.

2.1.4 CRYOPRESERVATION OF CELL LINES

Cryopreservation of cell lines is important for long storage of the cells and to ensure the availability of cells source for future studies or in case of contamination. Frozen stocks were prepared from 70% confluent flasks, cells were trypsinised as previously

described but using 0.1ml of trypsin-EDTA instead of 0.5ml and then resuspended in 5ml of medium. The mix was transferred into a 15ml sterile falcon tube and centrifuged at 1000rpm for 5mins. After, the medium was discarded and the pellet was resuspended in 1ml freezing medium, 10% dimethyl sulfoxide (Sigma, UK) and 90% of Fetal Calf Serum (FCS) or FBS (both from Invitrogen, UK) and kept in ice. The cells were gently pipetted up and down to ensure even distribution in the medium, then transferred into cryovials (NUNC, USA) and frozen at -20°C. After few hours the frozen vials were transferred to -80°C and left overnight. The following morning, the vials were placed in liquid nitrogen for permanent storage.

2.2 ANTIBODIES USED IN THIS STUDY

2.2.1 PRIMARY ANTIBODIES

The following primary antibodies were used in this study

Antibody	Specificity	Clonality	Origin
F4	ErbB1 intracellular domain	Mouse monoclonal	Gullick et al 1986
21N	ErbB2 intracellular domain	Rabbit polyclonal	Gullick et al 1987
CB11	ErbB2 intracellular domain	Mouse monoclonal	Abcam, UK
RTJ2	ErbB3 intracellular domain	Mouse monoclonal	(Rajkumar et al., 1996)
49.3	ErbB3 intracellular domain	Rabbit polyclonal	Prigent et al 1992
HFR1	ErbB4 intracellular domain	Mouse monoclonal	(Srinivasan et al., 1998)
Anti-glucagon	Pancreatic glucagon	Mouse monoclonal	Sigma, UK

2.2.2 SECONDARY ANTIBODIES

The secondary antibodies used in this study were the following:

Antibody	Applied to	Origin
AlexaFluor 546 goat anti-mouse IgG conjugate	IF* (cells)	Invitrogen, UK
Qdots 525 goat anti-mouse IgG conjugate	IF (cells and FFPE tissues)	Invitrogen, UK
Qdot 585 goat anti-rabbit IgG conjugate	IF (cells and FFPE** tissues)	Invitrogen, UK
Rabbit anti-mouse IgG Horse radish peroxidase (HRP) conjugated secondary antibody	Western Blotting	DAKO, UK
Swine anti-rabbit IgG Horse radish peroxidase (HRP) conjugated secondary antibody	Western Blotting	DAKO,UK

*IF :Immunofluorescence

**FFPE: Formalin fixed paraffin embedded

2.3 CELL IMMUNOFLUORESCENCE

Cells were plated in 24-well plates, containing coverslips, and left to grow overnight up to 80% confluence. The following day, after removing the media, three washes with PBS were performed. Cells were fixed with 4% paraformaldehyde/PBS pH 7.4 for 10mins and washed three times in PBS. Cell were also permeabilised with 0.1% Triton X-100 (Sigma,UK) in PBS for 10mins and rinsed in PBS three times. To avoid non-specific binding cells were incubated with 1% goat serum (Calbiochem, Merck, UK) in 1% BSA/PBS and blocking buffer for 30minutes. The blocking buffer was removed and coverslips were transferred on a sheet of fibre-free paper placed in humidified chamber where the cells were incubated with primary antibodies at an appropriate dilution in 1%BSA/PBS solution for 1 h at room temperature. Omission of primary antibody or blocking with immunised peptide was used. For the control with the

peptide, the primary antibody/peptide solution was prepared in advance: 150µg of peptide was added to 150µl of its corresponding antibody dilution and the mixture was incubated on a rotating wheel for 30min. Then the coverslips were transferred back to the plate and washed three times in PBS. Cells were then incubated with secondary antibody at an appropriate dilution in 1% goat serum/1%BSA/PBS for 1h at room temperature in the dark. Cells were rinsed again three times in PBS, mounted on glass slides using mowiol and stored at 4°C. All the steps were performed at room temperature.

For the double labelling, was followed the same protocol with the only difference that for the primary antibody incubation, were used two primary antibodies (one mouse monoclonal and the other rabbit polyclonal), for the secondary antibody incubation was used a dilution of anti-mouse and anti-rabbit secondary antibodies.

Antibody	Peptide
F4	2E
RTJ2	49.3
49.3	49.3
21N	21N
HFR1	96.4

2.4 TRANSFORMATION OF E.COLI WITH PLASMID DNA

Agar plates, Luria Bertani (LB) broths and stocks of antibiotics were prepared in advance. 25mg/ml of Ampicillin and 10mg/ml of Kanamycin (both from Sigma, UK) were made up in dH₂O, filter sterilised and stored at -20°C until required. LB agar was first sterilised by autoclaving and then left to cool. 50µg/ml of ampicillin or 30µg of kanamycin was added to the agar which then was aliquoted in petri dishes and left to

2-MATERIAL AND METHODS

set under the microbiological hood. Plates were stored at 4°C. Transformation was undertaken using 50µl E.Coli DH5α (Invitrogen, UK) competent cells, previously aliquoted and stored at -80°C. After thawing DH5α cells on ice, 1µl of plasmid was added to the aliquot and left on ice for 30min. The mix was heated for 20sec at 37-42°C in a pre-warmed water bath and returned back to the ice for 2min. To improve cloning efficiency, 0.95ml of SOC medium (Invitrogen, UK), instead of normal LB broth, was added to the tube and shaken at 37°C for 1h in an incubator shaker (Stuart Scientific, UK). Finally, 75µl of the mixture was spread over pre-warmed agar plates and incubated overnight at 37°C. The following day, 5ml of LB broth, with the appropriate antibiotic, was added in a sterile falcon tube. Single colonies were picked off using a yellow tip and dropped into the falcon tube that was then incubated overnight in a shaker incubator at 37°C at 225rpm. After 16h-18h the amplified DNA was extracted from the cells using the QIAprep Spin Miniprep Kit (Qiagen, UK) according to the manufacturer's instructions. DNA concentrations were then determined using the SmartSpec™ 3000 (Bio-Rad, UK) at an absorbance of 260nm in a quartz cuvette.

SOC medium composition
(Invitrogen, UK)

Tryptone	2%
Yeast extract	0.5%
NaCl	10mM
KCL	2.5mM
MgCl ₂	10mM
MgSO ₄	10mM
Glucose	20mM

2.5 TRANSIENT TRANSFECTION

Transfection was undertaken using Lipofectamine 2000 transfect reagent (Invitrogen, UK). Firstly, cells were plated in 24 well plate or 35mm tissue culture dishes (depending on the experiment) and incubated until 70% confluent. In one cryovial, DNA was diluted in Opti-MEM Reduced Serum Medium; in another cryovial Lipofectamine 2000 was also diluted in Opti-MEM and incubated for 5min at room temperature. Afterward, the diluted Lipofectamine was added to the diluted DNA and the mixture was incubated for 20min at room temperature to allow the DNA-Lipofectamine complexes to form. The mixture was then added to the cells and incubated at 37°C in 95% air and 5% CO₂ for 24h until ready to test for protein expression. All transfection procedure was carried out in a laminar flow tissue culture hood.

DNA and reagents volumes vary with the surface area of the culture vessel. In this study 24 well plates and 35mm dishes were used. The respective volumes for these tissue culture plates are reported in the following table.

Culture vessel	Volume of plating medium (ml)	DNA (µg) and dilution volume of Opti-MEM medium (µl)	Lipofectamine 2000 (µl) and dilution volume of Opti-MEM medium (µl)
35mm	2	4µg in 250µl	10µl in 250µl
24-well	0.5	0.8µg in 50µl	2µl in 50µl

2.6 WESTERN BLOTTING

2.6.1 CELL LYSIS

Cells were pre-plated in 35mm polystyrene tissue culture dishes and incubated in 95% air and 5% CO₂ until 70% confluent. Cells were washed twice with ice cold 2mM ethylene glycol tetra-acetic acid in PBS (EGTA-PBS) and then lysed in 200 µl of ice cold lysis buffer (containing 50mM Tris HCl pH 7.4, 150mM NaCl, 1% Triton X-100, 5mM

EDTA and protease inhibitor cocktail (Sigma, UK)) for 1-2min. After confirming the cell lysis under a microscope, the lysates were collected in 1.5 ml pre-cooled eppendorf tubes and cleared by centrifugation at 13,000 rpm for 10min at 4°C. Supernatant was aspirated and transferred into a new 1.5ml eppendorf and 50 µl of 5x sample buffer, was added to the supernatant. To denature proteins, cell lysates were heated at 100°C for 5min in a heat block (Stuart Scientific, UK) and then stored at -20°C.

2.6.2 SDS-PAGE GEL ELECTROPHORESIS

The 'Mighty Small II' Mini Vertical Unit obtained from Amersham Biosciences (Little Chalfont, UK) was used to run SDS-Page gel. Gel glass plates and spacers were cleaned first with dH₂O, wiped to dry and then treated with acetone before being assembled according to the supplier's instruction.

A 7.5% resolving gel was prepared and poured into the plate until ¾ full. To the top of the gel was added a layer of water saturated iso-1-butanol to allow the gel to set flat. Once the resolving gel was set, the saturated iso-1-butanol was discarded and a 3.75% stacking gel was made and poured on the top of the resolving gel. Quickly a comb 1.5mm thick with sample wells 5mm across was inserted. Once the stacking gel was set, the gel apparatus was transferred to a running tank filled with 1X running buffer and the comb was removed. Samples were heated at 100°C for 5min in a heat block (Stuart Scientific, UK) and loaded into the separate wells. 5µl of Dual colour molecular weight markers (M.W. 10-250kDa) (Bio-Rad, UK) was also loaded. Electrophoresis was initially run at 60V, once the samples had passed the stacking gel the voltage was increased to 120V until the dye front reached the bottom of the resolving gel.

2-MATERIAL AND METHODS

Preparation of 7.5% resolving gel:

Acrylamide / Bis solution 29:1	7.5%
Tris-HCl pH 8.8, 2M	0.37M
SDS	0.1%
N,N,N,N'-Tetra-methyl-ethylenediamine (TEMED)	10 μ l*
10 % Ammonium persulfate (Dapson)	0.1%
dH ₂ O to bring to volume	

*Amount is referred to 30ml of 7.5% resolving gel

Preparation of 3.75% stacking gel:

Acrylamide / Bis solution 29:1	3.75%
Tris-HCl pH 6.8, 2M	0.1M
SDS	0.1%
N,N,N,N'-Tetra-methyl-ethylenediamine (TEMED)	10 μ l*
10 % Ammonium persulfate (Dapson)	0.5%
dH ₂ O to bring to volume	

*Amount is referred to 10ml of 3.75% stacking gel

1X running buffer (pH8.6):

Tris- HCl	0.025M
Glycine	0.192M
SDS	1%
dH ₂ O	1 L

2.6.3 PROTEIN ELECTRO BLOTTING

After running the SDS-gel, a wet blotting procedure was performed using the Trans-Blot cell wet apparatus from Bio-Rad, UK. The blot apparatus was prepared first following the supplier's instructions. Two pads were pre-wetted in blotting buffer (10% of 10X running buffer (10% methanol, 0.1% SDS and dH₂O to bring to volume), two pieces of filter paper (Whatman, UK) of the dimension of the cassette and a piece of nitrocellulose membrane (Amersham Biosciences, UK) per gel, were cut and soaked also in blotting buffer. After removing the gel from the running apparatus the stacking gel was cut off. Then, the gel, the nitrocellulose membranes, filter papers and pads were sandwiched together in the cassette, after making sure that all air babbles between the gel and the membrane were removed. After, the cassette was tightly clamped and placed in the tank filled with the blotting buffer. The electrophoresis transfer was performed either at 100mA overnight or at 400mA for 3h at room temperature.

2.6.4 IMMUNODETECTION AND DEVELOPING

To check whether the proteins were successful transferred to the nitrocellulose membrane, a reversible staining method using Ponceau S red stain was applied to the blots. The blots were incubated for 1min in Ponceau S red stain solution (0.1% Ponceau, 5% acetic acid, dH₂O) and rinsed in dH₂O until completely destained, this was repeated for 3 times. To reduce not specific binding, the blots then were shaken in blocking buffer containing 5% of dried skimmed milk in 0.5% Tween-20/PBS(Sigma, UK) for 1h. The blots were then probed with primary antibodies, diluted in blocking buffer, for 1.5h at room temperature or at 4°C overnight. Blots then, were washed five times in 0.1% Tween 20/PBS and probed for 1h at room temperature with horse radish peroxidase (HRP) conjugated secondary antibody (1:1000 dilution; DAKO, UK) and washed again five times in 0.1% Tween 20/PBS. Detection of proteins bands was carried out with enhanced chemiluminescent ECL system. Blots were incubated for 1min in two ECL solutions, solution 1* and 2**, combined 1:1 ratio, and then exposed

2-MATERIAL AND METHODS

to X-ray film (Amersham Biosciences, UK) and the film was developed using a compact x4 hyper processor (Xograph Imaging Systems, UK).

*Solution 1

100mM Tris-HCl pH 8.5

2.5mM

0.4mM p-Cumaric acid

**Solution 2

100mM Tris-HCl pH 8.5

0.02% H₂O₂

2.7 TISSUES USED FOR IMMUNOHISTOCHEMICAL AND IMMUNOFLUORESCENT STUDIES

2.7.1 TISSUES SOURCES

Formalin fixed embedded tissues of rat pancreas prepared in this lab were used for optimisation experiments (for tissue preparation procedure see next section). The following tissues microarrays (TMA) were also used in this study.

Tissue microarray	Core size (mm)	Thickness (µm)	Array Type	Origin
HRC041	4.5	4	Human breast cancer HER2 IHC control array	US Biomax
CBA 3	2	4	Human breast cancer – metastasis-normal	Super Bio Chips
Herceptin treated	0.6	4	Primary breast cancer	Nottingham City Hospital

2.7.2 PREPARATION OF FFPE SECTIONS OF RAT PANCREAS

First day:

Rat tissue was dissected and each piece was placed into a 50ml falcon tube containing 10% Buffered Formal Saline (Thermo Scientific,UK) and left until required for use. Rat tissue was chopped up into smaller pieces and placed in 30% IMS for 30min, then in 60% IMS (diluted in dH₂O) and left overnight.

Second day:

Rat tissue was placed in 90% IMS for 2h room temperature (RT), 100% IMS for 2h then in 100% IMS and left overnight.

Third day:

Rat tissue was placed in 50% HistoClear/50%IMS for 2h at RT, 100% HistoClear for 3h and then in 100% HistoClear overnight.

Fourth day:

Wax beads were melted in the oven at 60°C and rat tissue was placed in the melted beads, and left overnight at room temperature.

Fifth day:

The wax containing the tissue was melted again and replaced 2-3 times to ensure that residues of HistoClear were removed from the tissue. Fresh molten wax was poured into plastic moulds and tissues were added separately in each mould and allowed to set to form blocks. The moulds were floated on cold water to ensure hardening and then mounted.

The blocks were finally cut using a microtome (Shandon AS325, UK). 5µm rat pancreas sections were then floated in a pre-warmed water bath at 40°C, placed on glass slide spositive charged (Superfrost plus, ThermoScientific, UK) and left to dry in the oven for 1h at 40°C.

2.8 IMMUNOHISTOCHEMICAL STUDY

2.8.1 STAINING PROCESS

The tissue sections were incubated in a drying oven at 60°C for 1h when required. The sections were dewaxed in three passages of 4min each in HistoClear and rehydrated in graded ethanols (100%, 100%, 70%) for 4min each. Then they were rinsed in distilled water (5min) and equilibrated in PBS (5min). Endogenous peroxidase activity was quenched by incubating the slides for 10min in 3% hydrogen peroxide solution made in distilled water. After one wash in distilled water (5min) followed by an additional wash in PBS (5min) slides were incubated for 1 h at room temperature with the primary antibody at the appropriate concentration diluted in 1%BSA/PBS. Subsequently, slides were rinsed first with distilled water and then PBS, and then incubated for 30min with Strep ABC complex/ HPR from DAKO kit. Sections were rinsed in dH₂O and incubated with the chromogenic substrate DAB (Cambridge Bioscience, UK and Diagnostic BioSystem, UK) freshly made for approximately 1min for colour change to occur. After rinsing with running distilled water for 5min, the slides were counterstained with 50% dilution in dH₂O of Gill's haematoxylin (Merk, Germany) for 30 seconds and rinsed under running tap water for 5min. Therefore the slides were dehydrated through graded alcohols (70%, 100% and finally 100% ethanol) for 4min each; then they were cleared with three passages in HistoClear, the first two for 4min each and the last one for 10min. Most of the HistoClear was removed from the slides by gently shaking and carefully wiping the slides making sure that the specimens had not dried out. Finally, slides were mounted with DPX mounting medium (Fisher Scientific, UK) and stored in the dark at room temperature.

2.8.2 SCORING SYSTEM

The scoring system is based on the intensity of brown stain against the haematoxylin background colour. Levels of protein expression in tissue sections stained by IHC were evaluated by two people using double-headed microscope (Olympus BX40, Germany). In accordance to the IHC interpretation criteria recommended by the American Society

of Clinical Oncology/College of American Pathologist (ASCO-CAP), the scoring was divided into quartiles. Cases were considered as negative (0) when no staining was present, 1+ when weak membrane stain was observed, 2+ if moderate stain was present and 3+ if or strong stain was present.

2.9 IMMUNOFLUORESCENT STAINING OF FFPE TISSUES

2.9.1 FFPE TISSUE IMMUNOFLUORESCENCE OF RAT PANCREAS

To develop a protocol for immunofluorescent staining with Qdots, 4µm thick sections formalin fixed paraffin embedded (FFPE) tissues of rat pancreas were used. The following staining procedure was adapted from [Xing et al 2007](#). Sections were dewaxed with three passages in Histoclear 5min each and then rehydrated through an alcohol gradient as follows: 100%, 95% and 75% ethanol for 2min each. Then they were placed on water for 2min and washed in PBS three times for 5min each. The slides were then incubated in blocking buffer with 2%BSA, 5% goat serum/PBS for 30min and then with primary antibody, diluted in blocking buffer, for 1.5h at room temperature. Sections were washed three times in PBS (5min each) and incubated with the secondary antibody, diluted in blocking buffer, for 2h at room temperature or overnight at 4°C in the dark. Finally, the slides were washed vigorously three times in PBS for 5min each, mounted in 90% glycerol/PBS and stored at 4°C in the dark.

2.9.2 OPTIMISATION OF QDOT IMMUNOFLUORESCENT PROTOCOL

FFPE sections of rat pancreas were also used to optimise the immunofluorescent staining procedure with Qdots. Both incubation time and concentration of the secondary antibody were optimised. The specimens were treated as described in the previous section until the incubation with the secondary antibody. To optimise the incubation time, the reaction was stopped at different time points; to optimise the secondary antibody concentrations, different dilutions were made and all tissue

sections were incubated for 2h. Omission of primary antibody was used as the control. Finally, slides were washed and mounted as already described.

2.9.3 QDOT IMMUNOFLOUORESCENT STAINING OF BREAST CANCER TISSUE ARRAYS

Qdot immunofluorescence was carried out on FFPE breast cancer tissues. All breast cancer tissue arrays were treated as described in section 2.9.1. Only when required, before starting the staining, tissue arrays were incubated in a dry oven at 60°C for 1h to remove the paraffin layer.

2.10 MICROSCOPY

2.10.1 LIGHT MICROSCOPY

An Olympus CKX31 inverted microscope was used to observe tissue cultures. Tissue sections stained by IHC were examined using a double-headed upright microscope (Olympus BX40, Germany) and images were taken using a Leica Leitz DMRB microscope (Leica Microsystems, Germany).

2.10.2 FLUORESCENCE MICROSCOPY

Images of fluorescent cells were taken using Leica AS MDW (Application Solution Multidimensional Workstation) with 63x magnification lens. Qdot 525 were excited with 490nm laser.

2.10.3 CONFOCAL MICROSCOPY

A Leica TCSP2 AOBS laser scanning confocal microscope (Leica Microsystem, Germany) was used to acquire images of fluorescent cells and FFPE tissue sections stained with AlexaFluor 546 (Invitrogen, UK) and Qdots.

2.11 AUTOFLUORESCENCE

2.11.1 METHOD TO REDUCE AUTOFLUORESCENCE

Confocal microscope was used to quench the autofluorescence in a FFPE breast cancer tissue section. The section was exposed for different lengths of time to repetitive scans using the 488nm laser line with 100% power and the 63x lens. Images were acquired using 63x magnification lens and the 40x magnification lens after 0mins, 10min, 30min and 60min exposure. The effects of photobleaching were also examined every 24h up to 144h and images were acquired using the 40x objective.

ACQUISITION PARAMETERS

DIODE LASER 488NM LINE	100% POWER
PMT* 1 OFFSET	2.30
PMT* 1 VOLTAGE	566.2V
FRAME AVERAGE	4
LINE AVERAGE	4

*PMT: Photomultiplier tube

2.11.2 DETERMINATION OF AUTOFLUORESCENCE PROFILE

Immunofluorescent staining of FFPE tissue sections was carried out as described in section 2.9.1, with the only difference that the specimens were incubated with PBS instead of primary and secondary antibodies. Slides were then examined using the confocal microscope and the 63x magnification lens. Tissues were excited with the 405nm laser line and gain, offset, frame average and line average were first optimised, depending on the tissue, in the region of the spectrum that corresponds to the autofluorescence emission. Then a series of images were automatically acquired, at different positions on the light spectrum (wavelength scan) with an increment of 10nm within the chosen wavelength range. After the scan, data were analysed using the

stack profile tool in the confocal software which generated a plot of the intensity emission versus wavelength.

2.12 QUANTUM DOT STUDIES

2.12.1. DETERMINATION OF Qdot SPECTRA PROFILE

On a microscope slide a small area was marked with a PAP water resistant pen, which creates a hydrophobic ring that limits the spread of the solution. A drop of concentrated Qdot nanocrystals solution was placed in the centre of the PAP pen ring and then covered with a coverslip. The slide was then examined using The Leica SP2 confocal microscope and the oil immersion 63x/1.4 objective lens. Qdots were excited with the 405nm wavelength diode laser and parameters for images acquisition were optimised in the region of the spectrum that corresponds to the nanocrystal emission: first the automatic gain function was used which helped to find the correct gain level and then the gain and offset were adjusted using the Look up table (LUT) to obtain an image with full dynamic range within the grey scale values. Then 20 lambda stacks were collected at different emission wavelengths (from 485nm to 725nm) with 10nm step size. All images were captured with a frame size of 512 by 512 pixels and 8 bit grey resolution. Finally, the spectra profile was determined using Leica Lite confocal software.

ACQUISITION PARAMETERS FOR QDOT 525

DIODE LASER 405NM LINE	25% POWER
PMT 1 OFFSET	0.6
PMT 1 VOLTAGE	677.0V
FRAME AVERAGE	8
LINE AVERAGE	1

ACQUISITION PARAMETERS FOR QDOT 585

DIODE LASER 405NM LINE	50% POWER
PMT 2 OFFSET	0.3
PMT 2 VOLTAGE	785.8
FRAME AVERAGE	8
LINE AVERAGE	1

2.13 PROCEDURE FOR IMAGE ACQUISITION

2.13.1 TESTING CONFOCAL CALIBRATION

A slide with a section of a plant (Corvallaria lily of the valley), supplied by Leica microsystems, was used to check the stability of the diode laser and PMTs.

Laser stability testing

After the laser was pre-warmed for 1h, an image was acquired at time 0 and after 8h during which time the laser was maintained turned on. The same procedure was repeated for 3 days. All images were also acquired using the same setting previously optimised for the acquisition of images from the breast cancer sections.

Testing PMTs efficiency

The same gain, same offset and same spectral window of 20nm, between 575nm and 595nm, were applied to each PMT separately. Other parameters were also maintained constant in each acquisition. Three images were taken in turn, one with PMT1, one with PMT2 and one with PMT3. The mean intensity was calculated for each image using the confocal software.

2.13.2 DETERMINATION OF PARAMETERS FOR IMAGE ACQUISITION

The diode laser was warmed up for 1h, in the meantime a standard slide with 20nm dilution of Qdot 585 (same dilution used for the staining), was prepared (see section

2.12.1). Before starting, images were acquired using the control slide supplied by Leica mycosystems to check the laser and PMTs. Images of Qdot 585 were collected using xyz mode.

ACQUISITION PARAMETERS FOR QDOT 585

DIODE LASER 405NM LINE	50% POWER
PMT 3 OFFSET	0.6
PMT 3 VOLTAGE	785.0V
SPECTRAL WINDOW	575NM-595NM
FRAME AVERAGE	8
LINE AVERAGE	1

This setting was then tested on breast cancer sections stained with Qdot 585 using the “look up table” indicator. Laser level, gain and offset of PMT1 (for the autofluorescence) and PMT 3 (for the specific signal) were optimised to balance signal intensity and background noise including all the values available within the grey scale range.

2.13.2 IMAGES ACQUISITION

Breast cancer sections stained with Qdot 585 were examined using a Leica SP2 laser scanning confocal microscope and a 63x magnification lens. Qdot 585 were excited by 405nm wavelength light and images acquired in two channels corresponding to two different spectral positions: one for the autofluorescence (between 485nm and 505nm) and the second for the Qdot 585 emission between (575nm and 595nm). Depending on the size of the core, 2mm or 0.6mm, three or two images respectively were acquired from different areas of each core. Each time, before starting to acquire the images, the laser was warmed up for 1h and an image with the standard sample was acquired to check whether the microscope was performing consistently.

ACQUISITION PARAMETERS FOR QDOT 585

DIODE LASER 405NM LINE	50% POWER
PMT 1 OFFSET	0.6
PMT 1 VOLTAGE	620.8V
PMT 3 OFFSET	0.6
PMT 3 VOLTAGE	693.7
FRAME AVERAGE	8
LINE AVERAGE	1

2.14. IMAGE QUANTIFICATION ANALYSIS

Each image was segmented for tumour areas and autofluorescent areas separately. Within an image, a single area or multiple areas were defined using the region of interest (ROI) tool available in the Leica Lite Confocal Software. Quantification data for each defined area were generated by the software and then transferred to Microsoft Office Excel 2007. A thresholding of 50 units on the grey value scale, from 0 to 50, was then applied. Mean intensity of Qdot 585 signal and autofluorescent signal, generated in the same spectra window, and were calculated for each defined tumour area and autofluorescent area separately. The formula used to calculate the mean intensity is the following:

$$\mu(I) = \frac{1}{N_{\text{pixel}}} \sum_{\text{pixel}} (I)$$

where (μ) is the mean, (I) is the pixel intensity, (N) is the pixel number and Σ is the sum of pixel intensities. (I) was obtained multiplying the grey level by the corresponding number of pixels.

An average of the Qdot 585 and autofluorescence mean intensities obtained from all of all images acquired in each section were calculated. The background

(autofluorescence) intensity was then removed by subtracting the mean intensity of the autofluorescence from the mean intensity of the Qdot 585 specific signal.

2.15 STATISTICAL ANALYSIS

The following software and statistical tests were performed:

- R software was used to execute Spearman's rank correlation
- Microsoft Office Excel 2007 was used for image quantification.
- SPSS was used to validate Qdot technology versus IHC, determine cut-offs point and perform Kaplan Meier survival analysis.

3 – DETECTION OF ErbB RECEPTOR EXPRESSION

3.1. INTRODUCTION

In order to develop a system that generates a more linear and scalable measurement of ErbB receptors in formalin fixed paraffin embedded (FFPE) breast cancer tissues using quantum dot nanotechnology, we first assessed ErbB receptor expression in FFPE cancer tissues by immunohistochemistry. In this chapter we evaluate the specificity of a series of antibodies and their performance in different systems. Several well characterised antibodies to the ErbB family were available in the laboratory. F4 is a monoclonal antibody directed to the cytoplasmic domain of the ErbB1 receptor. This antibody was developed using a synthetic peptide 2E and has been used to detect ErbB1 expression in human cervical, ovarian and vulval carcinomas (Gullick et al., 1985; Gullick et al., 1986). The 21N polyclonal antibody was raised to a synthetic peptide, called 21N, from the intracellular domain of ErbB2 (Gullick et al., 1987). Another antibody to ErbB2, NCL-CB11, employed here (Corbett et al., 1990) is a monoclonal antibody raised to a synthetic peptide from the intracellular domain of ErbB2. Two antibodies to the ErbB3 receptor, one polyclonal (49.3) and one monoclonal (RTJ2), generated against 49.3 synthetic peptide, from the cytoplasmic domain of ErbB3 receptor (Prigent and Gullick, 1994); (Rajkumar and Gullick, 1994) were also used in this work. The HFR1 monoclonal antibody, raised against a synthetic peptide called 96.4 matching to the intracellular domain of ErbB4 receptor, was used to detect this receptor (Srinivasan et al., 1998).

Despite these antibodies being well characterised as reported in the associated references, cell immunofluorescence and Western blotting techniques were used in this study to confirm antibody specificity. Cell lines were chosen over expressing each one of the four receptors as tools for this characterisation. From the literature it is well established that A431 cells over express ErbB1 receptor and SKBR3 breast cancer cells have high expression of ErbB2 receptor. Two stable transfected cell lines HEK293-ErbB3 and NIH 3T3-ErbB4 which over express their respective receptors were also used.

In order to demonstrate the specific reactions of each antibody with its respective receptor, selected antibodies were then used in immunofluorescent studies with Qdots in cell lines that over express individual receptors. We also compared Qdots performance in both epi-fluorescence microscopy and confocal microscopy. In order to test the ability of Qdot to label two receptors simultaneously, we then employed a breast cancer cell line, MDA-MDB453, that over express both ErbB2 and ErbB3 receptors (Knuefermann et al., 2003).

In order to develop a comparable data set, which can be used to evaluate IHC staining versus Qdots staining, the last series of experiment presented in this chapter examines the performance of the F4, 21N, RTJ2 and HFR1 antibodies in immunohistochemistry and the receptor expression on a series of formalin fixed paraffin embedded breast cancer sections derived from 60 breast cancer tumours. Sections from the same tumour will be then used to quantify receptors expression by Qdot immunofluorescence as described in the following chapter (see chapter 5).

3.2. AIMS

- I. Confirm specificity of primary antibody.
- II. Test the ability of Qdot to detect individual receptors.
- III. Investigate the ability of Qdot to detect multiple receptors in the same specimen.
- IV. Evaluate the performance of the antibodies in immunohistochemistry and receptor expression in breast cancer tissues.

3.3. RESULTS

3.3.1. IMMUNOFLUORESCENCE STUDY

3.3.1.1. DETERMINATION OF PRIMARY ANTIBODY SPECIFICITY

A431, SKBR3, HEK-293-ErbB3 and NIH 3T3-ErbB4 cell line were stained respectively with F4, 21N, RTJ2 and HFR1 antibodies. The concentration of each antibody was previously optimised within a range of 0.1µg/ml, 0.5µg/ml, 1µg/ml, 2µg/ml, 2.5µg/ml and 5µg/ml (data not shown); as optimal concentration for the experiments 2.5µg/ml was chosen. As all these antibodies are directed to the cytoplasmic domain of the receptor, cells were permeabilised with 0.1% Triton X-100/PBS which is a detergent that dissolves lipids from the cell membrane allowing the antibody to access the antigen. Cells were then incubated with the appropriate antibody. The antibody bound to the receptor molecules was detected indirectly by using a second anti-mouse antibody labelled with AlexaFluor 546. Figure 3.1 (A, C, E and G) shows positive membrane staining with each antibody, suggesting that the antibody reacted with the antigen. In order to determine whether the antibodies reacted specifically, a control pre-incubating the antibody with the immunising peptide was performed at the same time. No membrane staining was observed on cells incubated with the antibody-peptide mixture (Fig. 3.1 B, D, F and H) confirming that the antibody reaction was specific and the immunofluorescence was associated with receptor expression.

Expression of ErbB2 was also determined by using CB11 mouse monoclonal antibody (Fig. 3.2 A) which is commercial available. As the peptide to which this antibody was raised was not available, to ensure that there was not specific binding, omission of primary antibody was carried out as control. In this case no fluorescent cells were seen (Fig. 3.2 B).

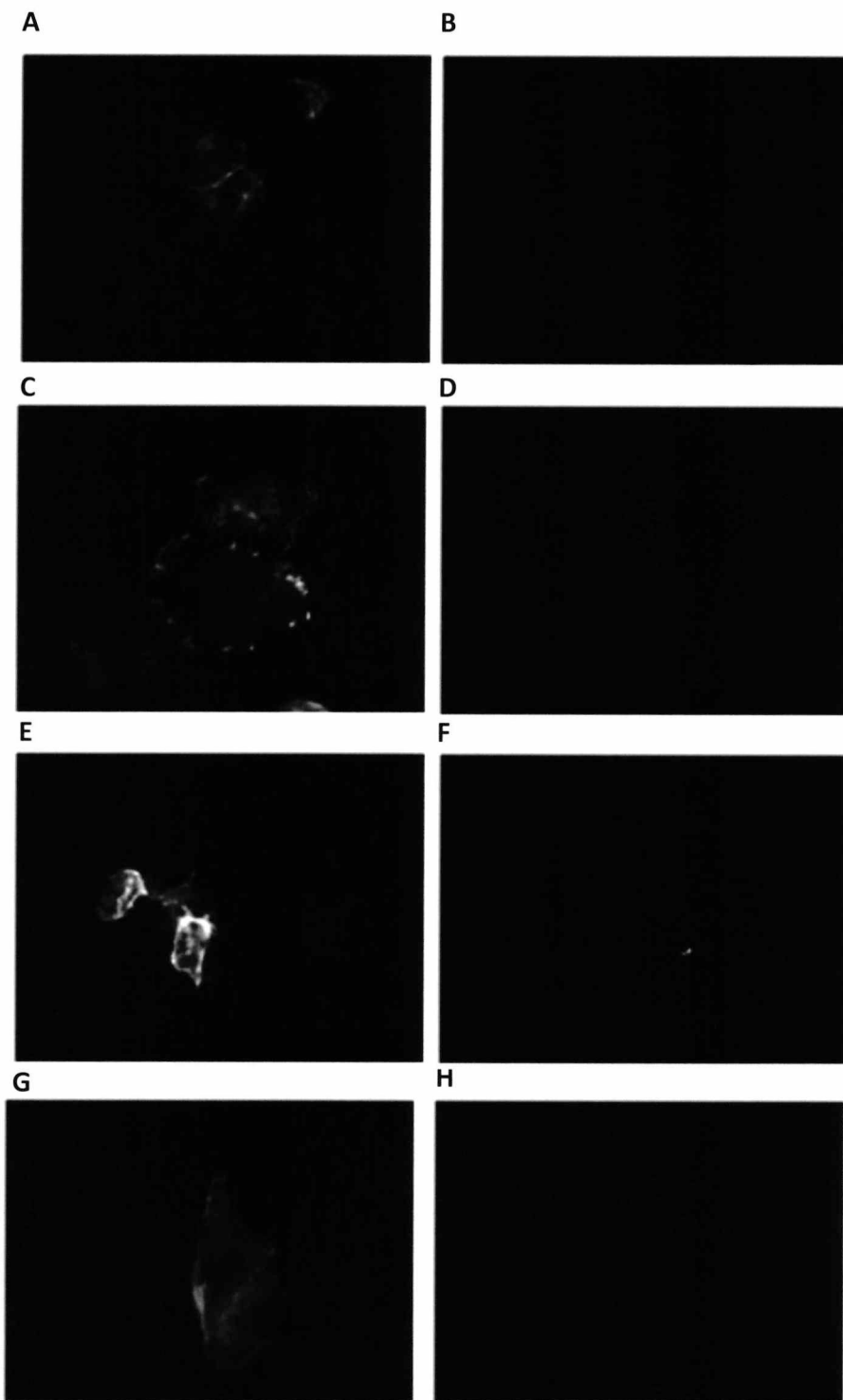


Figure 3.1 Detection of ErbB receptors with AlexaFluor 546. ErbB1 was detected in A431 cells with F4 antibody (A), ErbB2 in SKBR3 cells with 21N (C), ErbB3 in HEK293-ErbB3 cells with RTJ2 (E) and ErbB4 in NIH 3T3 cells with HFR1 antibody (G). (B), (D), (F), (H) Control cells treated with the antibody pre-incubated with the cognate peptide. All the images were desaturated, the brightness was increased by 10% and the contrast by 60% using Adobe Photoshop version 6.0.

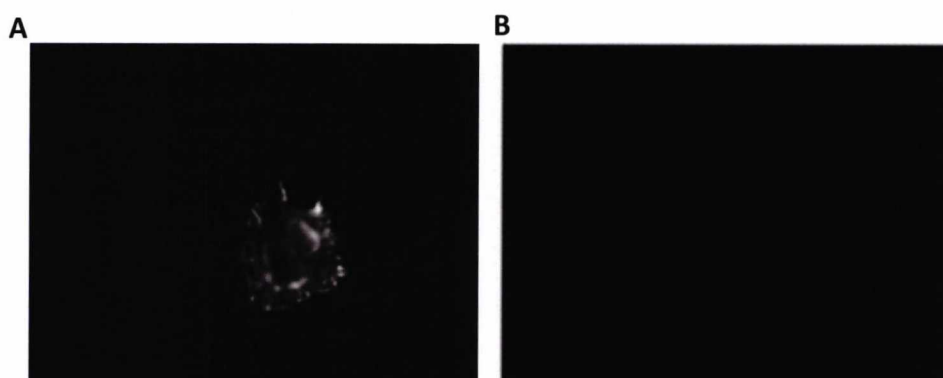


Figure 3.2 Immunofluorescent staining of SKBR3 cells with CB11 primary antibody and to detect ErbB2 (A); (B) control with omission of primary antibody. Anti-mouse immunoglobulin labelled with Alexafluor546 was used to detect the first antibody. The images were desaturated, the brightness was increased by 10% and the contrast by 60% using Adobe Photoshop version 6.0.

3.3.1.2. DETECTION OF ERBB RECEPTORS BY QDOT

Once we ensured by immunofluorescent staining that the antibody reaction was specific, we next examined the ability of Qdot to label specific targets on the cell membrane. Immunofluorescent staining was carried out as described previously with the only difference that a secondary goat anti-mouse antibody labelled with Qdot 525 was used instead of AlexaFluor546. Images were acquired using a wide-field fluorescence microscope (Leica AS MDW) with 490nm laser excitation and filter sets suitable for fluorescein isothiocyanate (FICT) detection. Membrane staining of ErbB1, ErbB2, ErbB3 and ErbB4 were observed in each cell line respectively as expected (Fig. 3.3 A, C, E and G). Control pre-incubation with the immunising peptide also confirmed the specificity of the stain (Fig. 3.3 B, D, F). Omission of primary antibody was chosen as a control for ErbB2 detected with CB11 for the reason explained in section 3.3.1. (Fig. 3.3 H).

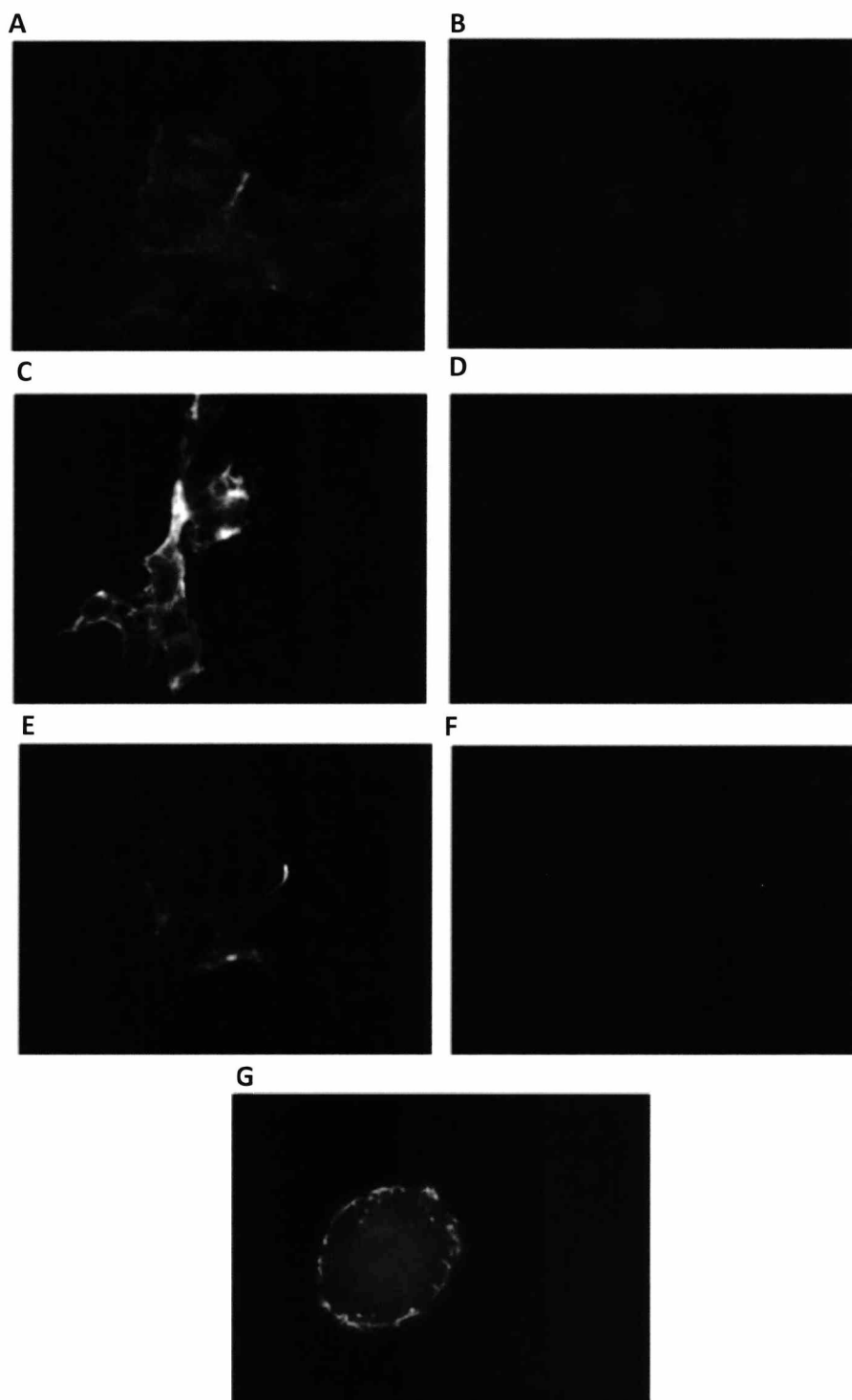


Figure 3.3. Evaluation of immunofluorescent staining with anti-mouse Qdot 525 secondary antibody of: A431 cells expressing ErbB1 (A), HEK293-HER3 cells expressing ErbB3 (C), NIH3T3-ErbB4 cells which overexpress ErbB4 (E) and SKBR3 cells expressing ErbB2 (G). Immunofluorescent staining in presence of the cognate peptide are shown in (B), (D) and (F). All the images were desaturated, the brightness was increased by 10% and the contrast by 60% using Adobe Photoshop version 6.0.

In order to obtain images with higher resolution and better quality, we employed a laser scanning confocal microscope. Wide-Field microscopy represents an easy and rapid method to collect data for immunofluorescent studies; however the resolution of the images captured is lower than the resolution that is possible to achieve using a confocal microscope. Furthermore the excitation light and the filter sets available with the Leica AS MDW were not optimised for Qdots emissions. Images of A431, HEK293-ErbB3 and NIH 3T3-ErbB4 cells stained with F4, RTJ2 and HFR1 monoclonal antibodies and anti-mouse Qdot 525 secondary antibody were therefore acquired with a Leica TCSP2 AOBS laser scanning confocal microscope (Fig. 3.4 A, C, and D). Images of SKBR3 cells stained with 21N antibody and anti-rabbit Qdot 585 secondary antibody were also captured with the Leica TCSP2 AOBS laser scanning confocal microscope (Fig. 3.4 B). Both Qdot 525 and Qdot 585 labelled secondary antibodies were excited with 405nm diode laser line. In order to maximise Qdots signals the bandwidths of the emission filters were set up at 20nm, between 515nm and 535 for Qdot 525, and between 575nm and 595nm for Qdot 585. Laser power, photomultiplier tubes, gain and off-set were also optimised. Clearly confocal images showed higher resolution, improved signal to noise ratio, higher light intensity and sharper image (Fig. 3.4 A, B, C, and D). Control with the immunised peptide (Fig. 3.4 A, B, C, and D third column) was performed. In order to examine how much the secondary antibodies labelled with Qdots contribute to the background (not specific signal) controls in absence of primary antibodies were carried out (Fig. 3.4 A, B, C, and D second column). No fluorescence was seen in all control experiments.

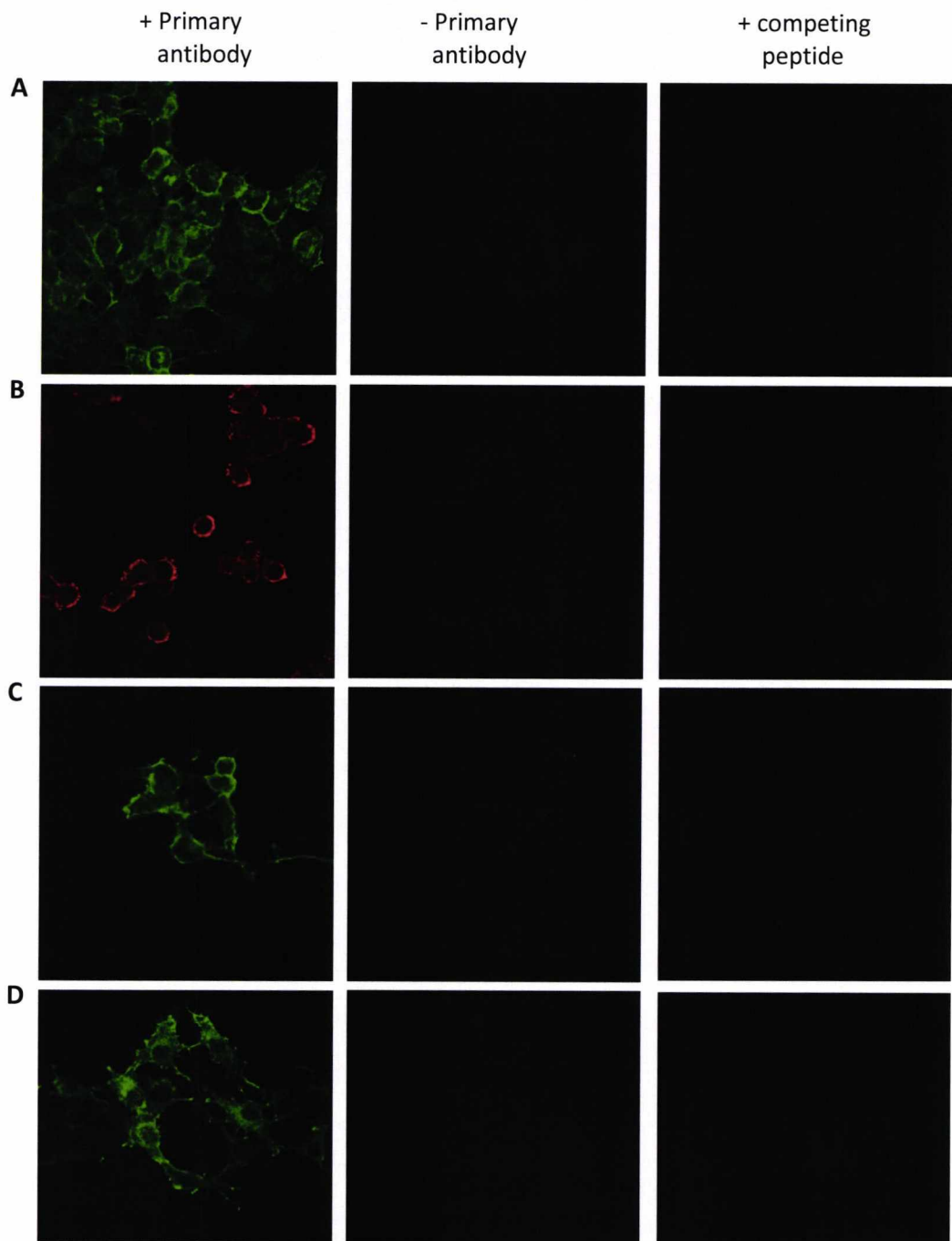


Figure 3.4 Immunofluorescent staining with anti-mouse Qdot 525 (row A, C and D) and antirabbit Qdot 585 (row B). Images were acquired with Leica TCSP2 AOBS laser scanning confocal microscope. On the left expression of ErbB1 in A431 cells stained with F4 monoclonal antibody and anti-mouse Qdot 525(A), ErbB2 in SKBR3 cells stained with 21N polyclonal antibody and anti-rabbit Qdot 585 (B), ErbB3 in HEK293-ErbB3 cells stained with RTJ2 monoclonal antibody and anti-mouse Qdot 525 (C) and ErbB4 in NIH 3T3-ErbB4 cells stained with HFR1 monoclonal antibody and anti-mouse Qdot 525 (D). In the column in the middle are shown the respective controls with the omission of the primary antibody and on the right column are shown the respective control with the immunising peptide.

3.3.1.3. DOUBLE LABELLING OF ErbB2 AND ERBB3 WITH QDOT

In order to explore the possibility to use Qdot to label multiple targets simultaneously, we performed immunofluorescence staining using MDA-MB453 breast cancer cells. This cell line was chosen because it expresses equal levels of ErbB2 and ErbB3 receptors (Knuefermann et al., 2003) and thus represented an excellent tool for the purpose of this study. Cells were fixed, permeabilised and incubated with a mixture of two antibodies RTJ2 mouse monoclonal antibody (directed to ErbB3) and 21N rabbit polyclonal antibody (directed to ErbB2). Negative controls with the competing peptides, 49.3 for RTJ2 and 21N for 21N, were also carried out to ensure that there was no non-specific binding of the antibodies. Anti-mouse Qdot 525 and Anti-rabbit Qdot 585 were used as secondary antibody to detect ErbB3 and ErbB2 respectively. Both Qdots were excited with the 405nm laser (laser power 25%) and images acquired using a confocal microscope and a 63x magnification lens. When specimens are labelled with more than one fluorophore bleed-through artefacts can occur. As the amount of bleed-through depends on laser intensity level and gain used for the image acquisition, in order to avoid bleed-through the setting for the image acquisition was optimised. The setting optimisation was carried out using a control specimen where only one dye was present while the two detection channels were active (data not shown). The optimised setting was then used for the image acquisition of the double labelled specimen (Fig.3.5 C). Specific staining of the cell surface was seen for both receptors with immunofluorescent signal at 525nm, in the green region of the spectrum, associated to ErbB3 expression (Fig. 3.5 A) and ErbB2 expression in the red region of the spectrum, corresponding to 585nm wavelength (Fig. 3.5 B). In the control experiment in which the first antibody was pre-incubated with the immunised peptide and then with the appropriate second antibody labelled with Qdot, no evident and specific signal was observed (Fig. 3.5 D). The results demonstrated that the two cellular targets, ErbB2 and ErbB3, were successfully detected in the same cell using Qdot with different wavelength emissions (Fig. 3.5 C).

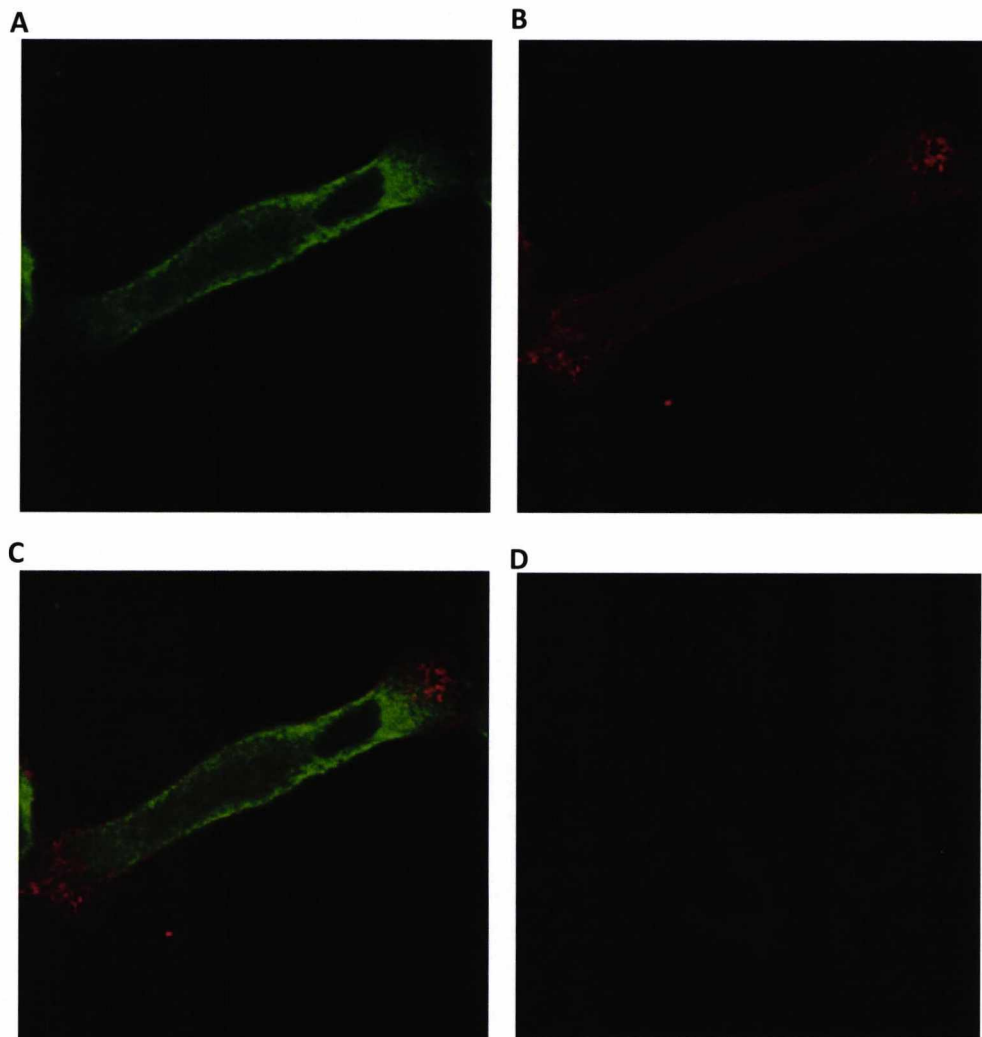


Figure 3.5 Double labelling of MDA-MB453 cells. (A) Detection of ErbB3 with green fluorescent quantum dots (Qdot 525). (B) Shows ErbB2 expression detected with red fluorescent quantum dots (Qdot 585). (C) Merged image: detection of both receptors expressed in the same cell. (D) Negative control with the immunising peptide. Qdot 525 and Qdot 585 were excited with 405nm laser at 25% power. Qdot 525 was imaged setting the gain level at 728.6 V, the offset at 1 on the PMT and the bandwidth between 515nm and 535nm. Qdot 585 were imaged setting the gain level at 658.9, the offset at 1 on a different PMT and the bandwidth between 575nm and 595nm. The control images were acquired with the same setting. All Images were adjusted for the input (103) and output (140).

In order to exclude that there was no bleed-through of one wavelength signal into the other one we examined the emission spectra of Qdot 525 and Qdot 585 performing a wavelength scan on MDA-MB453 cells labelled with both Qdots. Confocal microscopy

was used to collect a series of images across a defined range of wavelengths (from 453nm to 655nm) with a bandwidth of 10nm (Fig. 3.6).



Figure 3.6 Lambda stacks on MDA-MB453 cells double stained with Qdot 525 and Qdot 585. The brightness was increased by 10% and contrast by 60%.

The lambda stacks were then plotted by the confocal software on a graph where the x-axis reported the pixel intensities and the y-axis the wavelengths. Figure 3.7 shows two emission spectra profiles with a good separation of the emission peak at 525nm and 585nm. The two peaks where one corresponds to ErbB3 expression and the second one to ErbB2 expression, have the same intensity level which suggests that, in MDA-MB453 cells, both receptors are expressed in equal levels consistently with what has been reported in the literature.

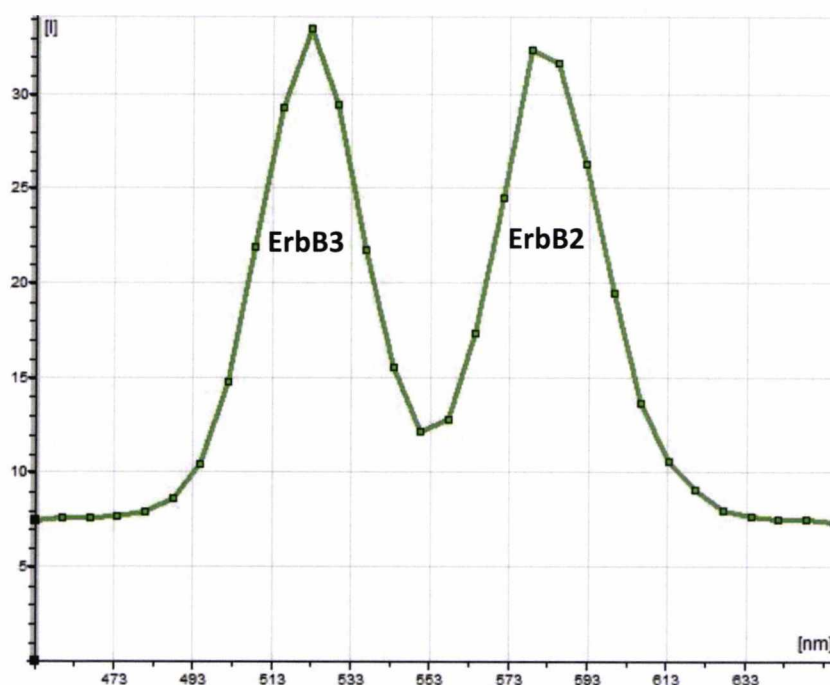


Figure 3.7 Emission Spectrum of Qdot 525 and Qdot 585. The graph shows the spectral separation between the emission profiles of QD525 and QD585 in double stained MDA-MB453 cells.

3.3.2. WESTERN BLOT STUDY

3.3.2.1. DETECTION OF ErbB RECEPTORS IN CELL LINES

Antibody specificity and expression of ErbB receptors in the same cell lines used for immunofluorescence studies, were also determined by Western blotting. Four blots with cell lysates of A431, SKBR3, HEK293-ErbB3 and NIH3T3-ErbB4 cells (Fig.3.8 A, B, C and D, track 1-2-3-4), were probed respectively with F4, 21N, RTJ2 and HFR1 antibodies. The antibodies specifically recognised ErbB1 (Fig.3.8 A, track 1), ErbB2 (Fig.3.8 B, track 2) and ErbB4 (Fig.3.8 D, track 4). The presence of additional lower intensity bands corresponding to each receptor were also observed in each track. The presence of extra bands below the molecular weight expected for ErbB2 were observed in SKBR3 cell lysate (Fig. 3.8 B track 2). This could be due to the presence of a truncated form of ErbB2 corresponding to 95kDa (see section 1.12.5). ErbB2 shedding occurs following a proteolytic cleavage mediated by metalloproteinases which release

the ErbB ectodomain in the blood stream and producing the membrane-bound fragment p95 (Codony-Servat et al., 1999); (Molina et al., 2001). It was not possible to detect a specific band using RTJ2 antibody (Fig.3.8, track 3). Several attempts were undertaken, both by myself and colleagues within the laboratory, to detect ErbB3 by Western blotting using RTJ2 antibody. These were unsuccessful. In contrast, the blot probed with the polyclonal antibody 49.3, raised to the same peptide as RTJ2, revealed a band of approximately 160kDa in the HEK293-ErbB3 cell lysate (Fig. 3.8 E, track 1), which was absent in the HEK293 cell lysate (Fig. 3.8 D, track 2) as expected.

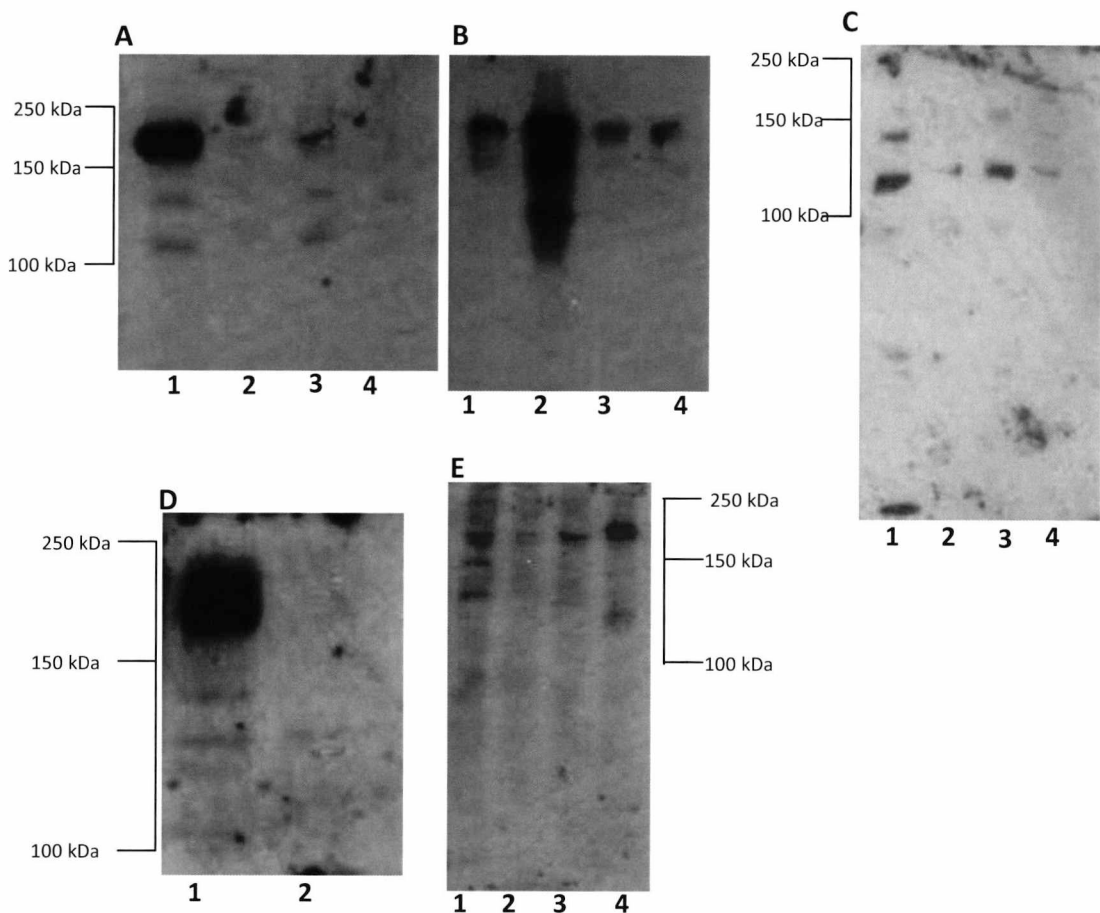


Figure 3.8 Evaluation of antibody specificity by Western blotting. In A), (B), (C) and (D) cell lysates from A431 (track 1), SKBR3 (track 2), HEK293-ErbB3 (track 3) and NIH3T3-ErbB4 (track 4) were used to detect receptor expression by immunoblotting. (A) 5 μ g/ml of F4 monoclonal antibody was used to detect ErbB1 (track 1). (B) ErbB2 (track 2) was detected using 3 μ g/ml of 21N polyclonal antibody; extra bands below the expected molecular weight were also observed. (C) Immunoblotting was performed using 5 μ g/ml RTJ2 monoclonal antibody, however no specific band corresponding to ErbB3 was observed (track 3). (D) Western blotting with 49.3 polyclonal antibody, HEK293-ErbB3 cell lysate is shown in track 1 and HEK293 cell lysate is shown in track 2. (E) A band corresponding to ErbB4 (track 4) was detected using 5 μ g/ml of HFR1 monoclonal antibody.

3.3.2.2. DETECTION OF ErbB RECEPTORS IN TRANSFECTED CELLS

To exclude the possibility of the antibodies cross reacting with the other receptors, Western blotting with cell lysates from transfected COS7 was performed. COS7 cells have little or no endogenous receptor expression and therefore they should only or prevalently express the transfected protein. COS7 cells were transfected with pBABEpuro-ErbB1, pcDNA3.1-ErbB2, pBABEpuro-ErbB3 and pcDNA3.1-ErbB4 plasmids separately. After approximately 20h, the time necessary for the proteins to be expressed, cell lysates were prepared. Four SDS-PAGE gels, each of which were loaded with COS7-ErbB1, COS7-ErbB2, COS7-ErbB3, COS7-ErbB4 transfected and not transfected COS7 cell lysates were run; lysates from A431, SKBR3, HEK293-ErbB3, NIH 3T3-ErbB4 were also run in parallel as positive controls. After transfer to nitrocellulose, each blot was probed with F4, 21N and HFR1 antibodies respectively. A signal corresponding to ErbB1 was detected in A431 and COS7-ErbB1 cells (Fig. 3.9 A track 1) in the blot probed with F4, however bands of the same size were also present in the others lanes (Fig. 3.9 A track 2-3-4-5-6). This was not surprising as endogenous expression of ErbB1 in COS7 cells was reported in other studies (Kumagai et al., 2001; Wang et al., 2005). The blot probed with the 21N antibody shows a band in both COS7-ErbB2 and SKBR3 cells but not in the other lysates. The blot probed with HFR1 antibody showed a specific band only in NIH 3T3-ErbB4 (Fig. 3.9 D track 1) but not in COS7-ErbB4 cells (Fig. 3.9 D track 5). This was probably due to the low concentration of ErbB4 in the cells.

3 - DETECTION OF ERBB RECEPTOR EXPRESSION

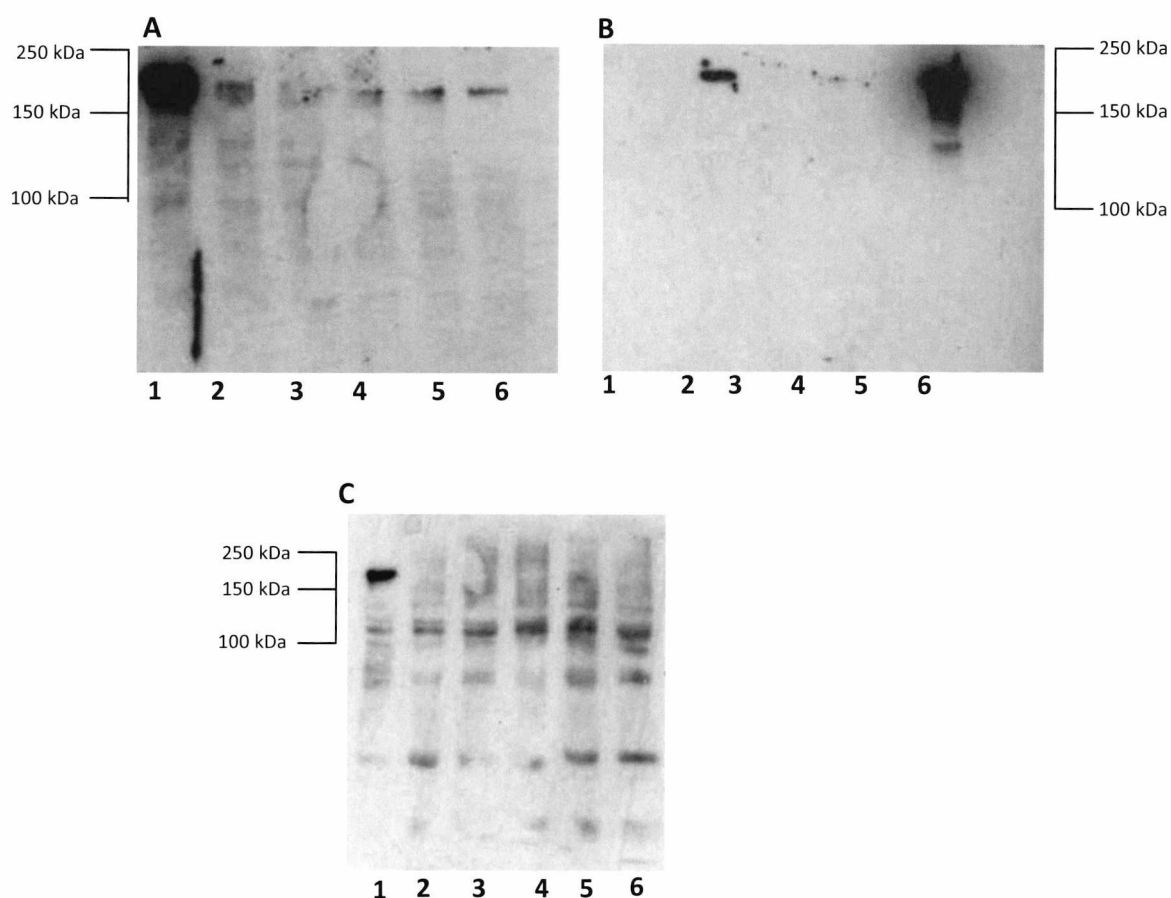


Figure 3.9 Western blot analysis for antibody cross-reactivity. (A) the blot was probed using 5µg/ml of F4 monoclonal antibody. Track 1 cell lysate from A431 cell, track 2 to 5 COS7 cells expressing ErbB1, ErbB2, ErbB3 and ErbB4, track 6 no transfected COS7 cells. (B) Immunoblotting of ErbB2 using 3µg/ml of 21N polyclonal antibody. Track 6 SKBR3 cell lysate, track 1 to 4 COS7-ErbB1, COS7-ErbB2, COS-ErbB3 and COS7-ErbB4. Track 5, COS7 cells. (C) Blot treated with 5µg/ml of HFR1 monoclonal antibody. Track 1, NIH 3T3-ErbB4 cell lysate, track 2 to 5 COS7-ErbB1, COS7-ErbB2, COS-ErbB3 and COS7-ErbB4, track 6 COS7.

1.1.1. IMMUNOHISTOCHEMICAL STUDIES OF RECEPTOR EXPRESSION IN BREAST CANCER

To examine the expression of ErbB receptors within a series of breast cancer tissues, immunohistochemical staining, using formalin fixed paraffin embedded (FFPE) breast cancer tissues, was performed. Immunohistochemistry (IHC) is a simple and commonly used method to determine the expression of proteins in a wide range of tumours. The IHC method is based on two types of detection systems, direct or indirect. The direct method involves a one-step process where a primary antibody conjugates to an enzyme, reacts directly with the antigen (Fig. 3.10 A). The indirect system is composed of two-steps which uses two layers. In the first layer, an unlabelled primary antibody binds the antigen, in the second layer a labelled secondary antibody reacts with the primary antibody (Fig. 3.10 B). The secondary antibody can be conjugated to an enzyme, such as peroxidase, alkaline phosphatase or glucose oxidase, or to fluofochromes. The most common IHC detection system, as shown in Figure 3.10 C, uses an additional layer represented by the avidin-biotin complex (ABC). This system has been used in this study. In this method the secondary antibody is conjugated to biotin molecules which have a high affinity for binding to avidin. Avidin is a large glycoprotein that has four binding sites per molecule for the biotin. By making a mixture of biotinylated enzyme and avidin in which on average only three of the four sites are occupied, therefore the fourth site is free to bind the biotinylated secondary antibody. Then a soluble chromogen, 3,3-diaminobenzidine (DAB), is converted by the peroxidase enzyme into a brown precipitate that is insoluble in water and in organic solvents (e.g. alcohol or histoclear). In principle a range of colour intensities of the brown stain will vary depending on the amount of antigen detected in the tissue. For this reason the method can also be used as a semi-quantitative measurement of protein expression.

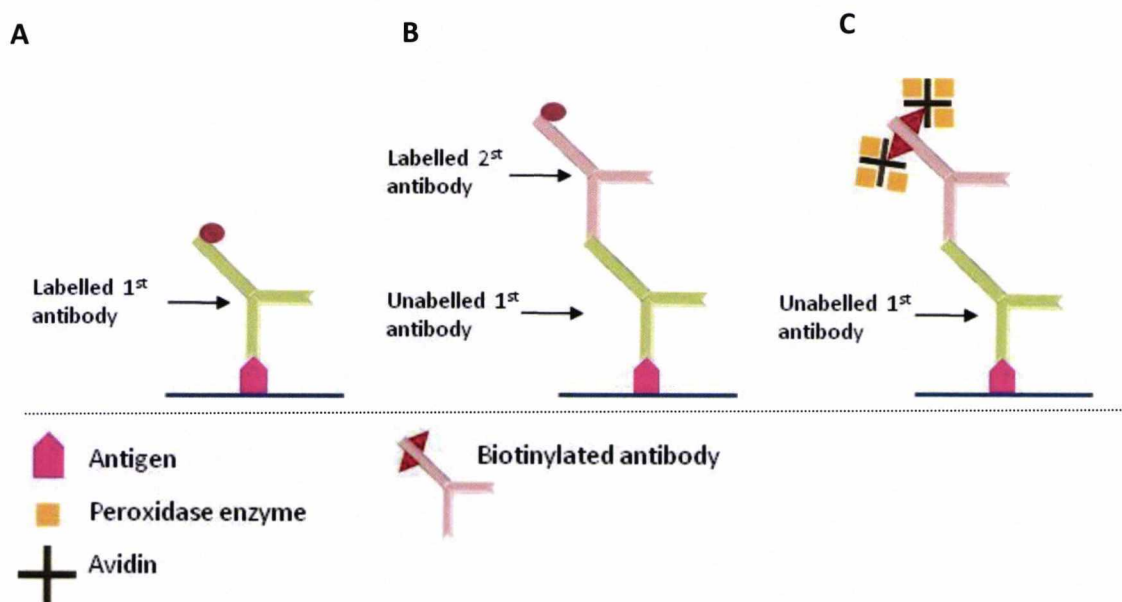


Figure 3.10 Different IHC methods. (A) direct method, (B) indirect method, (C) ABC method also used in this study.

1.1.1.1. IMMUNOHISTOCHEMICAL STAINING OF FOUR RECEPTORS IN BREAST CANCER TISSUE

The levels of expression of each ErbB receptor, in human breast cancer, were evaluated by immunohistochemical staining using multiple tissue arrays. Each array contained 60 unselected human breast cancers from patients with a typical range of receptor expression from 0 to 3+. The level of expression of each receptor was graded from 0 to 3+ on the basis of staining intensities. A score of zero corresponded to absence of staining, 1+ corresponded to weak staining, 2+ corresponded to moderate staining and 3+ to strong staining. The intensity of the brown staining was evaluated by two observers, myself and Prof. W. Gullick, on an Olympus BX40 microscope with a double head. Expression of ErbB1 receptor, shown in figure 3.11, was determined using F4 monoclonal antibody. Immunostaining was mainly cytoplasmic and there was no tumour showing high stain intensity scorable as 3+.

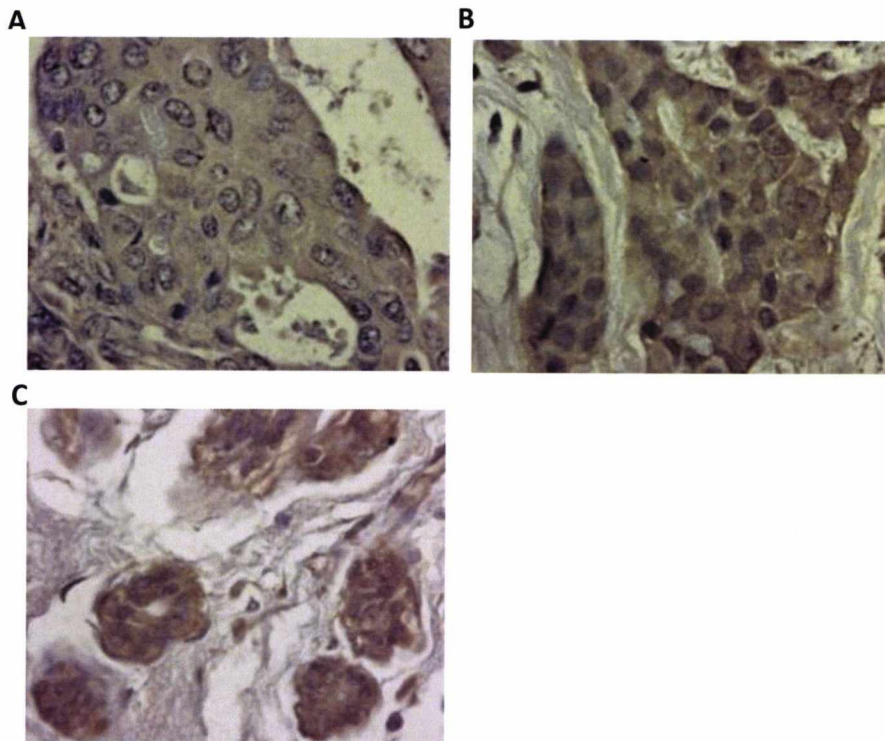


Figure 3.11 Immunohistochemical staining of ErbB1 in breast cancer tissues. Immunohistochemical staining was performed using 5 μ g/ml of F4 monoclonal antibody. The pictures show examples of staining for ErbB1 and the different levels of protein expression scored as 0 (A), 1+ (B), 2+ (C). Magnification: x63.

Different levels of expression of ErbB2 were examined using 21N polyclonal antibody. Increasing levels of ErbB2 expression are shown in figure 3.11. Distinct membrane staining characterised by a uniform and thick ring circumscribing the edges of the cells was observed in ErbB2 3+ breast cancers (Fig. 3.12 D).

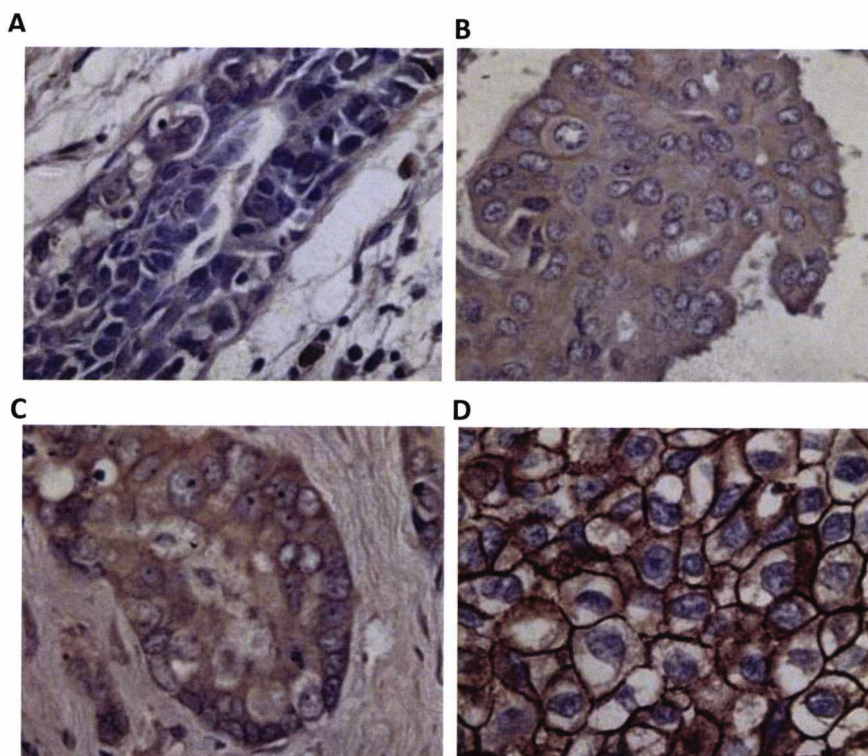


Figure 3.12 Immunohistochemical staining of ErbB2 in breast cancer tissues. Tissues were stained with 5 $\mu\text{g}/\text{ml}$ of 21N polyclonal antibody. Here is shown an example of ErbB2 negative staining (A), 1+ membrane staining (B), 2+ membrane staining (C), 3+ and uniform membrane staining (D). Magnification: x63

Immunohistochemical staining for ErbB3 and ErbB4 was carried out using RTJ2 monoclonal antibody (Fig 3.13) and HFR1 monoclonal antibody (Fig. 3.14) respectively. For both ErbB3 and ErbB4 receptors different staining intensity corresponding to different levels of expression were also determined.

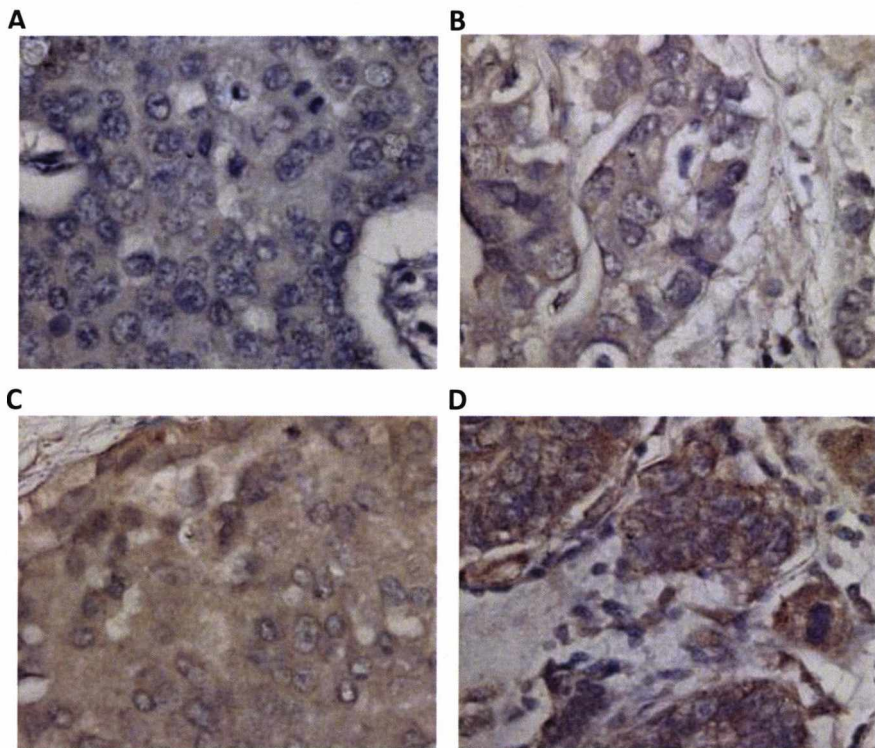


Figure 3.13 Immunohistochemical staining of ErbB3 in breast cancer tissues. ErbB3 expression was examined using 5 μ g/ml of RTJ2 monoclonal antibody. Examples of (A) negative, (B) 1+, (C) 2+ and (D) 3+ staining. Magnification: x63

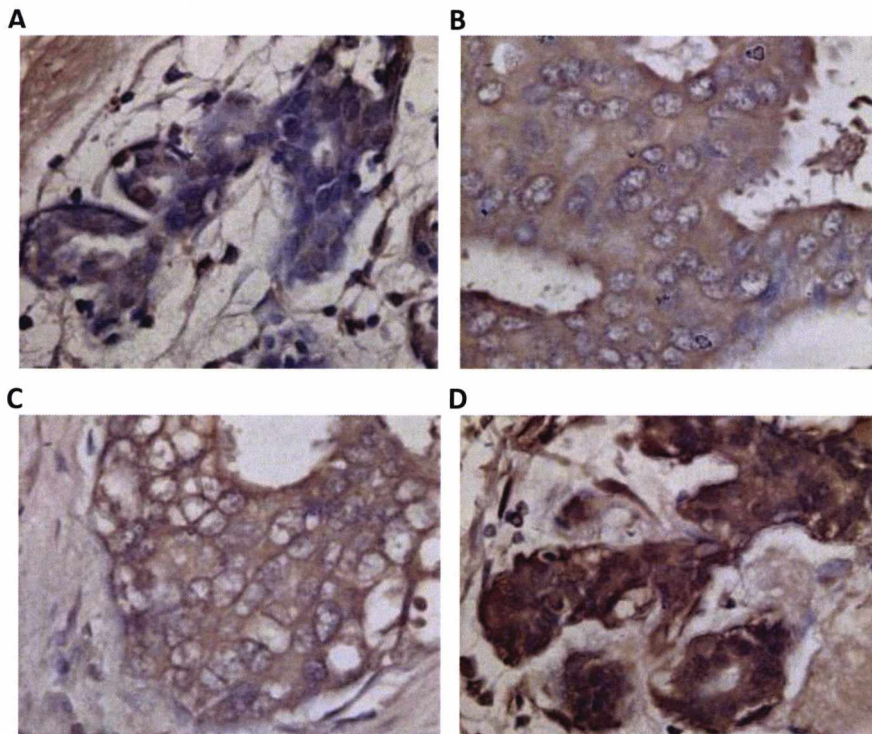


Figure 3.14 Immunohistochemical staining of ErbB4 in breast cancer tissues. Levels of expression of ErbB4 were evaluated using 1 μ g/ml HFR1 monoclonal antibody. Example of staining scoring of 0 (A), 1+ (B), 2+ (C) and 3+ (C). Magnification: x63

The number of cases scored for each receptor as 0, 1+, 2+ and 3+ is presented in the table 3.1 and summarised in Figure 3.14. 1.7% of the cases were not evaluable because samples were damaged or missing, therefore unscorable.

	ErbB1	ErbB2	ErbB3	ErbB4
total number of samples	56	57	58	54
samples scored as 0	17 (30.36%)	11 (19.3%)	7 (12%)	5 (9.2%)
samples scored as 1+	35 (62.5%)	18 (31.6%)	19 (32.7%)	32 (59.2%)
samples scored as 2+	4 (7.14%)	11 (19.3%)	19 (32.7%)	16 (29.6)
samples scored as 3+	0	17 (29.8%)	13 (22.4%)	1 (1.8%)

Table 3.1 ErbB receptor expression in a set of breast cancer samples.

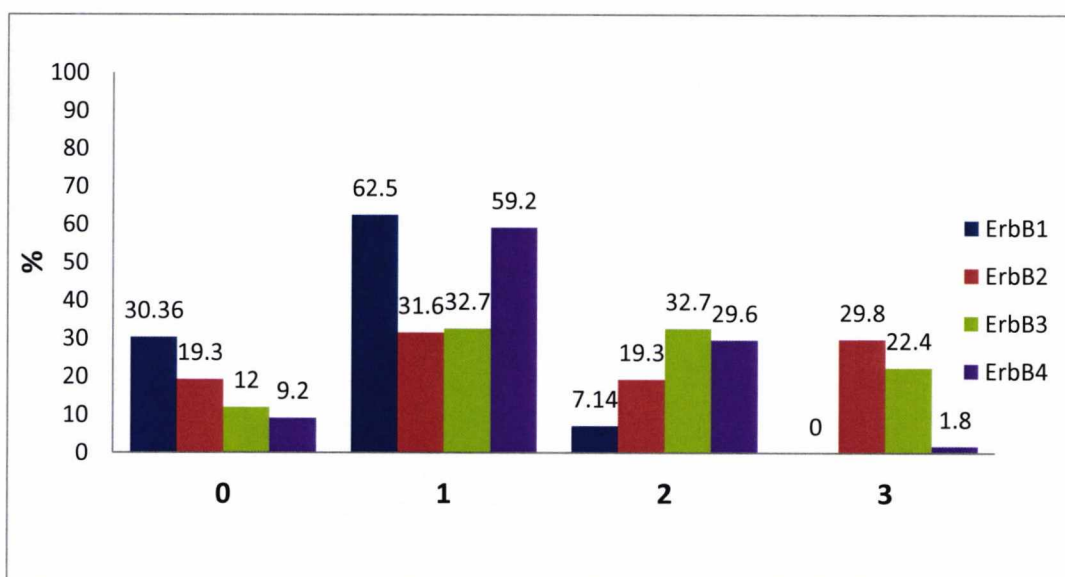


Figure 3.15 Percentage of breast cancer samples with low (0), weak (1+), moderate (2+), strong (3+) expression of ErbB1, ErbB2, ErbB3 and ErbB4 receptors.

1.1.1.2. CORRELATION BETWEEN ERBB2 EXPRESSION AND ERBB3 EXPRESSION IN BREAST CANCER

Like ErbB2, ErbB3 is also over expressed at high levels (3+ by immunohistochemistry) in approximately 20% of breast cancers but without gene amplification (Lemoine et al., 1992). In accordance with these reports, in our dataset we found that 29.8% of breast cancer samples stained for ErbB2 and 22.4% of the samples stained for ErbB3 have strong membrane staining and were scored as 3+ (Fig. 3.15). It has been reported in one study that co-expression of ErbB2 and ErbB3 often occurs in breast cancers and

that they are positively correlated (McIntyre et al.). Thus, we investigated whether within this new series of breast cancers co-expression of ErbB2 and ErbB3 was also present and whether the two events were correlated consistent with the published data. We found that 5 cases were scored 3+ for ErbB2 and ErbB3, which are approximately 9% of the total. In order to investigate possible associations between ErbB2 and ErbB3 over expression, Spearman's rank correlation statistical analysis was performed on these data using R statistical package. Spearman's rank correlation coefficient varies between -1 and 1 and gives an estimation of the strength of the association between two variables, in this case ErbB2 and ErbB3. Negative numbers (values comprise between 0 and -1) indicate that there is an inverse relationship: if one variable increases, the other decreases. Positive numbers (values from 0 to 1) indicate a positive relationship where if one variable increases the other increases. The Spearman rank correlation analysis gave a numerical value of 0.37 that corresponds to a weak correlation. As the same analysis (McIntyre et al.) was done in our laboratory on a larger sample size of 104 breast cancer tissues, we decided to use these data together with my own data. On this larger sample the Spearman's rank correlation resulted 0.48 suggesting that if one of the two receptors, either ErbB2 or ErbB3, is over expressed in a breast tumour, it is likely that the other receptor will be over expressed.

3.4. DISCUSSION

3.4.1. ANTIBODY SPECIFICITY

Both monoclonal and polyclonal antibodies are made by immunising animals (mouse, goat, rabbit, horse etc.) with purified antigens or synthetic peptides. The animal responds by producing antibodies that specifically recognise and bind the target protein. Monoclonal antibodies are produced mainly in mice (Kohler and Milstein, 1976) and rabbits. Polyclonal antibodies are produced in multiple animal species especially in rabbit, goat, horse and chicken. Compared to monoclonal antibodies, polyclonal antibodies have higher affinity and wide reactivity as they are more likely to recognise different isoforms of the proteins. While this can be an advantage, in the other hand this can also be a disadvantage as it increases the possibilities to cross-

react with similar epitopes in other protein. Therefore the specificity of polyclonal antibodies can vary from low to high. In contrast monoclonal antibodies have the advantage over polyclonal antibodies of having higher specificity which also reduces the possibility of cross-reaction.

In this study we used both monoclonal and polyclonal antibodies which were available in the laboratory. Despite the fact that all antibodies used in this study were well characterised, additional experiments were performed to show both their specificity and their absence of cross-reactivity with the other receptors. In order to determine whether the F4, RTJ2 and HFR1 monoclonal antibodies, and the 21N polyclonal antibody were able to detect specifically the target antigen, we used a cell system that comprises two natural cell lines, A431 and SKBR3, that over express ErbB1 and ErbB2 respectively, and two stably transfected cell lines, HEK293-ErbB3 and NIH 3T3-ErbB4. These four cell lines were used in both immunofluorescence and Western blotting studies. In immunofluorescent studies presented in Figure 3.1., 3.3 (A, C and E) and 3.4 it was shown that the antibodies detected receptor expression in each cell line. No fluorescence was observed in cells treated with the antibodies pre-incubated with the peptides to which they were raised (see section 3.1). This suggests that the antibodies were specifically reacting with the target receptor. We then tested the antibodies by Western blotting. ErbB1 was the first receptor studied and characterised. Among the four receptors in the family, ErbB1 is the easiest to detect as it does not have splice variants. The Western blot presented in Figure 3.8 A shows that the monoclonal antibody F4 specifically detected ErbB1 receptor in A431 cell lysate. The A431 cell line is derived from a squamous carcinoma of the vulva and highly over expresses ErbB1 with an average of 2×10^6 receptors per cell (Haigler et al., 1978) (Cohen, 1997) and consistent with this a band of 180kDa with high intensity was detected in the A431 cell lysate. The SKBR3 cell line is derived from a breast carcinoma with amplified and over expressed ErbB2. The full length of ErbB2 protein has a molecular weight of 185kDa, however the receptor is also present in a truncated form of 100kDa was also identified (Scott et al., 1993). Figure 3.8 B (track 2) shows a band at 185kDa and at 100kDa

suggesting that 21N polyclonal antibody has recognised both ErbB2 variants in SKBR3 cell lysate.

More challenging was the detection of ErbB3. Several attempts, using the monoclonal antibody RTJ2, failed to demonstrate the presence of ErbB3 protein in the cell lysate from HEK293 stably transfected with ErbB3. Several possibilities were taken into consideration to explain the absence of reaction. One explanation was that ErbB3 was proteolytically cleaved either as part of its natural life cycle or more likely due to the release of proteases during cell lysis. Another hypothesis was that the cell line lost the receptor expression after numerous passages or the antibody was not sensitive enough to detect ErbB3 by Western blotting. Hence we used the polyclonal antibody 49.3 which was raised against the same peptide used to raise the monoclonal antibody RTJ2 (Rajkumar et al., 1995). Figure 3.8 D shows that this antibody identified a 160kDa protein in the HEK293-ErbB3 cell lysate which was absent in the HEK293 cell lysate. This indicated both that the HEK293 stably transfected cells expressed ErbB3 and the intact protein was present in the lysate and that 49.3 give superior performance in Western blotting than the RTJ2 antibody.

To date several different sized isoforms of ErbB4 receptor have been identified (Elenius et al., 1999). Alternative splicing of ErbB4 pre-mRNA can occur at the extracellular juxtamembrane region or at the intracellular cytoplasmic tail, generating four different isoforms. HFR1 monoclonal antibody is able to recognise all four of the ErbB4 isoforms as it is directed to a sequence near the carboxy terminus of the protein (Hayes et al.). The isoform expressed in the cell line NIH 3T3 used as a control, is ErbB4-JMa. The blot presented in Figure 3.8 E shows that the monoclonal antibody HFR1 detected a 180kDa protein in NIH 3T3-ErbB4 cell lysate. The JMa but not the JMb of ErbB4 are subject to proteolytic cleavage upon binding to its cognate ligand, thus the cytoplasmic domain of the receptor is released as a lower molecular weight fragment (Carpenter and Liao, 2009). Therefore, the additional band of 80kDa also observed in the same track, it is likely that corresponds to a breakdown product of the protein.

Having shown that the antibodies reacted with the receptor to which they were raised, In order to determine whether there was cross-reactivity, we transiently transfected

COS7 cells with each receptor. We used the cell lysates from A431, SKBR3 and NIH 3T3-ErbB4 as positive controls and non transfected COS7 cells as the negative control. The F4, 21N and HFR1 antibodies detected ErbB1, ErbB2 and ErbB3 respectively in the positive controls (Fig. 3.9 A track 1, B track 2, C track 6). Figure 3.9 A shows a band of 180kDa in transfected COS7-ErbB1 cell lysate but also a much weaker band of the same size in all the other lanes. It has been shown that ErbB1 is expressed endogenously in COS7 cells (Kumagai et al., 2001), which can explain the band detected in non transfected COS7 (Fig. 3.9 A track 6). Therefore we concluded that it is more likely that F4 monoclonal antibody detected ErbB1 in all cell lysates and not that the antibody was cross-reacting with the other receptors. The blot presented in Figure 3.9 C shows a specific band of 180kDa, corresponding to ErbB4 and detected with HFR1 antibody, only in the positive control but not in the other lanes. The reason why the blot in Figure 3.9 C does not show a band in COS7-ErbB4 or why a band with higher intensity was not seen in COS7-ErbB1 cells in Figure 3.9 A may be due to the transfection efficiency. The 21N antibody detected ErbB2 only in the positive control and COS7-ErbB2 cell lysates.

The blots presented in Figure 3.8 A, B and E, apart from the band detected with the specific antibody, show in each cell lysate a band of approximately 180kDa with lower intensity. These bands correspond to endogenous expression of all receptors or could be due to cross-reaction of the antibody with the other receptors. However if F4 was cross-reacting with ErbB2 or ErbB4, bands with the same intensity of the band observed in Figure 3.8 B lane 2 and Figure 3.8 C lane 4 would have been seen. Taken together this data suggested that the antibodies do not cross-react with the other receptors.

3.4.2. CELL IMMUNOFLUORESCENCE WITH QDOTS

The use of Qdots in biology is a relatively new technology. Therefore, before applying Qdots technology to processed paraffin formalin embedded tissues, we evaluated their performance on a cellular system. We chose A431, SKBR3, HEK293-ErbB3 and NIH 3T3-ErbB4 cell lines as they were previously employed to detect the over expressed receptors by immunofluorescence using AlexaFluor 546 labelled secondary antibody (Fig. 3.1 A, C, E and G). The results presented in Figure 3.3 A, C, E and G demonstrate that the anti-mouse secondary antibody labelled with Qdot 525 reacted with the primary antibodies and detected the specific antigen. The Qdot525 signal for this preliminary experiment was visualised using Wide-Field microscopy and the images in Figure 3.3 were acquired using FITC excitation (490nm) and emission filter set (521nm) that is close to the emission of Qdot 525. In order to obtain better experimental results using Qdots optical properties, we subsequently employed laser scanning confocal microscopy (LSCM). As Qdots 525 have a high excitation coefficient in the ultraviolet region of the spectrum, we excited them with the 405nm diode laser line. Qdot signals were collected with 20nm bandwidth with emission centred at 525nm, for Qdot 525, and at 585nm for Qdot 585. Optimisation of other parameters such as laser power, photomultiplier tubes gain and offset were carried out to maximise the Qdots fluorescent signals and obtain brighter and sharper images with better signal to noise ratios. As a consequence the Qdots performance resulted in much higher signals when observed using confocal microscopy. The higher image quality obtained with this microscope is not only due to the more advanced features of laser scanning confocal microscopy, but also to the use of more appropriate excitation light and filter sets. Indeed, the specificity of the binding of the primary antibody was also confirmed with the immunised peptide (Fig. 3.4 third row). The control with omission of primary antibody showed a minimal background fluorescence proving that that Qdots fluorescent signal was also specific (Fig. 3.4 second row).

3.4.3. DOUBLE IMMUNOFLUORESCENCE USING QDOTS

One of the main complications in imaging experiments where specimens are labelled with two or more fluorophores is the bleed-through of fluorescence emission. Bleed-through is the appearance of fluorescence from one fluorophore in the detection channel set up to detect the other fluorophore. This phenomenon mainly occurs with dyes with emission spectra that exhibit a significant degree of overlap. This is due to the fact that the absorption and emission spectra for most organic fluorophores are asymmetrical and exhibit long skewed tails that cover a broad region (Fig. 3.16 A). Compared to the traditional organic fluorophores Qdots excitation and emission are quite different showing a narrow and symmetrical emission spectra profile (Fig. 3.16 B). This, together with their optical features, make Qdots particularly suited for simultaneous immunofluorescence detection of multiple targets.

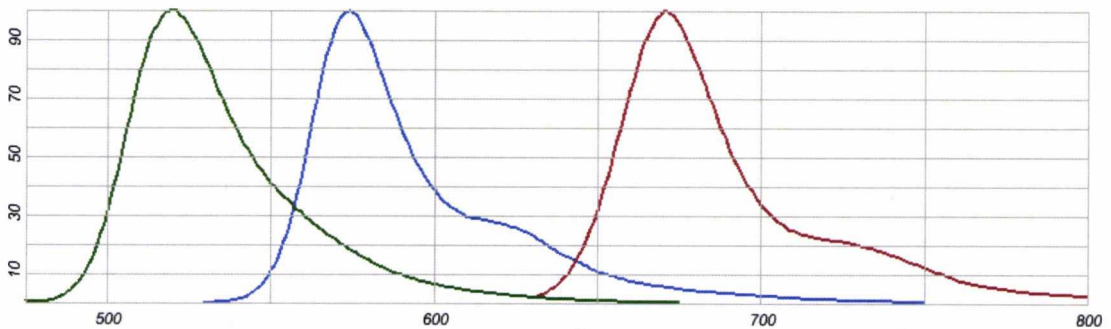
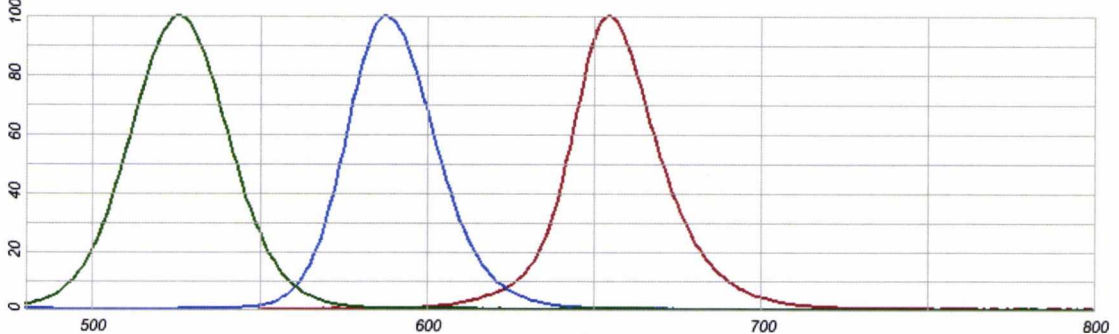
A**B**

Figure 3.16 Comparison between AlexaFluor and Qdot spectra profiles. (A) Emission spectra of AlexaFluor 488, 546 and 647. (B) Emission spectra of Qdot 525, 585 and 655. Figure adapted from <http://www.invitrogen.com/site/us/en/home/support/Research-Tools/FluorescenceSpectraViewer.htm>

First of all, unlike the organic fluorophores, all Qdots can be efficiently excited using a single wavelength in the ultraviolet/violet region of the spectra. Therefore the emission spectrum, which is independent from the excitation wavelength, only depends on the Qdot size. Furthermore, the fluorescence emission spectra have a narrow Gaussian distribution, which is symmetrical with the peak intensity in the centre of the curve. This allows the use of emission filters with narrow bandwidth (e.g. 10nm, 20nm) that reduces the bleed-through.

Double labelling of ErbB2 and ErbB3 in MDA-MB453 cells was carried out by using anti-mouse Qdot 525 and anti-rabbit Qdot 585 secondary antibodies. As the reference spectra of Qdot 525 and Qdot 585 show a minimal spectral overlap, we examined whether in our experiment there was the same low degree of overlap and to what extent this could generate bleed-through. The lambda scan presented in Figure 3.6 showed a presence of low intensity signal from 536nm and 564nm which could be due to the Qdot 525 and Qdot 585 spectra overlap in this area. This was confirmed by examining the plot presented in Figure 3.7. Here the overlapping region is represented by the area underneath the projections of the tail of each Qdot spectrum. However this minimal spectral overlapping did not result in bleed-through artefacts. Indeed the optical properties of Qdots (the symmetrical and narrow emission spectrum) enabled us to collect the images using a more efficient emission filter of only 20nm bandwidth (515nm-535nm and 575nm-595nm) which avoided the overlapping area of the spectra. Furthermore as each channel in the confocal microscope has a separate PMT tubes, different setting can be applied to image simultaneously different fluorophores.

3.4.3. IMMUNOHISTOCHEMICAL STUDIES

The tissue microarray (TMA) technology allows the rapid and effective examination of hundreds of samples simultaneously on a single microscope slide. TMAs can be used for both the detection of proteins, such as tumour markers and gene expression for instance by in situ hybridisation, on fixed paraffin embedded tissues. In this study four TMAs, with 60 cores of breast cancers were used to evaluate receptors expression by immunohistochemistry. Immunohistochemical staining was first introduced by Coons and Kaplan (Coons and Kaplan, 1950) using the direct method (see section 3.3.3).



Although this method was quick, it lacked sensitivity. Therefore, to make this detection system more sensitive, a few years later Coons et al. developed the two step method (Coons and Kaplan, 1950). Since then, different signal amplification methods to improve the sensitivity have been introduced. Among them the avidin-biotin method, which has been used in this study, is the most commonly used method for the detection of protein expression. The main drawback that any avidin-biotin system can have is the possibility of producing high background especially in tissues, such as liver and kidney that are rich of endogenous biotin. However this was not the case in these studies which employed breast cancer tissue or the omission of the first antibody as a control gave little or no signal. To be able to visualise the targeted antigens, the peroxidase enzyme was used. This enzyme reacts with a specific substrate and chromogen, called DAB (see section 3.3.3) and produces a brown coloured precipitate making the reaction of the primary antibody with the antigen visible. After the enzymatic reaction, Gill's haematoxylin stain was performed. The haematoxylin staining helps to visualise the tissue structure and makes it easier to determine the location of the proteins in relation to the tissue architecture.

Immunohistochemistry was performed using F4, RTJ2, HFR1 monoclonal antibodies to detect ErbB1, ErbB3 and ErbB4. The 21N polyclonal antibody was used to detect ErbB2. The performance of all these antibodies was found to be particularly good in this system producing high quality staining with a minimal background. This was evident from observing the signal to noise ratio which is given by the brown stain against the blue background. ErbB1, ErbB3 and ErbB4 gave mainly cytoplasmic immunoreactivity while expression of ErbB2 showed distinctive membranous immunoreactivity in 3+ cases and cytoplasmic staining only in 2+ and 3+ cases. Uniform and circumferential membrane staining has been related to the amplification of ErbB2 gene, whereas expression of the other receptors is not due to gene amplification.

The level of receptor expression in each breast cancer tissue was estimated in each array. The IHC interpretation criteria are based on two parameters: intensity of the stain and percentage of tumour cells stained. Even using these stringent criteria, two main problems need to be taken into consideration. The first one is the ambiguity of

borderline cases such as a strong 2+ or weak 3+. The second is the heterogeneity of the tissue structure and the heterogeneity of the staining. Therefore it is quite difficult to overcome these problems and inevitably it is not possible to completely eliminate a certain amount of subjectivity. In order to reduce the subjectivity of the judgment brown-coloured cytoplasmic and membranous staining were evaluated by two observers and scored after agreement was reached. Interestingly, expression of all four receptors was present in the first three quartiles, however only 1.8% of the breast cancers showed high levels of ErbB4 whereas ErbB2 and ErbB3 were expressed with substantial frequency in the 3+ quartile (Fig. 3.15) The role of ErbB4 in breast cancer is still controversial. While some studies have shown that over expression of ErbB4 is associated with poor prognosis (Abd El-Rehim et al., 2004), other studies linked its over expression to better outcome (well differentiated phenotype, longer survival) (Gullick, 2003; Suo et al., 2002; Witton et al., 2003).

More consistent results have been shown about ErbB3 in breast cancer. Over expression of ErbB3 has been correlated with poorer prognostic futures such as high grade and lymph node metastases (Koutras et al.). The role in breast cancer of ErbB3 receptor alone and when co-expressed with ErbB2 is also becoming clearer. Several studies have demonstrated that co-expression of ErbB2 and ErbB3 has a critical role in tumour progression and development of distant metastases (Alimandi et al., 1995). As explained in the introduction, ErbB3 preferentially forms heterodimers with the ErbB2 receptor and activates signalling pathways involved in cell proliferation, survival and transformation. Moreover, ErbB3 has recently been identified as one of the factors that contributes to drug resistance (Baselga and Swain, 2009) (Hamburger, 2008). A study carried out in the laboratory by a colleague has shown that targeting ErbB3 receptor in combination with Herceptin improves the activity of this drug in inhibiting the growth of breast cancer cells (Blackburn et al.). This evidence led us to focus our attention on ErbB2 and ErbB3 co-expression. We investigated whether there was a correlation between ErbB2 and ErbB3 expressed at the 3+ level using the data obtained from a cohort of approximately 60 breast cancers stained for ErbB2 and ErbB3 separately using Spearman's correlation. The Spearman's rank correlation is a

useful analysis as it tests for correlation between non parametric datasets. When the analysis was performed on 56 samples the result (0.37) showed a weak positive correlation. However when we added 96 samples from a previous study (McIntyre et al.) the correlation was stronger (0.48). This result indicates that if one of the receptors, either ErbB2 or ErbB3, is over expressed it is likely that the other one is also over expressed. The variation between these two results depends on the size of the two datasets used for the analysis, a larger dataset might establish a more reliable result.

4 – APPLICATION OF QDOT TECHNOLOGY ON FORMALIN FIXED PARAFFIN EMBEDDED TISSUES

4.1. INTRODUCTION

In the previous chapter we have shown the use of Qdots labelled secondary antibody for fluorescent immunostaining of cell lines. As the majority of clinical samples are FFPE tissues, in order to develop a system that can be used to quantify biomarkers in FFPE breast cancer tissues, the first objective of this study was to test the applicability of Qdots immunolabelling system on FFPE tissues. Contrarily to IHC method Qdot immunofluorescent staining is a new technique for which there is not a well characterised staining protocol. Therefore, in order to develop a Qdots immunofluorescent system for quantitative analysis of protein expression, our second goal was to create a standardised experimental procedure. For ethical reasons we carried out the work on FFPE rat pancreas tissues, prior to use the tissue arrays containing human tissues. Then we applied the standardised protocol on human breast cancer tissues. Thereafter, in a preliminary experiment, we tested the ability of Qdot525 to detect different levels of ErbB2 expression using an ErbB2 control arrays with four cores each, graded as 0, 1+, 2+ and 3+ by IHC.

Imaging experiments having fluorescent labels are often complicated by the presence of autofluorescence. The autofluorescence is the major source of unwanted background particularly in FFPE tissues. The autofluorescence is an intrinsic property of biological specimens generated by endogenous fluorophores and it is independent from the addition of fluorochromes. Biochemical sources of autofluorescence are flavins, NADH and NADPH, lipofuscins, collagen and elastin (Billinton and Knight, 2001). All these substances absorb light from UV (405nm) and blue (488nm) light and have a broad emission which can vary from approximately 420nm to 650nm. Another source of autofluorescence is also represented by fixatives which are used for the preservation of tissues. In order to overcome this problem, we used two different approaches. First we tried to reduce the autofluorescence by irradiating the specimen with a strong light (a method called photobleaching), second we studied the autofluorescence emission profile, generated by our samples, and we determined the

Qdot fluorescence emission in order to extract useful information to improve the signal to noise ratio.

4.2. AIMS

- I. Test the ability of Qdot secondary antibody to detect specific antigens on FFPE tissues.
- II. Develop a standard Qdot-immunofluorescence method.
- III. Apply the standardised protocol on breast cancer tissues to detect different levels of expression of ErbB2 by Qdot525.
- IV. Reduce the autofluorescence emission.
- V. Improve the signal to noise ratio.

4.3. RESULTS

4.3.1. DETECTION OF α -CELLS ON RAT PANCREAS

In order to investigate the ability of Qdot secondary antibody conjugates to specifically detect target proteins in FFPE, we used multi-blocks of rat tissues which were made in the laboratory (see section 2.7.2). Islets of Langerhan are special groups of cells in the pancreas, which make and secrete hormones. While the cytoarchitecture of the islet differs across species, the cell composition is the same. Each islet comprises at least five distinct cell types. In particular, in rat islets α -cells are located in the periphery of the islet and make and release glucagon, a hormone that raises the glucose level in the blood. This represented a useful control system as, due to the particular location of the α -cells, the staining pattern was easy to observe. Experiments were performed using anti-glucagon as primary antibody. We labelled α -cells in the Islet of Langerhan with a primary antibody directed to glucagon and we stained the tissues by IHC and by immunofluorescence using AlexaFluor546 labelled second antibody or Qdot 525 labelled secondary antibody. Specific signals were observed in all experiments. Rat sections stained by IHC exhibited brown staining colour in the expected position and pattern of the α -cells (Fig 4.1 A); Figure 4.2 A shows the islet of Langerhan stained with AlexaFluor546 secondary antibody (red fluorescent signal) and Fig. 4.3 A with Qdot 525 secondary antibody both of which specifically labelled α -cells. As a control, rat tissues were stained in the absence of primary antibody. No signals were observed in these tissues (Fig 4.1 B 4.2 B, 4.3 B) confirming the specificity of the staining.

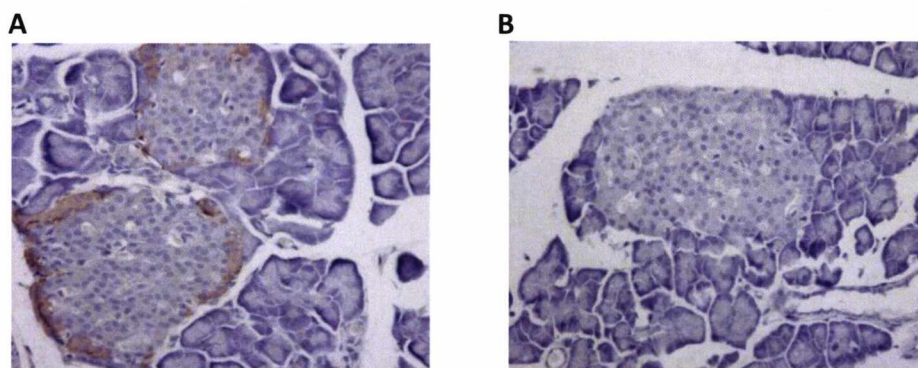


Figure 4.1 Immunohistochemical staining of rat pancreas tissues. (A) α -cells were stained (brown colour) using anti-glucagon primary antibody. (B) control in absence of primary antibody. Images were acquired with Leica Leitz DMRB microscope, original magnification x20.

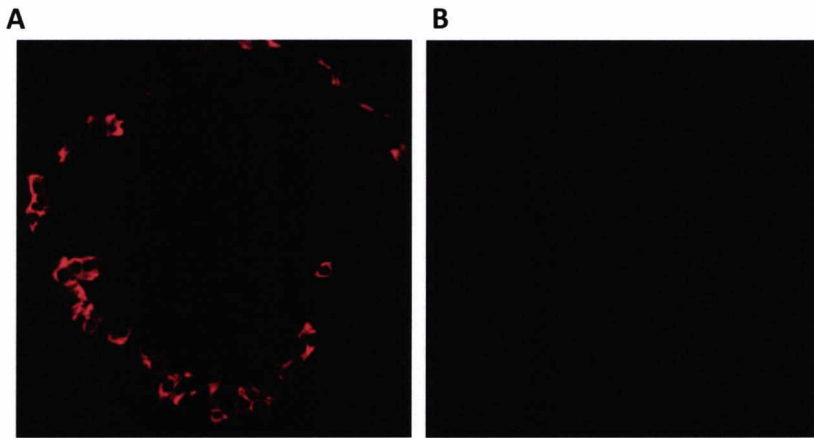
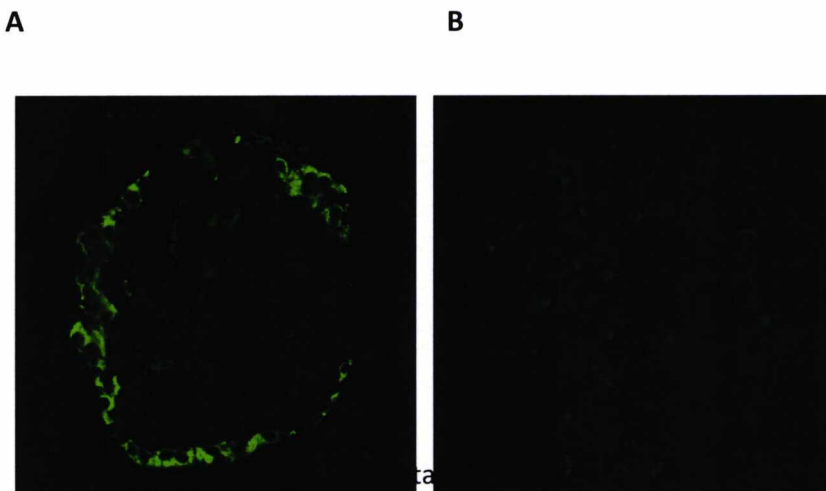


Figure 4.2 Immunofluorescent staining of rat pancreas tissue with AlexaFluor 546 anti-mouse secondary antibody. (A) α -cells stained with anti-glucagon primary antibody and AlexaFluor 546 secondary antibody. (B) control where primary antibody was omitted. Images were acquired with Leica SP2 confocal microscope. Original magnification 63x. AlexaFluor 546 was excited with HeNe 543nm laser line and the images were captured using emission filter 550nm-610nm.



anti-glucagon primary antibody and anti-mouse Qdot 525 secondary antibody. (A) Specific green fluorescent signal was observed in the expected pattern of α -cells. (B) Control with omission of primary antibody. Rat sections were incubated for 2h at room temperature with Qdot 525 secondary antibody. Images were acquired with Leica SP2 confocal microscope. Original magnification 63x. Qdot 525 were excited with 405nm laser line and images were captured with emission filter 515nm-535nm.

4.3.2. ESTABLISHING STANDARD PROTOCOL FOR QDOT LABELLING

In order to obtain reproducible and accurate measurements of fluorescent intensities, without them being affected by experimental procedures, we established a Qdot-immunofluorescence standard protocol (see section 2.9.1). The fluorescent signal of Qdot 525 was optimised first on FFPE rat pancreas tissues. We stained α -cells in the islets of Langerhan with anti-glucagon primary antibody and Quantum dots 525 secondary antibody. We stopped the incubation with the secondary antibody at different time points (15min, 1h, 2h, 4h and 8h) to determine the optimum time for treatment. No signal was observed in tissues incubated for 15min with Quantum dots 525 secondary antibody (Fig. 4.4 A) in comparison to the control. Green fluorescent signal was detected in tissues incubated for 1h (Fig. 4.4 B), 2h (Fig. 4.4 C), 4h (Fig. 4.4 D) and 8h (Fig. 4.4 E). However as shown in Figure 4.4 B the signal intensity obtained when tissues were incubated with the secondary antibody for 1h, was weaker than the signal intensities recorded with longer incubations (Fig. 4.4 C, D and E). As no major differences of fluorescence intensities were observed among 2h, 4h and 8h incubations we decided to choose 2h incubation in all subsequent experiments. Control with omission of the primary antibody was performed. The longest incubation time (8h) for the Qdot 525 secondary antibody was applied to the control section in which the first antibody was omitted and no fluorescent signal was observed (Fig. 4.4 F).

Once we established the secondary antibody incubation time, we optimised the concentration of the Qdot 525 secondary antibody. Figure 4.5 shows a comparison of the immunofluorescent staining of islets of Langerhan using the Qdot 525 secondary antibody at concentrations of 10nM, 20nM, 30nM and 40nM. Qdot 525 again showed fluorescent signal in the α -cells in the periphery of the islets. The section at 10nM (Fig. 4.5 A) showed a weaker signals compared to the sections stained with 20nM (Fig.4.5 B), 30nM (Fig. 4.5 C) and 40 nM (Fig. 4.5 D). Sections at 30nM and 40nM were over-stained. The highest concentration (40nM) for the Qdot 525 secondary antibody was applied to the control section and no fluorescent signal was observed (Fig. 4.5 E). The immunofluorescent staining results suggested that Qdot525 secondary antibody

at 20nM was the optimal concentrations giving a good signal to noise ratio and was ultimately used for this study.

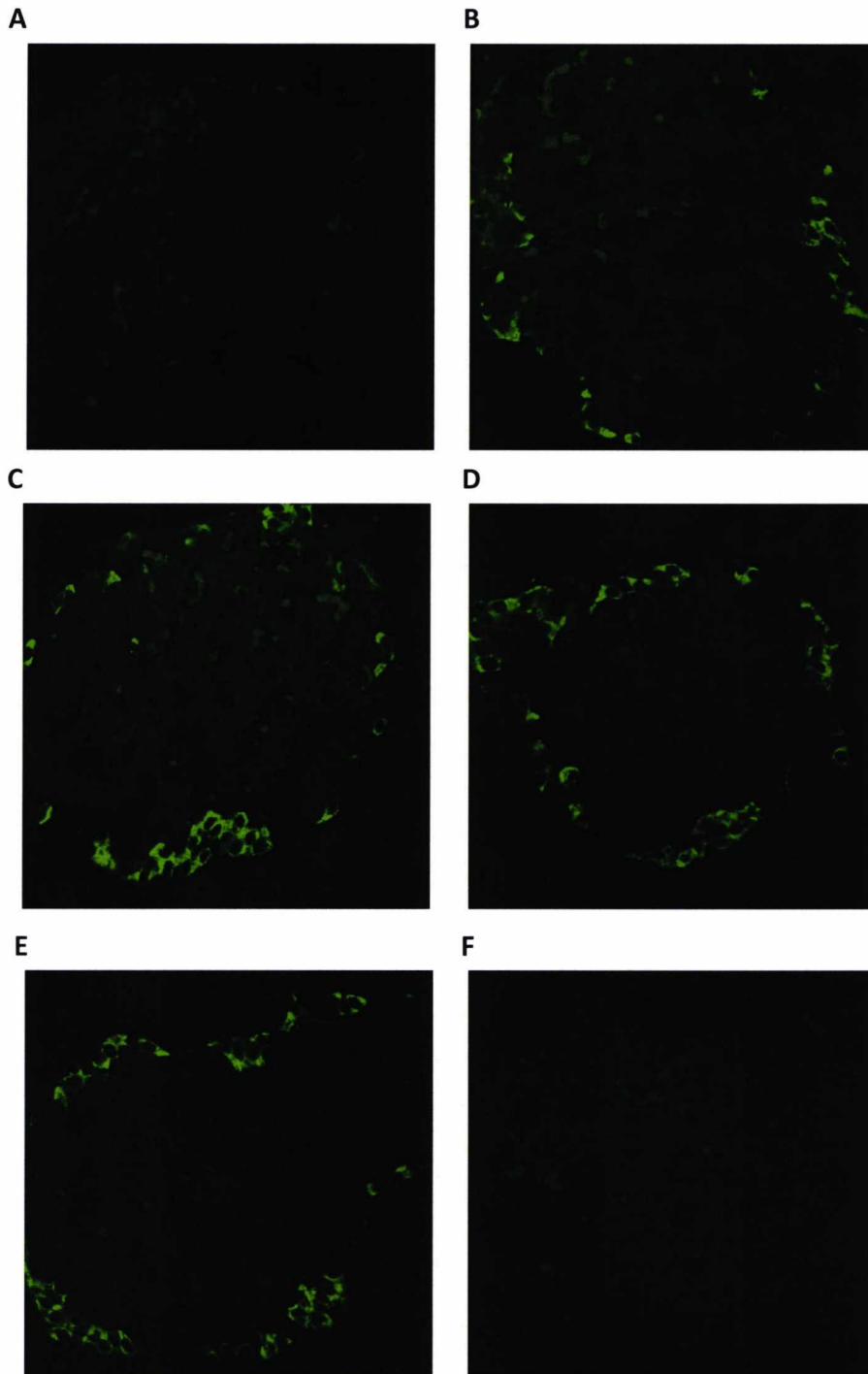


Figure 4.4 Optimisation of incubation time of Qdot 525 anti-mouse secondary antibody. (A) 15min incubation, (B) 1h incubation, (C) 2h incubation, (D) 4h incubation and (E) 8h incubation. (F) The control section, where primary antibody was omitted, was incubated with Qdot 525 secondary antibody for 8h. The same setting was used for all the image acquisition. All images were captured with Leica SP2 Laser Scanning Confocal Microscope using and 63x oil immersion lens.

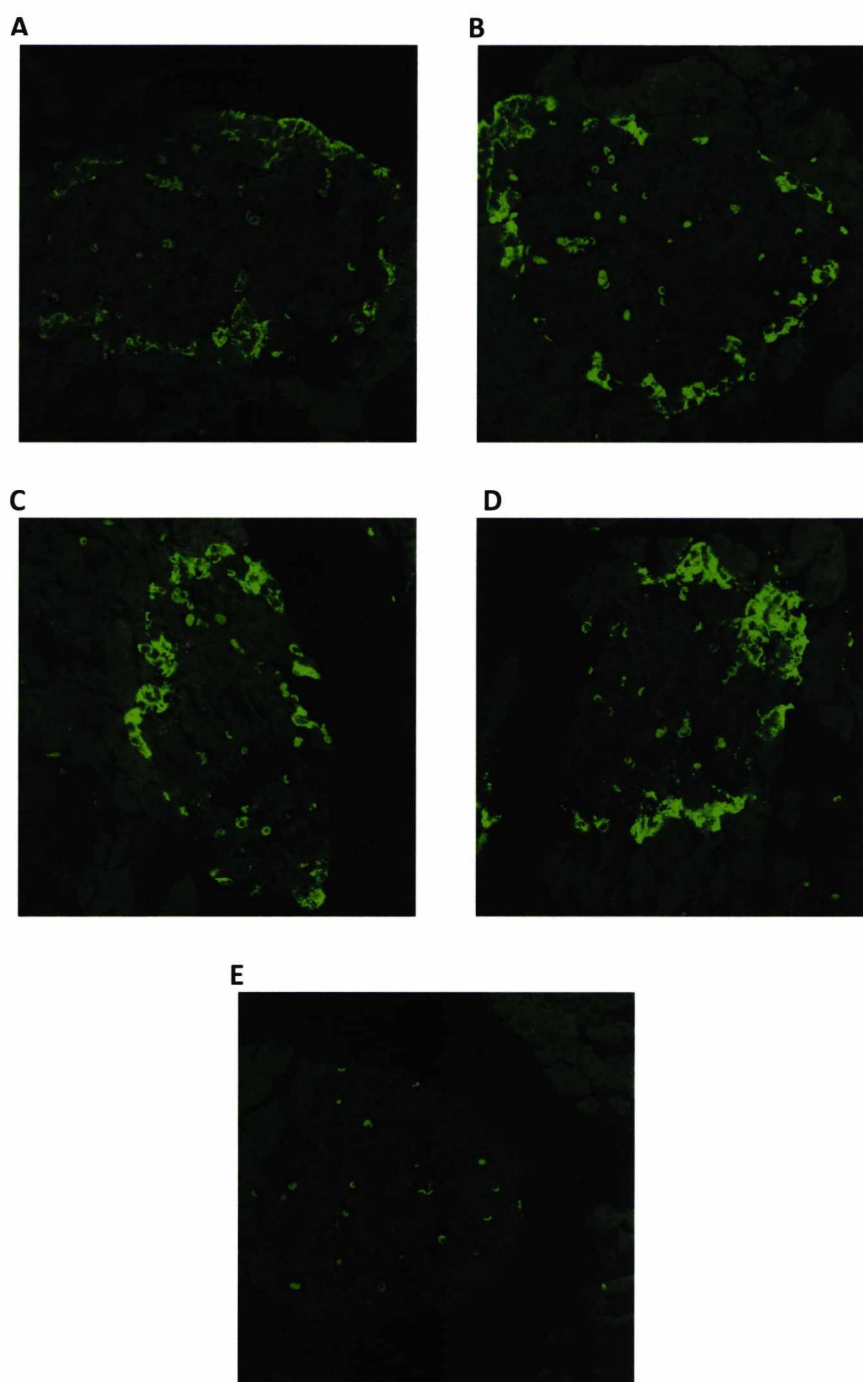


Figure 4.5 Optimisation of Qdot 525 anti-mouse secondary antibody concentration. All sections were incubated for two hours with different Qdot 525 secondary antibody concentrations: 10nM (A), 20nM (B), 30nM (C) and 40nM (D). 40nM concentration was used for the control where the primary antibody was omitted (E). Images were taken using Leica SP2 Laser Scanning Confocal Microscope and 63x oil immersion lens. The same setting was used to capture all the images.

4.3.3. DETECTION OF ERBB2 EXPRESSION IN A BREAST CANCER TISSUE ARRAY CONTROL

In order to evaluate the performance of Qdot 525 secondary antibody conjugates to assess ErbB2 status, an ErbB2 control microarray slide with four cores of breast cancer tissues that correspond to different level of ErbB2 expression graded as 3+, 2+, 1+ and 0 was used. Both conventional IHC (Fig. 4.6) and immunofluorescent staining with Qdot 525 secondary antibody (Fig. 4.7) were performed using the CB11 mouse monoclonal antibody.

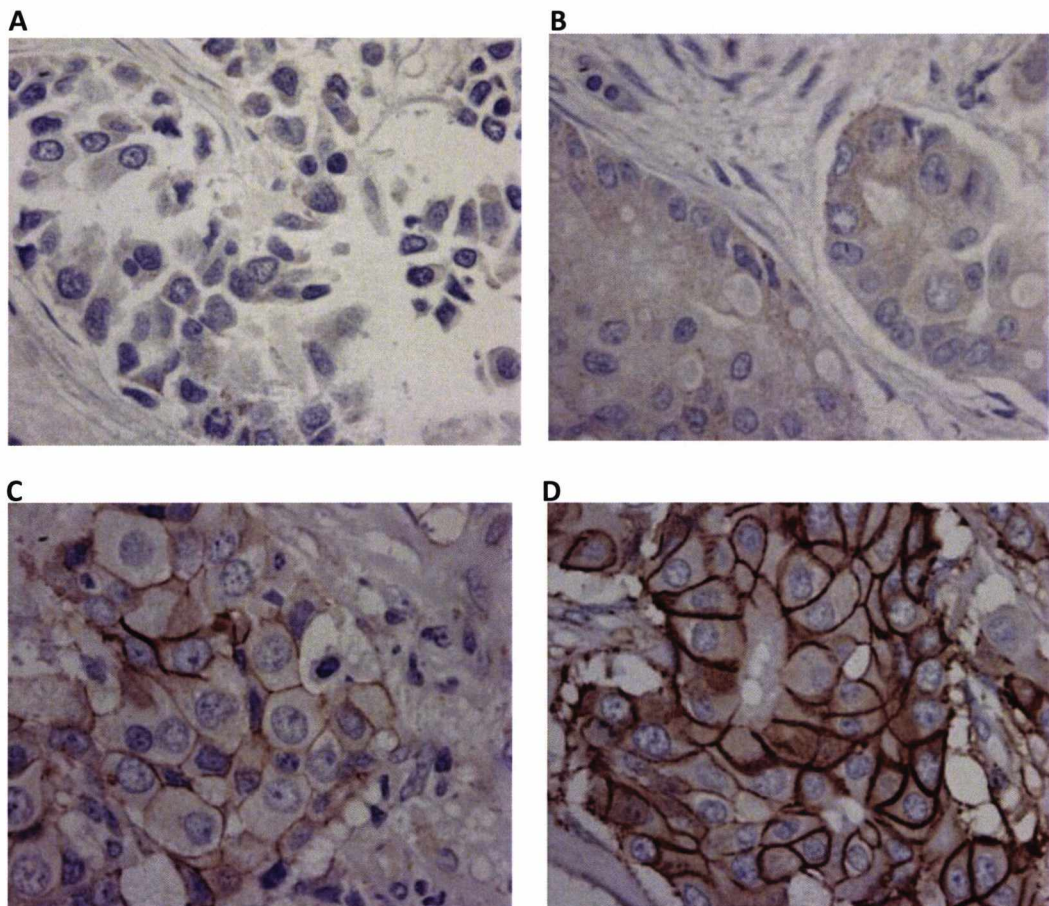


Figure 4.6 Immunohistochemistry (IHC) test performed on a control microarray slide with four cores of breast cancer tissues that correspond to different levels of ErbB2 expression graded as 0 (A), 1+ (B), 2+ (C) and 3+(D). Protein levels of expression are determined on the base of brown stain intensities.

Figure 4.7 shows immunofluorescent staining performed with Qdot 525 secondary antibody. Complete membrane staining forming a thick ring was observed when ErbB2 was expressed at 3+ levels (Fig. 4.7 D). Here the staining is represented by the green fluorescent signal, which is shown as a bright green (Figure 4.7 D). When the receptor was expressed at the lower level of 2+ it was still possible to see the specific signal represented by a thinner green fluorescent ring around the cell. However in this case, in order to distinguish the specific signal from the background, it was necessary to increase the gain and the magnification (Fig. 4.7 C). Despite the same higher gain and magnification being employed to detect ErbB2 at 1+ level, no specific signal was observed (Fig. 4.7 B). As expected, only tissue fluorescence emission from the sample, called autofluorescence (refer to section 4.3.3) was identified in the specimen graded as 0 (Fig.4.7 A).

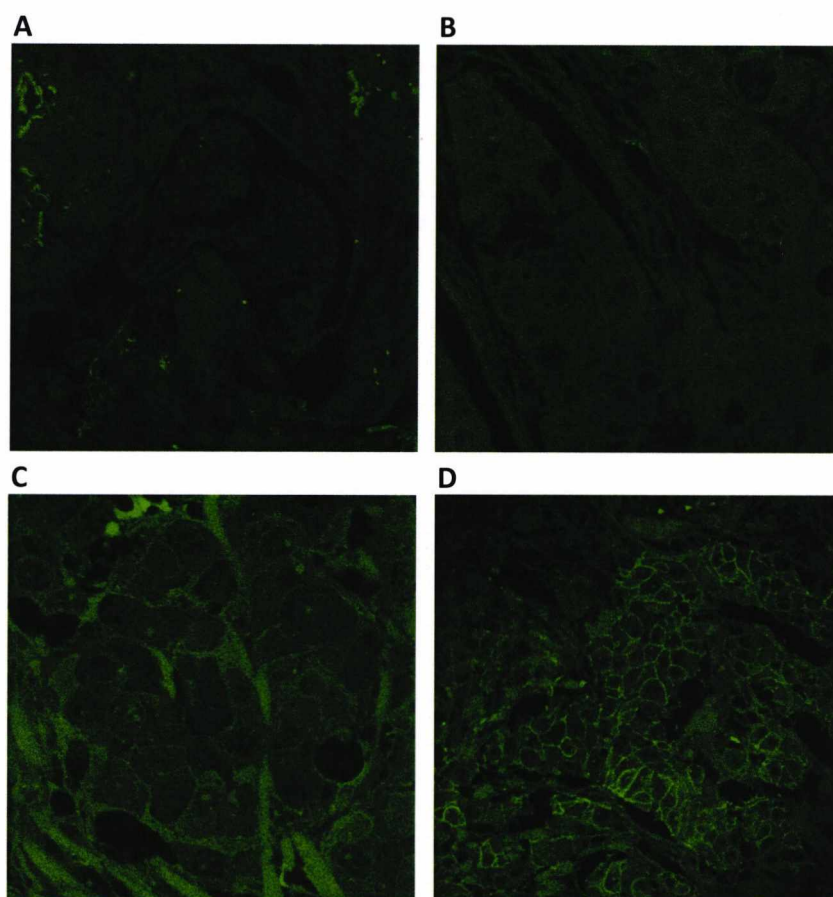


Figure 4.7 Breast cancer ErbB2 control array stained with CB11 mouse primary antibody and Qdot 525 anti-mouse secondary antibody. (A) correspond to ErbB2 scored as 0 by IHC, (B) correspond to ErbB2 scored as 1+ by IHC, (C) correspond to 2+ ErbB2 expression and (D) correspond to ErbB2 3+ expression by IHC. The balance and contrast of all images were increased by 25 % using Adobe Photoshop version 6.0.

The fluorescent green background that is visible in all the images in Figure 4.7 corresponds to the tissue autofluorescence. While the autofluorescence may be a useful tool to see the tissue structure and can help to identify the area of interest (e.g. tumour cells), on the other hand it is a significant problem as it often results in masking the specific fluorescent signal due its broad emission (section 4.1). In order to better evaluate the emission signal generated by the Qdot 525 in the four specimens examined, we tried to improve the separation between the autofluorescence signal and the specific signal by spectral unmixing. Spectral unmixing is a method of separating the signals from various fluorophores into individual channels based on their spectral profile (Kraus et al., 2007; Hibbs et al 2006). The Spectral Dye Separation tool, available in the Leica confocal software package is based on this linear unmixing method. To be able to unmix spectral data in our samples using this function, lambda stacks (with a spectral window of 10nm each) for each specimen were collected. Then reference spectra for both Qdot 525 and the autofluorescence were determined using chosen reference regions in the image. For the Qdot 525 a region was chosen where the fluorescent emission of the fluorochrome was particularly obvious and for the autofluorescence an area was identified with lowest signal and where no Qdot 525 signal was observed. Based on these reference spectra the computer unmixed the data and extracted regions of the specimen having a similar spectral fingerprint. In this way the software generated two separated images. Figure 4.8 shows an example of spectral separation based on the linear unmixing method applied to a lambda stack performed on the breast cancer sample scored as 3+ by IHC. Compared to Figure 4.7 D, Figure 4.8 A shows a sharper and brighter fluorescent signal around the cell membrane corresponding to the Qdot 525 signal. Figure 4.8 B shows in a pseudo-colour, only the background contribution. The same method was also applied to the lambda stacks recorded from the other three samples (data not shown).

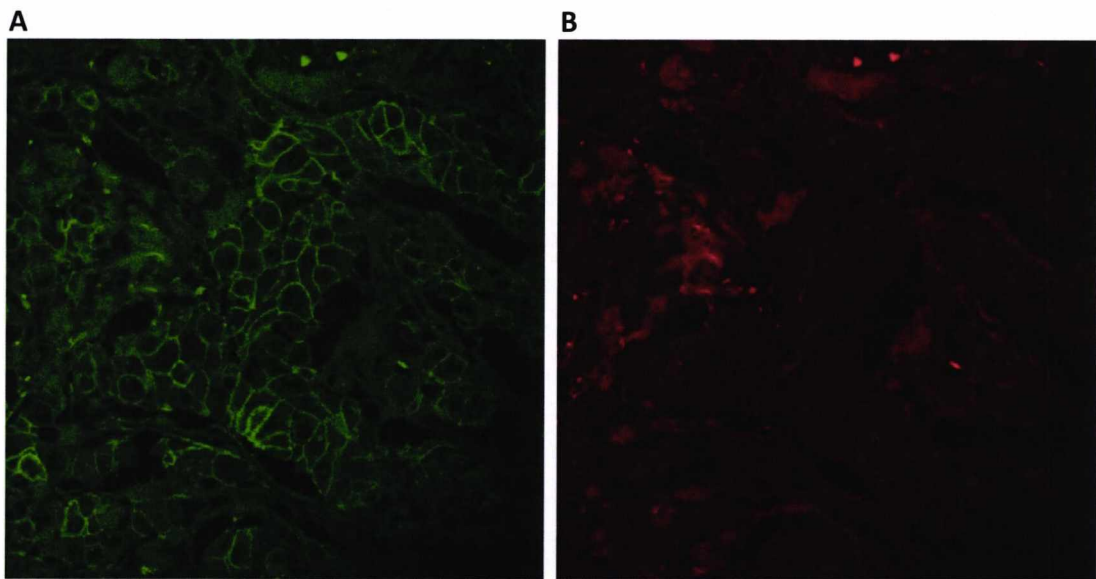


Figure 4.8 Spectral separation of Qdot 525 fluorescent signal and autofluorescent signal. The separation was obtained using the Spectral Dye Separation tool in the Leica Lite software. In this example we used a breast cancer tissue with ErbB2 3+ expression (Fig. 4.7 D). Two reference regions were chosen within the image, one for the autofluorescence and one for the Qdot 525 signal. Based on these reference regions the software generated two images, one with the Qdot 525 signal (A) and one with the autofluorescence (B). The separation between the two signals was improved compared to Figure 4.7 D. Although a brighter and sharper Qdot 525 signal is noticeable in (A), a strong background was still present. In both images the balance and the contrast were increase by 25% using Adobe Photoshop version 6.0.

Figure 4.9 shows the overlaid two-colour images from the four breast cancer specimens. The spectral unmixing method has enhanced the data quality as shown in the merged images. In these images it is possible to determine more clearly different Qdot 525 fluorescent intensities according to the different ErbB2 levels of expression in the four breast cancer tissues. However the separation from the background is not complete as it can be seen in the merged images presented in Figure 4.9 where the yellow/orange background indicates that there is still overlapping between the green pixels and the red pixels.

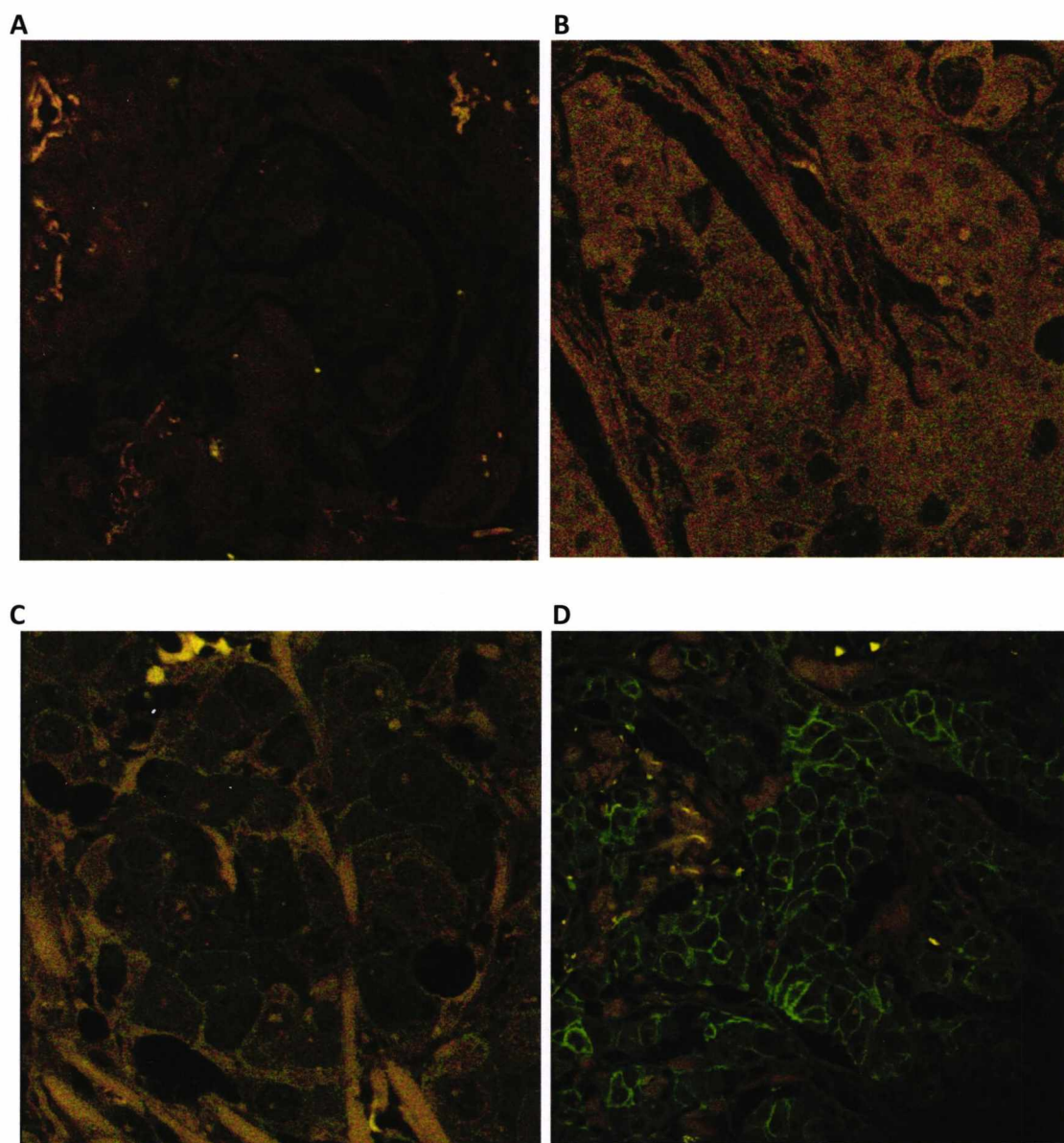


Figure 4.9 Merged two-colour images of the green and red channel after spectral reassignment. Breast cancer tissues with different ErbB2 levels of expression (A) 0, (B) 1+, (C) 2+ and (D) 3+. Brightness and contrast were increased by 25% in all images with Adobe Photoshop version 6.0.

4.3.4. AUTOFLUORESCENCE STUDIES IN FFPE TISSUES

In the following studies experiments were carried out to develop a method to reduce the background by quenching the autofluorescence first and then to examine in more details the autofluorescence profile in both rat tissues and breast cancer tissues in order to use this information to overcome this problem.

4.3.4.1. REDUCTION OF AUTOFLUORESCENCE BY PHOTBLEACHING

Photobleaching is a process whereby the amount of the light emitted by an excited fluorescent molecule decreases substantially with time. This phenomenon consists of a photochemical modification of the dye, induced by prolonged illumination, resulting in the irreversible loss of its ability to fluoresce. The photobleaching phenomena occurs when the absorption of radiation causes a shift of the ground energy level (S) to a higher energy level, either a singlet-excited state (S*) or triplet-excited state (T*) (Song et al., 1996). This temporary excess of energy can be dissipated by emission of fluorescence or by a process called intersystem crossing. In this process the fluorophore in the triplet-excited state reacts with oxygen, which is normally present in the environment as triplet ground state, generates singlet oxygen and returns to the lower energy level (ground state) (Di Aspro et al. 2006). During this process photons are emitted by the fluorophore until it is destroyed.

As this is true for any fluorescent molecule either exogenous or endogenous, we decided to reduce the autofluorescence by exposing the tissues to a strong light. Using confocal microscopy with an oil immersion 63x objective lens the specimens were irradiated with 488nm laser light at the maximum power for different times: 0min, 10min, 30min and 60min (Fig. 4.10 T0, T1, T2 and T3). After each exposure, images were acquired with the 40x objective lens to evaluate whether and to what extent the laser light illumination induced a reduction of autofluorescence. The mean intensity of the tissue fluorescence of a region of interest within the irradiated area was calculated at each time point using confocal software (Fig. 4.11). Figure 4.11 E shows that the autofluorescence intensity was significantly reduced after 60min exposure.

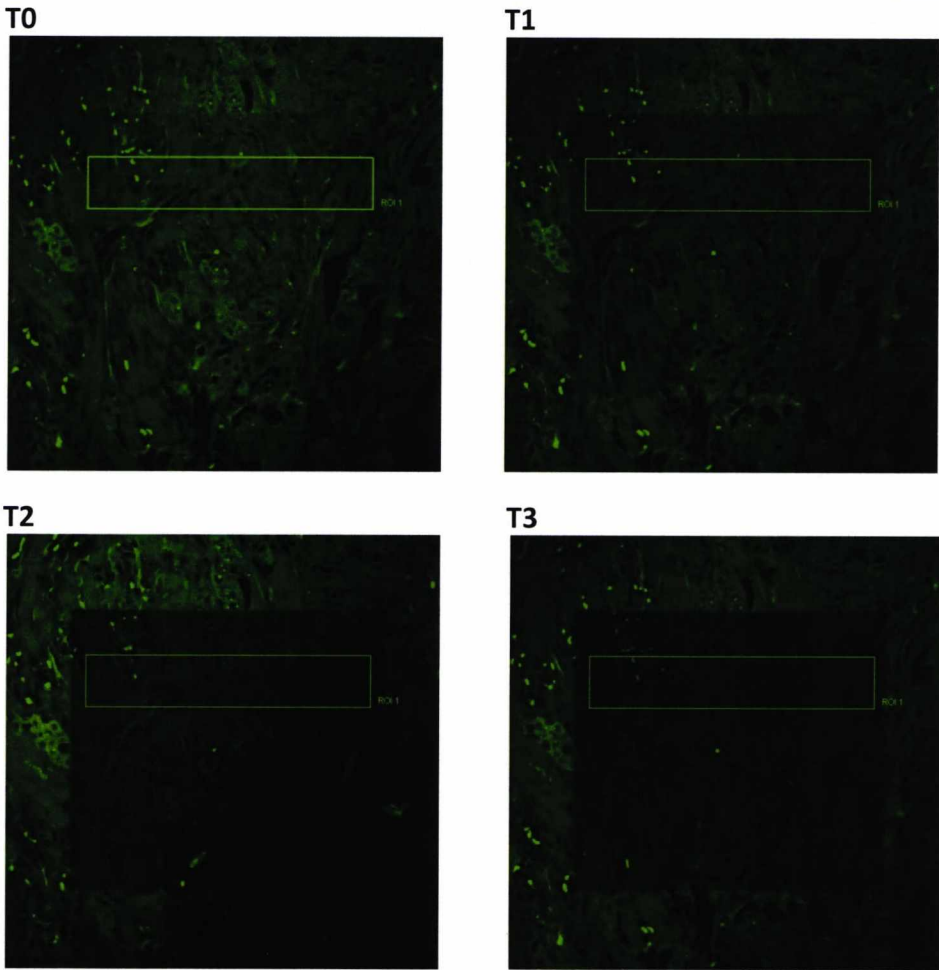


Figure 4.10 Photobleaching method to reduce the autofluorescence. A breast cancer section was irradiated with 488nm laser light through a 63x objective lens for different times: (T0) 0min, (T1) 10min, (T2) 30min and (T3) 60min. Images were acquired with 40x objective lens. (E)

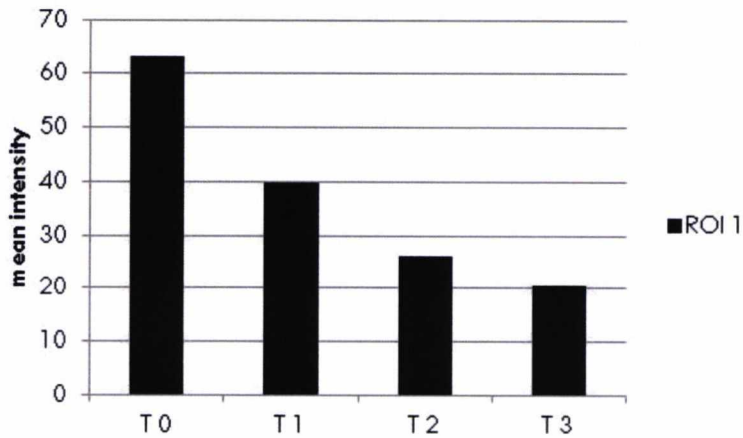


Figure 4.11 Photobleaching effect on the autofluorescence. In the histogram are reported the mean intensity values corresponding to region of interest (ROI) shown in Figure 4.10. The histogram demonstrates that autofluorescence was significantly reduced after 60min (T3).

4.3.4.2. STUDY OF AUTOFLUORESCENCE SPECTRA PROFILE IN RAT PANCREAS AND BREAST CANCER TISSUES

As mentioned above, the autofluorescence profile is very broad and might vary between tissues depending on the presence of different endogenous molecules and on the use of fixatives. Therefore we determined the spectral profile of the autofluorescence using a FFPE rat pancreas section where neither the primary antibody nor the secondary antibody was added. A lambda scan of the islet of Langerhans, from 418nm to 670nm, was recorded from this unstained section using 405nm laser line as the excitation source (image not shown). The emission signal of every lambda stack, of two defined regions of interest (ROI) (Fig. 4.12 A), was calculated with the Leica Lite confocal software and expressed as linear combination of the wavelength (Fig. 4.12 B). The graph in Figure 4.12 B shows that the two autofluorescent spectral profiles corresponding to two different regions in the specimen while differing in magnitude gave identical profiles at with peak emission at approximately 505nm.

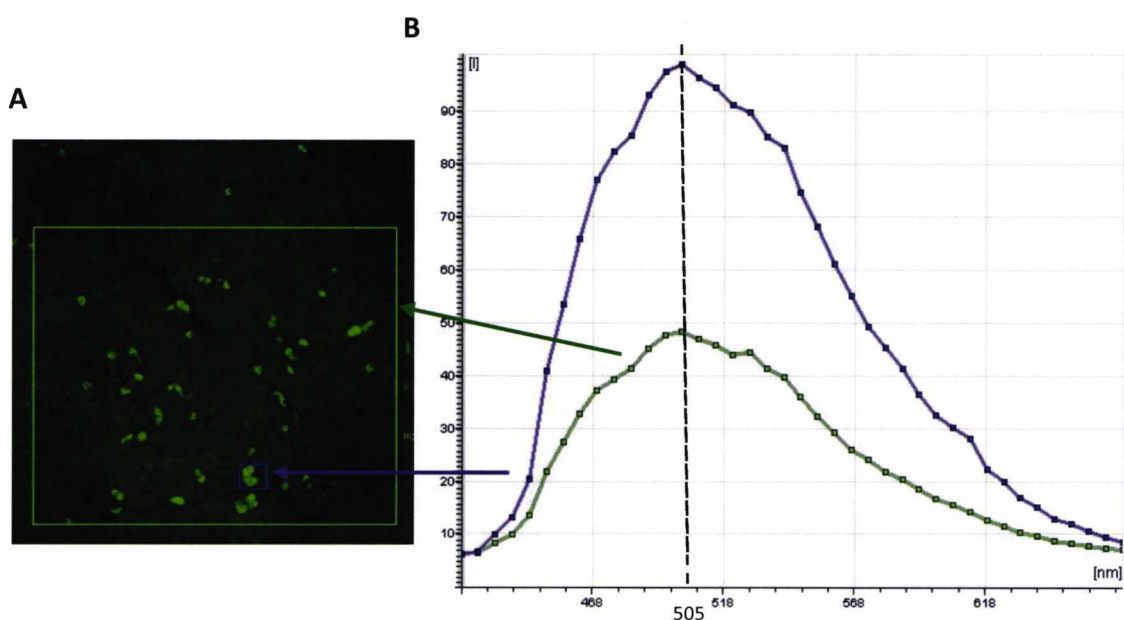


Figure 4.12 Autofluorescence in a FFPE rat pancreas tissue. (A) the image shows the autofluorescent signal only of an unstained islet of Langerhans in rat pancreas tissue. (B) shows the autofluorescence spectra profiles corresponding to two different regions which are indicated with purple and green colours. Autofluorescence peak emission is at 505nm.

We then determined the autofluorescence spectral profile in a series of breast cancer tissue sections using a breast cancer array with 60 cores. The experiment was carried out following the procedure described in section 2.9 with the difference that the incubations were performed with PBS only instead of primary and secondary antibodies. This allowed us to strictly evaluate the background signal and the spectra profile generated only by the tissue autofluorescence within different areas of the same core and also between cores. Five samples were analysed. Lambda stacks from five regions of each core were acquired using the same setting and then were examined with the Leica Lite confocal software. Figure 4.13 shows two representative examples of breast cancer tissues from two different cases which have very different autofluorescence emission intensity. Figure 4.14 and 4.15 show the emission spectra profile that corresponds to tissue area presented in Figure 4.13. The emission spectra that correspond to different areas of the same tissue show that autofluorescence emissions have similar magnitude and broad profile (Fig. 4.14 and 4.15). By comparing the emission spectra of two different cores, it was observed that, while the intensity of the autofluorescence is very different between cores, the spectral profiles are still similar. All graphs reported in Figure 4.14 and 4.15 show broad emission profile with the highest emission between 490nm and 535nm (shown in grey).

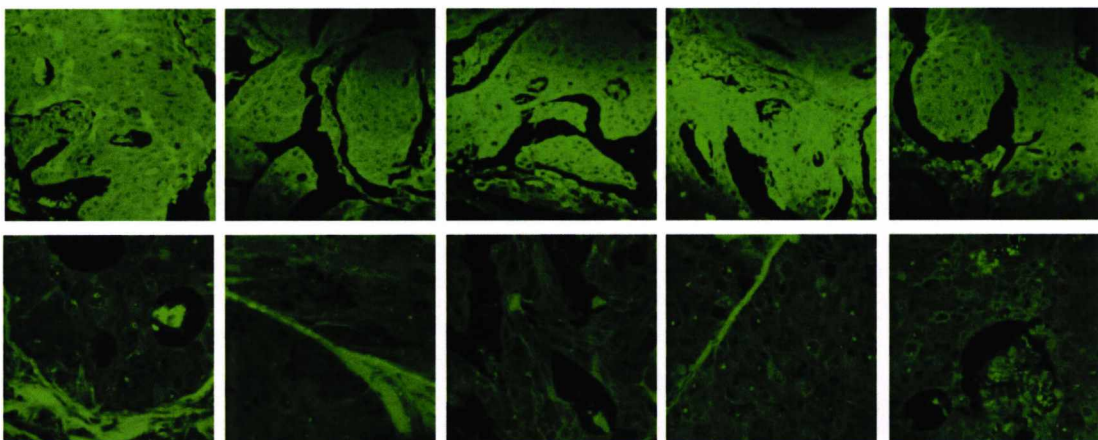


Figure 4.13 Variation of the autofluorescence between two different FFPE breast cancer tissues. Five images were taken from different areas within the same section.

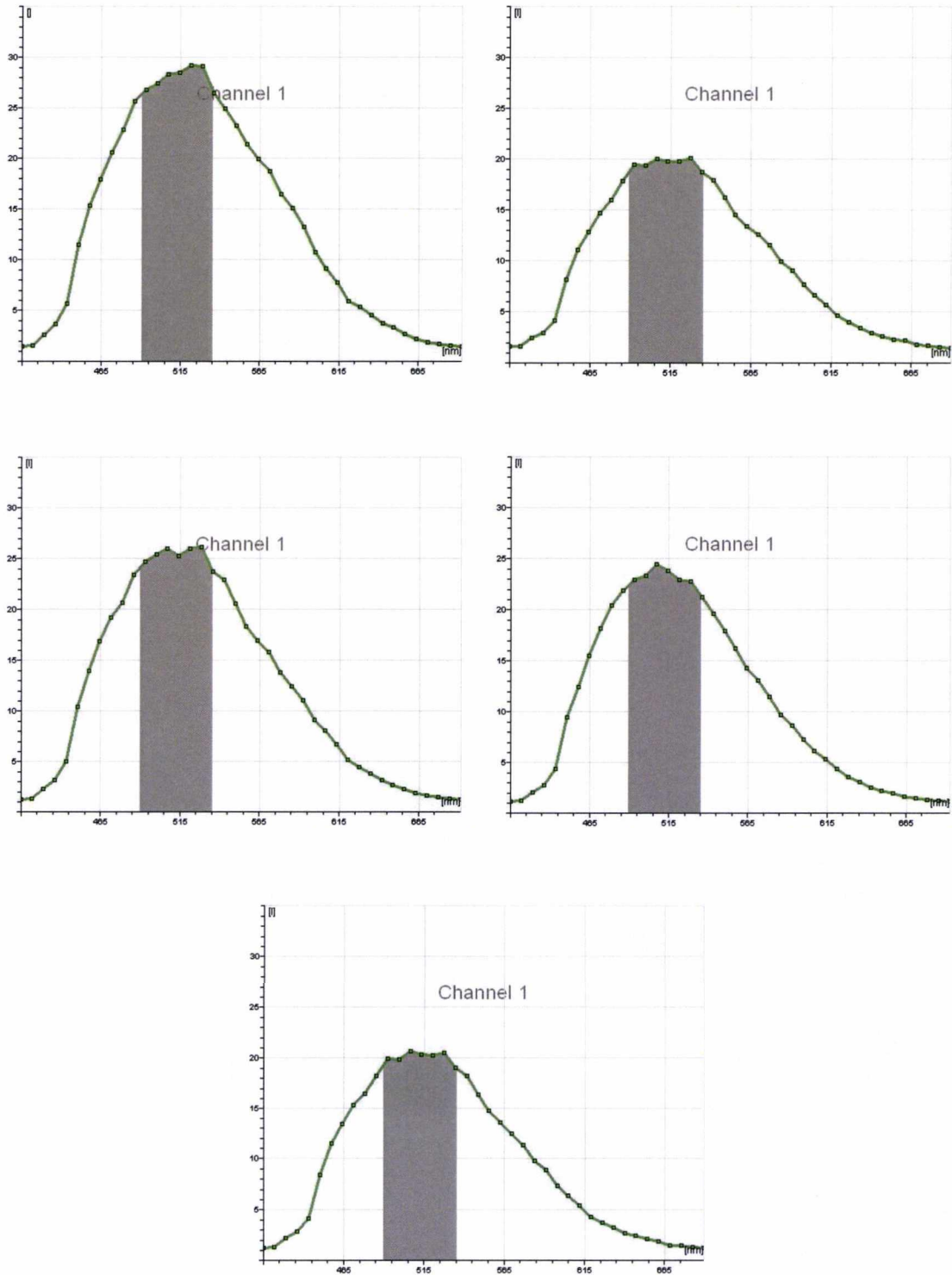


Figure 4.14 Autofluorescence emission spectra profiles from the tissue areas shown in Figure 4.13 first row. The highest emission of the autofluorescence was observed between 490nm and 535nm and it is indicated in grey.

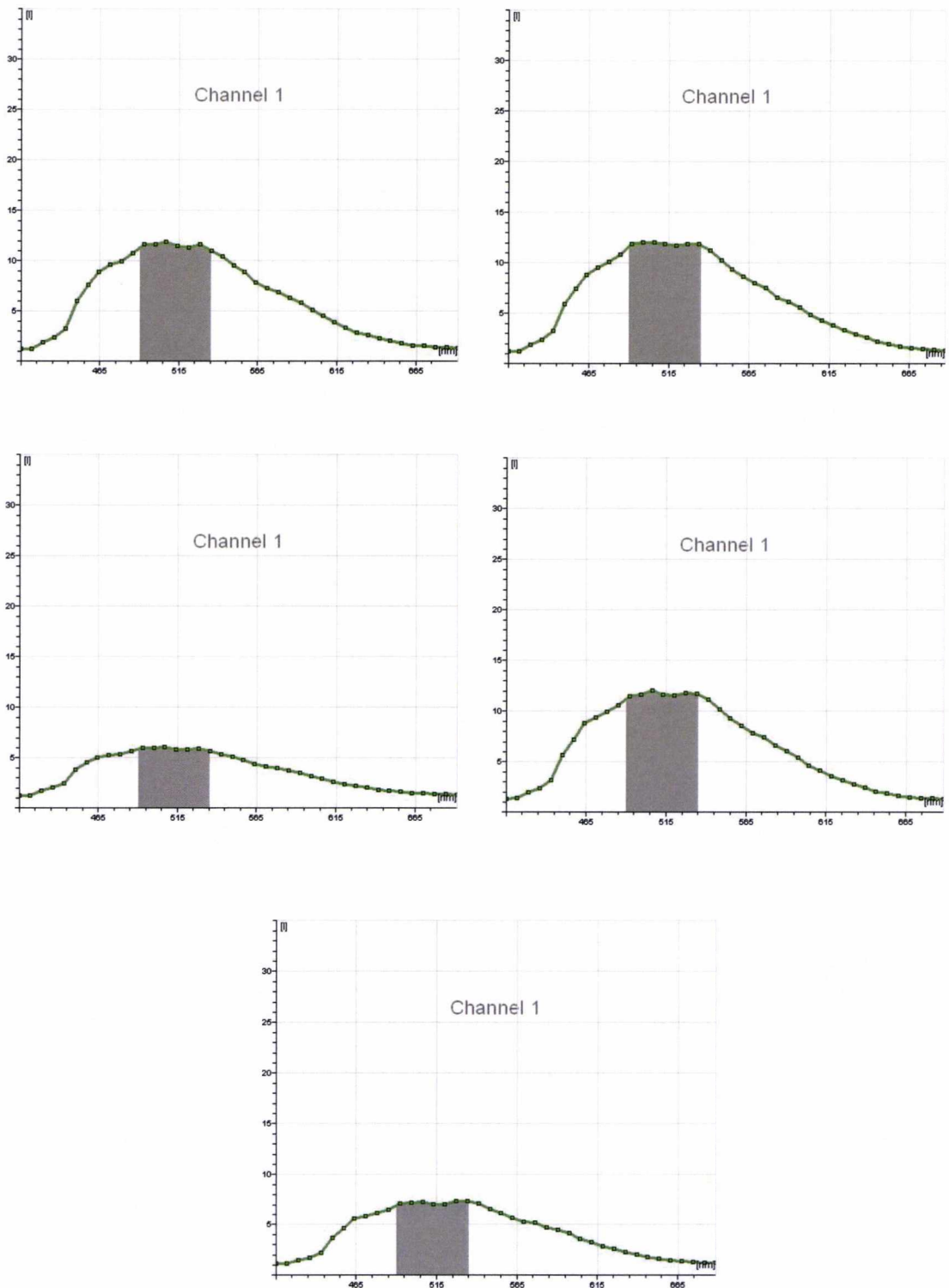


Figure 4.15 Autofluorescence spectra profile of the tissue areas shown in Figure 4.13 second row. The highest contribution of the autofluorescence, from 490nm to 535nm, is shown in grey.

4.3.4.2. Qdot 525 AND QDOT585 SPECTRA PROFILE AND REDUCTION OF AUTOFLUORESCENCE

As shown in the previous section, the highest autofluorescence emission intensity falls between 490nm and 535nm and then decreases until it becomes negligible. Figure 4.16 shows the spectra profile of Qdot525. It is clear that the Qdot525 emission occurs in the region of the spectrum where the autofluorescence emission is higher (Fig. 4.14 and 4.15). Therefore, in order to improve the signal to noise ratio by minimising the autofluorescence, we considered employing a Qdot conjugated secondary antibody that has its emission peak at 585nm (Fig. 4.17), where the autofluorescence emission is lower.

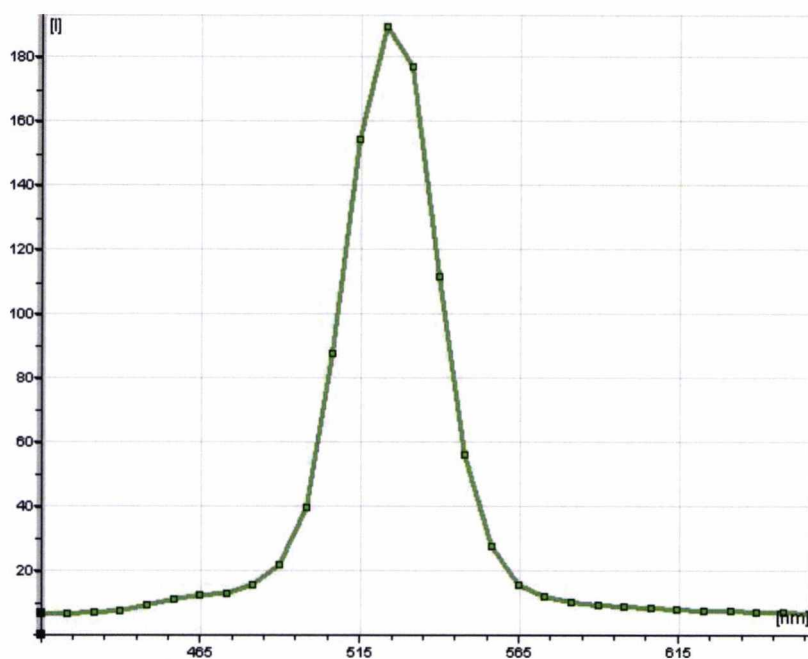


Figure 4.16 Emission profile of Qdot 525 when excited with 405nm laser light. The major contribution of Qdot 525 fluorescent signal is between 515nm and 535nm.

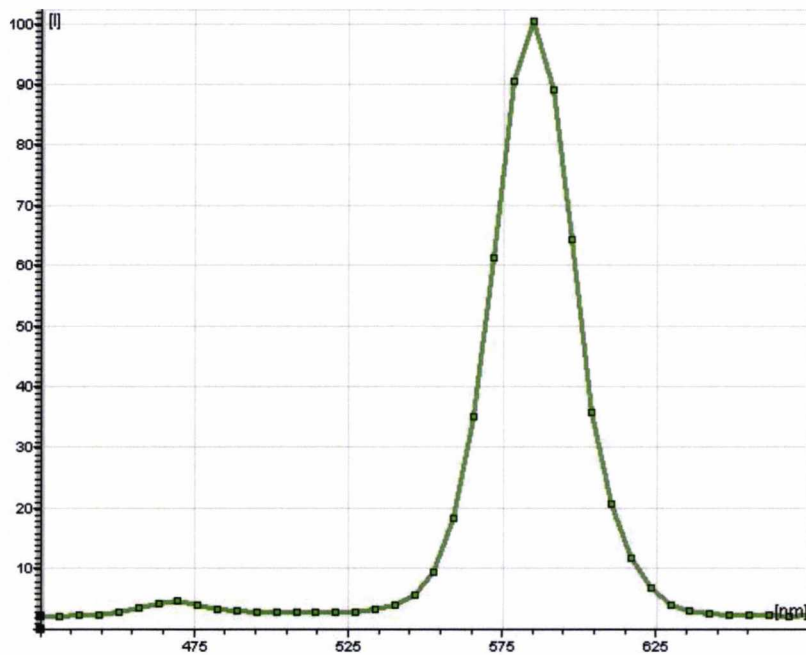


Figure 4.17 Emission spectra of Qdot 585. The highest emission of Qdot 585 was recorded between 575nm and 595nm.

4.4. DISCUSSION

4.4.1. DEVELOPMENT OF QDOT STANDARD PROTOCOL

The accuracy of quantitative measurements of fluorescence intensities in imaging microscopy depends on many different factors. Some of the most important aspects which can affect quantitative measurements are represented by the molecules and specimens being studied, the type of fluorophore used, the labelling procedures, the methods of image acquisition and image analysis. Therefore in order obtain maximum accuracy in quantitative fluorescence microscopy it is essential to develop a standard protocol for the immunofluorescent labelling first, and then to determine optimal conditions for image acquisition and analysis (see chapter 5).

In this study first we examined the applicability of Qdots in FFPE and then we established an optimised protocol for Qdot immunofluorescent staining to apply to all subsequent experiments. For ethical reasons these preliminary experiments were

performed on FFPE rat pancreas tissues which were readily available in the laboratory. We labelled α -cells in the Islet of Langerhans with a primary antibody directed to glucagon. In rat pancreas tissue the α -cells are located in the periphery of the islets and produce a strong signal around the edge of the islets. Therefore this represented a suitable model for this study. Qdot immunofluorescent staining (Fig. 4.3 A) was compared with IHC staining (Fig. 4.1 A) and immunofluorescent staining performed with AlexaFluor 546 (Fig. 4.2 A). The same staining pattern was observed in all experiments and no staining was present in the control slides (Fig. 4.1 B, 4.2 B and 4.3 B). These results demonstrated that Qdot 525 secondary antibody specifically labelled the α -cells.

IHC and FISH are two well characterised methods. In particular, for the assessment of ErbB2 in breast cancer, clear guidelines have been established by the ASCO/CAP to improve the accuracy of these two assays. The Qdot immunofluorescent staining procedure is a new technology and therefore there is not a well defined procedure for Qdot labelling. As different tissue treatments can produce fluctuation in the quantification of the fluorescent signal, we limited the variability of several experimental parameters. We optimised the incubation times (Fig.4.4) and the concentration (Fig. 4.5) of the Qdot 525 secondary antibody. We found that the best signal to noise ratio was achieved after 2h incubation (Fig. 4.4 C). We then showed that the optimum concentration of Qdot 525 secondary antibody corresponded to 20nM (Fig. 4.5 B). Therefore 2h incubation time and 20nM concentration of Qdot secondary antibody were chosen as standard procedure to apply to all Qdot immunofluorescent staining on breast cancer tissues.

4.4.2. APPLICATION OF QDOT TECHNOLOGY TO FFPE BREAST CANCER TISSUES

So far we have demonstrated that Qdot secondary antibody can be used for the detection of molecular targets in FFPE tissues and we established a standard protocol for Qdot immunofluorescent labelling procedure using FFPE rat pancreas tissues. As the aim of this work is to use Qdot immunofluorescence nanotechnology to measure different levels of protein expression in FFPE breast cancer tissues we then employed this technique to measure the expression levels of ErbB2 in breast cancer. To test the

ability of Qdot immunofluorescence method in detecting different levels of ErbB2 expression, an ErbB2 microarray control with four samples of breast cancers graded by IHC as negative (0), weak (1+), moderate (2+) and strong (3+) (Fig. 4.6), was used. Results presented in Figure 4.7 have shown that, according with the IHC staining (Fig.4.6), the Qdot immunofluorescence detection system was able to correctly discriminate between different levels of protein expression. Indeed a strong fluorescent signal around the cell membrane forming a uniform circumferential ring, typical of underlying gene amplification, was observed when ErbB2 was over expressed at 3+ levels (Fig. 4.7 D). No Qdot signal was detected in the ErbB2 negative breast cancer sample (Fig. 4.7 A). However, more challenging was the detection of ErbB2 at 2+ and 1+ levels. A weaker fluorescent signal was observed in the specimens expressing ErbB2 at 2+ level, however only after the gain and magnification were increased (Fig. 4.7 C). It was not possible to identify any specific Qdot signal in the breast cancer specimen over expressing ErbB2 at 1+ level (Fig. 4.7 B).

The major source of noise in the acquired images was introduced by a fluorescence background that was originating from the specimen autofluorescence. The specimens with Qdot signal corresponding to 2+ and 1+ ErbB2 expression, showed a small signal to background ratio which indicated that the intensity of the background was similar to the intensity of the Qdot signal. Therefore in the resulting images the Qdot signal was “lost” or hard to discriminate from the background. To overcome this problem we considered a computational method known as unmixing which is normally used to separate overlapping fluorescent signals from different fluorophores (Hibbs et al., 2006; Kraus et al 2007). Therefore we decided to treat the background fluorescence as another fluorophore. Using the spectral dye separation tool available in the confocal software we were able to obtain a better but not optimal separation between the Qdot 525 signal and the autofluorescence (Fig. 4.8 and 4.9) as strong background signal was still present. Although this method can be a useful tool for co-localisation studies, or identification of subcellular structures, it was not suitable for developing a scalable quantification system. The separation was computed on the basis of two reference regions chosen in the original image (one region for the Qdot 525 emission

and one for the autofluorescence emission); the choice of different reference regions would have lead to different outcomes (Fig. 4.18). The application of this method would have introduced arbitrariness and subjectivity in the fluorescence quantification system and would have also adversely affected the quantification.

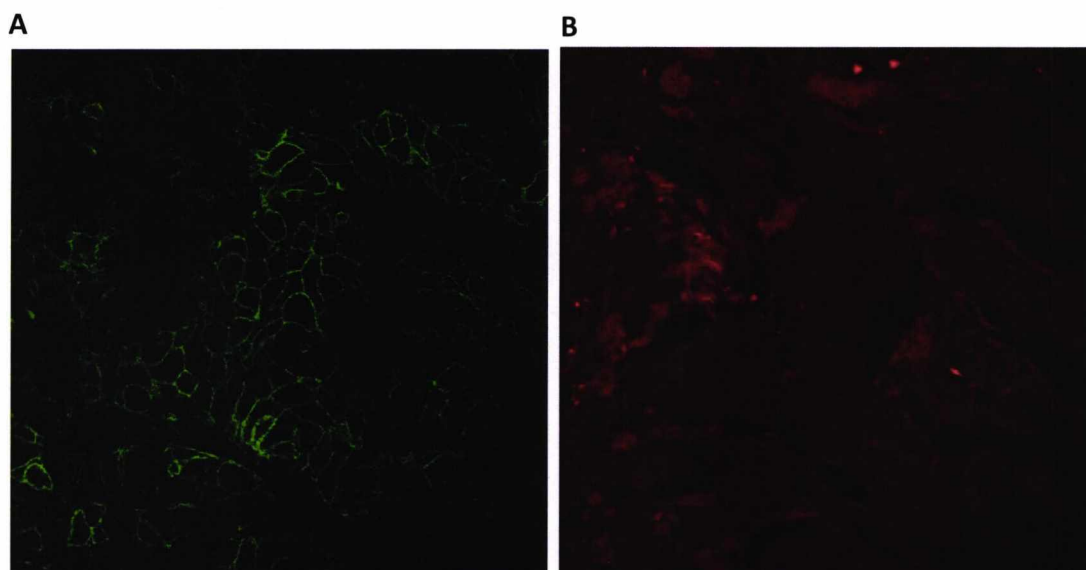


Figure 4.18 Spectral Dye Separation of Qdot 525 specific signal and autofluorescence. (A) Qdot 525 signal and (B) autofluorescence. In both images the balance and the contrast were increased by 25% using Adobe Photoshop version 6.0.

4.4.3. AUTOFLUORESCENCE STUDIES

The presence of background signals generated by tissue autofluorescence represents one of the main shortcomings in immunofluorescence imaging analysis. As mentioned before (see section 4.1), autofluorescence can be generated by a range of endogenous molecules, fixatives and embedding materials when they are excited at 380-490nm. In order to reduce the autofluorescence different approaches, such as chemical treatments, photochemical methods and digital imaging processing methods have been developed. Several chemical strategies include tissue treatments with ammonia-ethanol, borohydride, cupric sulfate and sudan black. It has been shown that they can reduce the autofluorescence more or less efficiently depending on tissue type, fixation,

and wavelength excitation light (Baschong et al., 2001; Schnell et al., 1999). Despite the encouraging results shown, it was decided that the chemical treatments would not be used in this study as manual chemical manipulation would make it more difficult to obtain comparable results.

A different method based on digital image processing has been reported by De Lest and co-workers. In this approach, the image with the autofluorescence emission only was subtracted from the image with the autofluorescence plus the fluorophore emission and then the specific fluorescent signal was calculated (Van de Lest et al., 1995). The digital method proposed by De Lest and colleagues was not suitable for this work as it requires two images from separate lasers to perform a digital subtraction of the autofluorescence; the first image from a laser with a wavelength which does not excite the fluorophore, to see the sample autofluorescence, the second image from a laser with wavelength which does excite the fluorophore emission. However, the Qdot emission can be generated by a laser with any wavelength within the usable spectrum and so this approach was not suitable in this context.

A photochemical approach is represented by photobleaching where a fluorescence emitted by a fluorophore decreases as a function of exposure (Billinton and Knight, 2001). Two different groups have described the effect of photobleaching on the autofluorescent emission. They have shown that maximal reduction of autofluorescence was achieved between 2 and 48 hours (depending on the intensity of UV irradiation) (Neumann and Gabel, 2002) (Viegas et al., 2007). Nonetheless, remaining autofluorescence was still present after the exposure. Better results were obtained by combining photobleaching and Sudan Black B (Viegas et al., 2007), or by irradiating the tissue with a mercury arc lamp through the objective lenses for 20min (Neumann and Gabel, 2002).

As Qdots are resistant to photobleaching (Wu et al., 2003) we decided to reduce the autofluorescence in breast cancer sections by photobleaching. By using a 488nm laser line at maximum power and the 63x lens, we have shown that the autofluorescence dramatically decreased after 60min irradiation (Fig. 4.10 D and 4.11). Although this was considered a possible approach it was not optimal for the purpose of this work.

We need to consider that, despite the Qdot's resistance to photobleaching, its capacity to fluoresce might be degraded after such heavy irradiation. We also considered the possibility of labelling the specimens with Qdots after bleaching the tissue. However this method was time consuming and expensive and therefore it would have been difficult to apply to a diagnostic system in a clinical practice. Therefore we choose to not take forward this approach.

In order to develop a different method to improve the signal to noise ratio, we analysed the features of autofluorescence spectra profiles with 405nm excitation. While the spectra of autofluorescence differed in magnitude, all spectra exhibited similar broad emission and highest emission between 490nm and 535 nm (Fig. 4.12 B and 4.14 and 4.15). We then examined the effect of autofluorescence on visualisation of Qdot 525 fluorescent signal by comparing the Qdot 525 spectra to the autofluorescence spectra. Figure 4.16 show that the Qdot 525 spectra profile exhibited its highest emission between 515nm and 535nm with the emission peak at 525nm. This indicates that the autofluorescence spectra completely overlays the Qdot 525 spectra. Therefore unless the Qdot 525 signal intensity is clearly higher than the maximum autofluorescence, it becomes difficult to detect a specific signal. This was observed in Fig. 4.7 where the Qdot 525 signal was strong enough to be detected when ErbB2 was expressed at 3+ level (Fig. 4.7 D) but not at 2+ and 1+ level where it was masked by the autofluorescence signal (Fig. 4.7 B and C). Spectra profiling of the autofluorescence showed nil that its contribution starts to decrease around 550nm and becomes almost null in the red region of the spectrum (Fig. 4.12 B). Therefore we decided to use a Qdot 585 which has the emission peak at 585nm (Fig. 4.17). The advantage of using Qdot 585 is that it is able to improve the signal to noise ratio by simply avoiding the region of the spectrum where the autofluorescence was stronger.

5 – QUANTIFICATION OF ErbB2 EXPRESSION IN BREAST CANCER TUMOURS BASED ON Qdot IMMUNOFLUORESCENCE IMAGING

5.1 INTRODUCTION

Among all members of the ErbB family, ErbB2 has become the most relevant molecular marker for the prognosis and management of breast carcinomas. ErbB2 over expression in human breast cancers was first reported in 1987 (Venter et al., 1987). Subsequently, ErbB2 gene amplification and/or protein over expression, which was found in 18-20% of breast cancers, were shown to be an independent adverse prognostic factor (Slamon et al., 1987). To date, the adverse prognostic significance of ErbB2 status has been evaluated in 107 published studies. Of these 107 studies, 95 have demonstrated a correlation between ErbB2 gene amplification and/or over expression and clinical outcome (Ross et al., 2009). In addition to its prognostic significance, what has made ErbB2 one of the most important molecular markers in breast cancer is its predictive value of response to Herceptin treatment. With the advent of Herceptin, the assessment of ErbB2 status has gained increasing relevance and it has become essential to identify those patients who can respond to the drug. Current testing and assessment of ErbB2 status, for selection of patients for treatment with the drug, relies initially on IHC and then on FISH for equivocal cases (IHC 2+) (refer to section 1.15). Despite the fact that there have been recommendations to standardise and improve the accuracy of ErbB2 testing (Ellis et al., 2000; Wolff et al., 2007), testing inaccuracy still remains a major issue and it can lead to patients misclassification (see section 1.15). According to the ASCO/CAP guidelines, approximately 20% of the ErbB2 testing is inaccurate (Wolff et al., 2007). Therefore it is important to improve the assessment of ErbB2, as this will allow better selection of patients who will most benefit from this drug.

In this study we are proposing a new system that can quantify more precisely ErbB2 levels of expression. In order to achieve a more objective, linear and scalable measurement of ErbB2 expression we have established a series of criteria to

standardise different stages of the process. Previously we have analysed the ability of the rabbit polyclonal antibody 21N in detecting ErbB2 expression in different systems including FFPE breast cancer tissues (see chapter 3), we have also studied the performance of Qdot secondary antibody and standardised the staining method on FFPE tissues (see chapter 3 and 4). Finally, after pondering different ways to improve the signal to noise ratio (which was affected by the presence of a strong autofluorescent signal), we have decided to use a secondary antibody labelled to a Qdot 585 with emission in region of the spectrum where the autofluorescence is lowest (chapter 4). In particular, our goal in this chapter is to measure the signal coming from the fluorophore (Qdot 585) labelled to ErbB2 receptor in FFPE breast cancer tissue which allows us to associate a number to different levels of ErbB2 expression. In order to be able to extract such information from each breast cancer specimen first we set up an imaging acquisition system that gives consistent results and is optimal for signal detection. Then we have defined a method for the image segmentation and quantification of the specific signal. Finally we have validated our results by comparing the Qdot-quantification system versus the IHC scoring system.

5.2. AIMS

- I. Find optimal conditions for imaging acquisition.
- II. Define a segmentation method.
- III. Establish criteria for quantification analysis.
- IV. Quantification of ErbB2
- V. Validation of the Qdot-quantification system versus IHC.

5.3. RESULTS

5.3.1. IMAGES ACQUISITION

In order to obtain reliable data from the images, we determined the optimal parameters for the acquisition first and then ensured that the chosen setting was consistent over time.

To help to understand the process involved in creating an optimal setting for the images acquisition, here we are going to provide a brief description of several components used in confocal microscopy and involved in this process. Some of these components include wavelength filtering devices, acousto-optical devices and light detector devices. As the Leica SP2 laser scanning confocal microscope was employed in this study, we will specifically refer to the components implemented by the Leica microsystem. The Leica SP2 laser scanning confocal microscope uses an Acousto-Optical Tunable filter (AOTF) device to select the exact light wavelength and direct it in the optical system. In addition the AOTF allows regulation of the intensity of the laser light reaching the sample. The AOTF substitute shutters, attenuation filters and line selection filters used in other instruments (<http://www.leica-microsystems-com/science-lab/white-confocal/confocal-excitation-from-filter-wheels-to-aotf/>).

Another element is represented by the Acousto-Optical Beam Splitter (AOBS) which replaces the primary dichroic mirrors to separate the illumination light (corresponding to the laser line used for the excitation) from the returning fluorescent light, which corresponds to the detection light (<http://www.leica-microsystems-com/science-lab/white-confocal/beam-splitting-dichroic-mirrors-and-acousto-optical-artwork-aobs/>). The detection system in the Leica confocal microscope is based on the following components: a spectral prism (SP) which replaces secondary dichroic mirrors and a system of slit, mirror and light detectors represented by the photomultiplier tubes (PMTs). The light emitted by the fluorochrome in the sample is refracted by the SP. The light can then pass through a movable slit (controlled by a computer software) equipped with a mirrored surface and be collected by a PMT detector. Alternatively the light can be reflected to one of the other PMTs. The output of the detectors is then

digitised in different channels (<http://www.leica-microsystems.com/science-lab/white-confocal/spectral-imaging-how-to-separate-the-colors/>).

5.3.1.1. ESTABLISHING STANDARD PARAMETERS FOR THE IMAGES ACQUISITION

Choosing the best acquisition setting is important in order to obtain optimal confocal images. As mentioned earlier, our goal is to measure different level of ErbB2 expression based on quantification of fluorescence values. In order to accomplish this goal we defined several parameters that are essential in determining the quality of the images (good signal to noise ratio) and the data that they contain (intensity values). In an 8-bit image the computer monitor displays the different intensity values as 256 grey levels (dynamic range). When generating an image with full dynamic range, with dim and bright areas, it is important not to lose any information from the signal. The parameters involved in this process include the laser intensity level, PMTs gain and offset and frame average. All these parameters can be controlled using the “Beam Path Setting” in the control panel of the microscope software.

The laser light is the actual light that reaches the sample and is used to excite the fluorophore. As mentioned earlier, the amount of light that reaches the sample can be controlled by using the AOTF device. The AOTF allows adjusting the laser intensity level between 0% and 100% of the laser power. If its power is set too low it may not be enough to excite the fluorophore and generate a true signal. If its power is set too high it may create bright images close to saturation point and at the same time it may damage the sample.

The gain level (or voltage) and the offset level of the PMT determine the signal produced by the detector and consequently the grey levels recorded in the image. They are used to adjust the image intensity values so that all the maximum levels of the grey values are included in the image. In particular the gain affects the bright features of the image, so a low gain will result in a duller image and high gain will create a brighter image. Therefore the gain level should be set just below the saturation; the images should contain only a few saturated pixels which correspond to the brightest areas of the image. The offset or black level control is used to ensure that

the dark features in the image are close to zero (black) or contain low grey level values. To ensure this, the offset should be set just above zero so that a low signal will not be lost. Using the confocal software it is possible to visualise both saturated pixels, displayed in blue colour, and the darkest pixels, displayed in green colour (Fig. 5.3). Optimal gain and offset level are also important in order to obtain an image which exhibits a significant amount of details (contained in the full dynamic range) and a good contrast and high resolution.

To create the appropriate setting for collecting images from a series of breast cancer tissues with different levels of ErbB2 labelled with Qdot 585, we started by using the spectral information previously obtained by using the pure fluorophore (see Fig. 4.17). The spectral profile presented in Figure 4.17 (chapter 4) shows that the highest signal emitted by the Qdot 585, occurs between 575nm and 595 nm. This is also shown in the wavelength scan presented in Figure 5.2. Therefore the PMT slider was positioned in this region of the spectrum. The confocal software was used to automatically determine the setting for optimal image acquisition of the fluorophore. These parameters were used as starting point to apply to the breast cancer specimens. The other parameter we have considered was the averaging. A specified number of frames of an individual image are repeatedly collected and the average of every image is calculated consecutively. This method reduces the noise, therefore it improves the image quality and the signal appears clearer. Obviously the result depends on the number of frames specified; the Leica confocal software allows to choose how many times, from 1 to 64, the section can be scanned. We applied this method to acquire images of the Qdot 585 using a specified number of scans from 1, 4, 8 to 12 (Fig. 5.2 A, B, C and D). It is noticeable that the amount of noise displayed in the image recorded with a single scan (Fig. 5.2 A) is higher than the noise present in the other images. The image in Figure 5.2 B still shows a certain amount of noise, which is considerably less in the images presented in Figure 5.2 C and D. As not a great difference was observed between 8 scans and 12 scans (Figure 5.2 C and D) we reckoned that 8 scans represented the optimal number of scans in order to obtain a sharp image with low noise (Fig. 5.2 C).

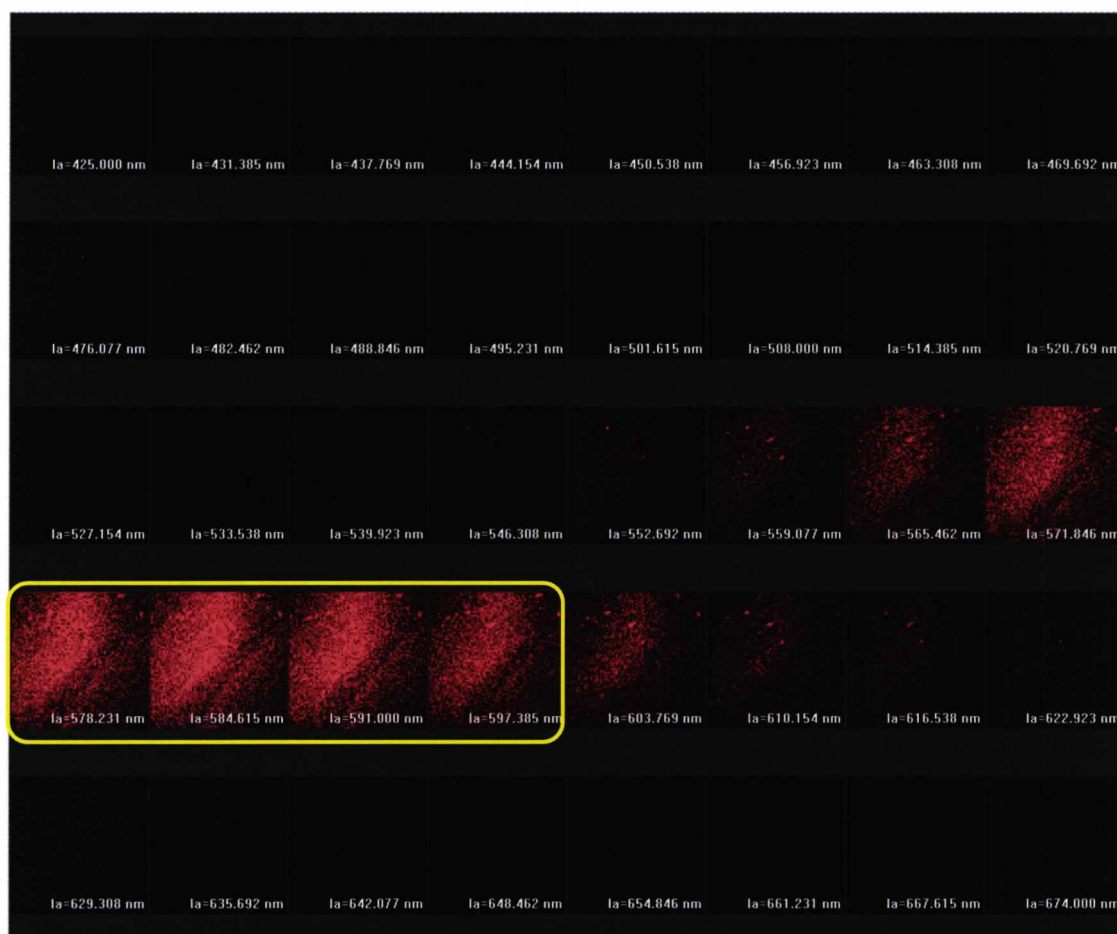


Figure 5.1 Wavelength scan of Qdot 585. A sample containing only Qdot 585 was prepared as described in section 2.12.1 and then its profile was analysed using the Leica SP2 LSCM and the leica Lite software. The image shows the emission signal of Qdot 585 from 425nm till 674nm. The emission has different intensities depending on the region of the light spectrum. In particular the image shows that Qdot 585 has the strongest emission approximately between 578nm and 597nm. The brightness was increased 10% and the contrast 60% with Photoshop CS2.

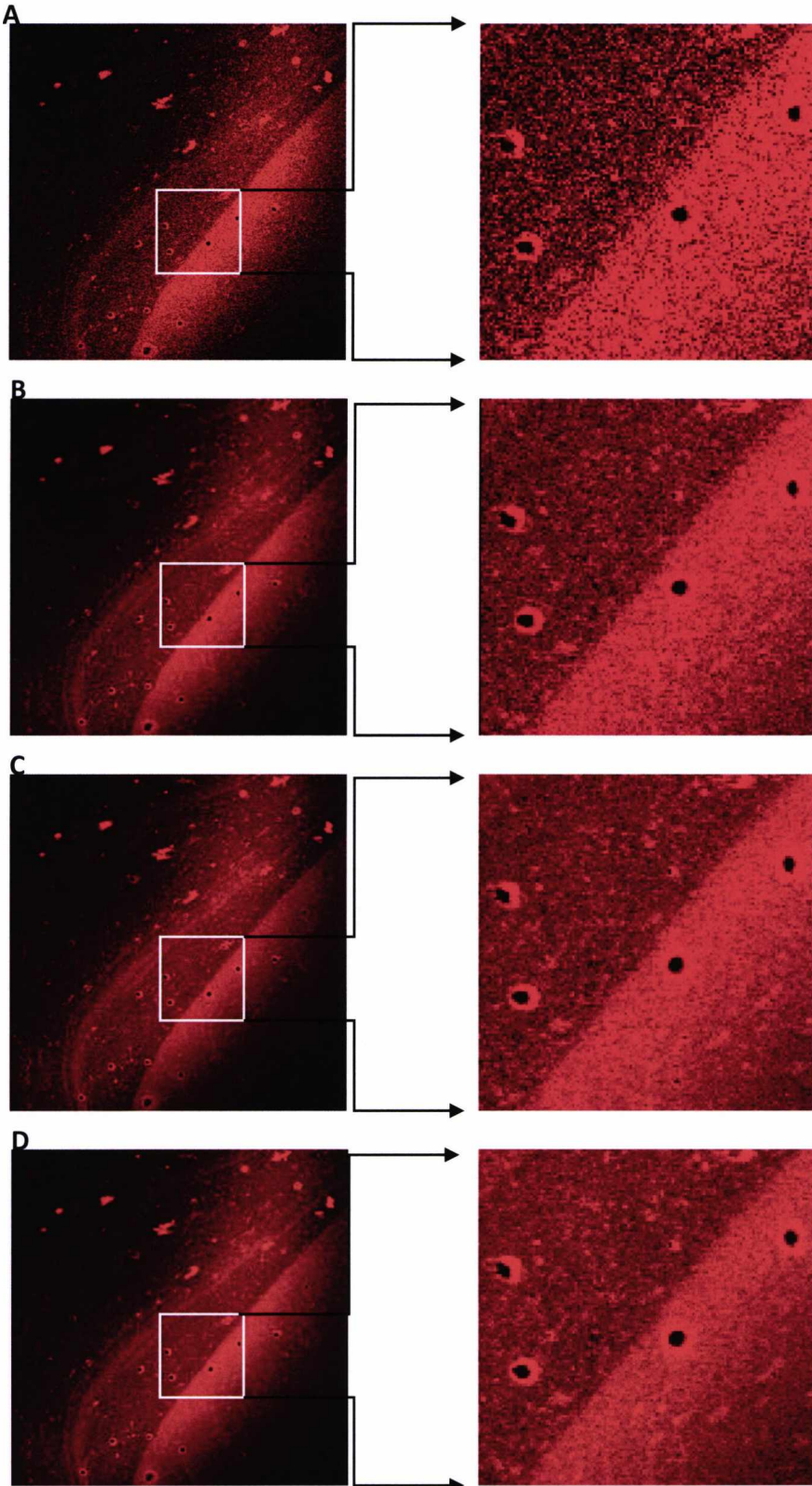


Figure 5.2 Reduction of noise by using the frame averaging method. The images were acquired choosing increasing number of scans: a single scan (A), 4 scans (B), 8 scans (C) and 12 scans (D). The zoomed images corresponding to areas in the white box reported on right show the decreased noise.

The breast cancer tissue array with the ErbB2 control samples, stained with 21N primary antibody and Qdot 585 secondary antibody was then used to establish the final setting for image acquisition. As this array contains four breast cancer tissues expressing ErbB2 at 3+, 2+, 1+ and 0, we deemed that this represented a good model for the purpose of this work. The tissues expressing ErbB2 at 3+ levels was used to determine the laser intensity level, the gain and the offset. Underexposed and saturated areas in the image were monitored by using the “Look Up Table” (LUT) in the confocal software. As mentioned earlier this function shows the darkest pixels in green and the brightest in blue (Fig. 5.3 A). The optimal setting will result with some pixels appearing green and some blue as shown in Figure 5.3 B.

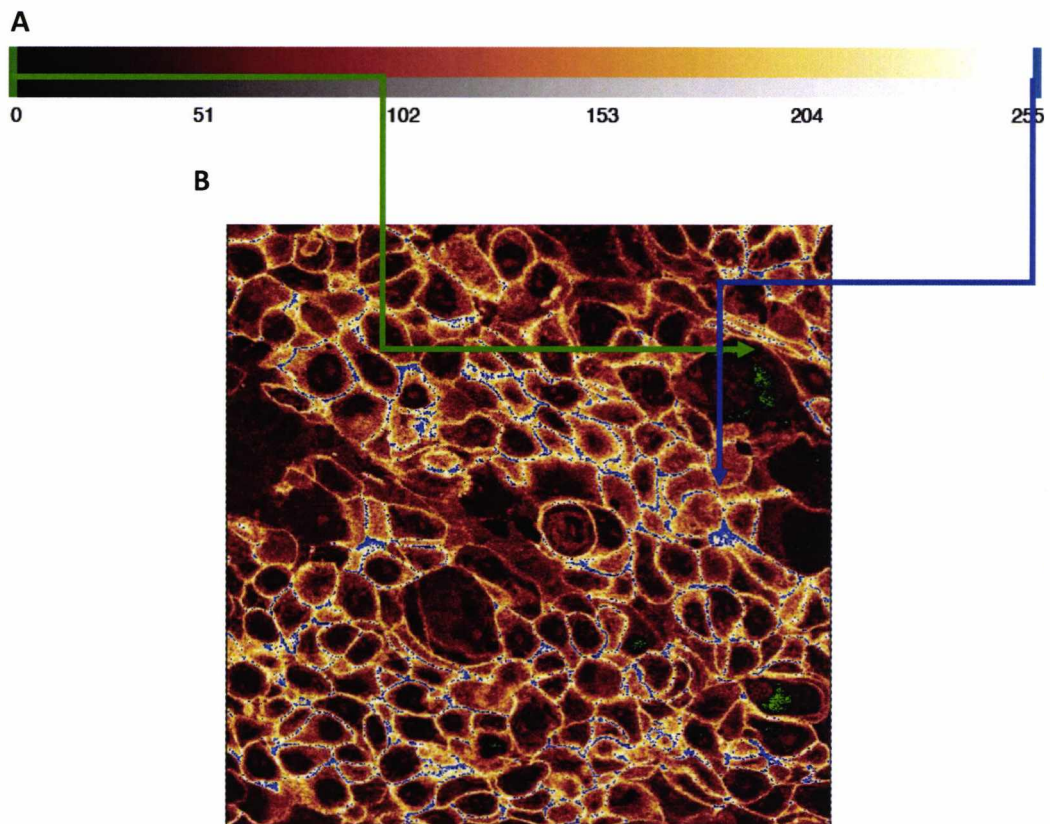


Figure 5.3 Application of “look up table” tool. (A) shows the look up table glow related to the grey scale. The black pixels are shown in green and the white pixels in blue. (B) Breast cancer tissue section expressing ErbB2 at 3+ level. The look up table was used to check underexposure and saturation levels in the image. The presence of some green pixels and blue pixels indicate that the images contains all the grey level values from 0 to 255. (A) was adapted from <http://www.zmb.uzh.ch/resources/download/CLSM.pdf>.

This setting was used to collect the images from all four breast cancer tissues with different expression levels of ErbB2. The results show that this setting was able to detect ErbB2 expressed at 3+, 2+, 1+ and 0 level. Figure 5.5 A shows intense Qdot 585 signal around the membrane that corresponds to ErbB2 expressed at 3+ level with optimum signal to noise ratio. Figure 5.5 B shows much weaker signal but still visible, corresponding to 2+ level of expression. No specific signal was discriminated in the specimen with ErbB2 expressed at 1+ level (Fig. 5.4 C), no Qdot 585 signal was present in the breast cancer specimen scored as 0 by IHC (Fig.5.4 D).

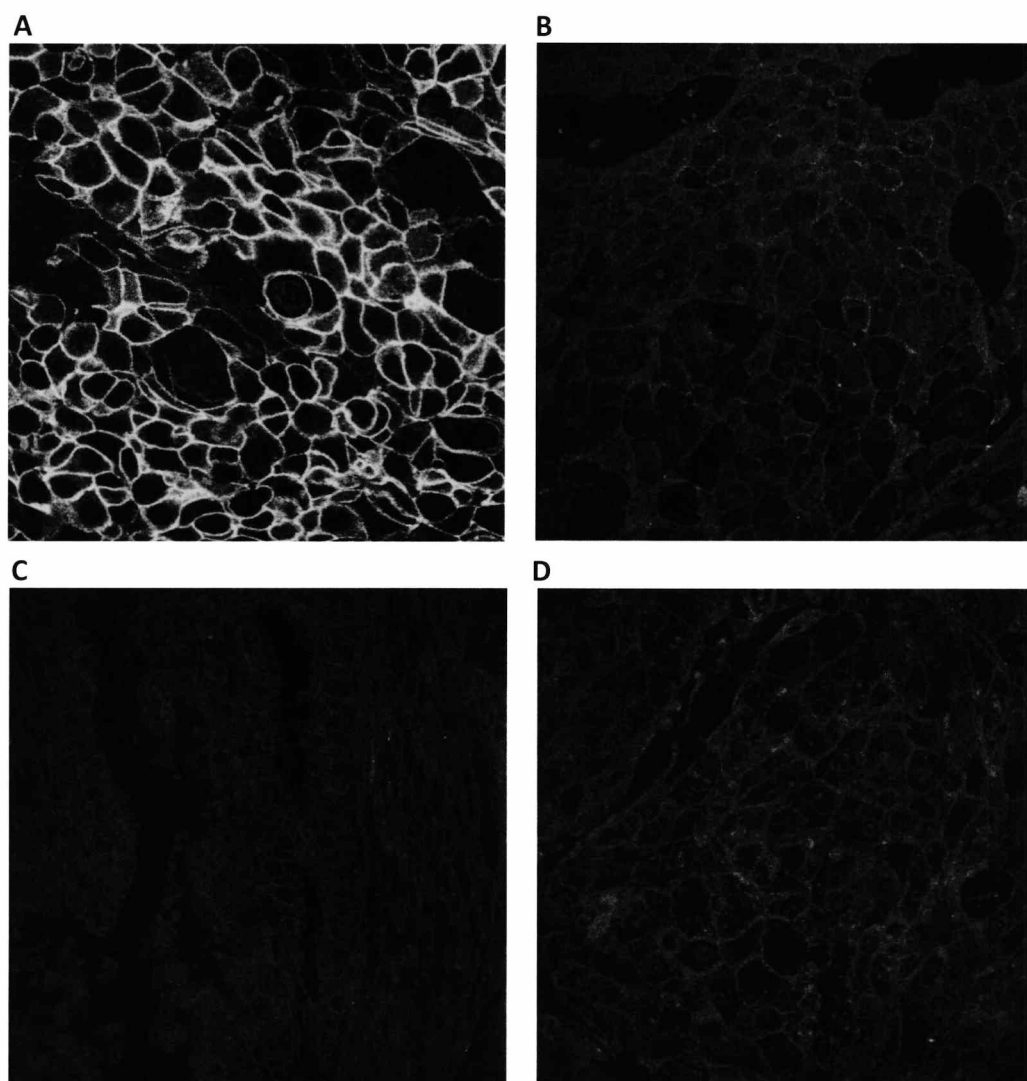


Figure 5.4 Breast cancer tissues expressing ErbB2 at 3+ (A), 2+ (B), 1+ (C) levels and 0 (D). The images were acquired with the same setting in the region of the light spectrum between 575nm and 595nm. The image balance was adjusted using Photoshop CS2 by increasing the brightness by 5% and the contrast by 45% in all the images.

Using Qdot 585 we have reduced the amount of the autofluorescence (see section 4.3.4.2), however some autofluorescent signal was still present (Fig. 5.4). In particular in the specimens with ErbB2 expression at 1+ level the Qdot 585 signal was not significantly higher than the background and this made the specific signal almost indistinguishable from the background. Therefore we decided to use the autofluorescence as an useful tool in distinguishing the specific signal from the background. Each image was simultaneously acquired in two channels (Fig. 5.5), one for the Qdot 585 signal (between 575 and 595nm) (Fig. 5.4) and one for the autofluorescence signal only (between 485nm and 505nm) (Fig. 5.6).

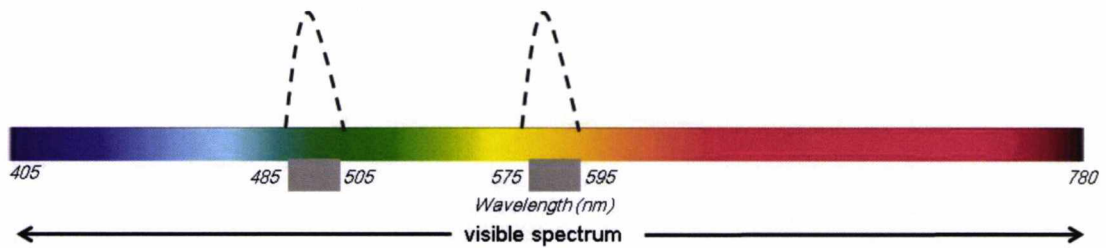


Figure 5.5 Channels used for the image acquisition. Two images were simultaneously generated in two different areas of the spectrum, one between 485nm and 505nm (for tissue autofluorescence only) and the second one between 575nm and 595nm (for the Qdot 585 signal)

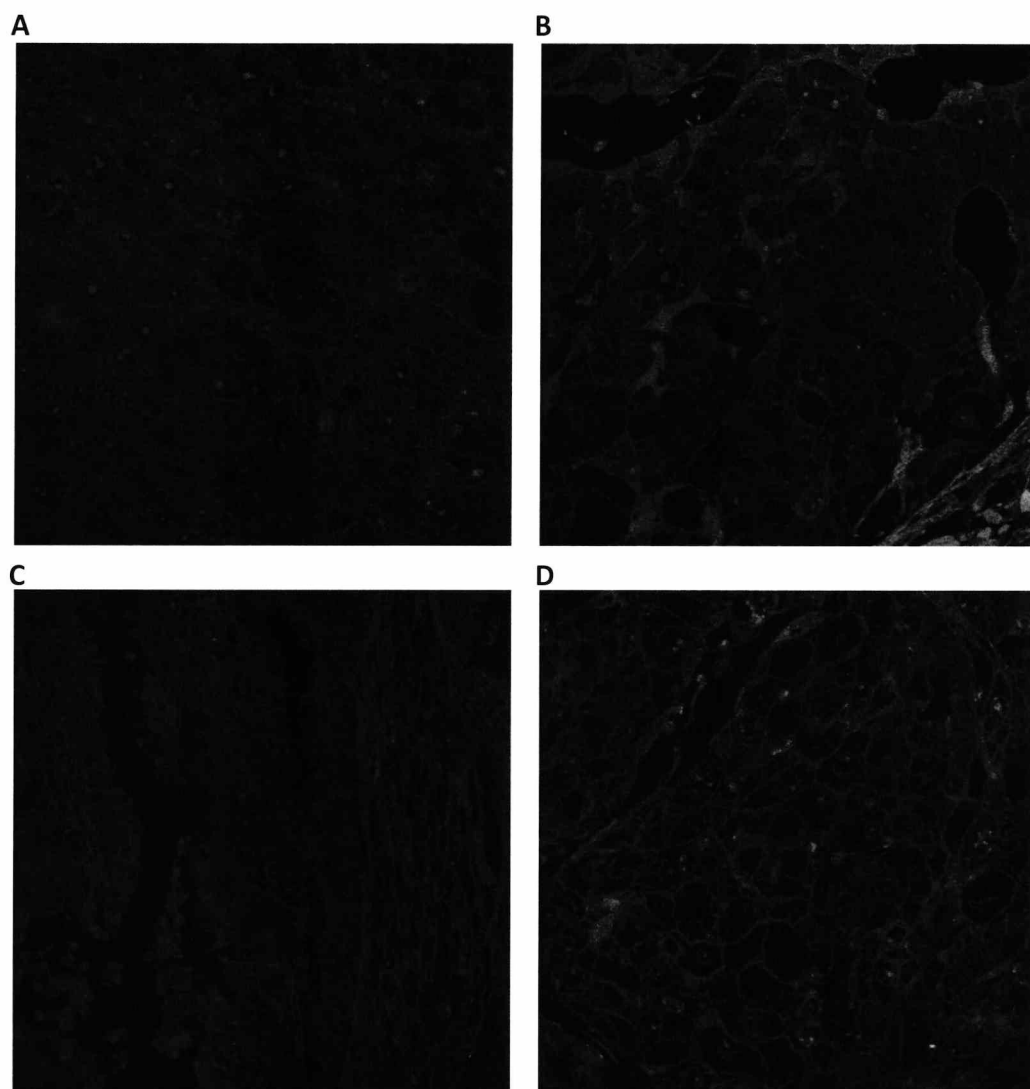


Figure 5.6 Images showing the autofluorescence of breast cancer tissues expressing ErbB2 at 3+ (A), 2+ (B), 1+ (C) levels and 0 (D). The images were acquired between 485nm and 505nm simultaneously with the images shown in Figure 5.5. In this region of the spectrum only autofluorescent signal (background) is present. Photoshop CS2 was used to adjust the image balance: brightness was increased by 5% and contrast by 45%.

By merging the images acquired in the two channels (Fig 5.7) it was possible to better discriminate the Qdot 585 signal and the autofluorescence in all four specimens. In particular in Figure 5.7 B and C the Qdot 585 signal became more visible on top of the autofluorescence (green background), while in Figure 5.7 D the two signal completely overlapped. This appears more evident by observing the histogram in Figure 5.8 that shows the mean intensities of the images acquired in the channel for both the autofluorescence (in green) and the Qdot 585 signal (in red).

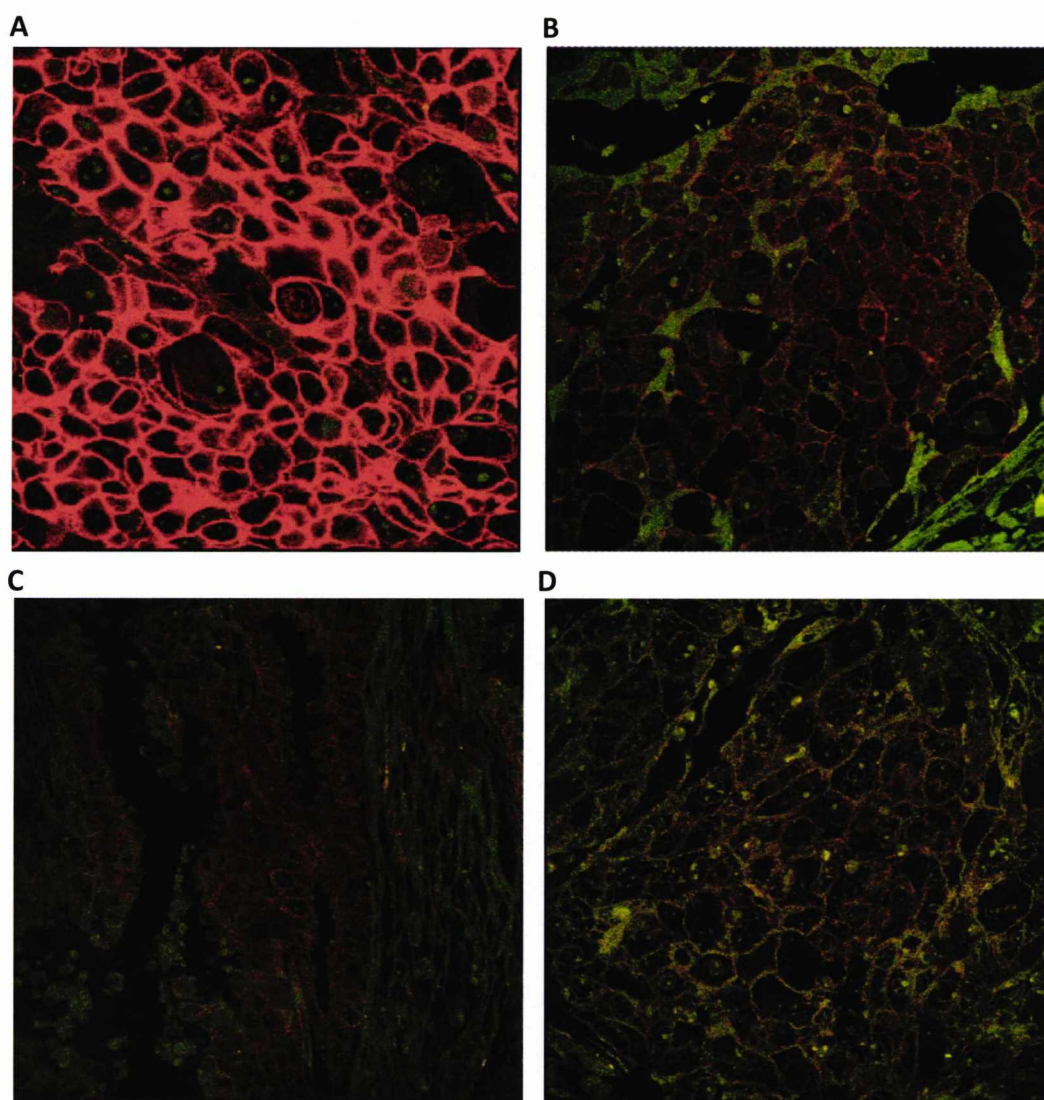


Figure 5.7 Merges of two colour images of the green (485nm-505nm) and red (575nm-595nm) channel. The green background corresponds to tissue autofluorescence and the red is the Qdot 585 fluorescent signal that corresponds to different levels of ErbB2. The images show four breast cancer tissues expressing ErbB2 at 3+ (A), 2+ (B), 1+ (C) levels and 0 (D). Photoshop CS2 was used to adjust the image balance: brightness was increased by 5% and contrast by 45%.

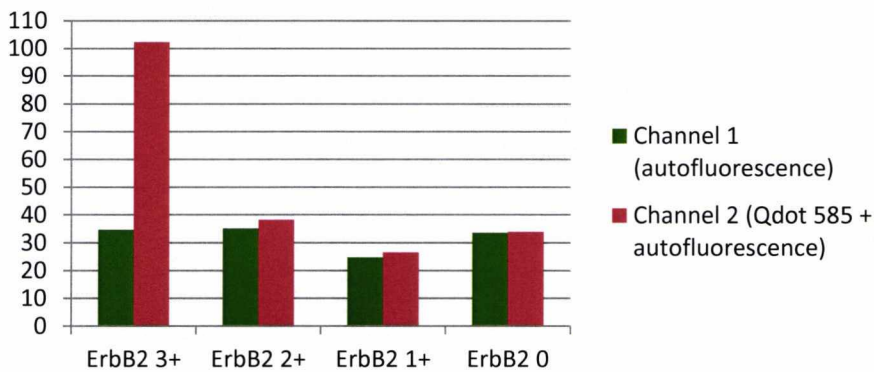


Figure 5.8 The histogram shows the mean intensities of the images in Figure 5.8. In green is reported the mean intensity of the autofluorescence only and in red is shown the mean intensity of the Qdot 585 signal with the contribution of the autofluorescence.

5.3.1.2. MAINTAINING CONSISTENCY OF THE CONFOCAL MICROSCOPE

The correct performance of each laser, light detectors etc. can influence every parameter involved in the image acquisition process and consequently the quantification of the intensity values. Therefore, we considered if necessary to ensure that the acquisitions performed at different times were consistent and comparable. Keeping the settings constant and using a control sample, supplied by Leica we tested whether the confocal microscope instrumentation was performing consistently. The control sample consisted in a thin transverse section of the rhizome with concentric vascular bundles from Lily of the Valley (*Convallaria majalis*). The advantage of using this sample resided in its morphology. The rhizome section has a clear and well defined structure. This allowed us to recognise and collect images from the same area every time we started the acquisition process. An images of the vascular bundles was acquired in both channels, one hour after that the microscope was started (T0) and after four hours (T1). The same test was repeated for four days (Fig. 5.9). At the end the average intensity of each image was calculated and reported on the histogram (Fig. 5.10 A and B). The intensity values obtained were compared and they showed that the microscope was performing consistently. The presence of small fluctuations in the intensities was within an acceptable range. This fluctuation can be explained by a small

shift in the xy and z position of the sample in the image rather than an inappropriate functioning of the instrument

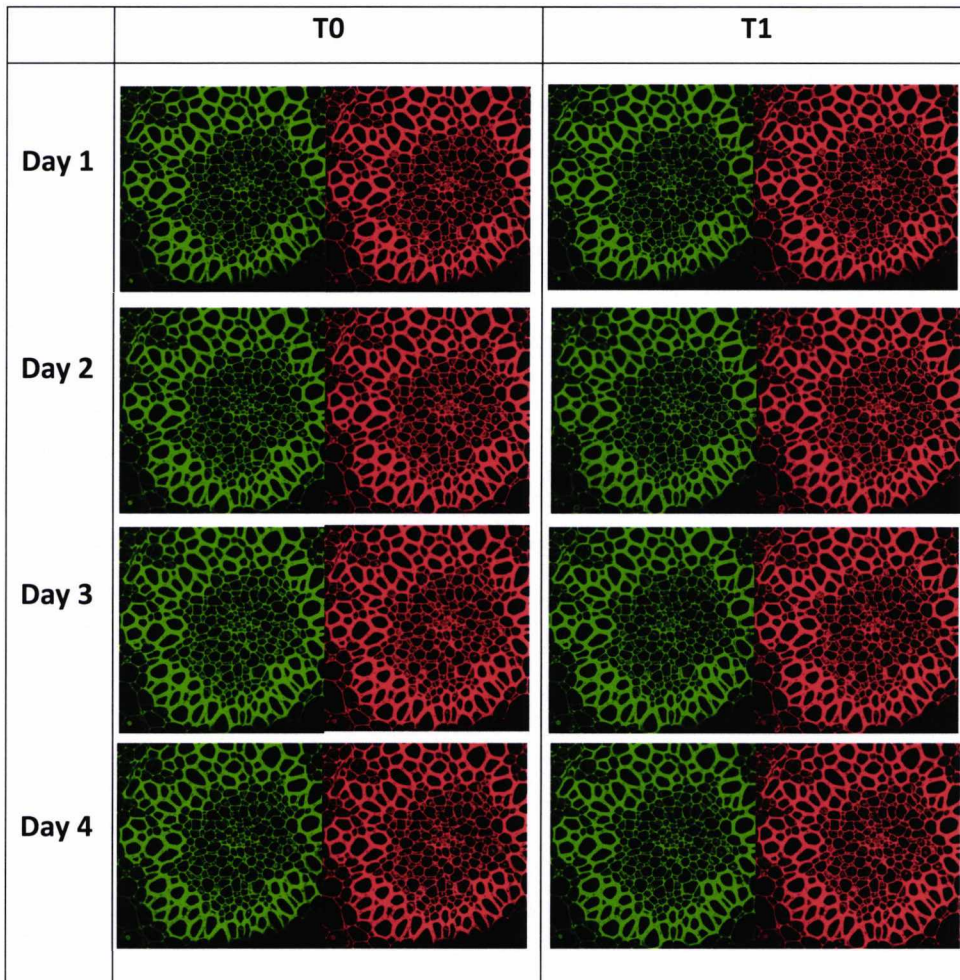


Figure 5.9 Vascular bundles from Lily of the Valley (*Convallaria majalis*). The images were acquired with the same settings under the same conditions for four days at 0 hours (T0) and after 4 hours (T1). Images were collected in both the green channel (485nm-505nm) and the red channel (575nm-595nm). The clear structure allowed using the same area of the section as control to test the confocal microscope performance.

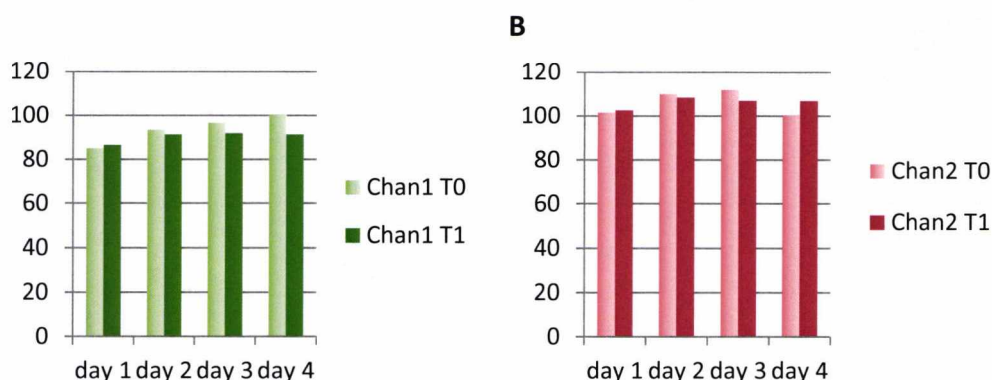


Figure 5.10 Comparison of the mean intensities from the control images shown in Figure 5.9. (A) Mean intensities of the images collected in each day in the green channel at T0 (light green) and T1 (in green). (B) Mean intensities of the images collected in each day in the red channel at T0 (light red) and T1 (in red).

An additional control was performed by using the breast cancer tissue array ErbB2 control slide stained with the Qdot 585 secondary antibody. An image from a specified area of each tissue was acquired simultaneously in the two channels over four days. Here we are showing as example four images collected from the breast cancer section with ErbB2 3+ expression (Fig. 5.11). The mean intensity of the whole frame was calculated and reported in a histogram (Fig. 5.12 A and B). The histogram in Figure 5.12 A shows the intensities of the images collected in channel 1 and that correspond to the autofluorescence; as expected the intensity values decrease slightly after each acquisition as consequence of photobleaching. The histogram in Figure 5.12 B correspond to the images acquired in channel 2 for the Qdot 585 emission; the histogram shows the combined signals representing the Qdot 585 signal intensity and the autofluorescence, that progressively decrease due photobleaching of both the fluorophore and the autofluorescence. Similar results were also obtained with images collected from the other sections (data not shown). These results suggested that the microscope was able to give consistent and reproducible results.

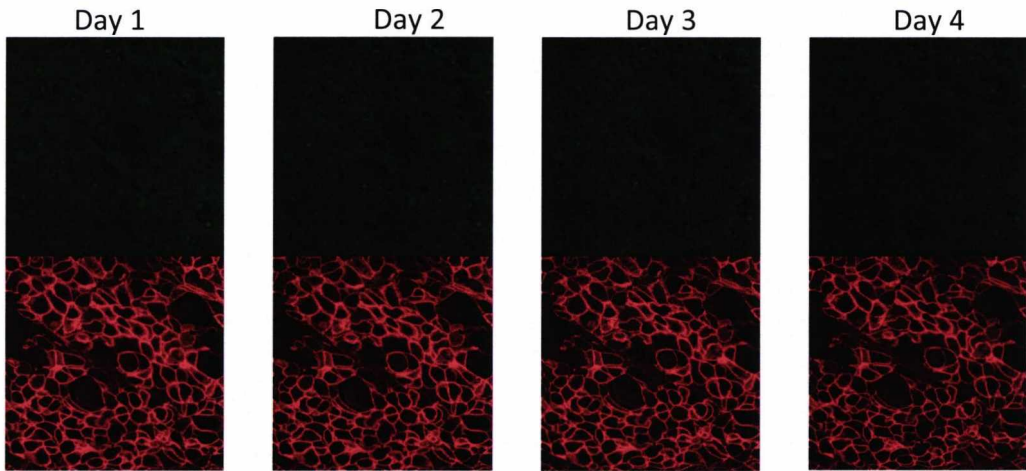


Figure 5.11 Comparison of images of ErbB2 3+ breast cancer tissue acquired simultaneously in two channels on different days. The green channel shows the tissue autofluorescence and the red channel shows the Qdot 585 signal. The acquisitions were performed with the same settings and conditions.

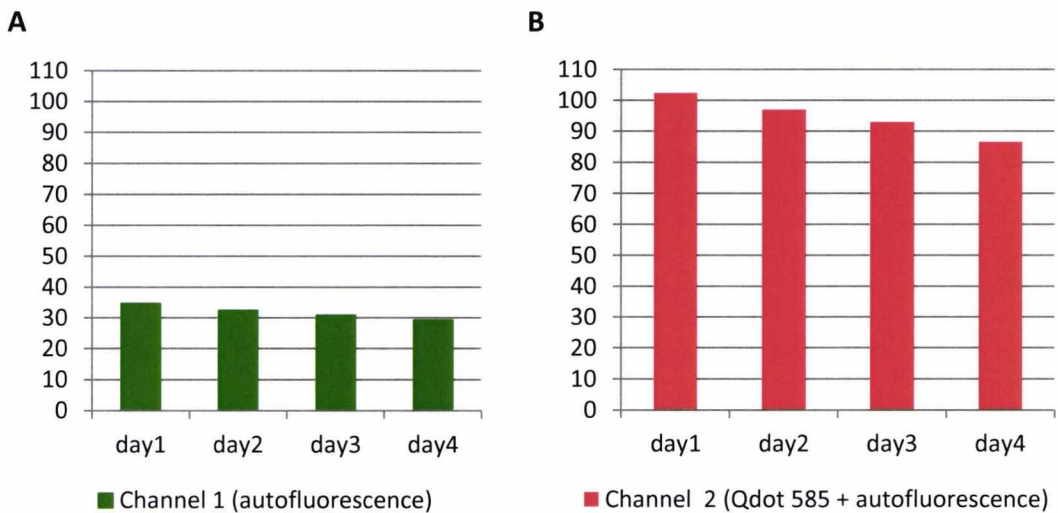


Figure 5.12 The histograms show the mean intensities of the images in Figure 5.11. (A) Mean intensities of the green channel (autofluorescence). (B) Mean intensities of the red channel (Qdot 585). Both histograms shows that the mean intensity values consistently decrease slightly as consequence of photobleaching

5.3.2. QUANTIFICATION ANALYSIS

In order to measure ErbB2 expression in breast cancer tissues and to translate this into a number we measured the pixels intensity values of the signal generated by the Qdot 585. As stated earlier, the fluorescent intensities of Qdot 585 depend on different amounts of protein present in the tissue and therefore by measuring the intensities it is possible to measure ErbB2 levels. All the operations were based on the Qdot 585 fluorescent signal and autofluorescent signal emitted in the red channel. The signal in the green channel was only used as supporting tool to identify the tissue morphology, tumour areas and tissue areas for the autofluorescence.

The quantification analysis of a fluorescent signal in a digital image involves several steps which include image segmentation, background removal by choosing a threshold and subtracting autofluorescence intensity values from the total signal and finally calculation of the mean intensity values of the specific signal. First of all we are going to consider the segmentation process. The Leica confocal software allows us to segment the image by “region of interest” (ROI). We used this tool to identify and separate areas containing tumour cells and areas, such as connective, fibrous, adipose tissue and stroma that not contain useful information and only contribute to the background. Therefore, the segmented image contains two groups of regions: one group formed by tumour areas with the specific signal (Fig. 5.13 A) and the background, and the second group representative only of the background of that specific tissue section (Fig. 5.13 B).

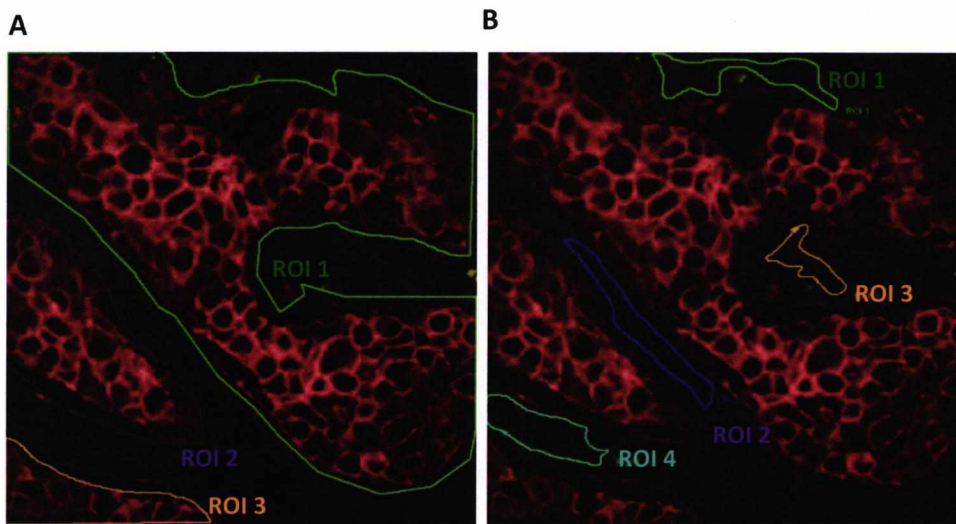


Figure 5.13 Example of segmented images. Images were segmented for the tumour (A) and the autofluorescence (B) using Leica lite software.

In order to extract the specific signal from the background we first estimated a threshold point. We analysed the grey level histograms that correspond to the tumour areas and the tissue areas in different sections.

The histogram in Figure 5.14 displays the distribution of pixel intensities within the image shown in Figure 5.13 A for the tumour areas (ROI 1-2-3). The pixel intensity (grey scale) reported on the x-axis is plotted against the number of pixels with that intensity (y-axis). The histogram shows that the large number of pixels is mainly in the left part of the histogram, more precisely they are spread over the first 30-40 units of the grey scale. Particularly ROI 1 shows a large number of dark pixels and this can be explained by the presence within the ROI 1 (Figure 5.13 A) of a black area, where no tissue is present. However the histogram also shows that different amount of pixels are distributed along all the grey levels indicating the presence of bright specific labelling.

We then analysed the histogram (Fig. 5.15) that corresponds to the tissue areas taken as background (Fig. 5.13 B). The histogram clearly shows that for each ROI all the pixels are spread within the first 50 units of the gray scale and no high intensity pixels are displayed.

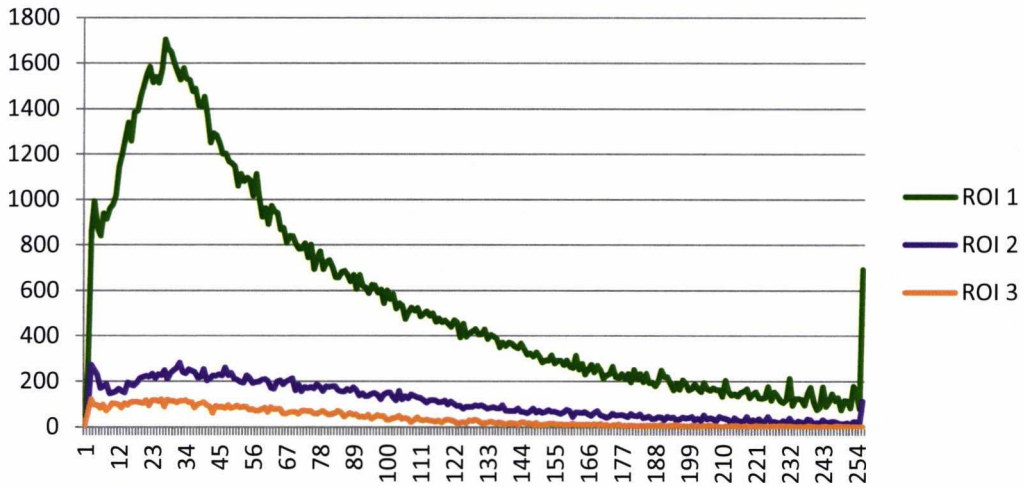


Figure 5.14 Histogram of the pixel intensities of the image collected in the red channel, within the three region of interest ROI 1-2-3 corresponding to the tumour areas (see Fig. 5.13A). The pixel intensity (grey scale values) is plotted on the x-axis and the number of pixels for each intensity level is plotted on the y-axis. The three curves, in particular the green one (ROI 1) are skewed on the left showing that the majority of the pixels are concentrated in the darkest region of the grey scale. The histogram also shows the presence of large number of high intensity pixels.

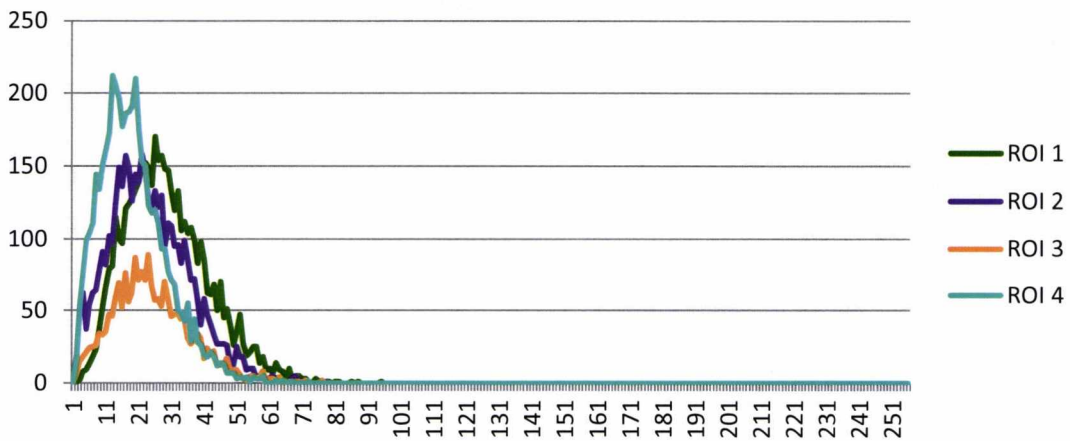


Figure 5.15 Histogram of the pixel intensities of the image collected in the red channel, within the four region of interest ROI 1-2-3-4 corresponding to background areas (see Fig. 5.13 B). The pixel intensity (grey scale values) is plotted on the x-axis and the number of pixels for each intensity level is plotted on the y-axis. Pixels are concentrated in the first 50 units of the grey scale and no high intensity pixels are present.

On the basis of these observation we chose 50 as threshold point on the grey scale as all the values below that point were part of the background and therefore not meaningful. Furthermore, as the majority of the pixels was spread within 0 and 50 units of the grey scale, including these pixels values when calculating the mean intensity would have skewed the results. All the pixels values above the threshold were used to calculate the mean intensity of the regions containing tumour cells and of the regions without tumour. To verify the quantification method we first applied this method to the ErbB 2 tissue array control with 3+, 2+, 1+ and 0 ErbB2 expression (Fig. 5.16 A from left to right) and we quantified the Qdot 585 signal. Figure 5.15 A shows segmented images for tumour areas (first row) and background areas (second row). For each area the mean intensity was determined and the average of the mean intensities was calculated. The histogram in Figure 5.15 B shows the average of the intensities of the tumour areas (in red) and the background areas (in lighter red). The average intensity obtained from the mean intensities of the areas containing the tumour is composed by the Qdot 585 signal and the background signal. Therefore in order to isolate the Qdot 585 signal it was necessary to subtract the mean intensity of the background from the mean intensity of the tumour. The histogram in Figure 5.16 C shows the quantification results of the Qdot 585 signal after subtraction of the background intensity signal. The results have shown good concordance with the level of ErbB2 expression in the four breast cancer sections as determined by IHC.

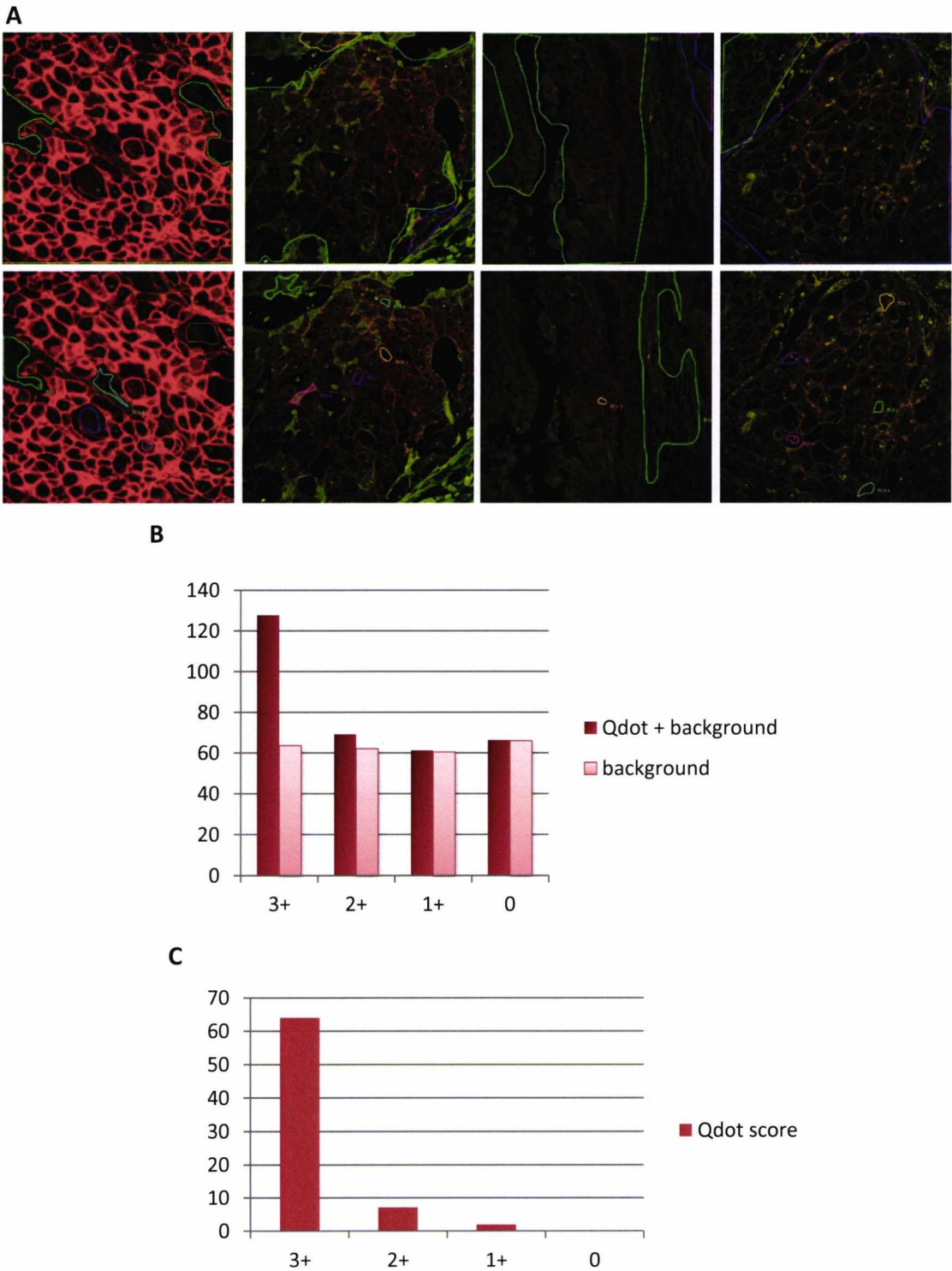


Figure 5.16 Qdot 585-Immunofluorescent staining of the control microarray slide with four cores of breast cancer tissues. (A) Images were segmented for the tumour areas (first row) and the background (second row). Qdot 585 signal and background signal were quantified. (B) shows the mean intensity of Qdot 585 signal with the contribution of the background and the background signal alone. (C) shows the mean intensity of the Qdot 585 signal after subtraction of the background.

5.3.2.1. QUANTIFICATION OF ERBB2 IN BREAST CANCER TISSUES

In order to see whether the system was able to produce a scalable measurement of ErbB2 expression we quantified ErbB2 expression in a larger set of unselected breast cancer specimens with different levels of ErbB2. We used a tissue array with 60 FFPE breast cancer samples taken from 60 breast tumours. Another sample from the same tumours was previously stained by IHC and scored visually (see section 3.3.4.1). In order to gain a good understanding of the overall ErbB2 expression in each tumour section, we acquired three images from different tumour areas in each tissue and proceeded to the quantification analysis as previously explained. As the fluorescent signal was uniform across different areas of the same tissue, here we are going to show only one image which is representative of each section. Figure 5.17 shows four examples of breast cancer tissue sections that correspond to tumours previously scored as 3+ by IHC. The images in the left were segmented for the tumour areas and the images in the right row were segmented for the autofluorescence. What appears evident from a first observation is that despite all these tumour sections belong to the same category (3+ IHC score), they show very different Qdot 585 fluorescent signals and therefore different expression of ErbB2 as also indicated in Figure 5.19 A. The histogram in Figure 5.19 A reports the mean intensities of the Qdot 585 fluorescent signals of 17 tumours which were scored as 3+ by IHC. The results presented in the histogram (Fig.5.19 A) show that this quantification system based on Qdot-immunofluorescence is able to detect different levels of ErbB2 expression within the 3+ category and generate a more linear and scalable measurement of ErbB2.

After we measured the Qdot 585 signal in a set of breast tumours that were previously scored as 3+ by IHC, we quantified the Qdot 585 signal in a set of tumours scored as 2+ by IHC. In Figure 5.18 are presented three examples of ErbB2 2+ breast cancers, the images on the left column shows images that were segmented for tissue areas containing tumour cells and the images on the right column shows images that were segmented for the tissue autofluorescence. Despite the Qdot 585 signal being much weaker (Fig. 5.18) the system was able to discriminate among different levels of intensities within this set of tumours as reported in the histogram in Figure 5.19 B.

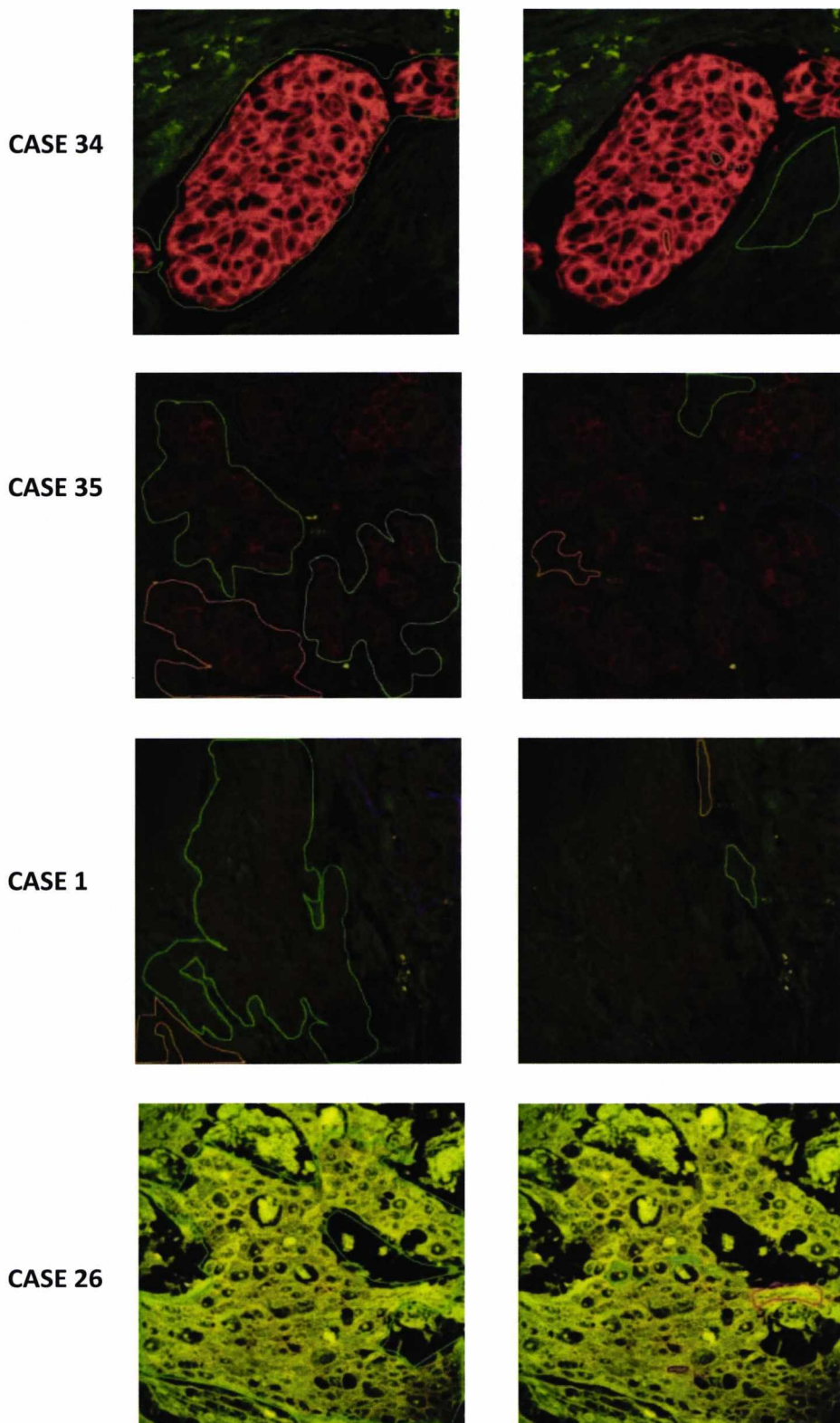


Figure 5.17 Qdot-immunofluorescent staining of breast cancer tissues. Examples of four breast cancer tissues (all scored 3+ by IHC). On left are shown images segmented for the tumour areas. On right are shown images segmented for the autofluorescence. Each case represents different levels of expression of the ErbB2 receptor.

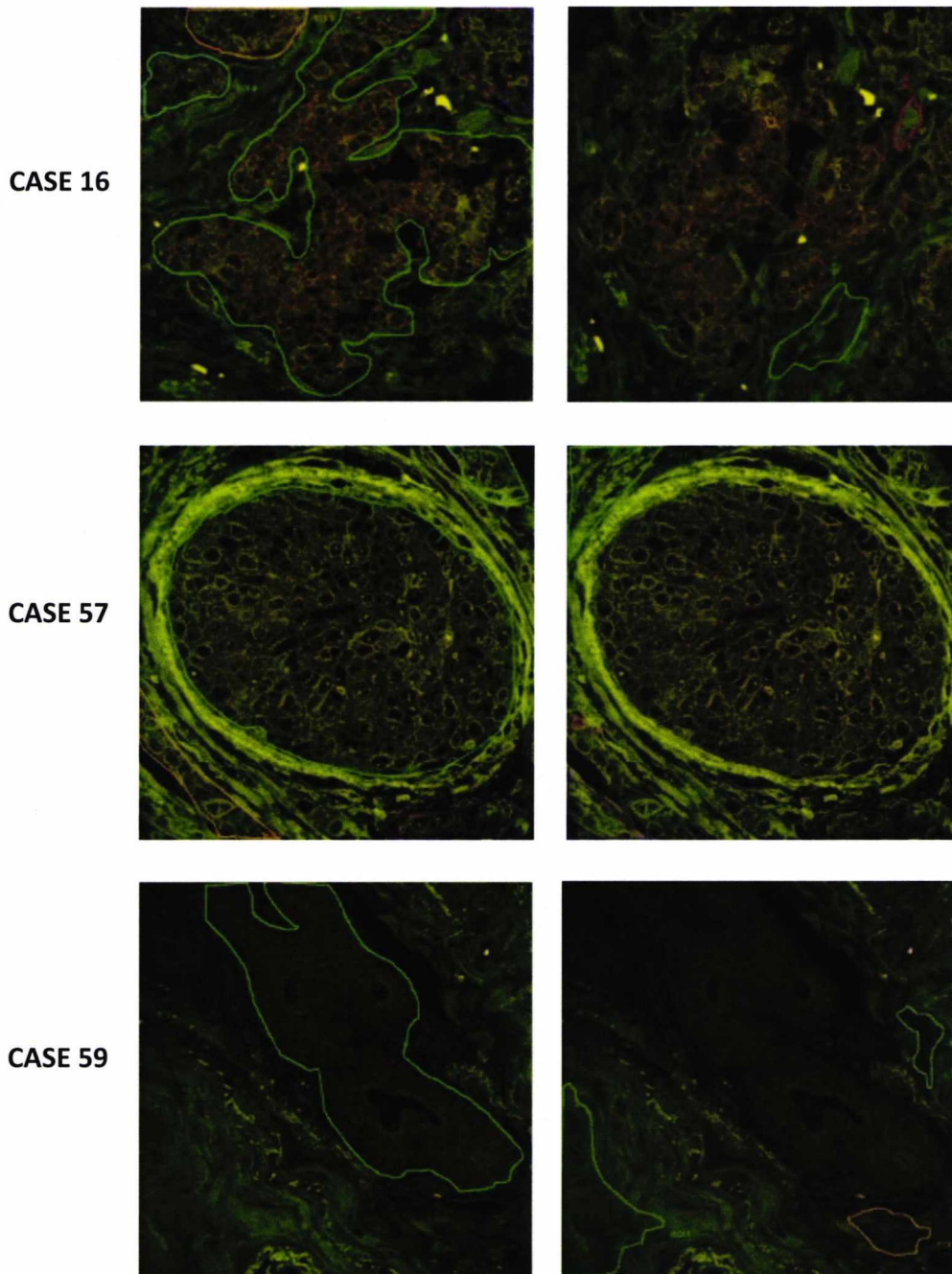


Figure 5.18 Qdot-immunofluorescent staining of breast cancer tissues. Examples of three breast cancer tissues (scored 2+ by IHC). On the left are shown images segmented for the tumour areas. On the right are shown images segmented for the autofluorescence. Each case represents different levels of expression of the ErbB2 receptor.

5 – QUANTIFICATION OF ErbB2 EXPRESSION IN BREAST CANCER TUOMOURS BASED ON Qdot IMMUNOFLUORESCENCE IMAGING

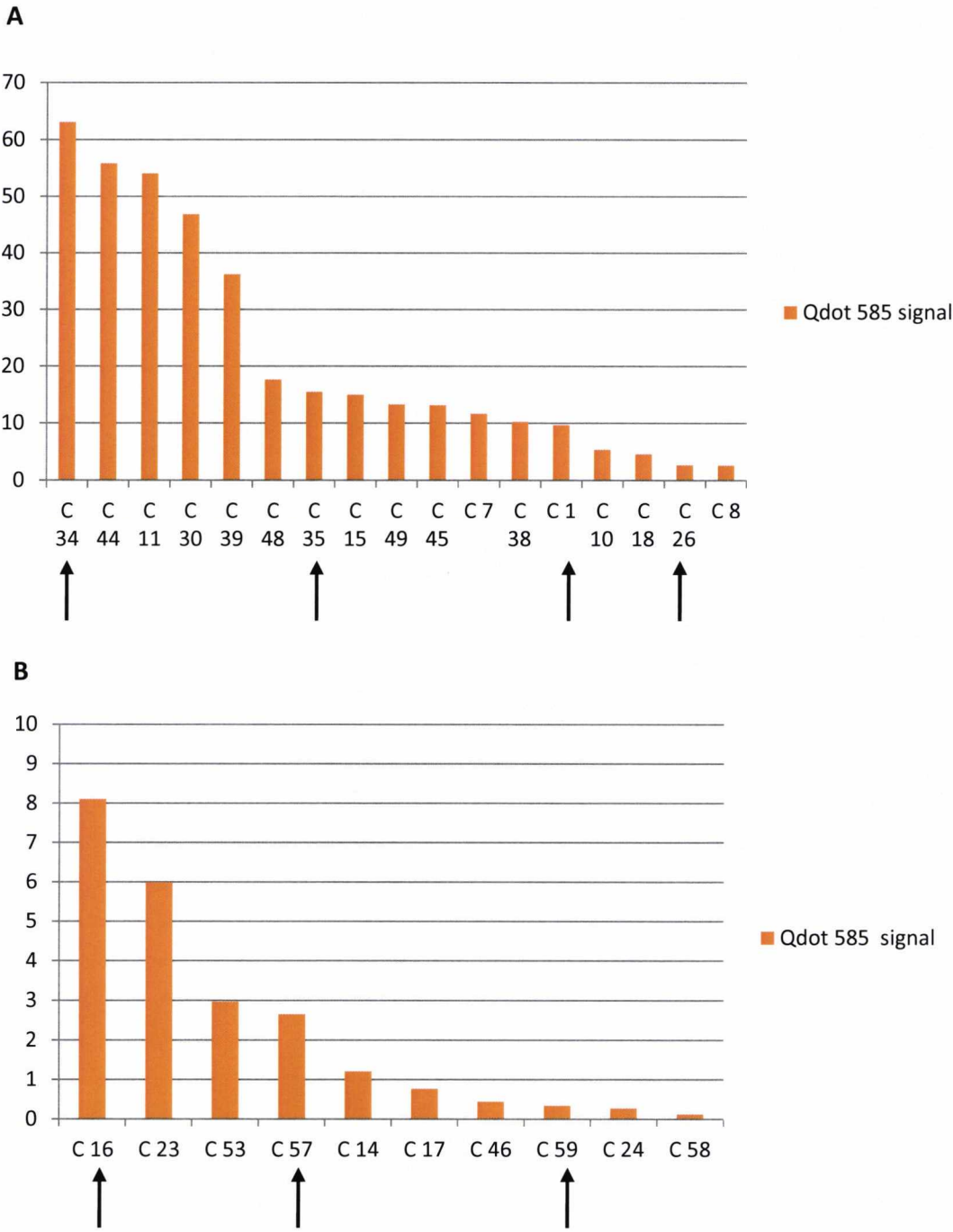


Figure 5.19 The two histograms show Qdot 585 signal quantification (mean intensity reported on the y-axis), of 3+ cases (A) and 2+ cases (B). Cases indicated by the arrows are shown in the images in Figure 5.16 and 5.17.

The strength of the Qdot 585 signal was very low in the group of tumours scored as 1+, and therefore it was not possible to quantify and generate a scalable measurement.

5.3.2.2. VALIDATION OF Qdot QUANTIFICATION SYSTEM VERSUS THE IHC SYSTEM

As mentioned earlier, the quantification of ErbB2 expression was performed on a series of breast cancer sections cut from the same set of tumours previously stained and scored by IHC (refer to section 3.3.4.1). As samples from the same tumours were used to determine ErbB2 expression by two different systems, it was possible to validate the Qdot quantification method by comparing the results obtained with this system with the IHC scoring results. The breast samples that were used to quantify ErbB2 by the Qdot system were ranked on the basis of the IHC score. The plot in Figure 5.20 shows a series of 2+ (blue circles) and 3+ (red circles) samples ordered and plotted versus the Qdot measurements (y-axis). As can be seen from the plot, Qdot quantification values, that correspond to the 2+ samples, show lower scores than the samples categorised as 3+ by IHC. This demonstrate that the Qdot quantification system is able to determine ErbB2 expression levels concordant with the IHC test. Furthermore the plots show that the Qdot system gives a range of values producing higher granularity instead of grouping tumours, with clearly different levels of ErbB2 expression, in the same category.

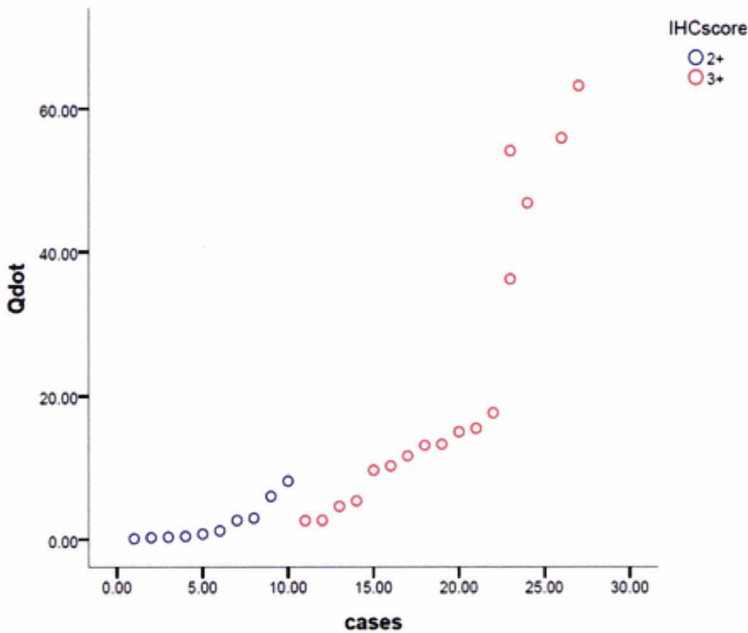


Figure 5.20 Validation of the Qdot quantification system versus the IHC test. As shown in the graph, 2+ samples are in the lower quartile of the Qdot measurements.

5.4. DISCUSSION

In this chapter we have described a system that has enabled us to obtain useful quantitative data from digital images of FFPE breast cancer tissues over expressing the ErbB2 receptor. Using Qdot nanocrystals, our objective was to develop a more linear and scalable measurement of ErbB2 by quantifying the intensity values of the Qdot fluorescent emission while quantitative information can be extracted from digital images, the reliability of these depends on the sample labelling process (see chapter 4), on the accuracy of the image collection and on the image analysis.

5.4.1. IMAGES COLLECTION

After the sample labelling, the image collection was the second important step in order to obtain high quality images for quantification. The image acquisition process started with the type of instrument involved in the process. In this work we used a laser scanning confocal microscope. Compared to conventional epi-fluorescence microscopes, confocal microscopes have several advantages such as better resolution, the ability to eliminate out-focus light, optical slice capability and multichannel detection. However confocal microscopes also have some disadvantages as they are expensive, complex instruments to operate and the laser source can damage the samples if used at high intensity or for a prolonged length of time. Obviously the choice of the instrument mostly depends on the objective of the study. During this work we considered the possibility of using a wide field microscope, however the results were not satisfactory and we reckoned that confocal microscopy was the most suited for this study. The images in Figure 5.21 were collected with a wide field microscope from the ErbB2 breast cancer tissue array control expressing ErbB2 at 3+, 2+, 1+ levels and 0 (Fig. 5.21 A, B, C and D). The images show a stronger background compared to the images acquired with the confocal microscope (Fig. 5.4). Furthermore the image in Figure 5.21 B, with lower expression of ErbB2, appears to have a stronger signal than the image in Figure 5.21 A giving potentially misleading the results.

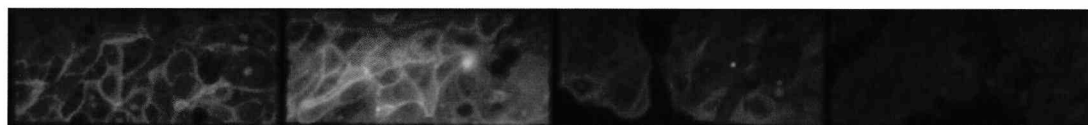


Figure 5.21 Breast cancer tissues expressing ErbB 2 at 3+ (A), 2+ (B), 1+ (C) levels and 0 (D) defined by IHC. The images were acquired with a wide field Olympus microscope and EM-CDD camera.

One explanation can be found in the out-of-focus light. While the images collected with an epi-fluorescence microscope will contain both in- focus and out-of-focus planes, confocal images will contain light from only in-focus planes (from the z-optical slice).The out-of-focus light from above and below the plane of focus is stopped by a pinhole. It can be argued that blocking the photons originating from the planes near to the in-focus object it will cut out useful information. This can be true in some situations, however not for this study. In this work we were using FFPE tissue sections of 4 μ m thickness with strong background due to the tissue autofluorescence; photons from the background can fill the detector reducing its capacity of collecting photons (from the signal) before the detector saturates (Waters, 2009). Excluding photons not originating from the plane of focus improved the signal to noise ratio and generated sharper and clearer images. However there were also other factors, related to the detection system, which need to be taken into consideration. For instance the filters used for the excitation and emission were suitable, but they were not optimised for the Qdot 585. Furthermore, the light detector used, an electron multiplier cooled charge-couple device (EM-CDD), is a very sensitive device with a high quantum efficiency (QE), which is the proportion of photons that reaches the detector that contribute to the output signal. This means that an EM-CDD camera can detect very low signals. Usually this can represent a very useful property, especially in experiments with cells where there are a small percentage of photons from the background that arrives at the detector.

The advantage of the detection system available in the Leica confocal laser scanning microscope (see section 5.3.1), is that it is a very flexible system. The main control panel allowed us to create the best setting for the image collection. It enabled us to

have a complete control of the laser light levels (using the AOTF filters), of the wavelength and the width of the band emission for collection by adjusting the movable slits and of the PMTs gain and offset; also the look up table enabled us to check if the chosen setting was correct for the acquisition or generating over/underexposed images. The first priority was to reduce the noise present in the images. In a confocal microscope there are two types of noise: the dark current noise (or electronic noise) and the shot noise (or photon or Poisson Noise). The dark current noise is created by the instrument even in absence of light. It is due to a leakage of current within the device. The dark current noise is shown in the image as few bright pixels randomly scattered. The shot noise is associated with the statistical nature of the light. The light is formed by photons and the number of photons that reach the detector at random time points is not always the same. This fluctuation in the number of detected photons (statistical uncertainty) is the shot noise. This means that each pixel in the image will contain different number of photons at random time points. Because the shot noise is related to the square root of the photons (signal) collected, increasing the signal intensity (number of photons collected) decreases the effect of the shot noise as the increase in the signal is greater than the increase in the noise. An example of an image containing noise is shown in Figure 5.2 A that was acquired with a single scan. However using the averaging method it was possible to reduce the noise and improve the image quality (Fig. 5.2 B, C and D).

We then have established an acquisition setting able to include in the image all the grey levels and therefore not exclude any information as shown in Figure 5.3 B. The images in Figure 5.3 B shows a breast cancer tissue with high intensity Qdot 585 signal corresponding to ErbB2 expression scored as 3+ by IHC. The setting also showed that it was also possible to detect different intensity signals corresponding to lower levels of ErbB2 expression corresponding to 2+, 1+ and 0 scored by IHC (Fig. 5.4 and 5.8 7 and C and D). The mean intensity values reported in the histogram in Figure 5.9 also confirmed what was observed in those images.

5.4.2. INSTRUMENT CONSISTENCY

In order to quantify the level of fluorescence between samples and on different days, it was important to ensure that the setting was identical each time. For this reason the laser stability and the general performance of the detection system was monitored by using a control section supplied by Leica. The advantage of this thin section of rhizome from Lily of the Valley resided in its morphology. The clear structure allowed recognising and performing a series of acquisitions using the same area in the rhizome (Fig. 5.9). This control was particularly useful. Indeed when we started using the confocal, it allowed us to spot a problem relative to the laser stability as shown in the histogram (Fig. 5.22).

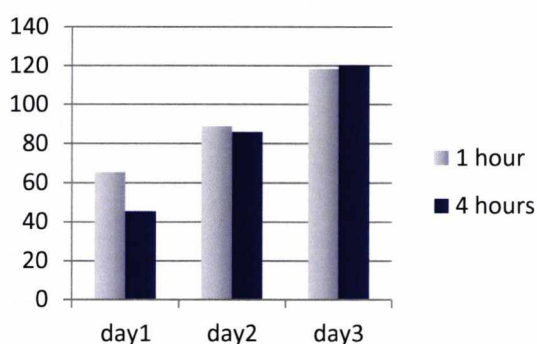


Figure 5.22 The histogram shows the mean intensities obtained from the images of the control section acquired in the red channel using the same setting. The histogram clearly shows the inconsistency of the instrument performance.

Subsequently the problem was corrected with the intervention of a Leica engineer. We then ran a new test using the control section of the rhizome and it showed that the laser was stable and the acquisition could have been performed consistently (Fig. 5.10 A and B). The presence of minor variations in the mean intensities are due to small shifts in the x-y position of the region of the rhizome acquired and also probably to a different position of the z-plane acquired. Considering these variables, we concluded that the small changes in the intensities were not due to an unacceptable performance

of the laser or the light detector. This was also confirmed by the results presented in Figure 5.11 and 5.12 A and B. Here the mean intensities were slightly decreasing with the time probably as consequence of the tissue and fluorophore photobleaching.

5.4.3. QUANTIFICATION ANALYSIS

In order to obtain an accurate measurement of the levels of expression of ErbB2 we identified areas containing cells and isolated the Qdot 585 signal from the background and the autofluorescence.

In Figure 5.8 we have shown how we used the tissue autofluorescence as a useful tool to facilitate the identification of the tumour areas versus other tissue structures. Here the images acquired in the green channel (485nm-505nm) showing the tissue autofluorescence only (Fig. 5.7) were merged with the images acquired in the red channel (575nm-585nm) (Fig. 5.5). In the two-colour images (Fig. 5.8) the Qdot 585 signal from the tumour cells appeared more obvious than in the images in Figure 5.5. In this way it was possible to segment the images for the tumours areas and the tissue autofluorescence (Fig. 5.13, 5.16, 5.17 and 5.18). The mean intensity of each area was calculated after applying a threshold of 50 grey levels (from 0 to 50 unit of the grey scale). In this way we excluded all the pixels corresponding to dark regions in the slide where no signal was present; in this way we also excluded the low intensity values of the background. As the majority of pixels were between 0 and 50 grey levels (Fig. 5.14 and 5.15), including these values would have skewed the results. However even after applying the threshold the background due to the tissue autofluorescence was still affecting the result (Fig 5.16 C). The autofluorescence in some tissues can be very strong showing high intensity values as shown in the image in Figure 5.17 case 26. This appears more evident by comparing the histogram in Figure 5.19 A where the autofluorescence was subtracted, with the histogram in Figure 5.23 where the mean intensities of the same cases without subtraction of the autofluorescence are reported. Here cases with weaker Qdot 585 signals have stronger fluorescent intensity than cases with higher Qdot 585 signal. However from the histogram it is clear that this is only due to the contribution of the autofluorescence.

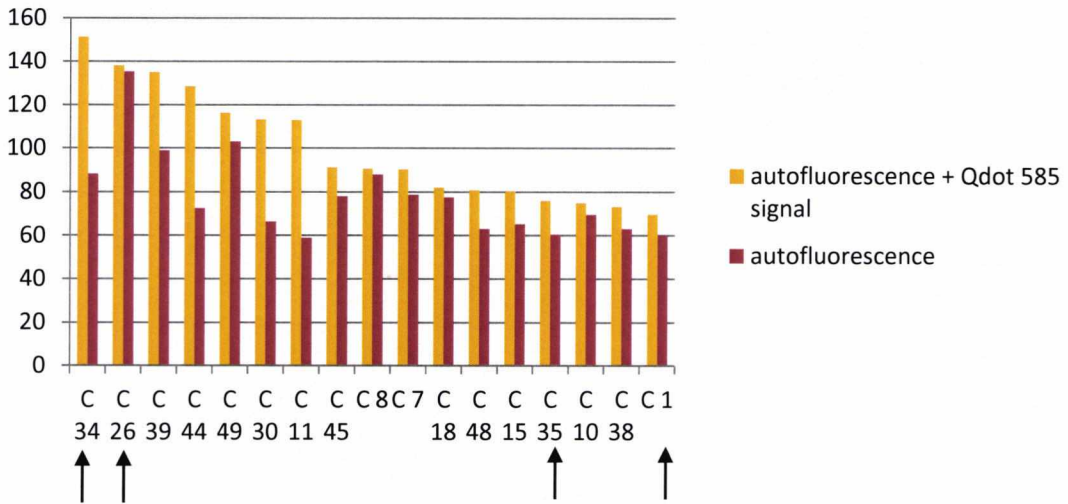


Figure 5.23 Quantification of Qdot 585 signal with the contribution of the autofluorescence and the autofluorescence only. The histogram shows how the autofluorescence can affect and the quantification results.

Therefore the average of the mean intensities of the background areas was subtracted from the average of the mean intensities of the tumour areas (Fig.5.19 A and B). As the images were acquired with a 63x magnification lenses and thus each image was representing only a small part of the tissue examined, we reckoned that analysing a larger tissue area would have given more accurate measurements even if we observed that the Qdot 585 signal was uniform within each section and therefore even a small area of that section could have represented the ErbB2 levels of expression in that section (Fig.5.24). Therefore all the measurements shown so far were based on the analysis of three images acquired for each 2mm core section. These covered between 70% and 80% of the tissue.

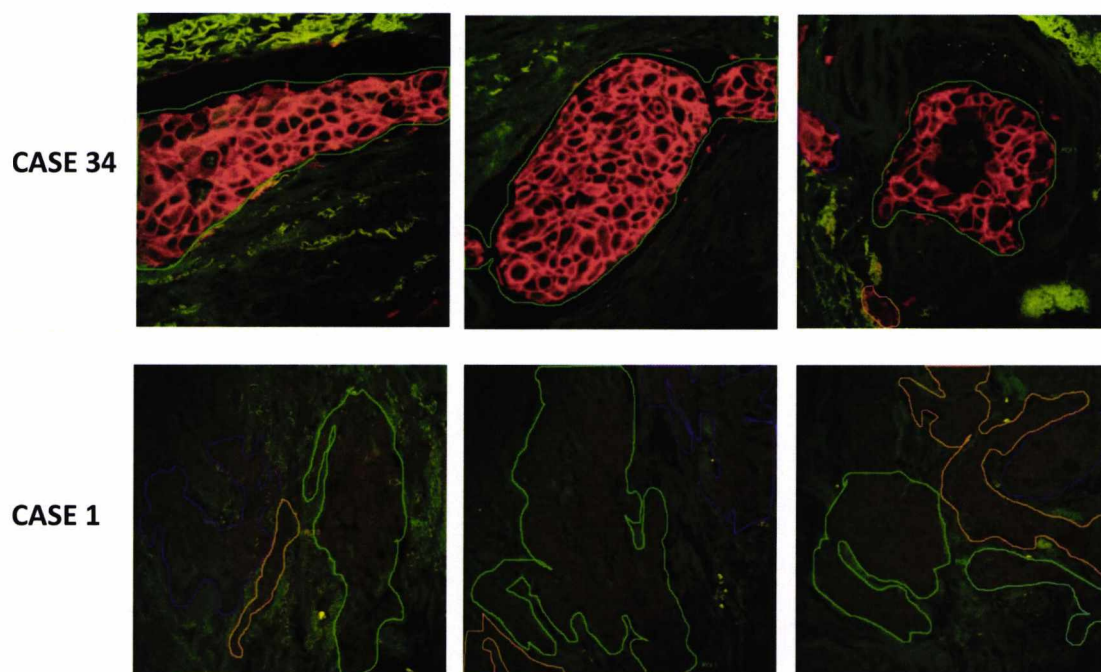


Figure 5.24 Two examples of three different tumour areas within the same section. The immunofluorescent staining with Qdot 585 generated a uniform signal throughout the section.

The quantification method was validated by comparing the results obtained from the quantification of the Qdot signals with the IHC score. In the plot in Figure in 5.20 we have shown that all the 2+ cases gave low scores and were located in the lower quartile of the Qdot measurements. The quantification results have demonstrated that Qdot immunofluorescent staining and the method that we have applied for the image acquisition and for the quantification analysis, have generated a more accurate and scalable measurement of ErbB2 expression in breast cancer tissues. Most important we have shown that the levels of expression of ErbB2 are very different within the same category of tumour scored as 3+ and 2+ (Fig. 5.19 and 5.20). Within the cases scored as 3+ by IHC there was a 60 fold range of ErbB2 expression which can be meaningful for screening patients for Herceptin treatment.

The system we developed was shown to be able to easily differentiate ErbB2 levels of expression in both 3+ and 2+ IHC categories, but it was not able to discriminate between low levels of ErbB2 expression in the 1+ IHC category. However our major

interest was focused on the 3+ and 2+ cases: the first group is the target for Herceptin treatment and the second group is formed from borderline cases that require an additional test (FISH) to assess the ErbB2 status to determine the eligibility of those patients for treatment.

On the other hand, to discriminate between low level of ErbB2 it would have been possible by improving the system sensitivity. This could have been done in different ways such as increasing the signal strength of the Qdot 585 and/or reducing the contribution of the autofluorescence to the signal (for instance by using strepavidin Qdot that emit in the infrared where there is little or no autofluorescence).

6 – QUANTIFICATION OF PRIMARY BREAST CANCER TREATED WITH HERCEPTIN

6.1 INTRODUCTION

One of the most significant breakthroughs in the treatment of breast cancer over the last 20 years has been the development and launch in 1998 of the monoclonal antibody Herceptin. This drug offered real improvement in relapse free interval and survival in patients with breast cancer over expressing ErbB2. Clinical studies, involving women with ErbB2 positive metastatic breast cancer that have progressed after chemotherapy, have shown the efficacy of Herceptin alone and in combination with chemotherapy (Meric et al., 2002). It has been recorded that the overall response rate to Herceptin as single agent, in patients with metastatic disease, is between 15% and 26% (Cobleigh et al., 1999; Vogel et al., 2002) and it becomes much higher, between 80% and 86%, when Herceptin is used in combination with other agents (Collins et al., 2009; Spigel and Burstein, 2003). This means that around 15%-20% of patients do not have any benefit from Herceptin treatment. It was observed that the efficacy of Herceptin was significantly greater in those patients over expressing ErbB2 at 3+ level measured by IHC or FISH positive compared to those patients with a score of 2+. These latter patients showed no response rate or any low benefit from the drug (Slamon et al., 2001; Vogel et al., 2002). Therefore the best way of predicting a patient's tumour response to Herceptin is by the assessment of ErbB2 over expression. As explained earlier, currently in clinical practice ErbB2 status is determined by detecting ErbB2 expression by IHC and/or ErbB2 gene amplification by FISH (see 1.15.1 and 1.15.2). It is recognised that both assays have advantages and disadvantages and although there have been international recommendations in order to improve the accuracy of the two tests, approximately 20% of the current ErbB2 tests can be inaccurate (Wolff et al., 2007).

Unlike the IHC, fluorescence is not affected by temperature, pH, substrate concentration or product inhibition, therefore the signal generated by the nanocrystal is proportional to the amount of the target present in the tissue. As shown in the previous chapter, the Qdot quantification system was able to discriminate between

different amounts of ErbB2 within the 3+ and 2+ categories giving a more scalable measurement. Using Qdot labelled antibodies and image analysis, this study aims to evaluate levels of HER2 receptors in patients with breast cancers treated with Herceptin and investigate whether there is a correlation between HER2 levels of expression, measured by Qdot, in patients who respond to Herceptin and who do not respond.

We believe that identifying sub-groups of breast cancers is important to improve the selection of patients for Herceptin treatment and for different targeted therapies.

6.2 AIMS

- I. Measure ErbB2 over expression by Qdot image analysis in a set of primary breast cancers treated with Herceptin.
- II. Compare Qdot measurements vs IHC scores
- III. Correlate Qdot ErbB2 status with clinical outcome

6.3. RESULTS

6.3.1. QUANTIFICATION OF ErbB2 IN A SERIES OF BREAST CANCERS TREATED WITH HERCEPTIN

In this study we have used the Qdot 585 labelled antibody and the image quantification system to test the expression levels of ErbB2 in a series of 145 FFPE primary breast carcinomas from women treated with Herceptin. All the samples were kindly supplied by Prof. Ian Ellis (Nottingham City Hospital). The tumour sections were organised on a tissue microarray and this allowed us to stain all the tissue together. The sections were 0.6mm in diameter and extracted from the central core of the tumour. This set of breast primary tumours contained 104 cases classified as ErbB2 3+ and 29 cases classified as ErbB2 2+ by IHC according to the international guidelines. However 10 cases were recorded as “999” meaning that both IHC and/or FISH data were not available or unknown. The 29 cases scored as 2+ were also tested as positive FISH and therefore were also eligible for Herceptin therapy. All this information was obtained from the patients’ clinical database.

The analysis was performed on 123 samples (88 3+ samples and 27 2+ samples/FISH positive) as some sections were damaged, missing or contained no scorable tissue. The tissue microarray was stained following the standardised protocol previously developed. The images were acquired by using the settings previously established (chapter 5) after controlling for the microscope performance by using the control slide supplied by the Leica Company. As the cores were smaller (0.6mm) compared to the cores on the tissue microarray previously used (2mm), two images were acquired instead of three. Images were then segmented and the Qdot 585 signal was quantified by applying the method described in the previous chapter. The images in Figure 6.1 show four examples of breast cancers scored as 3+ by IHC. The images in Figure 6.2 represent four examples of breast tumours classified as 2+ by IHC and FISH positive. All the images presented in both Figure 6.1 and 6.2 were segmented for the tumour areas, images segmented for the autofluorescence have not been shown. The data obtained have shown that applying Qdot quantification system to this series of breast

cancers, it was possible to identify a 40 fold range of expression of the ErbB2 protein (Fig. 6.3).

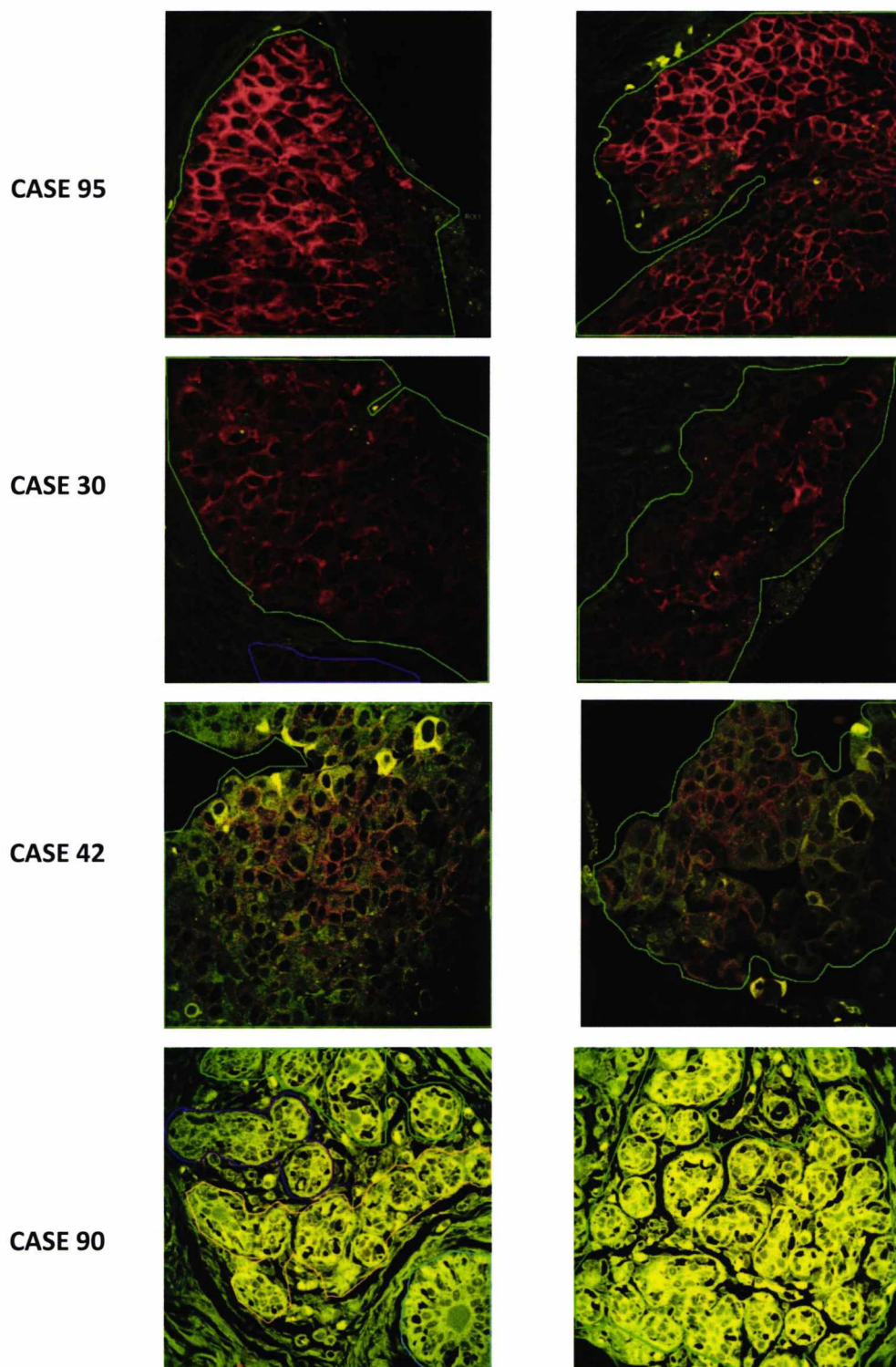
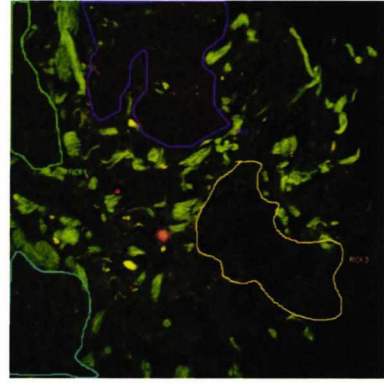
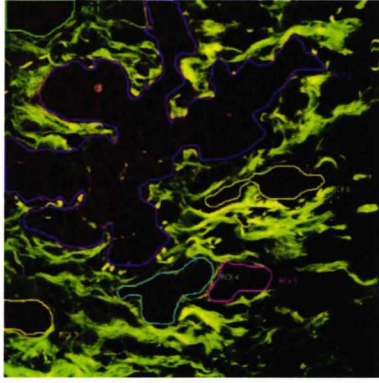
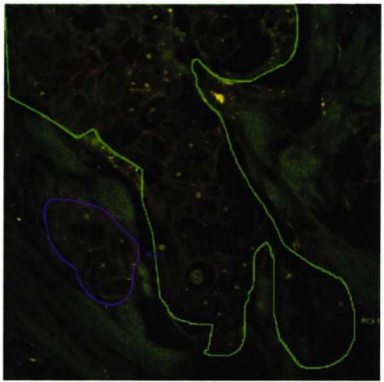
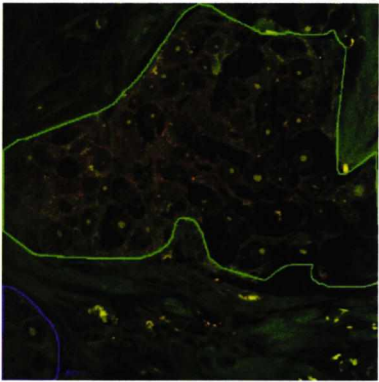


Figure 6.1 Qdot-immunofluorescent staining of primary breast cancer tissues. Examples of two images each from four breast cancer cases scored as 3+ by IHC. The shown images were segmented for the tumour areas.

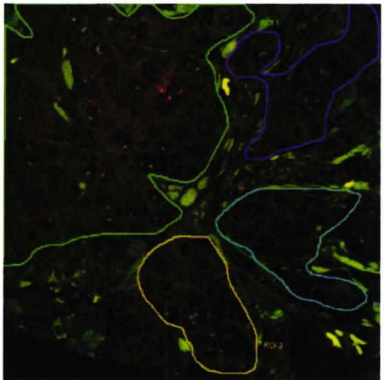
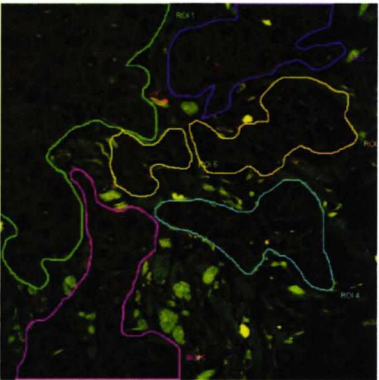
CASE 121



CASE 108



CASE 111



CASE 135

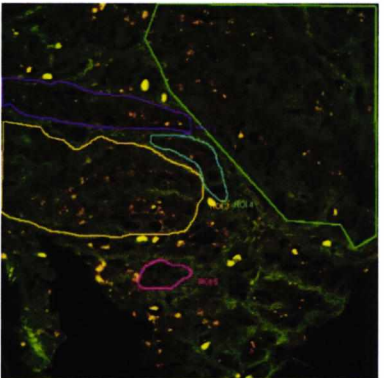
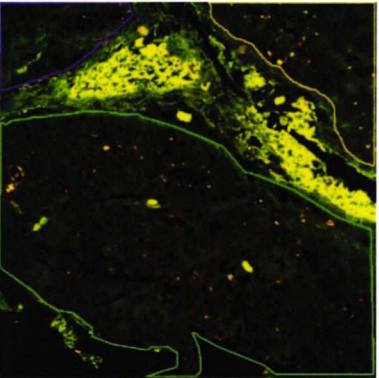


Figure 6.2 Qdot-immunofluorescent staining of primary breast cancer tissues. Examples of two images each from four breast cancer cases scored as 2+ by IHC. The images shown were segmented for the tumour areas.

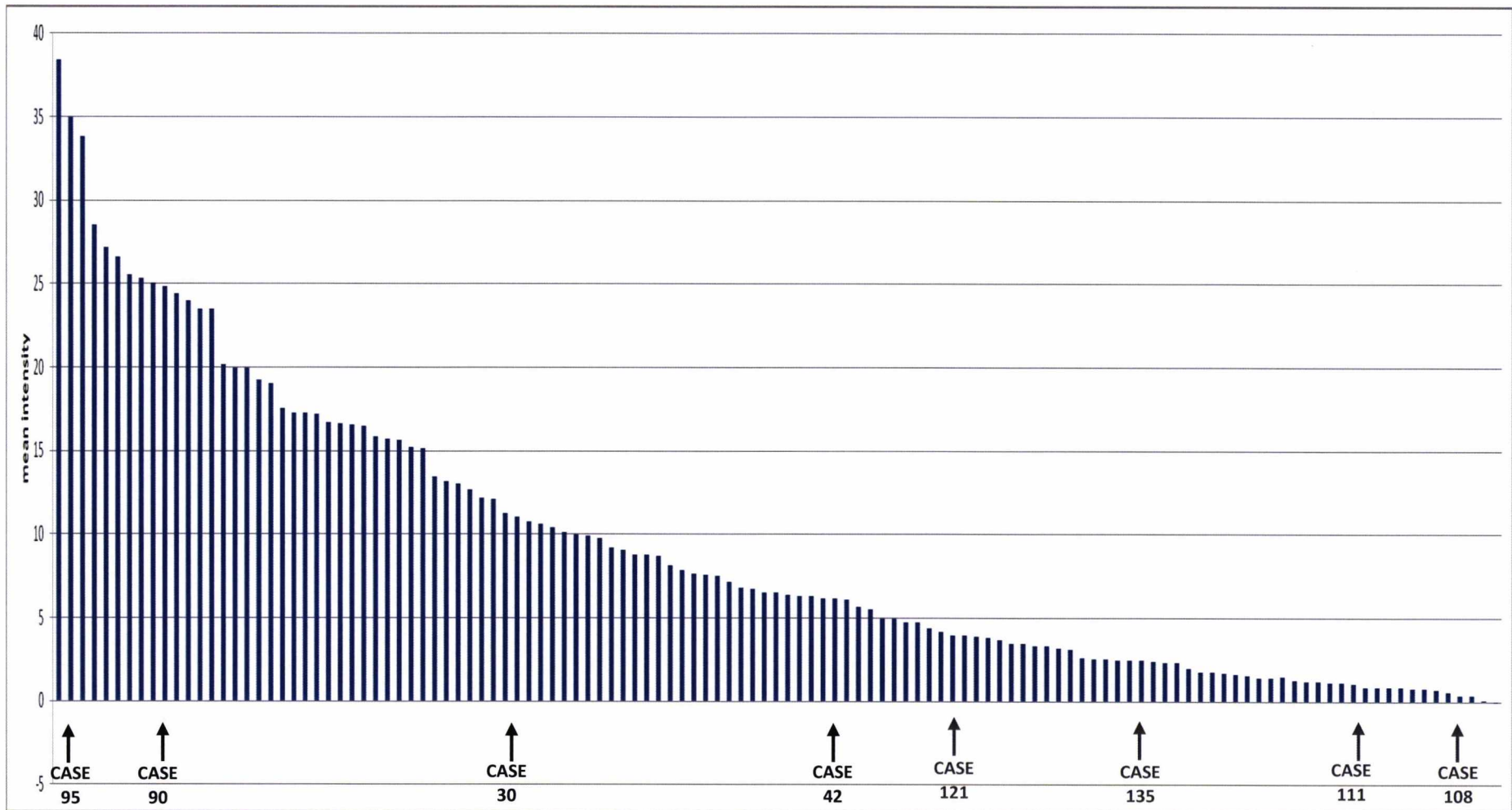


Figure 6.3 The histogram summarises the Qdot quantification results of 123 breast cancers over expressing ErbB2 at 2+ and 3+ levels. The black arrows indicate 3+ cases shown in Figure 6.1 and the grey arrows indicate the 2+ cases shown in Figure 6.2. The histogram demonstrates that this test can discriminate different levels of protein expression.

We then attempted to validate the Qdot ErbB2 score by comparing it with ErbB2 IHC status. The Qdot quantification data were ordered and ranked on a plot, according to IHC 2+, 3+ and not recorded “999” (Fig. 6.4). The plot in Figure 6.4 shows that the 27 patients classified as 2+ gave relatively low Qdot score and that they were in lowest quartile of the Qdot ErbB2 levels. This demonstrates that the Qdot system is able to correctly delineate levels of ErbB2 expression concordant with the IHC test.

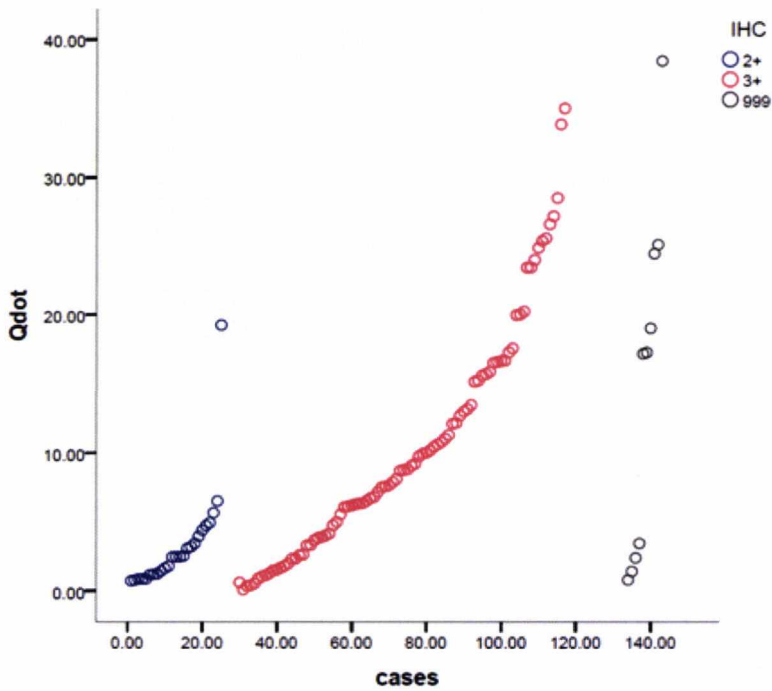


Figure 6.4 Validation of Qdot quantification values of 123 primary breast cancers over expressing ErbB2 versus IHC score. The graph shows that 2+ patients are in the lower quartile of the Qdot measurement. 999 are not recorded patients in the clinical database.

6.3.2 STATISTICAL ANALYSIS

We demonstrated that Qdot quantification system was able to determine different ErbB2 levels of expression producing a more scalable measurement compared to IHC. Then we addressed the question how the ErbB2 status measured by Qdot was related to patients’ outcome. In order to address this question, we first scrutinised the patients’ clinical database. The clinical data included a wide range of information about each patient. For instance some information were about patient’s age and patient’s

age at the time of the diagnosis, breast cancer family history, others were related to patients' tumour features such as tumour size, pathological tumour extent, pathological breast cancer type (e.g. invasive ductal carcinomas), tumour grade, oestrogen receptor status, pathological TNM stage (see section 1.12.3), lymph node status (positive or negative) and others relating to patient's treatment (radiotherapy, hormonal therapy, adjuvant chemotherapy and Herceptin treatment). However not all these data were used for the statistical analysis.

In this preliminary analysis, in order to correlate Qdot-ErbB2 status to clinical outcome, we decided to consider the disease status (disease free, recurrence, metastatic and death) at the last follow up (November 2010). The table 6.1 summarises the clinical outcomes obtained from the database.

Clinical outcome	Number of patients
Disease Free	102
Metastatic	6
Recurrent	1
Death	6

Table 6.1 Summary of the disease status in 115 breast cancer patients treated with Herceptin.

Initially we split the Qdot-ErbB2 scores in high and low to see if the patients with low ErbB2 levels measured by Qdot were those who benefited least from Herceptin. The cut-off point (6.52) was chosen as the median of the Qdot values (Fig. 6.5).

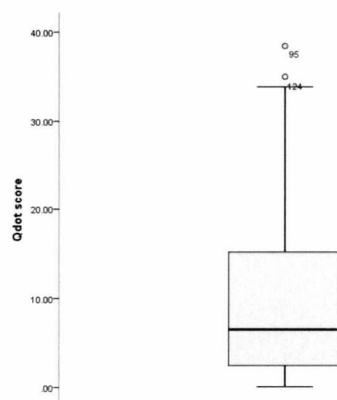


Figure 6.5 Median values of Qdot measurement. The median value (6.52) was calculated with SPSS PASW 18

Therefore we highlighted those patients who were disease free vs. recurrent, metastatic and dead. The majority of adverse events (recurrent, metastatic and death) observed were below the cut-off point (Fig. 6.6).

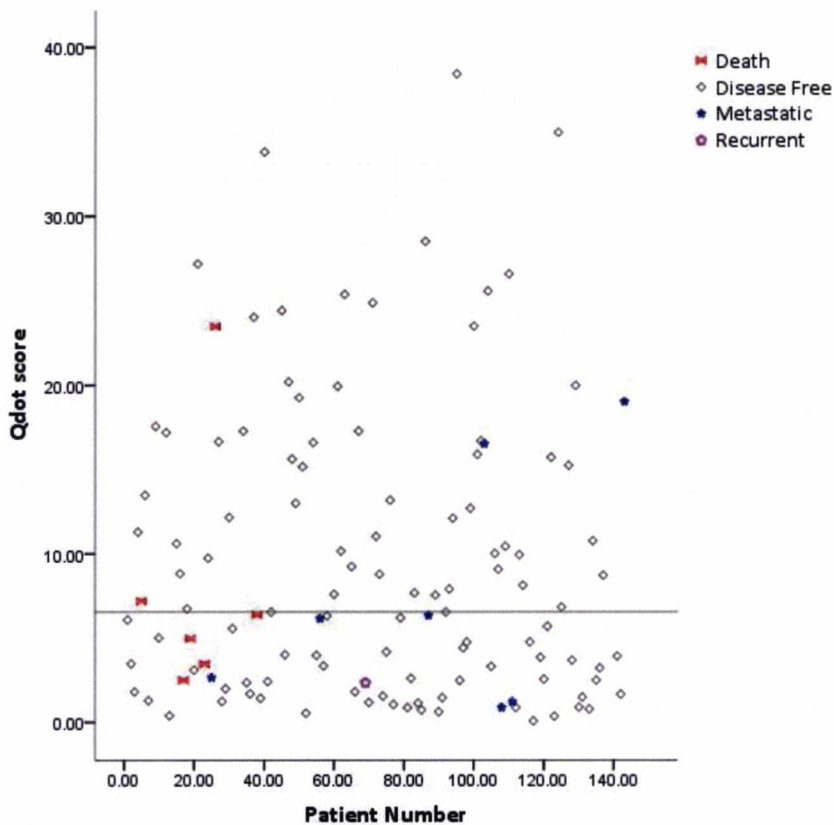


Figure 6.6 A median level was chosen as cut-off point to divide patients into two groups, one group with high Qdot score, and the other group with low Qdots score. Patients below the median level seem to have poorer clinical outcome.

Following this observation we hypothesised that patients in the group with low scores might have had less benefit from the drug. Therefore we next investigated this hypothesis by using the Kaplan-Meier survival analysis. The Kaplan-Meier plot is a widely used method in clinical studies for estimating the survival probabilities of a population over time. It plots the percentage of survival against time. The survival curve is drawn as a step function where each step represents an event occurring at time t . Every time that occur an event the curve drop by $1/n$ where n is the population at that time. The starting time ($t=0$) corresponds to the time when a study has started;

at this time all subjects are alive. As the time progresses to the time of the occurrence of a given event two situations can happen: the proportion of the population still alive decreases (the curve steps down) or does not change (the curve remains flat) (Bewick et al., 2004; Goel et al.). The Kaplan-Meier analysis also incorporates a series of different situations labelled as “right-censored” data. For example a censored observation can be marked if a patient entered the study later or dropped out the study before the end, if he/she has neither survived or died before the end of the study, or if for any reason the contact with the patient has been lost during the follow-up or they have died for another cause independently from the cause of interest (Lagakos, 1979). A censored point data is indicated on the curve by a tick “|” and every time a point data is censored the population is reduced by 1. The censored data represent at the same time a strength and weakness of the Kaplan-Meier curve. It is a strength because it allows to include in the analysis also the data related these patients. However, it can represent a weakness as a high number of censored data will reduce the size of the initial population changing on the curve the effect of the occurring events and reducing the reliability of the analysis.

This analysis is used to compare survival rates between two or more groups. For instance in this study we split the population into high and low ErbB2-Qdot score based on the cut-off point previously calculated. The size of the two groups was even as the group with high ErbB2-Qdot score included 57 patients and the group with low ErbB2-Qdot score included 58 patients. For each group a graph was plotted of time (x-axis) versus the proportion of people surviving (y-axis). All the adverse events (death, disease progression, recurrence) were included in the analysis. Figure 6.7 shows the overall survival (OS) for each group of patients. 3 adverse events were observed in the group with high ErbB2-Qdot score and 10 in the group with low ErbB2-Qdot score (Fig. 6.7). However there was no significant difference between the two curves, meaning that the probability of survival was the same for each population. As lymph node positivity is known to be associated with worse prognosis we applied the analysis to this subgroup of patients. Also in this case the majority of the adverse events were in the subgroup with low Qdot score (8 events vs. 2 events) however there was no significant difference between the two curves (Fig. 6.8).

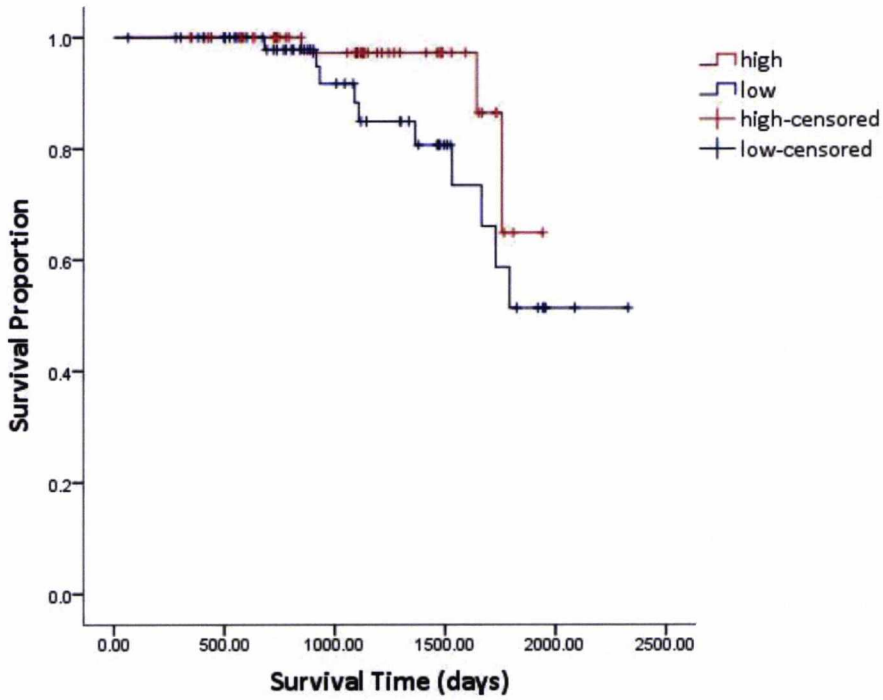


Figure 6.7 Kaplan Meier survival analysis of the whole population. The adverse events include death, metastasis and recurrence.

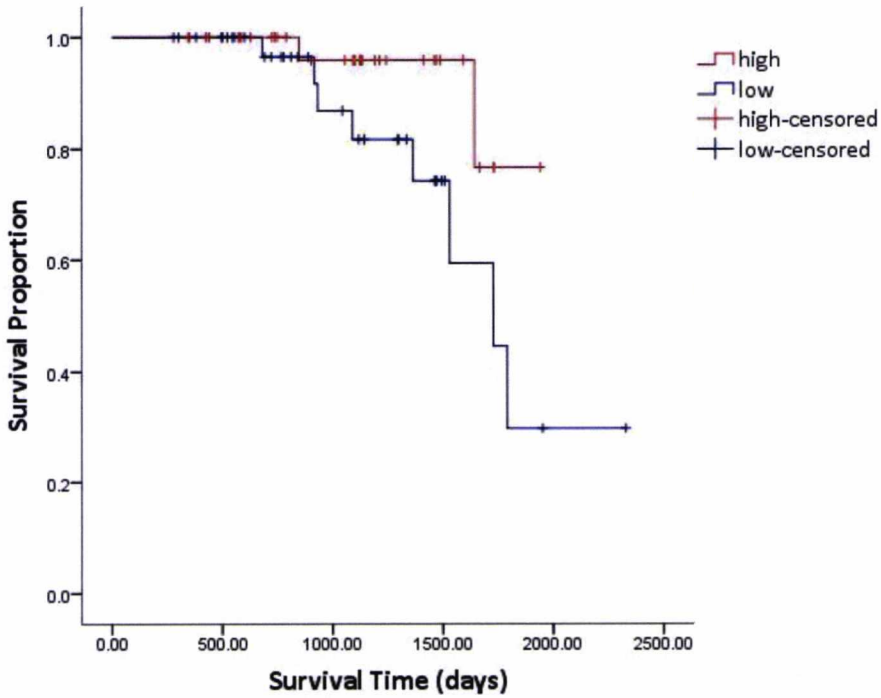


Figure 6.8 Kaplan Meier survival analysis in node positive patients including death, metastasis and recurrence as events.

6.4. DISCUSSION

6.4.1. ASSESSMENT OF ErbB2 STATUS BY Qdot

The availability of a very effective anti-ErbB2 treatment based on the use of the monoclonal antibody Herceptin, has made the assessment of ErbB2 fundamental in order to select those patients who are eligible for the drug. The use of Herceptin was first approved by the US FDA for the treatment of metastatic disease and more recently it has been recommended for the treatment of ErbB2 positive early breast cancers (NICE technology appraisal guidance 107). In this way we are seeking as hypothesis that what is clinically relevant is not just the over expression of the protein but the extent of that over expression. To date while there are no evidences that Herceptin is beneficial to patients in the 0 and 1+ category or low levels of gene amplification (Pauletti et al., 2000) there is much evidence that the clinical benefit from the drug is restricted to patients in the 3+ IHC category and 2+ FISH positive (Slamon et al., 2001) (Mass et al., 2005). There are several biologic mechanisms that can cause increased levels of ErbB2 expression in a cell. The most common mechanism is gene amplification. It has been suggested the polysomy of chromosome 17 is associated with ErbB2 over expression although this is uncertain (Kostopoulou et al., 2007; Torrisi et al., 2007). Elevated levels of ErbB2 also have been found in the absence of gene amplification or polysomy 17. In this case ErbB2 over expression can have arisen from an increased ErbB2 gene expression and mRNA production or decreased mRNA degradation. Different assays can be used to quantify mRNA over expression (e.g. qRT-PCR, Northern blot, slot blot, in situ hybridisation), or to determine gene amplification (e.g. PCR, Southern blot, in situ hybridisation) or to assess protein over expression (e.g. ELISA, IHC) (Barberis et al., 2008; Moelans et al.). However all the techniques that involve tissue homogenates, such as PCR, Northern blot, Southern blot, Western blot, ELISA are not practical as clinical test for several reasons. First these methods require a large amount of tissue sample which has to be destroyed in order to extract proteins, mRNA or DNA; then the extracts from different cellular compartments and from different cells types (tumour cells, stromal cells, normal cells),

can be mixed together producing misleading results (Rampaul et al., 2002). On the contrary to perform the IHC test can be used with a small tumour section preserving the rest of the tumour biopsy and the stained slide can be stored in case of further re-evaluation. Most important, this type of assay preserves the tissue architecture which also carries important information about the tumour. For this reason IHC is still the test most used in the clinical laboratory to determine ErbB2 status. However as discussed before the IHC test has several drawbacks: it is a semi-quantitative method, is dependent on temperature and pH making it difficult to standardise on a global scale. The other test widely used is FISH which is applied to confirm gene amplification in IHC equivocal cases. Despite the effort of the ASCO/CAP panel to standardise pre-analytic (tissue processing), analytic (tissue staining) and post-analytic (scoring criteria) factors, false-negative and false-positive ErbB2 IHC results are frequently documented (Dowsett et al., 2003; Gown, 2008; Sauter et al., 2009). This has brought the need for developing a test that allows improving the assessment of ErbB2 and therefore the patients' selection for the treatment.

In this study we have quantified the levels of ErbB2 expression by using the Qdot system in a tissue array of 145 breast cancers treated with Herceptin. The ErbB2 status of each breast cancer was previously determined by IHC and FISH tests at Nottingham City Hospital. The results have shown that the Qdot fluorescence imaging method has the potential to improve the ErbB2 assessment. First, like the IHC assays, it preserves the tissue morphology. This appears clear by observing the two colour images (autofluorescence plus Qdot signal); therefore such features can be used by a pathologist in order to identify tumour areas, stromal cells or other tissues areas meaningful for the final assessment. The advantage of using an image analysis system to extract quantification data is that it can contribute to decrease the scoring subjectivity and improve consistency and reproducibility. In addition the Qdot method can offer higher discrimination among different levels of ErbB2 expression compared to the IHC method. In Figure 6.3 we have shown that within the 2+ and 3+ category there is a wide range of expression of ErbB2 protein, over about 40 fold range and if we consider the Qdot quantification data presented in Figure 5.18 A we found even a wider range up to 60 fold. This appears even more evident in Figure 6.4 where the

Qdot scores were ranked according to the 2+ and 3+ categories. A paper published during this work by Chen and co-workers has shown that using Qdot labelling, ErbB2 levels in IHC 3+ cases varied over a 100 fold range (Chen et al.) confirming the data presented here. The higher score determined by Chen et al compared to ours may be due to the fact that they used a Qdot conjugated streptavidin probe which amplifies the signal.

6.4.2 CORRELATION BETWEEN QDOT QUANTIFICATION AND PATIENTS RESPONSE TO HERCEPTIN

Once we have measured ErbB2 status by Qdot in this set of patients treated with Herceptin we attempted to investigate how the quantitative measurements of ErbB2 based on Qdot analysis correlate to the patients clinical outcome following Herceptin treatment. The new method should improve the quantification of ErbB2 in order to identify those patients who are benefiting and who are not benefiting from the treatment. This will avoid exposing patients, who do not have chance to benefit from the drug, to the risk of side effects. It has been shown that the risk of developing brain metastases is higher for those patients who received Herceptin in the clinical trials (Sutherland et al.) and that Herceptin is associated with cardio toxicity specially in combination with anthracycline/cyclophosphamide (Singer et al., 2008) NICE technology appraisal guidance No34; National costing report: Early and locally advanced breast cancer/Advanced breast cancer 2009).

In this study we have divided the patients in two subgroups, choosing as the cut-off point the median value. Although it would be expected poorer clinical outcomes in patients with high levels of ErbB2 expression, as all the patients were treated with Herceptin, from preliminary observations we noticed that the majority of patients with poorer outcome were in the subgroup with lower Qdot score (Fig. 6.6). This suggested that the drug was more effective on the population with highest ErbB2 expression. A further analysis was done using the Kaplan-Meier curves to estimate the chance of survival in each group. The analysis was performed by using first the whole population and then only the lymph node positive patients. Although most of the adverse events were occurring in the population with low Qdot score, the results

showed that there was no significant difference between the two curves in each Kaplan-Meier analysis meaning that both population (with high and low Qdot score) had the same overall survival chances (Fig. 6.7 and 6.8). The small size of the sample, high number of censored patients and the small number of events represented the main limitations of this study. A longer term follow-up would have been valuable to further investigate our hypothesis and obtain more conclusive evidence. Recently a study in line with our preliminary results has been published by Lipton et al. By using a different quantitative technology called HERmark, they have shown a good correlation between increasing ErbB2 levels and response rate to Herceptin (Lipton et al.). However the same group in a subsequent analysis has observed a subgroup of patients with very high level of ErbB2 expression that appears to respond poorly to Herceptin (Bates et al., 2011; Joensuu et al., 2011).

7 – QUANTIFICATION OF ErbB3

7.1. INTRODUCTION

As discussed in section 1.9, aberrant expression of different members of the ErbB family is involved in the development and progression of different types of carcinomas. In particular over expression of ErbB1, ErbB2, ErbB3 and ErbB4 play an important role in breast cancers. From most of the studies published to date, it has emerged that, high levels of expression of ErbB1, ErbB2 and ErbB3 are associated with worse prognosis and resistance to different treatments. In contrast, over expression of ErbB4 in breast cancer is associated with inhibition of cell growth, more differentiated tumour morphology and thus with more favourable clinical outcome (see section 1.12.5). Therefore, it is becoming clear that the presence of different sets of ErbB receptors characterizes different subtypes of breast cancers that may respond differently to treatments. As mentioned in sections 1.10 and 1.12.7, the ErbB receptors have become a target for the development of anticancer drugs. Several monoclonal antibodies and TKIs, which can inhibit multiple receptors, are currently in clinical use (see section 1.12.6) for the treatment of breast cancer. Therefore, a more accurate characterisation of the different types of breast cancer can be important in stratifying patients for more tailored treatments. Having taken these considerations into account, we aimed to use the new Qdot quantification system to detect and measure the over expression other ErbB family members in breast cancers. As explained previously, ErbB3 is the obligatory dimerisation partner of ErbB2 and it is indispensable for ErbB2 to promote tumour development in ErbB2 over expressing tumours (Holbro et al., 2003) (Siegel et al., 1999) furthermore, ErbB2-ErbB3 heterodimers have the strongest mitogenic activity by activating the PI3K/Akt pathway (Tzahar et al., 1996) playing an important role in tumour progression and can contribute to resistance to anticancer treatments (Siegel et al., 1999) (Knuefermann et al., 2003). Therefore, to determine whether the Qdot system was able to detect different levels of expression of another ErbB family members (other than ErbB2), we first directed our attention on the detection of ErbB3 receptor expression.

To have a clear understanding whether the Qdot system was suitable for the detection of ErbB3, we decided to employ the same detection method previously applied to ErbB2. Therefore, in order to use the Qdot 585 anti-rabbit secondary antibody for the detection of ErbB3, we employed the polyclonal antibody 49.3. As this antibody, compared to RTJ2 monoclonal antibody, has previously been shown to recognise specifically ErbB3 by Western blotting (see Fig. 3.8 D), we decided to confirm the specificity of 49.3 polyclonal antibody when used immunofluorescence detection using HEK293-ErbB3 cell line. Following on these experiments the polyclonal antibody was used to detect ErbB3 expression by IHC first and then by the Qdot system using two arrays, containing respectively 60 FFPE breast cancer tissue samples from the same set of tumours.

7.2. AIMS

- I. Confirm the specificity of the 49.3 primary antibody and Qdot585 to detect ErbB3 receptor in immunofluorescence staining using genetically engineered cells.
- II. Evaluate the performance of the 49.3 primary antibody to detect different levels of ErbB3 expression in FFPE breast cancer tissues by IHC.
- III. Evaluate the ability of Qdot system to quantify different levels of ErbB3 expression in FFPE breast cancer tissues.

7.3. RESULT

7.3.1. TESTING THE 49.3 POLYCLONAL ANTIBODY IN IMMUNOFLUORESCENCE AND IMMUNOHISTOCHEMICAL STAINING

As previously shown in section 3.3.2.1, the polyclonal antibody 49.3, in contrast to the RTJ2 monoclonal antibody, was able to specifically detect ErbB3 receptor in HEK293-ErbB3 cell line by Western blotting (Fig. 3.8 D). Therefore we decided to verify its ability to detect ErbB3 in HEK293-ErbB3 cells also by the immunofluorescence technique. The experiment was carried out following the same protocol and using the same controls applied to the other antibodies employed in this study (see section 3.3.1). Therefore, HEK293-ErbB3 cells were stained with 49.3 polyclonal antibody and Qdot585 anti-rabbit secondary antibody. Specific membrane and cytoplasmic stain of ErbB3 were observed as expected (Fig. 7.1 A). Omission of the primary antibody was applied to evaluate the background (presence of a non specific signal) due to the secondary antibody labelled with Qdot585 (Fig. 7.1 B); finally, the control with the immunising peptide was performed to confirm the specificity of the 49.3 primary antibody (Fig. 7.1 C). In both controls no fluorescent signal was detected (Fig. 7.1 B and C).

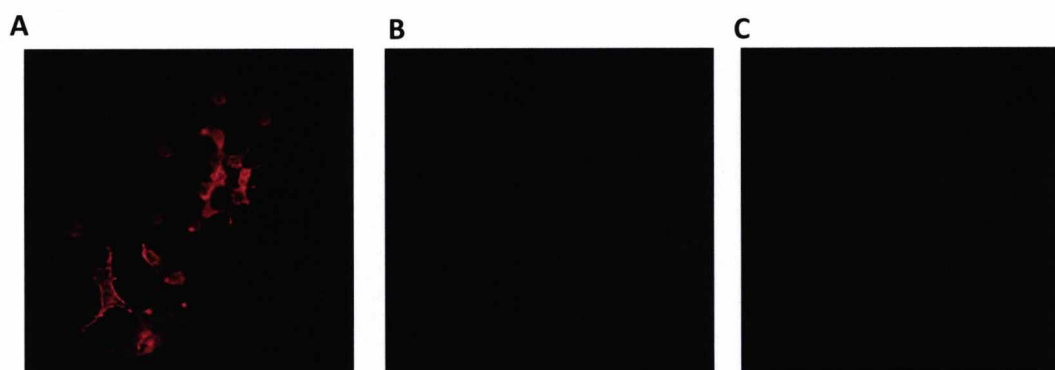


Figure 4.3.1 Immunofluorescence of HEK293-ErbB3 cells. (A) ErbB3 was detected using the 49.3 polyclonal antibody and anti-rabbit Qdot 585 secondary antibody; (B) control in presence of Qdot 585 secondary antibody conjugates and omission of primary antibody; (C) control with the 49.3 antibody pre-incubated with the immunising peptide and Qdot 585 secondary antibody conjugates.

In order to use 49.3 polyclonal antibody on FFPE human breast cancer tissues, we optimised the antibody concentration using FFPE rat kidney tissues (data not shown). We used kidney tissue as it was previously shown that it has moderate levels of ErbB3 expression (Prigent et al., 1992). The optimal concentration was then employed to evaluate the performance of 49.3 polyclonal antibody to detect different levels of expression of ErbB3 in FFPE breast cancer tissues using a microarray with 60 FFPE breast cancer samples. These samples were from the same set of 60 breast cancer tumours previously used to detect each receptor expression including ErbB3 that was detected using the RTJ2 monoclonal antibody (see section 3.3.4.1). The results showed predominantly cytoplasmic immunostaining as expected, and different staining intensities corresponding to different levels of ErbB3 (0, 1+, 2+ and 3+) were also observed (Fig. 7.2 A, B, C and D). The histogram in Figure 7.3 B summarised the scoring results and the table in Figure 7.3 A describes in more detail the number of samples scored as 0, 1+, 2+, and 3+.

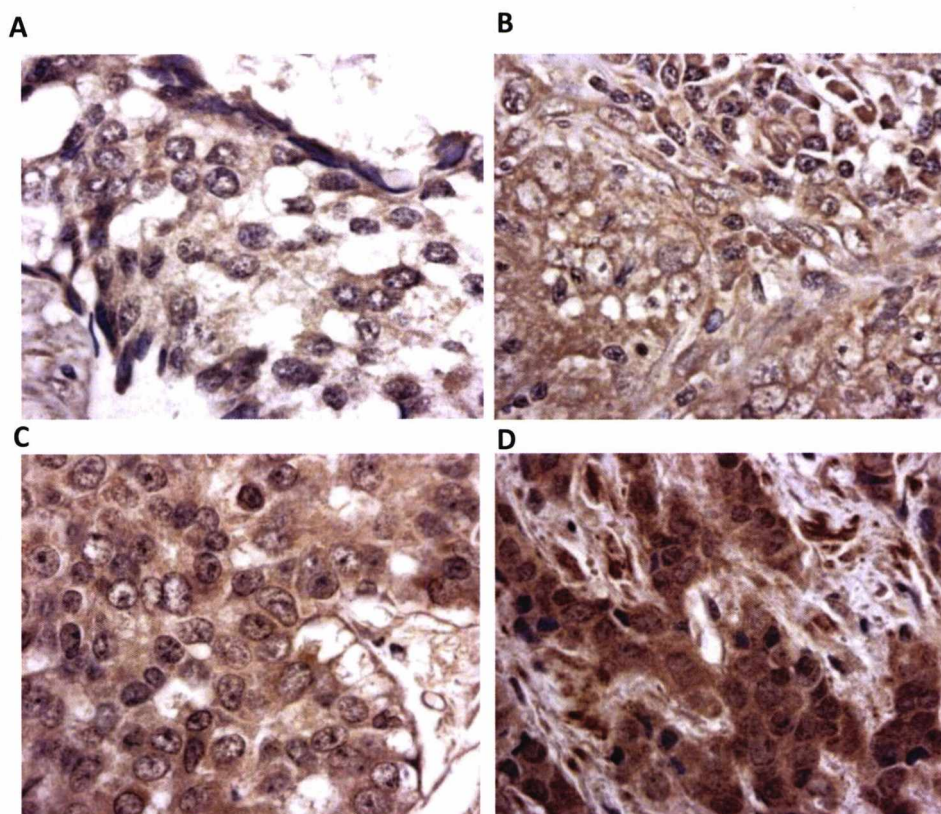


Figure 4.3.2 Immunohistochemical staining of ErbB3 in FFPE breast cancer tissues. Levels of ErbB3 expression were determined by using 49.3 polyclonal antibody. The images show an example of IHC staining scored as (A) 0, (B) 1+, (C) 2+ and (3+). Magnification x63

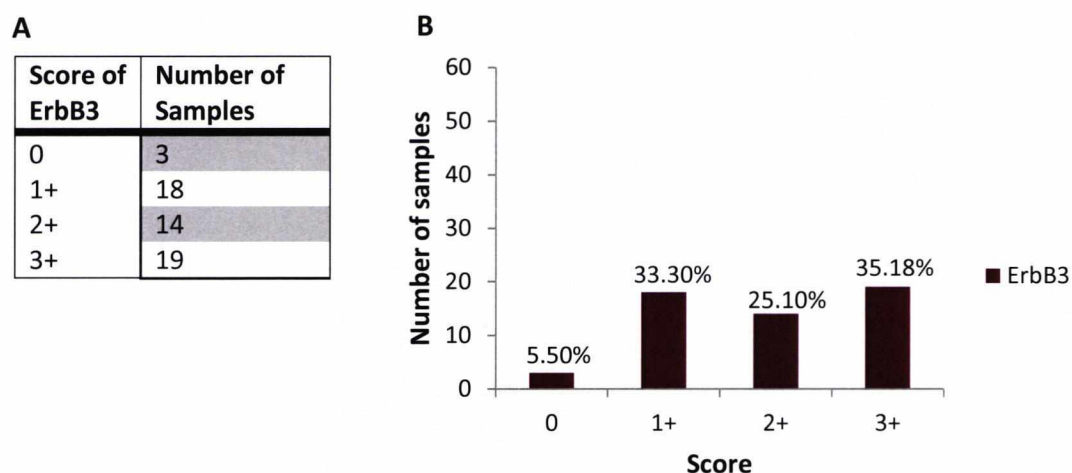


Figure 4.3.3 ErbB3 expression in a set of human breast cancer tissues. (A) In the table are reported the number of samples scored as 0, 1+, 2+ and 3+. (B) The histogram shows the percentage of breast cancer samples with the different levels of ErbB3 expression.

7.3.2. DETECTION OF ErbB3 BY Qdots IN BREAST CANCER TISSUES.

In order to evaluate the ability of the Qdot system to detect ErbB3 expression in FFPE breast cancer tissues, we stained a tissue array with 60 FFPE breast cancer tissues samples from the same set of tumours used for the IHC staining. By following this method we aimed to compare the IHC results versus the results obtained using the Qdot system and determine whether the system was correctly detecting the different levels of expression of ErbB3. Therefore for the Qdot-IF staining we used the 49.3 polyclonal antibody as primary antibody and anti-rabbit Qdot 585 as the secondary antibody. The same Qdot-IF protocol and image acquisition system used for the detection of ErbB2 (see chapter 5) were applied to the data obtained from this experiment. Figure 7.4 shows three images of three different breast tumours expressing ErbB3 at 3+ levels scored by IHC. The specific signal (Qdot 585) is shown in red and the background (autofluorescence) in green. The Qdot 585 signal shown in the images in Figure 7.4 was the strongest signal observed. Therefore, although the Qdot system was able to detect the presence of ErbB3 over expression in some breast tumours, the sensitivity of the technique is limited by its ability to clearly discriminate different levels of ErbB3 expression.

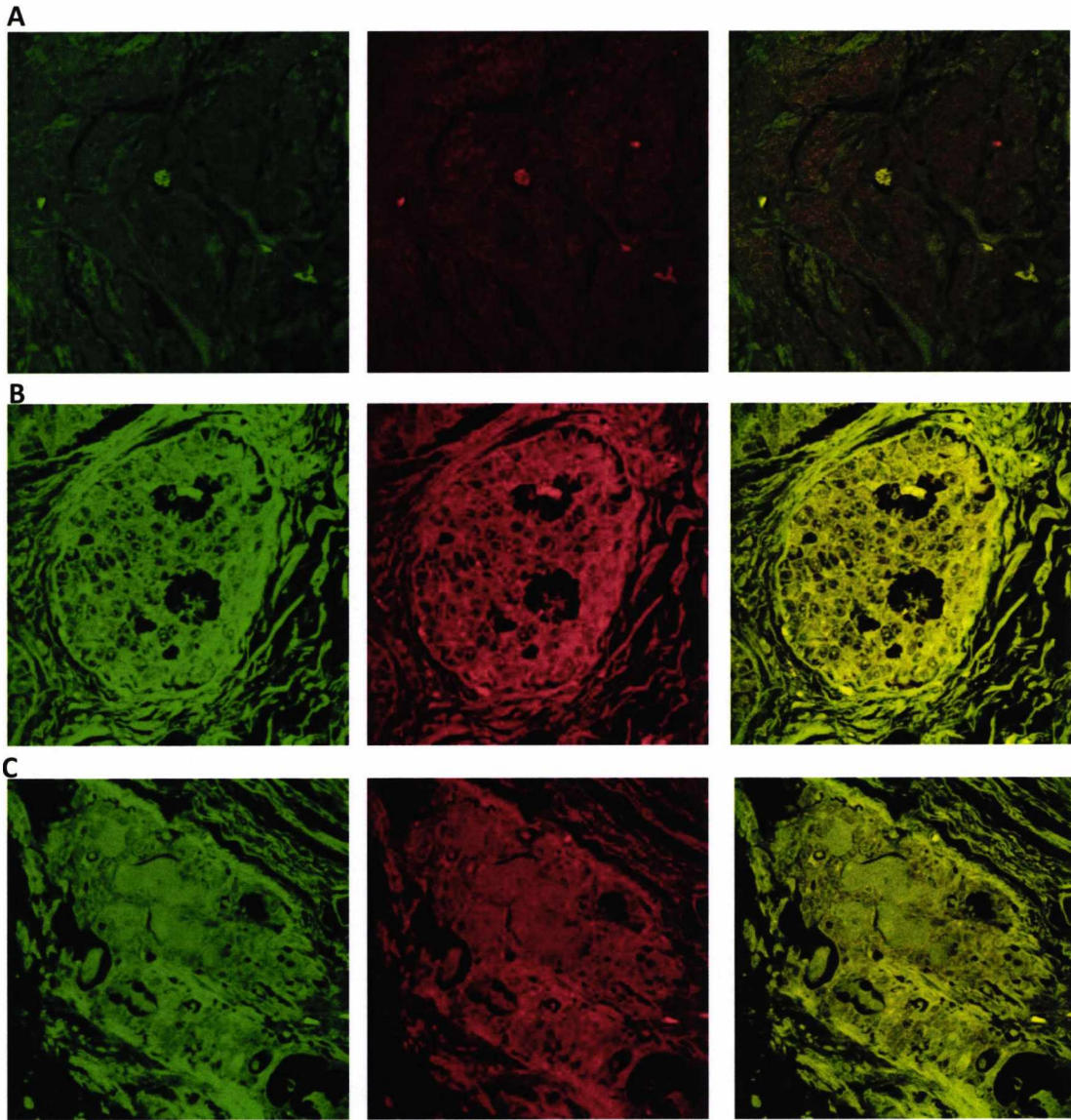


Figure 4.3.4 Qdot 585 immunofluorescent staining of FFPE breast cancer tissues. (A), (B) and (C) represent three images of three different breast tumour stained for ErbB3 and previously classified as 3+ by IHC. On the first column are shown images acquired in the green channel for the autofluorescence, on the second column are shown images acquired in the red channel for the Qdot signal and on the third column are shown the merged images. The Qdot 585 fluorescent signal in red is very low and almost completely overlaps with the autofluorescence background in green.

7.4. DISCUSSION

Two antibodies, the RTJ2 monoclonal antibody and the 49.3 polyclonal antibody, were employed in this study to detect ErbB3 receptors. Although these antibodies have been well characterised (see references in 3.1) additional experiments were undertaken in this work (see chapter 3). Compared to RTJ2 monoclonal antibody, the polyclonal antibody 49.3 showed superior performance in Western blotting (see Fig.3.8). Therefore, we decided to confirm its specificity and test its performance by immunofluorescence. In Figure 7.1 A we have shown that the antibody successfully detected ErbB3 in HEK293 cell line over expressing ErbB3 and no specific fluorescence was present when the antibody was blocked with the immunising peptide (Fig. 7.1 C). The antibody was then used to stain FFPE tissue samples by IHC. These tissues were obtained from 60 breast tumours previously used to examine ErbB3 expression with RTJ2 antibody and the other receptors expression with the respective antibody (see 3.3.4.1). As expected, the tissue immunoreactivity was mainly present in the cytoplasmic area rather than on the cell surface. The different brown intensities staining corresponding to different levels of ErbB3, were then graded from 0 to 3+. Comparing the scoring results obtained with 49.3 polyclonal antibody with the scoring results obtained with RTJ2 monoclonal antibody, we noticed that 20 cases were scored higher, 16 cases lower and to 17 cases it was given the same score. This difference can be explained by observing the two antibody's performance in IHC. The IHC staining performed with 49.3 polyclonal antibody generated higher background (Fig. 7.2) compared to the IHC staining carried out with the RTJ2 antibody (3.13). Indeed, the images in Figure 3.13 shows better signal to noise ratio, defined by the blue haematoxylin stain vs. the brown stain compared to the images in Figure 7.2. Our results were consistent with previously results, which showed that RTJ2 monoclonal antibody gave superior staining with lower background compared to the 49.3 polyclonal antibody (Rajkumar et al., 1993).

In summary, RTJ2 monoclonal antibody gave greater performance in IHC over the 49.3 polyclonal antibody. 49.3 polyclonal antibody gave a better performance in Western

Blotting. Both antibodies specifically recognised ErbB3 and produced good quality immunofluorescence staining in the HEK293-ErbB3 cell line.

Therefore, to use the anti-rabbit Qdot 585 secondary antibody and the same parameters for the image acquisition previously established, we decided to employ the 49.3 polyclonal antibody. Another array with 60 FFPE breast cancer tissue samples from the same series of tumours was then used to test the ability of the Qdot system to detect ErbB3 levels of expression. The results shown in the images in Figure 7.3 have revealed a limit in the system related to its sensitivity. The images presented in Figure 7.3 correspond to three examples of breast tumours scored as 3+ by IHC and to the strongest signals observed. From the images, it appears clear that the Qdot signal is too low to give reliable information and it mainly overlaps with the tissue autofluorescence. Indeed, although ErbB3 is over expressed at significant levels in breast cancer, its levels of expression are lower to those observed for ErbB2. This is because the ErbB2 is gene amplified and it is expressed at very high levels with definite membrane staining pattern, ErbB3 over expression is not due to gene amplification but mainly to upregulation of ErbB3 gene transcription (Lemoine et al., 1992). Therefore in order to quantify ErbB3 it would be necessary to improve the sensitivity of the technique. This can be achieved by meliorating the signal to noise ratio in different ways. For instance, it would be possible to increase the signal strength (e.g. by using a streptavidin Qdot conjugate), or reduce the background autofluorescence by using Qdots antibodies/or a streptavidin conjugate that emit in the far red where the contribution of the autofluorescence is very low. Furthermore, the development of software, tailored for a Qdot-based assay, would allow improvement the system sensitivity for the detection and quantification of biomarkers expressed in more modest amounts in FFPE breast cancers.

8 – GENERAL DISCUSSION

8.1. DISCUSSION

One of the most important advances in breast cancer translational research has been the identification of several prognostic and predictive biomarkers which can determine both the course of the disease and the response of the cancer to a therapeutic treatment. The biomolecular characterisation of various types breast cancers has been crucial for the development of targeted therapeutic strategies with reduced drug toxicity and increased efficacy. Therefore, along with the new generation of selective drugs, the accurate identification of those patients with greatest likelihood of response to a particular drug or chemotherapy has become of importance. There are three molecular markers which are routinely used in clinical practise to predict response to treatment: two of these markers, ER and PR, are used to select patients who respond to endocrine therapy and the third one, ErbB2, which has been introduced more recently in clinical practice, is used to predict patients response to Herceptin treatment (Pusztai et al., 2006). The significance of ErbB2 was first determined in 1987 by Slamon and colleagues who discovered that ErbB2 gene was amplified and correlated with more aggressive tumour behaviour and poorer clinical outcome (Slamon et al., 1987). In the same year Venter and colleagues found that ErbB2 protein over expression was present in 18-20% of breast tumours (Venter et al., 1987). Subsequently the development of the monoclonal antibody Herceptin has made a significant breakthrough in the treatment of ErbB2 over expressing metastatic breast cancer and now also as an adjuvant therapy, in the treatment of early stage breast cancer. The patients' eligibility for the clinical trials to test efficacy and safety of the drug alone and in combination with other therapeutic agents was based on the IHC assay. This assay was used to assess ErbB2 status in patients with breast cancer. Only patients with ErbB2 over expressed at 2+ and 3+ levels with uniform cell membrane stain in more than 10% of the tumour cells, were enrolled in these early studies. The results from the clinical trials showed that only patients with ErbB2 expression at 3+ level benefited from Herceptin and patients with ErbB2 expression at 2+ level did not respond or had a

low response making treatment uneconomic (Cobleigh et al., 1999) (Slamon et al., 2001) Vogel (Vogel et al., 2002). Currently, Herceptin is widely used for the treatment of both metastatic breast cancer (<http://www.fda.gov/Drugs/Development-Approval-Process/HowDrugsareDevelopedandApproved/ApprovalApplications/TherapeuticBiologicApplications/ucm080591.htm>) and early stage breast cancer (<http://www.fda.gov/NewsEvents/Newsroom/PressAnnouncements/2006/ucm108788.htm>) and only in patients with high levels of expression (3+ cases by IHC) or gene amplification determined by FISH. Therefore, the assessment of ErbB2 status has become crucial in order to identify those patients who most benefit from this drug. IHC (HercepTest™ Dako IHC kit) and FISH (PathVysion® ErbB2 DNA probe kit or Pathway™ Ventana Kit) are the only assays for ErbB2 testing approved by the FDA and internationally recommended by the ASCO/CAP experts. These assays are routinely employed in clinical practice to select those patients who are eligible to receive the anti-ErbB2 Herceptin treatment. Advantages and disadvantages of these assays (see section 1.13.1) have been widely recognised and documented (Gown, 2008; Shah and Chen) (Seidenfeld et al 2008). Therefore the ASCO/CAP experts have tried to address the issues regarding the ErbB2 testing accuracy by releasing a series of detailed recommendations. These guidelines covered all pre-analytic, analytic and post-analytic steps aiming to standardise and reduce those sources of variability which can cause test inaccuracy and inconsistency across different laboratories (Wolff et al., 2007). For instance, increasing the cut-off point of tumour cells with dark and uniform membrane staining, from 10% to 30%, has improved the accuracy of ErbB2 testing (Hameed et al., 2007). However despite the ASCO/CAP has reported that 20% of ErbB2 tests are inaccurate (Wolff et al., 2007).

Although there have been great advances in breast cancer (e.g. identification of biomarkers, development of new targeted therapies) the advances in the assays have not kept pace. There are still important problems that do not allow the most accurate and efficient way to select patients.

In this work we tackled the important issue of ErbB2 testing in breast cancer by proposing an alternative method able to assess ErbB2 status in a more linear and

scalable fashion. The quantification values corresponding more directly to ErbB2 expression, allow greater differentiation of receptor levels of expression and therefore more detailed and potentially more accurate information.

The system that we have developed is based on the use of FFPE breast tumour tissues, immunofluorescence and quantum dots. The development of an assay that employs FFPE tissue slices rather than tissue homogenates has several advantages. In the FFPE tissue sections the tissue and cell morphology are well preserved. This information can be used by a pathologist to identify invasive cells, tumour areas and to evaluate the receptor expression on the membrane of these cells. Contrarily, different types of assays such as PCR, ELISA, Western Blotting and Southern Blotting, require the use of tissue homogenates which are typically obtained from a larger amount of tissue. Furthermore the tissue including homogenates can contain a mixture of DNA, mRNA or proteins from different parts of the tissues including invasive cancer cells and normal and inflammatory cells that can mislead the results.

The choice of using Qdots instead of the conventional organic dyes has been made based on the optical properties of the Qdots, which we have discussed in section 1.14. In particular, Qdots are brighter than the traditional organic dyes therefore more sensitive. In immunofluorescence experiment on FFPE tissue, the sensitivity of the fluorophore is a relevant feature as it improves the signal to noise ratio which is affected by the tissue autofluorescence. Another important property of the Qdots is their narrow and symmetric emission profile which we have shown in Figure 4.16 and 4.17. This is important in studies that require the simultaneous detection of multiple targets as it allows to minimise the spectra overlapping and therefore bleed-through phenomena (Fig. 3.5 and 3.6). Furthermore the use of Qdots for the detection of ErbB2 in breast cancer cells and FFPE breast cancer tissues, has been described and it appears technically feasible, sensitive and produces reproducible, linear measurements (Wu et al., 2003) (Xing et al., 2007). Furthermore during the course of this study a paper showing the potentiality of Qdots for the quantitative measurement of ErbB2 has been published (Chen et al., 2009).

The immunofluorescence method represents a valuable alternative to IHC as it is more reproducible as the latter depends on an enzymatic reaction which can be affected by

different variables and therefore it is more difficult to standardise. Theoretically a fluorescence signal is a linear function of the concentration of the fluorophore in a sample. This means that the intensity of the emitted light is proportional to the concentration of the fluorophore attached to the targeted proteins. In addition the fluorescence intensities can be divided in 256 points on a scale rather than just 4. Therefore the immunofluorescence technique represents an useful tool for gathering quantitative data and to generate a scalable measurement of the protein of interest.

In order to develop an assay that is not affected by analytic and post-analytic steps, our first concern was to evaluate the specificity and performance of the primary antibody. The polyclonal antibody 21N and the monoclonal antibody CB11 were used for the detection of ErbB2. Both these antibody have been well characterised as reported in the reference (Corbett et al., 1990; Gullick et al., 1987). In this work we confirmed their specificity and performance in different systems (see chapter 3). A study that compared the sensitivity and specificity in IHC of 7 polyclonal and 20 monoclonal antibodies, including 21N and CB11, has reported 100% specificity for both antibodies and a difference in sensitivity of 4% between them (Press et al., 1994). Also in our study both antibodies have demonstrated high performance when they were used in IHC. They detected different levels of expression of ErbB2, graded from 0 to 3+ in FFPE breast cancer tissues (Fig.3.12 and 4.6) and they have shown distinct membrane staining associated with ErbB2 over expression with no or minimum background. As there was no significant difference in the ability of the two antibodies to detect ErbB2 level of expression and both were producing good quality immunostaining, we decided to take forward for this study the 21N polyclonal antibody. This was available in the laboratory and as it was raised in rabbit we showed that it could be used with the mouse monoclonal antibody RTJ2 for the simultaneous detection of ErbB2 and ErbB3 (Fig. 3.5).

Our second aim was to evaluate the Qdots ability to detect specific antigens in cell lines before applying Qdots technology to FFPE tissues. Therefore we used four cell lines over expressing individual receptors to detect ErbB1, ErbB2, ErbB3 and ErbB4 by immunofluorescence with Qdot labelled antibodies. The results presented in Figure 3.3

A, C, D and G and in Figure 3.4 (chapter 3), demonstrated that both the anti-mouse Qdot 525 and the anti-rabbit Qdot 585 secondary antibodies allowed the specific detection of the target proteins. In the final phase of this characterisation we demonstrated that Qdot immunolabelling system successfully worked also on FFPE rat pancreas tissues where Qdot 525 secondary antibody bound to a monoclonal antibody specifically labelling the α -cells (Fig. 4.3).

As Qdot nanocrystals are relatively new and their application in biology and medicine is still being studied, currently there are not well characterised experimental protocols for their use. In addition, the linearity of the fluorescence signal can be affected by different factors including high fluorophore concentration. At the same time a low fluorophore concentration can result in loss of sensitivity or an underestimation of the fluorescent signal. Therefore it was necessary and important to optimise the concentration and the incubation time for Qdot immunofluorescence on FFPE tissues. This allowed us to obtain high quality staining with a good compromise between system sensitivity, i.e. the fluorescence signal emitted and signal to noise ratio (Fig. 4.4 and 4.5). The established protocol was then applied to all the subsequent Qdot immunofluorescence experiments on FFPE tissues carried out in this work. This was essential to obtain reproducible and comparable measurements of fluorescent intensities across samples, without them being affected by experimental procedures. Therefore we started to investigate whether Qdot immunofluorescent labelling was suitable for detecting different levels of protein expression in FFPE breast cancer tissues. For this purpose we used a control microarray slide with four cores of breast cancer tissues that correspond to different level of ErbB2 expression graded as 3+, 2+, 1+ and 0. The microarrays were stained by IHC and by immunofluorescence with Qdot 525 (Fig.4.6 and Fig.4.7). The Qdot immunofluorescence system correctly showing a strong fluorescent signal when ErbB2 was over expressed at 3+ level (Fig. 4.7 D) and no signal was present in the ErbB2 negative breast cancer tissue (Fig. 4.7 A). However it was not possible to observe any specific signal in the specimen over expressing ErbB2 at 1+ signal (Fig. 4.7 B) and only a weak fluorescent signal was observed in the specimen expressing ErbB2 at 2+ level (Fig. 4.7 C). The main problem we encountered at this stage was the presence of a strong fluorescence background (autofluorescence)

originating from the FFPE tissues. On the one hand the autofluorescence represents an useful tool as it allows identification of the tissue structure and morphology. On the other hand it represents one of the main shortcomings in immunofluorescence studies. Indeed the presence of the autofluorescence was strongly affecting the signal to noise ratio masking low Qdot fluorescent signals and interfering with the detection of ErbB2 expressed at lower levels. Therefore, after pondering different ways how to overcome this problem, we decided to apply a method known as unmixing by using the Leica Lite confocal software (Fig 4.8 and 4.9). However this method proved to be unsuitable for this study (see 4.4.2). As it has been shown recently that Qdots are particularly resistant to photobleaching (Wu et al., 2003), we therefore tried to reduce the tissue autofluorescence by photobleaching. As shown in Figure 4.10 and 4.11 the autofluorescence was successfully reduced. However this approach required the exposure of the specimen to high intensity laser light for a long length of time (60 mins). This could have also affected the Qdots signal despite their resistance to photobleaching. Furthermore this method was time consuming and not suitable for a possible application in clinical practice. The following studies on the autofluorescence spectral profile (see section 4.3.4.2) revealed that the Qdot 525 and the autofluorescent emissions were completely overlapping and this was causing the loss in sensitivity. For this reason we decided to employ a Qdot conjugated secondary antibody that has emission peak shifted away from the highest autofluorescence emission (Fig. 4.17). At the same time we exploited the autofluorescence in order to discriminate the specific signal from the background by acquiring the images in two channels (Fig 5.5). This, together with the use of the Qdot 585 conjugate secondary antibody, clearly improved the signal to noise ratio and allowed clear detection of different intensities of Qdot fluorescent signal emissions that correspond to different levels of ErbB2 expression graded from 3+ to 0 by IHC (Fig. 5.7).

As our goal was to measure in a more objective, linear and scalable way the different intensities emitted from the Qdot 585 nanocrystal labelled to ErbB2 receptor in the FFPE breast cancer specimens, we established a series of criteria. These enabled us to standardise those stages of the process which involved the imaging acquisition and the image quantification analysis (chapter 5). The images were acquired with a laser

scanning confocal microscope which has been shown to be the most suitable choice for the purpose of this work (see section 5.4.1). The flexibility of the detection system available in the Leica Laser scanning confocal microscope (see section 5.3.1) allowed us to generate an optimal setting for image collection. Furthermore, by monitoring the consistency of the setting over time (see section 5.3.1.1), we ensured that the data generated in the images were reliable and comparable.

To correctly quantify the fluorescent signal produced by the Qdot 585 secondary antibody conjugate and consequently to obtain useful information about the levels of expression of ErbB2 receptor in the breast cancer samples, we tackled two issues. The first was related to the strong background signal which could have led to a wrong interpretation of the quantification results (Fig. 5.15 B and 5.22). The second was related to the presence of dark areas in the slide where no signals were present. If we included the pixel values of these regions, then the results would have been skewed toward zero (Fig. 5.13 and 5.14). The first issue was overcome by segmenting the images by region of interest. The tissue autofluorescence was used to identify areas of interest containing tumour cells versus areas that only contributed to the background such as connective, fibrous, adipose tissue etc. (Fig. 5.12 and 5.15 A). The second issue was overcome by applying a threshold of 50 grey levels from 0 to 50 units of the grey scale (see section 5.3.2). The mean intensities of the background areas and of the areas of interest were calculated. The average intensity of the background regions was then subtracted from the average intensity of the areas of interest which still contained the Qdot 585 signal with the contribution of the autofluorescence (Fig. 5.15 B and 5.22). In this way we obtained the values of the specific signal only generated by the Qdot 585 secondary antibody bound to the ErbB2 receptor. As we have shown in Figure 5.15 A and C, where applied in this way the Qdot quantification system was able to correctly discriminate and quantify ErbB2 levels of expression in the ErbB2 control array with four breast cancer tissues with ErbB2 expression graded by IHC as 3+, 2+, 1+ and 0.

We then applied this system to a tissue array containing 60 FFPE breast cancer tissues taken from 60 unselected breast cancers that were previously scored by IHC (Table 3.1

and Fig. 3.15). We showed that the system was able to differentiate ErbB2 levels of expression within both the 3+ and 2+ categories producing a more scalable and linear measurement (Fig. 5.18). As expected the Qdot values corresponding to the 2+ cases showed lower scores than the samples categorised as 3+ by IHC (Fig.5.19). However, a few samples of the 2+ category showed higher values than the lowest cases of the 3+ category. This was not surprising as it is generally recognised that the separation between the 2+ and the 3+ category is not always evident by IHC especially for borderline 2+/3+ cases and therefore for those cases an additional test is required (FISH).

In this work we also employed the Qdot quantification system that we developed to measure ErbB2 in a set of breast tumours from patients treated with Herceptin. The tissue array employed in the study was kindly supplied by Prof. Ian Ellis (Nottingham City Hospital) along with the patients clinical data. The array included 145 primary breast carcinomas from women treated with the drug. The ErbB2 status in these breast tumours was previously assessed by IHC and FISH at Nottingham City Hospital. The results obtained from the Qdot quantification system have shown that it can produce higher discrimination among different levels of the ErbB2 expression compared to the IHC test. Indeed, it has shown that within the 3+ and 2+ categories exists a wide range of expression of ErbB2 protein. The magnitude of this range was over 40 fold in this set of tumours (Fig. 6.3 and 6.4) and up to 60 fold if we consider the data presented in Figure 5.18 A. These data are supported by work subsequently published by Chen and colleagues who found, by using Qdots that ErbB2 expression can vary by up to 100 fold in IHC 3+ cases (Chen et al.).

Thus, as previously reported, the patients response to Herceptin depends on the levels of expression of ErbB2. In this work we have demonstrated that these levels are highly variable within the 3+ and 2+ categories. Our hypothesis is that the patients with the highest level of ErbB2 expression may be the most likely to respond to the drug. Therefore, we considered addressing the following question: how are the levels of ErbB2 receptor measured by Qdot correlated to the patients' response? In order to attempt to answer this question, we divided the patients treated with the drug in two

subgroups, high Qdot score and low Qdot score, choosing as the cut-off point the median value. The majority of patients with poorer outcomes were in the subgroup with lower Qdot score (low level of ErbB2) and patients with better outcome were in the high Qdot score (high level of ErbB2) (Fig. 6.6). This suggested that the drug was more effective on the population with high ErbB2 levels. We further investigated these preliminary observations performing a Kaplan-Meier analyses on the whole cohort of patients first (Fig. 6.7) and then in a subgroup of patients lymph node positive (Fig. 6.8). Despite the fact that most of the adverse events were occurring in the population with low Qdot score, the difference between the two survival curves was not significant in both Kaplan-Meier analysis. The main limitations in this work were the small size of the sample, high number of censored data and the small numbers of events. It would be interesting to take this study further and obtain more conclusive evidences using a bigger cohort of patients and a longer term follow-up. It would be interesting to compare the group of patients treated with Herceptin with a group of patients not treated with Herceptin to individuate the right cut-off point to establish where the drug is most effective

The correlation between ErbB2 levels, calculated by a different technology called HERmark (see section 1.13.2), and response rate to Herceptin, have been shown in two studies which were published in the course of this work. One study showed a good correlation between increasing levels of ErbB2 and response rate to Herceptin (Lipton et al.), the other study, published by the same group, has identified a subgroup of patients with very high levels of ErbB2 expression that appears to respond poorly to Herceptin (Bates et al., 2011) (Joensuu et al., 2011). Therefore it becomes evident that a new evaluation of ErbB2 levels of expression and response rate to Herceptin, based on a more accurate assessment of its levels and new evaluated cut-off points, is of importance for an optimal selection of patients. It has been recorded that the overall response rate to Herceptin as single agent, in patients with metastatic disease, is 23% and it becomes much higher, between 80% and 86%, when Herceptin is used in combination with other agents (Collins et al., 2009; Spigel and Burstein, 2003). This means that around 15%-20% of patients fail to respond to Herceptin treatment. It has

also been shown that the risk of developing brain metastases is higher for those patients who receive Herceptin in the clinical trials (Sutherland et al.) and that Herceptin is associated with cardiotoxicity (NICE technology appraisal guidance No34; National costing report: Early and locally advanced breast cancer/Advanced breast cancer 2009). Therefore an optimal selection of patients for treatment with Herceptin will avoid adverse effects to patients who should have not been eligible for Herceptin and at the same time will avoid unnecessary cost to the Health Service.

As explained before (chapter 1), in order to activate downstream signalling pathways, the ErbB2 receptor has to dimerise with one of the other members of the Epidermal growth factor family. Furthermore both ErbB1 and ErbB3 have been found to be over expressed in breast cancer (see section 1.12.6) and ErbB3 in particular has been linked to the mechanisms of resistance to Herceptin (see section 1.12.5). It has been shown that ErbB2/ErbB3 is the most oncogenic heterodimer (Tzahar et al., 1996) as it activates the PI3K/Atk signalling pathway which determines cell proliferation and survival. For this reason, therapeutic strategies that target multiple receptors have been developed (see section 1.12.7). Furthermore, a work carried out in the laboratory has shown that the combination of Herceptin with the SGP1 monoclonal antibody, which targets ErbB3, improved the effect of Herceptin by inhibiting the growth of breast cancer cells (Blackburn et al.). Therefore the detection and the assessment of other receptors in breast cancers may be relevant in stratifying patients for a more personalised treatment.

In this study we found that ErbB3 was the receptor with the highest frequency of expression at 3+ (Fig. 3.15) levels beside ErbB2. Additionally, the Spearman's rank analysis has shown that there was a weak positive correlation between the two receptors expression (see section 3.3.4.2). For these reasons we decided to start testing the Qdot system to quantify ErbB3 receptor expression in FFPE breast cancer tissues. In this case the system showed itself to be limited by its sensitivity. Indeed, even when ErbB3 was expressed at 3+ levels (scored by IHC) the signal detected corresponding to ErbB3 (Qdot 585 emission) was too low to be quantified (Fig. 7.3). Even if ErbB3 is expressed at significant levels in breast cancer, its levels of expression

are not as high as those seen for ErbB2 (Fig 3.12, 3.13 and 7.1), this because the ErbB3 gene is not amplified like ErbB2. Furthermore, while ErbB2 immunostaining shows a clear and strong uniform membrane staining with typical “chicken wire” pattern, ErbB3 immunostaining is mainly cytoplasmic. This was a relevant factor for the detection of ErbB3 by Qdots as in the Qdot immunofluorescent system, this more cytoplasmic distribution makes it more difficult to separate the specific signal and the autofluorescence, therefore requiring higher sensitivity and an enhanced signal to noise ratio in future experiments. This can be achieved in different ways, for example, by using the Qdot streptavidin conjugate and/or Qdots that emit in the far red where the contribution of the autofluorescence is lower or totally absent (Fig. 4.14) and by developing a software tailored for the Qdot-based assay. Once these problems are overcome this method has the potential to be applied for the detection and measurement of any biomarker, included ER and PR. Furthermore it offers the potential for a simultaneous detection of multiple biomarkers.

8.1.1. CONCLUSION

In this study we have tested a new way of measuring ErbB2 expression. This new technology, based on Qdot-immunofluorescence and imaging analysis, has shown to have the potential to improve the current method for the assessment of ErbB2. Interestingly, using our new method, we have found that ErbB2 is expressed at very different levels in cases currently scored the same using IHC and we hypothesise that this could have important influence on patients’ response to treatment. We believe that a more accurate assessment of ErbB2 status in breast cancer can have a relevant clinical impact for both patients and the NHS. However in order to establish this additional testing on a larger cohort of patients treated with Herceptin is essential. To determine the eligibility of a patient for a therapeutic treatment, it is also important to determine a new cut-off point based on Qdot score rather than IHC and then calculate the quality-adjusted life years (QALY) and thus the cost versus benefit for the newly identified group of patients.

Overall the method that we have developed can offer a valid alternative to the IHC; however it still needs to be developed further. The main drawback is represented by

the sensitivity of the system. However as mentioned above there are different ways that can be developed in order to improve this.

REFERENCES

- Abd El-Rehim, D.M., Pinder, S.E., Paish, C.E., Bell, J.A., Rampaul, R.S., Blamey, R.W., Robertson, J.F., Nicholson, R.I., and Ellis, I.O. (2004). Expression and co-expression of the members of the epidermal growth factor receptor (EGFR) family in invasive breast carcinoma. *Br J Cancer* *91*, 1532-1542.
- Abe, Y., Odaka, M., Inagaki, F., Lax, I., Schlessinger, J., and Kohda, D. (1998). Disulfide bond structure of human epidermal growth factor receptor. *J Biol Chem* *273*, 11150-11157.
- Alaoui-Jamali, M.A., Song, D.J., Benlimame, N., Yen, L., Deng, X., Hernandez-Perez, M., and Wang, T. (2003). Regulation of multiple tumor microenvironment markers by overexpression of single or paired combinations of ErbB receptors. *Cancer Res* *63*, 3764-3774.
- Alimandi, M., Romano, A., Curia, M.C., Muraro, R., Fedi, P., Aaronson, S.A., Di Fiore, P.P., and Kraus, M.H. (1995). Cooperative signaling of ErbB3 and ErbB2 in neoplastic transformation and human mammary carcinomas. *Oncogene* *10*, 1813-1821.
- Alizart, M., Saunus, J., Cummings, M., and Lakhani, S.R. (2010). Molecular classification of breast carcinoma. *Diagnostic Histopathology* *18*, 97-103.
- Allison, M. The HER2 testing conundrum. *Nat Biotech* *28*, 117-119.
- Amit, I., Wides, R., and Yarden, Y. (2007). Evolvable signaling networks of receptor tyrosine kinases: relevance of robustness to malignancy and to cancer therapy. *Mol Syst Biol* *3*, 151.
- Arkin, M., and Moasser, M.M. (2008). HER2 directed small molecule antagonists. *Curr Opin Investig Drugs* *9*, 1264-1276.
- Arora, A., and Scholar, E.M. (2005). Role of tyrosine kinase inhibitors in cancer therapy. *J Pharmacol Exp Ther* *315*, 971-979.
- Badra, F.A., Karamouzis, M.V., Ravazoula, P., Likaki-Karatza, E., Tzorakoleftherakis, E., Koukouras, D., Iconomou, G., Xiros, N., Siablis, D., Papavassiliou, A.G., *et al.* (2006). Non-palpable breast carcinomas: correlation of mammographically detected malignant-appearing microcalcifications and epidermal growth factor receptor (EGFR) family expression. *Cancer Lett* *244*, 34-41.
- Barberis, M., Pellegrini, C., Cannone, M., Arizzi, C., Coggi, G., and Bosari, S. (2008). Quantitative PCR and HER2 testing in breast cancer: a technical and cost-effectiveness analysis. *Am J Clin Pathol* *129*, 563-570.

Barok, M., Tanner, M., Koninki, K., and Isola, J. Trastuzumab-DM1 causes tumour growth inhibition by mitotic catastrophe in trastuzumab-resistant breast cancer cells in vivo. *Breast Cancer Res* 13, R46.

Baschong, W., Suetterlin, R., and Laeng, R.H. (2001). Control of autofluorescence of archival formaldehyde-fixed, paraffin-embedded tissue in confocal laser scanning microscopy (CLSM). *J Histochem Cytochem* 49, 1565-1572.

Baselga, J. (2010). Treatment of HER2-overexpressing breast cancer. *Ann Oncol* 21 *Suppl* 7, vii36-40.

Baselga, J. (2001). The EGFR as a target for anticancer therapy--focus on cetuximab. *Eur J Cancer* 37 *Suppl* 4, S16-22.

Baselga, J. (2002). Why the epidermal growth factor receptor? The rationale for cancer therapy. *Oncologist* 7 *Suppl* 4, 2-8.

Baselga, J., Cortes, J., Kim, S.B., Im, S.A., Hegg, R., Im, Y.H., Roman, L., Pedrini, J.L., Pienkowski, T., Knott, A., *et al.* (2012). Pertuzumab plus trastuzumab plus docetaxel for metastatic breast cancer. *N Engl J Med* 366, 109-119.

Baselga, J., and Swain, S.M. (2009). Novel anticancer targets: revisiting ERBB2 and discovering ERBB3. *Nat Rev Cancer* 9, 463-475.

Bates, M., Sperinde, J., Kostler, W.J., Ali, S.M., Leitzel, K., Fuchs, E.M., Paquet, A., Lie, Y., Sherwood, T., Horvat, R., *et al.* (2011). Identification of a subpopulation of metastatic breast cancer patients with very high HER2 expression levels and possible resistance to trastuzumab. *Ann Oncol*.

Baulida, J., Kraus, M.H., Alimandi, M., Di Fiore, P.P., and Carpenter, G. (1996). All ErbB receptors other than the epidermal growth factor receptor are endocytosis impaired. *J Biol Chem* 271, 5251-5257.

Bazley, L.A., and Gullick, W.J. (2005). The epidermal growth factor receptor family. *Endocr Relat Cancer* 12 *Suppl* 1, S17-27.

Beerli, R.R., and Hynes, N.E. (1996). Epidermal growth factor-related peptides activate distinct subsets of ErbB receptors and differ in their biological activities. *J Biol Chem* 271, 6071-6076.

Bennasroune, A., Gardin, A., Aunis, D., Cremel, G., and Hubert, P. (2004). Tyrosine kinase receptors as attractive targets of cancer therapy. *Crit Rev Oncol Hematol* 50, 23-38.

Bewick, V., Cheek, L., and Ball, J. (2004). Statistics review 12: survival analysis. *Crit Care* 8, 389-394.

Billinton, N., and Knight, A.W. (2001). Seeing the wood through the trees: a review of techniques for distinguishing green fluorescent protein from endogenous autofluorescence. *Anal Biochem* 291, 175-197.

Bilous, M., Dowsett, M., Hanna, W., Isola, J., Lebeau, A., Moreno, A., Penault-Llorca, F., Ruschoff, J., Tomasic, G., and van de Vijver, M. (2003). Current perspectives on HER2 testing: a review of national testing guidelines. *Mod Pathol* 16, 173-182.

Biscardi, J.S., Maa, M.C., Tice, D.A., Cox, M.E., Leu, T.H., and Parsons, S.J. (1999). c-Src-mediated phosphorylation of the epidermal growth factor receptor on Tyr845 and Tyr1101 is associated with modulation of receptor function. *J Biol Chem* 274, 8335-8343.

Blackburn, E., Zona, S., Murphy, M.L., Brown, I.R., Chan, S.K., and Gullick, W.J. (2011) A monoclonal antibody to the human HER3 receptor inhibits Neuregulin 1-beta binding and co-operates with Herceptin in inhibiting the growth of breast cancer derived cell lines. *Breast Cancer Res Treat* 134, 53-59.

Bose, R., and Zhang, X. (2009). The ErbB Kinase Domain: Structural Perspectives into Kinase Activation and Inhibition. *Exp Cell Res* 315, 649-658.

Bouyain, S., Longo, P.A., Li, S., Ferguson, K.M., and Leahy, D.J. (2005). The extracellular region of ErbB4 adopts a tethered conformation in the absence of ligand. *Proc Natl Acad Sci U S A* 102, 15024-15029.

Breuleux, M. (2007). Role of heregulin in human cancer. *Cell Mol Life Sci* 64, 2358-2377.

Brown, J.P., and Pinder, S.E. (2010). Ductal carcinoma in situ: current morphological and molecular subtypes. *Diagnostic Histopathology* 18, 112-118.

Brunelli, M., Manfrin, E., Martignoni, G., Bersani, S., Remo, A., Reghellin, D., Chilosi, M., and Bonetti, F. (2008). HER-2/neu assessment in breast cancer using the original FDA and new ASCO/CAP guideline recommendations: impact on selecting patients for herceptin therapy. *Am J Clin Pathol* 129, 907-911.

Burgess, A.W., Cho, H.S., Eigenbrot, C., Ferguson, K.M., Garrett, T.P., Leahy, D.J., Lemmon, M.A., Sliwkowski, M.X., Ward, C.W., and Yokoyama, S. (2003). An open-and-shut case? Recent insights into the activation of EGF/ErbB receptors. *Mol Cell* 12, 541-552.

Burke, P., Schooler, K., and Wiley, H.S. (2001). Regulation of epidermal growth factor receptor signaling by endocytosis and intracellular trafficking. *Mol Biol Cell* 12, 1897-1910.

Busfield, S.J., Michnick, D.A., Chickering, T.W., Revett, T.L., Ma, J., Woolf, E.A., Comrack, C.A., Dussault, B.J., Woolf, J., Goodearl, A.D., *et al.* (1997). Characterization of a neuregulin-related gene, Don-1, that is highly expressed in restricted regions of the cerebellum and hippocampus. *Mol Cell Biol* *17*, 4007-4014.

Capri, G., Chang, J., Chen, S.C., Conte, P., Cwiertka, K., Jerusalem, G., Jiang, Z., Johnston, S., Kaufman, B., Link, J., *et al.* (2009). An open-label expanded access study of lapatinib and capecitabine in patients with HER2-overexpressing locally advanced or metastatic breast cancer. *Ann Oncol* *21*, 474-480.

Carpenter, G. (1999). Employment of the epidermal growth factor receptor in growth factor-independent signaling pathways. *J Cell Biol* *146*, 697-702.

Carpenter, G. (2000). The EGF receptor: a nexus for trafficking and signaling. *Bioessays* *22*, 697-707.

Carpenter, G., and Liao, H.J. (2009). Trafficking of receptor tyrosine kinases to the nucleus. *Exp Cell Res* *315*, 1556-1566.

Casalini, P., Iorio, M.V., Galmozzi, E., and Menard, S. (2004). Role of HER receptors family in development and differentiation. *J Cell Physiol* *200*, 343-350.

Chan, S.K., Hill, M.E., and Gullick, W.J. (2006). The role of the epidermal growth factor receptor in breast cancer. *J Mammary Gland Biol Neoplasia* *11*, 3-11.

Chen, C., Peng, J., Xia, H.S., Yang, G.F., Wu, Q.S., Chen, L.D., Zeng, L.B., Zhang, Z.L., Pang, D.W., and Li, Y. (2009). Quantum dots-based immunofluorescence technology for the quantitative determination of HER2 expression in breast cancer. *Biomaterials* *30*, 2912-2918.

Chen, C., Xia, H.S., Gong, Y.P., Peng, J., Peng, C.W., Hu, M.B., Zhu, X.B., Pang, D.W., Sun, S.R., and Li, Y. (2009). The quantitative detection of total HER2 load by quantum dots and the identification of a new subtype of breast cancer with different 5-year prognosis. *Biomaterials* *31*, 8818-8825.

Cho, H.S., and Leahy, D.J. (2002). Structure of the extracellular region of HER3 reveals an interdomain tether. *Science* *297*, 1330-1333.

Citri, A., Skaria, K.B., and Yarden, Y. (2003). The deaf and the dumb: the biology of ErbB-2 and ErbB-3. *Exp Cell Res* *284*, 54-65.

Citri, A., and Yarden, Y. (2006). EGF-ERBB signalling: towards the systems level. *Nat Rev Mol Cell Biol* *7*, 505-516.

Clayton, A.H., Walker, F., Orchard, S.G., Henderson, C., Fuchs, D., Rothacker, J., Nice, E.C., and Burgess, A.W. (2005). Ligand-induced dimer-tetramer transition during the

activation of the cell surface epidermal growth factor receptor-A multidimensional microscopy analysis. *J Biol Chem* **280**, 30392-30399.

Cobleigh, M.A., Vogel, C.L., Tripathy, D., Robert, N.J., Scholl, S., Fehrenbacher, L., Wolter, J.M., Paton, V., Shak, S., Lieberman, G., *et al.* (1999). Multinational study of the efficacy and safety of humanized anti-HER2 monoclonal antibody in women who have HER2-overexpressing metastatic breast cancer that has progressed after chemotherapy for metastatic disease. *J Clin Oncol* **17**, 2639-2648.

Codony-Servat, J., Albanell, J., Lopez-Talavera, J.C., Arribas, J., and Baselga, J. (1999). Cleavage of the HER2 ectodomain is a pervanadate-activable process that is inhibited by the tissue inhibitor of metalloproteases-1 in breast cancer cells. *Cancer Res* **59**, 1196-1201.

Cohen, G.B., Ren, R., and Baltimore, D. (1995). Modular binding domains in signal transduction proteins. *Cell* **80**, 237-248.

Cohen, S. (1997). EGF and its receptor: historical perspective. Introduction. *J Mammary Gland Biol Neoplasia* **2**, 93-96.

Collins, D., Hill, A.D., and Young, L. (2009). Lapatinib: a competitor or companion to trastuzumab? *Cancer Treat Rev* **35**, 574-581.

Coons, A.H., and Kaplan, M.H. (1950). Localization of antigen in tissue cells; improvements in a method for the detection of antigen by means of fluorescent antibody. *J Exp Med* **91**, 1-13.

Corbett, I.P., Henry, J.A., Angus, B., Watchorn, C.J., Wilkinson, L., Hennessy, C., Gullick, W.J., Tuzi, N.L., May, F.E., Westley, B.R., *et al.* (1990). NCL-CB11, a new monoclonal antibody recognizing the internal domain of the c-erbB-2 oncogene protein effective for use on formalin-fixed, paraffin-embedded tissue. *J Pathol* **161**, 15-25.

D'Antonio, A., Losito, S., Pignata, S., Grassi, M., Perrone, F., De Luca, A., Tambaro, R., Bianco, C., Gullick, W.J., Johnson, G.R., *et al.* (2002). Transforming growth factor alpha, amphiregulin and cripto-1 are frequently expressed in advanced human ovarian carcinomas. *Int J Oncol* **21**, 941-948.

Dapson, R.W. (1993). Fixation for the 1990's: a review of needs and accomplishments. *Biotech Histochem* **68**, 75-82.

Daub, H., Wallasch, C., Lanckenau, A., Herrlich, A., and Ullrich, A. (1997). Signal characteristics of G protein-transactivated EGF receptor. *EMBO J* **16**, 7032-7044.

Dawson, J.P., Berger, M.B., Lin, C.C., Schlessinger, J., Lemmon, M.A., and Ferguson, K.M. (2005). Epidermal growth factor receptor dimerization and activation require

ligand-induced conformational changes in the dimer interface. *Mol Cell Biol* 25, 7734-7742.

de Bono, J.S., and Rowinsky, E.K. (2002). The ErbB receptor family: a therapeutic target for cancer. *Trends Mol Med* 8, S19-26.

Downward, J., Yarden, Y., Mayes, E., Scrace, G., Totty, N., Stockwell, P., Ullrich, A., Schlessinger, J., and Waterfield, M.D. (1984). Close similarity of epidermal growth factor receptor and v-erb-B oncogene protein sequences. *Nature* 307, 521-527.

Dowsett, M., Bartlett, J., Ellis, I.O., Salter, J., Hills, M., Mallon, E., Watters, A.D., Cooke, T., Paish, C., Wencyk, P.M., *et al.* (2003). Correlation between immunohistochemistry (HercepTest) and fluorescence in situ hybridization (FISH) for HER-2 in 426 breast carcinomas from 37 centres. *J Pathol* 199, 418-423.

Dunn, M., Sinha, P., Campbell, R., Blackburn, E., Levinson, N., Rampaul, R., Bates, T., Humphreys, S., and Gullick, W.J. (2004). Co-expression of neuregulins 1, 2, 3 and 4 in human breast cancer. *J Pathol* 203, 672-680.

Elenius, K., Choi, C.J., Paul, S., Santiestevan, E., Nishi, E., and Klagsbrun, M. (1999). Characterization of a naturally occurring ErbB4 isoform that does not bind or activate phosphatidylinositol 3-kinase. *Oncogene* 18, 2607-2615.

Elenius, K., Corfas, G., Paul, S., Choi, C.J., Rio, C., Plowman, G.D., and Klagsbrun, M. (1997). A novel juxtamembrane domain isoform of HER4/ErbB4. Isoform-specific tissue distribution and differential processing in response to phorbol ester. *J Biol Chem* 272, 26761-26768.

Ellis, L.M., and Hicklin, D.J. (2009). Resistance to Targeted Therapies: Refining Anticancer Therapy in the Era of Molecular Oncology. *Clin Cancer Res* 15, 7471-7478.

Erickson, S.L., O'Shea, K.S., Ghaboosi, N., Loverro, L., Frantz, G., Bauer, M., Lu, L.H., and Moore, M.W. (1997). ErbB3 is required for normal cerebellar and cardiac development: a comparison with ErbB2-and heregulin-deficient mice. *Development* 124, 4999-5011.

Falls, D.L. (2003). Neuregulins: functions, forms, and signaling strategies. *Exp Cell Res* 284, 14-30.

Fedi, P., Pierce, J.H., di Fiore, P.P., and Kraus, M.H. (1994). Efficient coupling with phosphatidylinositol 3-kinase, but not phospholipase C gamma or GTPase-activating protein, distinguishes ErbB-3 signaling from that of other ErbB/EGFR family members. *Mol Cell Biol* 14, 492-500.

Ferguson, K.M., Berger, M.B., Mendrola, J.M., Cho, H.S., Leahy, D.J., and Lemmon, M.A. (2003). EGF activates its receptor by removing interactions that autoinhibit ectodomain dimerization. *Mol Cell* *11*, 507-517.

Filardo, E.J. (2002). Epidermal growth factor receptor (EGFR) transactivation by estrogen via the G-protein-coupled receptor, GPR30: a novel signaling pathway with potential significance for breast cancer. *J Steroid Biochem Mol Biol* *80*, 231-238.

Filardo, E.J., Quinn, J.A., Bland, K.I., and Frackelton, A.R., Jr. (2000). Estrogen-induced activation of Erk-1 and Erk-2 requires the G protein-coupled receptor homolog, GPR30, and occurs via trans-activation of the epidermal growth factor receptor through release of HB-EGF. *Mol Endocrinol* *14*, 1649-1660.

Fizman, G.L., and Jasnis, M.A. Molecular Mechanisms of Trastuzumab Resistance in HER2 Overexpressing Breast Cancer. *Int J Breast Cancer* *2011*, 352182.

Franklin, M.C., Carey, K.D., Vajdos, F.F., Leahy, D.J., de Vos, A.M., and Sliwkowski, M.X. (2004). Insights into ErbB signaling from the structure of the ErbB2-pertuzumab complex. *Cancer Cell* *5*, 317-328.

Friess, H., Yamanaka, Y., Kobrin, M.S., Do, D.A., Buchler, M.W., and Korc, M. (1995). Enhanced erbB-3 expression in human pancreatic cancer correlates with tumor progression. *Clin Cancer Res* *1*, 1413-1420.

Fry, W.H., Kotelawala, L., Sweeney, C., and Carraway, K.L. (2009). Mechanisms of ErbB receptor negative regulation and relevance in cancer. *Exp Cell Res* *315*, 697-706.

Garrett, T.P., McKern, N.M., Lou, M., Elleman, T.C., Adams, T.E., Lovrecz, G.O., Kofler, M., Jorissen, R.N., Nice, E.C., Burgess, A.W., *et al.* (2003). The crystal structure of a truncated ErbB2 ectodomain reveals an active conformation, poised to interact with other ErbB receptors. *Mol Cell* *11*, 495-505.

Garrett, T.P., McKern, N.M., Lou, M., Elleman, T.C., Adams, T.E., Lovrecz, G.O., Zhu, H.J., Walker, F., Frenkel, M.J., Hoyne, P.A., *et al.* (2002). Crystal structure of a truncated epidermal growth factor receptor extracellular domain bound to transforming growth factor alpha. *Cell* *110*, 763-773.

Gassmann, M., Casagrande, F., Orioli, D., Simon, H., Lai, C., Klein, R., and Lemke, G. (1995). Aberrant neural and cardiac development in mice lacking the ErbB4 neuregulin receptor. *Nature* *378*, 390-394.

Goel, M.K., Khanna, P., and Kishore, J. Understanding survival analysis: Kaplan-Meier estimate. *Int J Ayurveda Res* *1*, 274-278.

Gown, A.M. (2008). Current issues in ER and HER2 testing by IHC in breast cancer. *Mod Pathol* *21 Suppl 2*, S8-S15.

Gullick, W.J. (2001). The Type 1 growth factor receptors and their ligands considered as a complex system. *Endocr Relat Cancer* 8, 75-82.

Gullick, W.J. (2003). c-erbB-4/HER4: friend or foe? *J Pathol* 200, 279-281.

Gullick, W.J. (2009). The epidermal growth factor system of ligands and receptors in cancer. *Eur J Cancer* 45 *Suppl* 1, 205-210.

Gullick, W.J., Berger, M.S., Bennett, P.L., Rothbard, J.B., and Waterfield, M.D. (1987). Expression of the c-erbB-2 protein in normal and transformed cells. *Int J Cancer* 40, 246-254.

Gullick, W.J., Bottomley, A.C., Lofts, F.J., Doak, D.G., Mulvey, D., Newman, R., Crumpton, M.J., Sternberg, M.J., and Campbell, I.D. (1992). Three dimensional structure of the transmembrane region of the proto-oncogenic and oncogenic forms of the neu protein. *EMBO J* 11, 43-48.

Gullick, W.J., Downward, J., and Waterfield, M.D. (1985). Antibodies to the autophosphorylation sites of the epidermal growth factor receptor protein-tyrosine kinase as probes of structure and function. *EMBO J* 4, 2869-2877.

Gullick, W.J., Marsden, J.J., Whittle, N., Ward, B., Bobrow, L., and Waterfield, M.D. (1986). Expression of epidermal growth factor receptors on human cervical, ovarian, and vulval carcinomas. *Cancer Res* 46, 285-292.

Gutierrez, C., and Schiff, R. HER2: biology, detection, and clinical implications. *Arch Pathol Lab Med* 135, 55-62.

Guy, C.T., Cardiff, R.D., and Muller, W.J. (1996). Activated neu induces rapid tumor progression. *J Biol Chem* 271, 7673-7678.

Haigler, H., Ash, J.F., Singer, S.J., and Cohen, S. (1978). Visualization by fluorescence of the binding and internalization of epidermal growth factor in human carcinoma cells A-431. *Proc Natl Acad Sci U S A* 75, 3317-3321.

Hamburger, A.W. (2008). The role of ErbB3 and its binding partners in breast cancer progression and resistance to hormone and tyrosine kinase directed therapies. *J Mammary Gland Biol Neoplasia* 13, 225-233.

Hameed, O., Chhieng, D.C., and Adams, A.L. (2007). Does using a higher cutoff for the percentage of positive cells improve the specificity of HER-2 immunohistochemical analysis in breast carcinoma? *Am J Clin Pathol* 128, 825-829.

Harari, D., and Yarden, Y. (2000). Molecular mechanisms underlying ErbB2/HER2 action in breast cancer. *Oncogene* 19, 6102-6114.

Harding, J., and Burtness, B. (2005). Cetuximab: an epidermal growth factor receptor chimeric human-murine monoclonal antibody. *Drugs Today (Barc)* 41, 107-127.

Hayes, N.V., Blackburn, E., Boyle, M.M., Russell, G.A., Frost, T.M., Morgan, B.J., and Gullick, W.J. Expression of neuregulin 4 splice variants in normal human tissues and prostate cancer and their effects on cell motility. *Endocr Relat Cancer* 18, 39-49.

Higashiyama, S., Horikawa, M., Yamada, K., Ichino, N., Nakano, N., Nakagawa, T., Miyagawa, J., Matsushita, N., Nagatsu, T., Taniguchi, N., *et al.* (1997). A novel brain-derived member of the epidermal growth factor family that interacts with ErbB3 and ErbB4. *J Biochem* 122, 675-680.

Holbro, T., Beerli, R.R., Maurer, F., Koziczak, M., Barbas, C.F., 3rd, and Hynes, N.E. (2003). The ErbB2/ErbB3 heterodimer functions as an oncogenic unit: ErbB2 requires ErbB3 to drive breast tumor cell proliferation. *Proc Natl Acad Sci U S A* 100, 8933-8938.

Huang H.E., Chin S.F., Ginestier C., *et al.* (2004). A Recurrent Chromosome Breakpoint in Breast Cancer at the NRG1/Neuregulin 1/Heregulin Gene. *Cancer Res* 64, 6840–6844

Huang, W., Reinholz, M., Weidler, J., Yolanda, L., Paquet, A., Whitcomb, J., Lingle, W., Jenkins, R.B., Chen, B., Larson, J.S., *et al.* Comparison of central HER2 testing with quantitative total HER2 expression and HER2 homodimer measurements using a novel proximity-based assay. *Am J Clin Pathol* 134, 303-311.

Hubbard, S.R. (1999). Structural analysis of receptor tyrosine kinases. *Prog Biophys Mol Biol* 71, 343-358.

Hubbard, S.R. (2006). EGF receptor activation: push comes to shove. *Cell* 125, 1029-1031.

Hubbard, S.R., and Till, J.H. (2000). Protein tyrosine kinase structure and function. *Annu Rev Biochem* 69, 373-398.

Hurvitz, S.A., and Kakkar, R. The potential for trastuzumab emtansine in human epidermal growth factor receptor 2 positive metastatic breast cancer: latest evidence and ongoing studies. *Ther Adv Med Oncol* 4, 235-245.

Hynes, N.E., Horsch, K., Olayioye, M.A., and Badache, A. (2001). The ErbB receptor tyrosine family as signal integrators. *Endocr Relat Cancer* 8, 151-159.

Irish, J.C., and Bernstein, A. (1993). Oncogenes in head and neck cancer. *Laryngoscope* 103, 42-52.

Ito, Y., Higashiyama, S., Takeda, T., Yamamoto, Y., Wakasa, K.I., and Matsuura, N. (2001). Expression of heparin-binding epidermal growth factor-like growth factor in pancreatic adenocarcinoma. *Int J Pancreatol* 29, 47-52.

Iwamoto, R., and Mekada, E. (2006). ErbB and HB-EGF signaling in heart development and function. *Cell Struct Funct* 31, 1-14.

Iwamoto, R., Yamazaki, S., Asakura, M., Takashima, S., Hasuwa, H., Miyado, K., Adachi, S., Kitakaze, M., Hashimoto, K., Raab, G., *et al.* (2003). Heparin-binding EGF-like growth factor and ErbB signaling is essential for heart function. *Proc Natl Acad Sci U S A* 100, 3221-3226.

Jackson, L.F., Qiu, T.H., Sunnarborg, S.W., Chang, A., Zhang, C., Patterson, C., and Lee, D.C. (2003). Defective valvulogenesis in HB-EGF and TACE-null mice is associated with aberrant BMP signaling. *EMBO J* 22, 2704-2716.

Jarzab, M., Rozanowski, P., Kowalska, M., Zebracka, J., Rudnicka, L., Stobiecka, E., Jarzab, B., Stachura, J., and Pawlega, J. (2008). Optimization of the method of RNA isolation from paraffin blocks to assess gene expression in breast cancer. *Pol J Pathol* 59, 85-91.

Joensuu, H., Sperinde, J., Leinonen, M., Huang, W., Weidler, J., Bono, P., Kataja, V., Kokko, R., Turpeenniemi-Hujanen, T., Jyrkkio, S., *et al.* (2011). Very high quantitative tumor HER2 content and outcome in early breast cancer. *Ann Oncol*.

Jorissen, R.N., Epa, V.C., Treutlein, H.R., Garrett, T.P., Ward, C.W., and Burgess, A.W. (2000). Characterization of a comparative model of the extracellular domain of the epidermal growth factor receptor. *Protein Sci* 9, 310-324.

Jorissen, R.N., Walker, F., Pouliot, N., Garrett, T.P., Ward, C.W., and Burgess, A.W. (2003). Epidermal growth factor receptor: mechanisms of activation and signalling. *Exp Cell Res* 284, 31-53.

Jura, N., Endres, N.F., Engel, K., Deindl, S., Das, R., Lamers, M.H., Wemmer, D.E., Zhang, X., and Kuriyan, J. (2009a). Mechanism for activation of the EGF receptor catalytic domain by the juxtamembrane segment. *Cell* 137, 1293-1307.

Jura, N., Shan, Y., Cao, X., Shaw, D.E., and Kuriyan, J. (2009b). Structural analysis of the catalytically inactive kinase domain of the human EGF receptor 3. *Proc Natl Acad Sci U S A* 106, 21608-21613.

Kallioniemi, O.P., Kallioniemi, A., Kurisu, W., Thor, A., Chen, L.C., Smith, H.S., Waldman, F.M., Pinkel, D., and Gray, J.W. (1992). ERBB2 amplification in breast cancer analyzed by fluorescence in situ hybridization. *Proc Natl Acad Sci U S A* 89, 5321-5325.

Karunakaran, D., Tzahar, E., Beerli, R.R., Chen, X., Graus-Porta, D., Ratzkin, B.J., Seger, R., Hynes, N.E., and Yarden, Y. (1996). ErbB-2 is a common auxiliary subunit of NDF and EGF receptors: implications for breast cancer. *EMBO J* 15, 254-264.

Kew, T.Y., Bell, J.A., Pinder, S.E., Denley, H., Srinivasan, R., Gullick, W.J., Nicholson, R.I., Blamey, R.W., and Ellis, I.O. (2000). c-erbB-4 protein expression in human breast cancer. *Br J Cancer* *82*, 1163-1170.

Kim, E.S., Khuri, F.R., and Herbst, R.S. (2001). Epidermal growth factor receptor biology (IMC-C225). *Curr Opin Oncol* *13*, 506-513.

Kinugasa, Y., Ishiguro, H., Tokita, Y., Oohira, A., Ohmoto, H., and Higashiyama, S. (2004). Neuroglycan C, a novel member of the neuregulin family. *Biochem Biophys Res Commun* *321*, 1045-1049.

Klijn, J.G., Berns, P.M., Schmitz, P.I., and Foekens, J.A. (1992). The clinical significance of epidermal growth factor receptor (EGF-R) in human breast cancer: a review on 5232 patients. *Endocr Rev* *13*, 3-17.

Knuefermann, C., Lu, Y., Liu, B., Jin, W., Liang, K., Wu, L., Schmidt, M., Mills, G.B., Mendelsohn, J., and Fan, Z. (2003). HER2/PI-3K/Akt activation leads to a multidrug resistance in human breast adenocarcinoma cells. *Oncogene* *22*, 3205-3212.

Kohler, G., and Milstein, C. (1976). Derivation of specific antibody-producing tissue culture and tumor lines by cell fusion. *Eur J Immunol* *6*, 511-519.

Kolibaba, K.S., and Druker, B.J. (1997). Protein tyrosine kinases and cancer. *Biochim Biophys Acta* *1333*, F217-248.

Kostopoulou, E., Vageli, D., Kaisaridou, D., Nakou, M., Netsika, M., Vladica, N., Daponte, A., and Koukoulis, G. (2007). Comparative evaluation of non-informative HER-2 immunoreactions (2+) in breast carcinomas with FISH, CISH and QRT-PCR. *Breast* *16*, 615-624.

Koutras, A.K., Fountzilias, G., Kalogeras, K.T., Starakis, I., Iconomou, G., and Kalofonos, H.P. The upgraded role of HER3 and HER4 receptors in breast cancer. *Crit Rev Oncol Hematol* *74*, 73-78.

Kumagai, T., Davis, J.G., Horie, T., O'Rourke, D.M., and Greene, M.I. (2001). The role of distinct p185neu extracellular subdomains for dimerization with the epidermal growth factor (EGF) receptor and EGF-mediated signaling. *Proc Natl Acad Sci U S A* *98*, 5526-5531.

Lammerts van Bueren, J.J., Bleeker, W.K., Brannstrom, A., Jansson, M., Peipp, M., Schneider-Merck, T., Valerius, T., van de Winkel, J.G., and Parren, P.W. (2012). Retraction for Lammerts van Bueren et al. The antibody zalutumumab inhibits epidermal growth factor receptor signaling by limiting intra- and intermolecular flexibility. *Proc Natl Acad Sci U S A*. *A 109*, 5548

Lammerts van Bueren JJ, Bleeker WK, Brännström A, von Euler A, Jansson M, Peipp M, Schneider-Merck T, Valerius T, van de Winkel JG, Parren PW. (2008). Proc Natl Acad Sci U S A. A *105*, 6109-14.

Larson, J.S., Goodman, L.J., Tan, Y., Defazio-Eli, L., Paquet, A.C., Cook, J.W., Rivera, A., Frankson, K., Bose, J., Chen, L., *et al.* (2010). Analytical Validation of a Highly Quantitative, Sensitive, Accurate, and Reproducible Assay (HERmark) for the Measurement of HER2 Total Protein and HER2 Homodimers in FFPE Breast Cancer Tumor Specimens. *Patholog Res Int* *2010*, 814176.

Lee, J.W., Soung, Y.H., Seo, S.H., Kim, S.Y., Park, C.H., Wang, Y.P., Park, K., Nam, S.W., Park, W.S., Kim, S.H., *et al.* (2006). Somatic mutations of ERBB2 kinase domain in gastric, colorectal, and breast carcinomas. *Clin Cancer Res* *12*, 57-61.

Lemmon, M.A. (2009). Ligand-induced ErbB receptor dimerization. *Exp Cell Res* *315*, 638-648.

Lemmon, M.A., Bu, Z., Ladbury, J.E., Zhou, M., Pinchasi, D., Lax, I., Engelman, D.M., and Schlessinger, J. (1997). Two EGF molecules contribute additively to stabilization of the EGFR dimer. *EMBO J* *16*, 281-294.

Lemmon, M.A., and Schlessinger, J. Cell signaling by receptor tyrosine kinases. *Cell* *141*, 1117-1134.

Lemoine, N.R., Barnes, D.M., Hollywood, D.P., Hughes, C.M., Smith, P., Dublin, E., Prigent, S.A., Gullick, W.J., and Hurst, H.C. (1992). Expression of the ERBB3 gene product in breast cancer. *Br J Cancer* *66*, 1116-1121.

Lenferink, A.E., Pinkas-Kramarski, R., van de Poll, M.L., van Vugt, M.J., Klapper, L.N., Tzahar, E., Waterman, H., Sela, M., van Zoelen, E.J., and Yarden, Y. (1998). Differential endocytic routing of homo- and hetero-dimeric ErbB tyrosine kinases confers signaling superiority to receptor heterodimers. *EMBO J* *17*, 3385-3397.

Lerdrup, M., Bruun, S., Grandal, M.V., Roepstorff, K., Kristensen, M.M., Hommelgaard, A.M., and van Deurs, B. (2007). Endocytic Down-Regulation of ErbB2 Is Stimulated by Cleavage of Its C-Terminus. *Mol Biol Cell* *18*, 3656-3666.

Leu, M., Bellmunt, E., Schwander, M., Farinas, I., Brenner, H.R., and Muller, U. (2003). ErbB2 regulates neuromuscular synapse formation and is essential for muscle spindle development. *Development* *130*, 2291-2301.

Leyland-Jones, B., and Smith, B.R. Serum HER2 testing in patients with HER2-positive breast cancer: the death knell tolls. *Lancet Oncol* *12*, 286-295.

Li, Q., Ahmed, S., and Loeb, J.A. (2004). Development of an autocrine neuregulin signaling loop with malignant transformation of human breast epithelial cells. *Cancer Res* *64*, 7078-7085.

Li, S., Schmitz, K.R., Jeffrey, P.D., Wiltzius, J.J., Kussie, P., and Ferguson, K.M. (2005). Structural basis for inhibition of the epidermal growth factor receptor by cetuximab. *Cancer Cell* 7, 301-311.

Lipton, A., Kostler, W.J., Leitzel, K., Ali, S.M., Sperinde, J., Weidler, J., Paquet, A., Sherwood, T., Huang, W., and Bates, M. Quantitative HER2 protein levels predict outcome in fluorescence in situ hybridization-positive patients with metastatic breast cancer treated with trastuzumab. *Cancer* 116, 5168-5178.

Luetkeke, N.C., Qiu, T.H., Fenton, S.E., Troyer, K.L., Riedel, R.F., Chang, A., and Lee, D.C. (1999). Targeted inactivation of the EGF and amphiregulin genes reveals distinct roles for EGF receptor ligands in mouse mammary gland development. *Development* 126, 2739-2750.

Luttrell, D.K., and Luttrell, L.M. (2004). Not so strange bedfellows: G-protein-coupled receptors and Src family kinases. *Oncogene* 23, 7969-7978.

Lyne, J.C., Melhem, M.F., Finley, G.G., Wen, D., Liu, N., Deng, D.H., and Salup, R. (1997). Tissue expression of neu differentiation factor/herregulin and its receptor complex in prostate cancer and its biologic effects on prostate cancer cells in vitro. *Cancer J Sci Am* 3, 21-30.

Martin-Fernandez, M., Clarke, D.T., Tobin, M.J., Jones, S.V., and Jones, G.R. (2002). Preformed oligomeric epidermal growth factor receptors undergo an ectodomain structure change during signaling. *Biophys J* 82, 2415-2427.

Mass, R.D., Press, M.F., Anderson, S., Cobleigh, M.A., Vogel, C.L., Dybdal, N., Leiberman, G., and Slamon, D.J. (2005). Evaluation of clinical outcomes according to HER2 detection by fluorescence in situ hybridization in women with metastatic breast cancer treated with trastuzumab. *Clin Breast Cancer* 6, 240-246.

McIntyre, E., Blackburn, E., Brown, P.J., Johnson, C.G., and Gullick, W.J. The complete family of epidermal growth factor receptors and their ligands are co-ordinately expressed in breast cancer. *Breast Cancer Res Treat* 122, 105-110.

Mendelsohn, J., and Baselga, J. (2003). Status of epidermal growth factor receptor antagonists in the biology and treatment of cancer. *J Clin Oncol* 21, 2787-2799.

Meric, F., Hung, M.C., Hortobagyi, G.N., and Hunt, K.K. (2002). HER2/neu in the management of invasive breast cancer. *J Am Coll Surg* 194, 488-501.

Miettinen, P.J., Berger, J.E., Meneses, J., Phung, Y., Pedersen, R.A., Werb, Z., and Derynck, R. (1995). Epithelial immaturity and multiorgan failure in mice lacking epidermal growth factor receptor. *Nature* 376, 337-341.

Moasser, M.M. (2007). Targeting the function of the HER2 oncogene in human cancer therapeutics. *Oncogene* 26, 6577-6592.

Moelans, C.B., de Weger, R.A., Van der Wall, E., and van Diest, P.J. Current technologies for HER2 testing in breast cancer. *Crit Rev Oncol Hematol* 80, 380-392.

Molina, M.A., Codony-Servat, J., Albanell, J., Rojo, F., Arribas, J., and Baselga, J. (2001). Trastuzumab (herceptin), a humanized anti-Her2 receptor monoclonal antibody, inhibits basal and activated Her2 ectodomain cleavage in breast cancer cells. *Cancer Res* 61, 4744-4749.

Monton, H., Nogues, C., Rossinyol, E., Castell, O., and Roldan, M. (2009). QDs versus Alexa: reality of promising tools for immunocytochemistry. *J Nanobiotechnology* 7, 4.

Mosesson, Y., and Yarden, Y. (2004). Oncogenic growth factor receptors: implications for signal transduction therapy. *Semin Cancer Biol* 14, 262-270.

Muller, W.J., Sinn, E., Pattengale, P.K., Wallace, R., and Leder, P. (1988). Single-step induction of mammary adenocarcinoma in transgenic mice bearing the activated c-neu oncogene. *Cell* 54, 105-115.

Nahta, R., and Esteva, F.J. (2006). Herceptin: mechanisms of action and resistance. *Cancer Lett* 232, 123-138.

Negro, A., Brar, B.K., and Lee, K.F. (2004). Essential roles of Her2/erbB2 in cardiac development and function. *Recent Prog Horm Res* 59, 1-12.

Neumann, M., and Gabel, D. (2002). Simple method for reduction of autofluorescence in fluorescence microscopy. *J Histochem Cytochem* 50, 437-439.

Nik-Zainal, S., Van Loo, P., Wedge, D.C., Alexandrov, L.B., Greenman, C.D., Lau, K.W., Raine, K., Jones, D., Marshall, J., Ramakrishna, M., *et al.* The life history of 21 breast cancers. *Cell* 149, 994-1007.

Nishikawa, R., Ji, X.D., Harmon, R.C., Lazar, C.S., Gill, G.N., Cavenee, W.K., and Huang, H.J. (1994). A mutant epidermal growth factor receptor common in human glioma confers enhanced tumorigenicity. *Proc Natl Acad Sci U S A* 91, 7727-7731.

Normanno, N., Bianco, C., De Luca, A., and Salomon, D.S. (2001). The role of EGF-related peptides in tumor growth. *Front Biosci* 6, D685-707.

Normanno, N., De Luca, A., Bianco, C., Strizzi, L., Mancino, M., Maiello, M.R., Carotenuto, A., De Feo, G., Caponigro, F., and Salomon, D.S. (2006). Epidermal growth factor receptor (EGFR) signaling in cancer. *Gene* 366, 2-16.

Normanno, N., Kim, N., Wen, D., Smith, K., Harris, A.L., Plowman, G., Colletta, G., Ciardiello, F., and Salomon, D.S. (1995). Expression of messenger RNA for amphiregulin, heregulin, and cripto-1, three new members of the epidermal growth factor family, in human breast carcinomas. *Breast Cancer Res Treat* 35, 293-297.

Ogiso, H., Ishitani, R., Nureki, O., Fukai, S., Yamanaka, M., Kim, J.H., Saito, K., Sakamoto, A., Inoue, M., Shirouzu, M., *et al.* (2002). Crystal structure of the complex of human epidermal growth factor and receptor extracellular domains. *Cell* 110, 775-787.

Olayioye, M.A., Neve, R.M., Lane, H.A., and Hynes, N.E. (2000). The ErbB signaling network: receptor heterodimerization in development and cancer. *EMBO J* 19, 3159-3167.

Pauletti, G., Dandekar, S., Rong, H., Ramos, L., Peng, H., Seshadri, R., and Slamon, D.J. (2000). Assessment of methods for tissue-based detection of the HER-2/neu alteration in human breast cancer: a direct comparison of fluorescence in situ hybridization and immunohistochemistry. *J Clin Oncol* 18, 3651-3664.

Pedersen, M.W., Meltorn, M., Damstrup, L., and Poulsen, H.S. (2001). The type III epidermal growth factor receptor mutation. Biological significance and potential target for anti-cancer therapy. *Ann Oncol* 12, 745-760.

Pegram, M.D., Pauletti, G., and Slamon, D.J. (1998). HER-2/neu as a predictive marker of response to breast cancer therapy. *Breast Cancer Res Treat* 52, 65-77.

Penuel, E., Akita, R.W., and Sliwkowski, M.X. (2002). Identification of a region within the ErbB2/HER2 intracellular domain that is necessary for ligand-independent association. *J Biol Chem* 277, 28468-28473.

Perou, C.M., Sorlie, T., Eisen, M.B., van de Rijn, M., Jeffrey, S.S., Rees, C.A., Pollack, J.R., Ross, D.T., Johnsen, H., Akslén, L.A., *et al.* (2000). Molecular portraits of human breast tumours. *Nature* 406, 747-752.

Pinaud, F., Michalet, X., Bentolila, L.A., Tsay, J.M., Doose, S., Li, J.J., Iyer, G., and Weiss, S. (2006). Advances in fluorescence imaging with quantum dot bio-probes. *Biomaterials* 27, 1679-1687.

Plaut, K. (1993). Role of epidermal growth factor and transforming growth factors in mammary development and lactation. *J Dairy Sci* 76, 1526-1538.

Porter, A.C., and Vaillancourt, R.R. (1998). Tyrosine kinase receptor-activated signal transduction pathways which lead to oncogenesis. *Oncogene* 17, 1343-1352.

Prenzel, N., Fischer, O.M., Streit, S., Hart, S., and Ullrich, A. (2001). The epidermal growth factor receptor family as a central element for cellular signal transduction and diversification. *Endocr Relat Cancer* 8, 11-31.

Press, M.F., Hung, G., Godolphin, W., and Slamon, D.J. (1994). Sensitivity of HER-2/neu antibodies in archival tissue samples: potential source of error in immunohistochemical studies of oncogene expression. *Cancer Res* 54, 2771-2777.

Prigent, S.A., and Gullick, W.J. (1994). Identification of c-erbB-3 binding sites for phosphatidylinositol 3'-kinase and SHC using an EGF receptor/c-erbB-3 chimera. *EMBO J* 13, 2831-2841.

Prigent, S.A., Lemoine, N.R., Hughes, C.M., Plowman, G.D., Selden, C., and Gullick, W.J. (1992). Expression of the c-erbB-3 protein in normal human adult and fetal tissues. *Oncogene* 7, 1273-1278.

Pusztai, L., Mazouni, C., Anderson, K., Wu, Y., and Symmans, W.F. (2006). Molecular classification of breast cancer: limitations and potential. *Oncologist* 11, 868-877.

Qi, C.F., Liscia, D.S., Normanno, N., Merlo, G., Johnson, G.R., Gullick, W.J., Ciardiello, F., Saeki, T., Brandt, R., Kim, N., *et al.* (1994). Expression of transforming growth factor alpha, amphiregulin and cripto-1 in human breast carcinomas. *Br J Cancer* 69, 903-910.

Qiu, Y., Ravi, L., and Kung, H.J. (1998). Requirement of ErbB2 for signalling by interleukin-6 in prostate carcinoma cells. *Nature* 393, 83-85.

Rajkumar, T., Gooden, C.S., Lemoine, N.R., Gullick, W.J., and Goden, C.S. (1993). Expression of the c-erbB-3 protein in gastrointestinal tract tumours determined by monoclonal antibody RTJ1. *J Pathol* 170, 271-278.

Rajkumar, T., and Gullick, W.J. (1994). A monoclonal antibody to the human c-erbB3 protein stimulates the anchorage-independent growth of breast cancer cell lines. *Br J Cancer* 70, 459-465.

Rajkumar, T., Majhi, U., Malligarjuna, V., and Gullick, W. (1995). Prevalence of C-erbb3 expression in squamous-cell carcinomas of the cervix as determined by the monoclonal-antibody rtj2. *Int J Oncol* 6, 105-109.

Rajkumar, T., Stamp, G.W., Hughes, C.M., and Gullick, W.J. (1996). c-erbB3 protein expression in ovarian cancer. *Clin Mol Pathol* 49, M199-M202.

Rakha, E.A., Reis-Filho, J.S., Baehner, F., Dabbs, D.J., Decker, T., Eusebi, V., Fox, S.B., Ichihara, S., Jacquemier, J., Lakhani, S.R., *et al.* Breast cancer prognostic classification in the molecular era: the role of histological grade. *Breast Cancer Res* 12, 207.

Rampaul, R.S., Pinder, S.E., Gullick, W.J., Robertson, J.F., and Ellis, I.O. (2002). HER-2 in breast cancer--methods of detection, clinical significance and future prospects for treatment. *Crit Rev Oncol Hematol* 43, 231-244.

Reid, A., Vidal, L., Shaw, H., and de Bono, J. (2007). Dual inhibition of ErbB1 (EGFR/HER1) and ErbB2 (HER2/neu). *Eur J Cancer* 43, 481-489.

Robinson, D.R., Wu, Y.M., and Lin, S.F. (2000). The protein tyrosine kinase family of the human genome. *Oncogene* 19, 5548-5557.

Roepstorff, K., GrÃ¸vdal, L., Grandal, M., Lerdrup, M., and van Deurs, B. (2008). Endocytic downregulation of ErbB receptors: mechanisms and relevance in cancer. *Histochem Cell Biol* 129, 563-578.

Roskoski, R., Jr. (2004). The ErbB/HER receptor protein-tyrosine kinases and cancer. *Biochem Biophys Res Commun* 319, 1-11.

Ross, J.S., Slodkowska, E.A., Symmans, W.F., Pusztai, L., Ravdin, P.M., and Hortobagyi, G.N. (2009). The HER-2 receptor and breast cancer: ten years of targeted anti-HER-2 therapy and personalized medicine. *Oncologist* 14, 320-368.

Rowinsky, E.K. (2004). The erbB family: targets for therapeutic development against cancer and therapeutic strategies using monoclonal antibodies and tyrosine kinase inhibitors. *Annu Rev Med* 55, 433-457.

Roy, V., and Perez, E.A. (2009). Beyond trastuzumab: small molecule tyrosine kinase inhibitors in HER-2-positive breast cancer. *Oncologist* 14, 1061-1069.

Saeki, T., Stromberg, K., Qi, C.F., Gullick, W.J., Tahara, E., Normanno, N., Ciardiello, F., Kenney, N., Johnson, G.R., and Salomon, D.S. (1992). Differential immunohistochemical detection of amphiregulin and cripto in human normal colon and colorectal tumors. *Cancer Res* 52, 3467-3473.

Salomon, D.S., Brandt, R., Ciardiello, F., and Normanno, N. (1995). Epidermal growth factor-related peptides and their receptors in human malignancies. *Crit Rev Oncol Hematol* 19, 183-232.

Sauter, G., Lee, J., Bartlett, J.M., Slamon, D.J., and Press, M.F. (2009). Guidelines for human epidermal growth factor receptor 2 testing: biologic and methodologic considerations. *J Clin Oncol* 27, 1323-1333.

Schlessinger, J. (2000). Cell signaling by receptor tyrosine kinases. *Cell* 103, 211-225.

Schlessinger, J. (2002). Ligand-induced, receptor-mediated dimerization and activation of EGF receptor. *Cell* 110, 669-672.

Schlessinger, J., and Lemmon, M.A. (2003). SH2 and PTB domains in tyrosine kinase signaling. *Sci STKE* 2003, RE12.

Schlessinger, J., and Lemmon, M.A. (2006). Nuclear signaling by receptor tyrosine kinases: the first robin of spring. *Cell* 127, 45-48.

Schneider, M.R., and Wolf, E. (2009). The epidermal growth factor receptor ligands at a glance. *J Cell Physiol* 218, 460-466.

Schnell, S.A., Staines, W.A., and Wessendorf, M.W. (1999). Reduction of lipofuscin-like autofluorescence in fluorescently labeled tissue. *J Histochem Cytochem* 47, 719-730.

Scott, G.K., Robles, R., Park, J.W., Montgomery, P.A., Daniel, J., Holmes, W.E., Lee, J., Keller, G.A., Li, W.L., Fendly, B.M., *et al.* (1993). A truncated intracellular HER2/neu receptor produced by alternative RNA processing affects growth of human carcinoma cells. *Mol Cell Biol* 13, 2247-2257.

Sebastian, J., Richards, R.G., Walker, M.P., Wiesen, J.F., Werb, Z., Derynck, R., Hom, Y.K., Cunha, G.R., and DiAugustine, R.P. (1998). Activation and function of the epidermal growth factor receptor and erbB-2 during mammary gland morphogenesis. *Cell Growth Differ* 9, 777-785.

Shah, S., and Chen, B. Testing for HER2 in Breast Cancer: A Continuing Evolution. *Patholog Res Int* 2011.

Shi, F., Telesco, S.E., Liu, Y., Radhakrishnan, R., and Lemmon, M.A. ErbB3/HER3 intracellular domain is competent to bind ATP and catalyze autophosphorylation. *Proc Natl Acad Sci U S A* 107, 7692-7697.

Shigematsu, H., and Gazdar, A.F. (2006). Somatic mutations of epidermal growth factor receptor signaling pathway in lung cancers. *Int J Cancer* 118, 257-262.

Shigematsu, H., Takahashi, T., Nomura, M., Majmudar, K., Suzuki, M., Lee, H., Wistuba, II, Fong, K.M., Toyooka, S., Shimizu, N., *et al.* (2005). Somatic mutations of the HER2 kinase domain in lung adenocarcinomas. *Cancer Res* 65, 1642-1646.

Sibilia, M., Steinbach, J.P., Stingl, L., Aguzzi, A., and Wagner, E.F. (1998). A strain-independent postnatal neurodegeneration in mice lacking the EGF receptor. *EMBO J* 17, 719-731.

Siegel, P.M., Ryan, E.D., Cardiff, R.D., and Muller, W.J. (1999). Elevated expression of activated forms of Neu/ErbB-2 and ErbB-3 are involved in the induction of mammary tumors in transgenic mice: implications for human breast cancer. *EMBO J* 18, 2149-2164.

Sierke, S.L., Cheng, K., Kim, H.H., and Koland, J.G. (1997). Biochemical characterization of the protein tyrosine kinase homology domain of the ErbB3 (HER3) receptor protein. *Biochem J* 322 (Pt 3), 757-763.

Singer, C.F., Kostler, W.J., and Hudelist, G. (2008). Predicting the efficacy of trastuzumab-based therapy in breast cancer: current standards and future strategies. *Biochim Biophys Acta* 1786, 105-113.

Sithanandam, G., and Anderson, L.M. (2008). The ERBB3 receptor in cancer and cancer gene therapy. *Cancer Gene Ther* 15, 413-448.

Slamon, D.J., Clark, G.M., Wong, S.G., Levin, W.J., Ullrich, A., and McGuire, W.L. (1987). Human breast cancer: correlation of relapse and survival with amplification of the HER-2/neu oncogene. *Science* 235, 177-182.

Slamon, D.J., Godolphin, W., Jones, L.A., Holt, J.A., Wong, S.G., Keith, D.E., Levin, W.J., Stuart, S.G., Udove, J., Ullrich, A., *et al.* (1989). Studies of the HER-2/neu proto-oncogene in human breast and ovarian cancer. *Science* 244, 707-712.

Slamon, D.J., Leyland-Jones, B., Shak, S., Fuchs, H., Paton, V., Bajamonde, A., Fleming, T., Eiermann, W., Wolter, J., Pegram, M., *et al.* (2001). Use of chemotherapy plus a monoclonal antibody against HER2 for metastatic breast cancer that overexpresses HER2. *N Engl J Med* 344, 783-792.

Smith, A.M., Dave, S., Nie, S., True, L., and Gao, X. (2006). Multicolor quantum dots for molecular diagnostics of cancer. *Expert Rev Mol Diagn* 6, 231-244.

Soltoff, S.P., and Cantley, L.C. (1996). p120cbl is a cytosolic adapter protein that associates with phosphoinositide 3-kinase in response to epidermal growth factor in PC12 and other cells. *J Biol Chem* 271, 563-567.

Soltoff, S.P., Carraway K.L., Prigent S.A., Gullick W.G., and Cantley L.C. (1994). ErbB3 Is Involved in Activation of Phosphatidylinositol 3-Kinase by Epidermal Growth Factor. *Mol Cell Biol* 14, 3550-3558

Song, L., Varma, C.A., Verhoeven, J.W., and Tanke, H.J. (1996). Influence of the triplet excited state on the photobleaching kinetics of fluorescein in microscopy. *Biophys J* 70, 2959-2968.

Sorkin, A., and Goh, L.K. (2008). Endocytosis and intracellular trafficking of ErbBs. *Exp Cell Res* 314, 3093-3106.

Spigel, D.R., and Burstein, H.J. (2003). Trastuzumab regimens for HER2-overexpressing metastatic breast cancer. *Clin Breast Cancer* 4, 329-337; discussion 338-329.

Srinivasan, R., Gillett, C.E., Barnes, D.M., and Gullick, W.J. (2000). Nuclear expression of the c-erbB-4/HER-4 growth factor receptor in invasive breast cancers. *Cancer Res* 60, 1483-1487.

Srinivasan, R., Poulson, R., Hurst, H.C., and Gullick, W.J. (1998). Expression of the c-erbB-4/HER4 protein and mRNA in normal human fetal and adult tissues and in a survey of nine solid tumour types. *J Pathol* 185, 236-245.

Stamos, J., Sliwkowski, M.X., and Eigenbrot, C. (2002). Structure of the epidermal growth factor receptor kinase domain alone and in complex with a 4-anilinoquinazoline inhibitor. *J Biol Chem* 277, 46265-46272.

Stein, R.A., and Staros, J.V. (2000). Evolutionary analysis of the ErbB receptor and ligand families. *J Mol Evol* 50, 397-412.

Strachan, L., Murison, J.G., Prestidge, R.L., Sleeman, M.A., Watson, J.D., and Kumble, K.D. (2001). Cloning and biological activity of epigen, a novel member of the epidermal growth factor superfamily. *J Biol Chem* 276, 18265-18271.

Sundvall, M., Iljin, K., Kilpinen, S., Sara, H., Kallioniemi, O.P., and Elenius, K. (2008). Role of ErbB4 in breast cancer. *J Mammary Gland Biol Neoplasia* 13, 259-268.

Suo, Z., Risberg, B., Kalsson, M.G., Willman, K., Tierens, A., Skovlund, E., and Nesland, J.M. (2002). EGFR family expression in breast carcinomas. c-erbB-2 and c-erbB-4 receptors have different effects on survival. *J Pathol* 196, 17-25.

Sutherland, S., Ashley, S., Miles, D., Chan, S., Wardley, A., Davidson, N., Bhatti, R., Shehata, M., Nouras, H., Camburn, T., *et al.* Treatment of HER2-positive metastatic breast cancer with lapatinib and capecitabine in the lapatinib expanded access programme, including efficacy in brain metastases--the UK experience. *Br J Cancer* 102, 995-1002.

Sweeney, C., and Carraway, K.L., 3rd (2000). Ligand discrimination by ErbB receptors: differential signaling through differential phosphorylation site usage. *Oncogene* 19, 5568-5573.

Sweeney, C., and Carraway, K.L., 3rd (2004). Negative regulation of ErbB family receptor tyrosine kinases. *Br J Cancer* 90, 289-293.

Tholouli, E., Sweeney, E., Barrow, E., Clay, V., Hoyland, J.A., and Byers, R.J. (2008). Quantum dots light up pathology. *J Pathol* 216, 275-285.

Threadgill, D.W., Dlugosz, A.A., Hansen, L.A., Tennenbaum, T., Lichti, U., Yee, D., LaMantia, C., Mourton, T., Herrup, K., Harris, R.C., *et al.* (1995). Targeted disruption of mouse EGF receptor: effect of genetic background on mutant phenotype. *Science* 269, 230-234.

Tidcombe, H., Jackson-Fisher, A., Mathers, K., Stern, D.F., Gassmann, M., and Golding, J.P. (2003). Neural and mammary gland defects in ErbB4 knockout mice genetically rescued from embryonic lethality. *Proc Natl Acad Sci U S A* 100, 8281-8286.

Torrisi, R., Rotmensz, N., Bagnardi, V., Viale, G., Curto, B.D., Dell'orto, P., Veronesi, P., Luini, A., D'Alessandro, C., Cardillo, A., *et al.* (2007). HER2 status in early breast cancer:

relevance of cell staining patterns, gene amplification and polysomy 17. *Eur J Cancer* 43, 2339-2344.

Travis, A., Pinder, S.E., Robertson, J.F., Bell, J.A., Wencyk, P., Gullick, W.J., Nicholson, R.I., Poller, D.N., Blamey, R.W., Elston, C.W., *et al.* (1996). C-erbB-3 in human breast carcinoma: expression and relation to prognosis and established prognostic indicators. *Br J Cancer* 74, 229-233.

True, L.D., and Gao, X. (2007). Quantum dots for molecular pathology: their time has arrived. *J Mol Diagn* 9, 7-11.

Tsai, M.S., Shamon-Taylor, L.A., Mehmi, I., Tang, C.K., and Lupu, R. (2003). Blockage of heregulin expression inhibits tumorigenicity and metastasis of breast cancer. *Oncogene* 22, 761-768.

Tsang, R.Y., and Finn, R.S. Beyond trastuzumab: novel therapeutic strategies in HER2-positive metastatic breast cancer. *Br J Cancer* 106, 6-13.

Tsutsui, S., Kataoka, A., Ohno, S., Murakami, S., Kinoshita, J., and Hachitanda, Y. (2002). Prognostic and predictive value of epidermal growth factor receptor in recurrent breast cancer. *Clin Cancer Res* 8, 3454-3460.

Tvorogov, D., Sundvall, M., Kurppa, K., Hollmen, M., Repo, S., Johnson, M.S., and Elenius, K. (2009). Somatic mutations of ErbB4: selective loss-of-function phenotype affecting signal transduction pathways in cancer. *J Biol Chem* 284, 5582-5591.

Tzahar, E., Waterman, H., Chen, X., Levkowitz, G., Karunagaran, D., Lavi, S., Ratzkin, B.J., and Yarden, Y. (1996). A hierarchical network of interreceptor interactions determines signal transduction by Neu differentiation factor/neuregulin and epidermal growth factor. *Mol Cell Biol* 16, 5276-5287.

Van de Lest, C.H., Versteeg, E.M., Veerkamp, J.H., and Van Kuppevelt, T.H. (1995). Elimination of autofluorescence in immunofluorescence microscopy with digital image processing. *J Histochem Cytochem* 43, 727-730.

Venter, D.J., Tuzi, N.L., Kumar, S., and Gullick, W.J. (1987). Overexpression of the c-erbB-2 oncoprotein in human breast carcinomas: immunohistological assessment correlates with gene amplification. *Lancet* 2, 69-72.

Viegas, M.S., Martins, T.C., Seco, F., and do Carmo, A. (2007). An improved and cost-effective methodology for the reduction of autofluorescence in direct immunofluorescence studies on formalin-fixed paraffin-embedded tissues. *Eur J Histochem* 51, 59-66.

Vogel, C.L., Cobleigh, M.A., Tripathy, D., Gutheil, J.C., Harris, L.N., Fehrenbacher, L., Slamon, D.J., Murphy, M., Novotny, W.F., Burchmore, M., *et al.* (2002). Efficacy and

safety of trastuzumab as a single agent in first-line treatment of HER2-overexpressing metastatic breast cancer. *J Clin Oncol* 20, 719-726.

Wang, Q., Villeneuve, G., and Wang, Z. (2005). Control of epidermal growth factor receptor endocytosis by receptor dimerization, rather than receptor kinase activation. *EMBO Rep* 6, 942-948.

Wang, S.E., Narasanna, A., Perez-Torres, M., Xiang, B., Wu, F.Y., Yang, S., Carpenter, G., Gazdar, A.F., Muthuswamy, S.K., and Arteaga, C.L. (2006). HER2 kinase domain mutation results in constitutive phosphorylation and activation of HER2 and EGFR and resistance to EGFR tyrosine kinase inhibitors. *Cancer Cell* 10, 25-38.

Ward, C.W., Garrett, T.P.J., McKern, N.M., Lou, M., Cosgrove, L.J., Sparrow, L.G., Frenkel, M.J., Hoyne, P.A., Elleman, T.C., Adams, T.E., *et al.* (2001). The three dimensional structure of the type I insulin-like growth factor receptor. *Mol Pathol* 54, 125-132.

Waters, J.C. (2009). Accuracy and precision in quantitative fluorescence microscopy. *J Cell Biol* 185, 1135-1148.

Weigelt, B., Geyer, F.C., and Reis-Filho, J.S. Histological types of breast cancer: how special are they? *Mol Oncol* 4, 192-208.

Weigelt, B., Geyer, F.C., and Reis-Filho, J.S. (2012). Histological types of breast cancer: how special are they? *Mol Oncol* 4, 192-208.

Weigelt, B., Hu, Z., He, X., Livasy, C., Carey, L.A., Ewend, M.G., Glas, A.M., Perou, C.M., and Van't Veer, L.J. (2005). Molecular portraits and 70-gene prognosis signature are preserved throughout the metastatic process of breast cancer. *Cancer Res* 65, 9155-9158.

Wetzker, R., and Bohmer, F.D. (2003). Transactivation joins multiple tracks to the ERK/MAPK cascade. *Nat Rev Mol Cell Biol* 4, 651-657.

Wiley, H.S. (2003). Trafficking of the ErbB receptors and its influence on signaling. *Exp Cell Res* 284, 78-88.

Wiley, H.S., and Burke, P.M. (2001). Regulation of receptor tyrosine kinase signaling by endocytic trafficking. *Traffic* 2, 12-18.

Wiseman, S.M., Makretsov, N., Nielsen, T.O., Gilks, B., Yorida, E., Cheang, M., Turbin, D., Gelmon, K., and Huntsman, D.G. (2005). Coexpression of the type 1 growth factor receptor family members HER-1, HER-2, and HER-3 has a synergistic negative prognostic effect on breast carcinoma survival. *Cancer* 103, 1770-1777.

Witton, C.J., Reeves, J.R., Going, J.J., Cooke, T.G., and Bartlett, J.M. (2003). Expression of the HER1-4 family of receptor tyrosine kinases in breast cancer. *J Pathol* 200, 290-297.

Wolff, A.C., Hammond, M.E., Schwartz, J.N., Hagerty, K.L., Allred, D.C., Cote, R.J., Dowsett, M., Fitzgibbons, P.L., Hanna, W.M., Langer, A., *et al.* (2007). American Society of Clinical Oncology/College of American Pathologists guideline recommendations for human epidermal growth factor receptor 2 testing in breast cancer. *J Clin Oncol* 25, 118-145.

Wong, A.J., Ruppert, J.M., Bigner, S.H., Grzeschik, C.H., Humphrey, P.A., Bigner, D.S., and Vogelstein, B. (1992). Structural alterations of the epidermal growth factor receptor gene in human gliomas. *Proc Natl Acad Sci U S A* 89, 2965-2969.

Wu, M., Rivkin, A., and Pham, T. (2008). Panitumumab: human monoclonal antibody against epidermal growth factor receptors for the treatment of metastatic colorectal cancer. *Clin Ther* 30, 14-30.

Wu, X., Liu, H., Liu, J., Haley, K.N., Treadway, J.A., Larson, J.P., Ge, N., Peale, F., and Bruchez, M.P. (2003). Immunofluorescent labeling of cancer marker Her2 and other cellular targets with semiconductor quantum dots. *Nat Biotechnol* 21, 41-46.

Xing, Y., Chaudry, Q., Shen, C., Kong, K.Y., Zhau, H.E., Chung, L.W., Petros, J.A., O'Regan, R.M., Yezhelyev, M.V., Simons, J.W., *et al.* (2007). Bioconjugated quantum dots for multiplexed and quantitative immunohistochemistry. *Nat Protoc* 2, 1152-1165.

Xing, Y., and Rao, J. (2008). Quantum dot bioconjugates for in vitro diagnostics & in vivo imaging. *Cancer Biomark* 4, 307-319.

Yamauchi, T., Ueki, K., Tobe, K., Tamemoto, H., Sekine, N., Wada, M., Honjo, M., Takahashi, M., Takahashi, T., Hirai, H., *et al.* (1998). Growth hormone-induced tyrosine phosphorylation of EGF receptor as an essential element leading to MAP kinase activation and gene expression. *Endocr J* 45 Suppl, S27-31.

Yamauchi, T., Ueki, K., Tobe, K., Tamemoto, H., Sekine, N., Wada, M., Honjo, M., Takahashi, M., Takahashi, T., Hirai, H., *et al.* (1997). Tyrosine phosphorylation of the EGF receptor by the kinase Jak2 is induced by growth hormone. *Nature* 390, 91-96.

Yamauchi, T., Yamauchi, N., Ueki, K., Sugiyama, T., Waki, H., Miki, H., Tobe, K., Matsuda, S., Tsushima, T., Yamamoto, T., *et al.* (2000). Constitutive tyrosine phosphorylation of ErbB-2 via Jak2 by autocrine secretion of prolactin in human breast cancer. *J Biol Chem* 275, 33937-33944.

Yarden, Y., and Sliwkowski, M.X. (2001). Untangling the ErbB signalling network. *Nat Rev Mol Cell Biol* 2, 127-137.

Zepeda-Castilla, E.J., Recinos-Money, E., Cuellar-Hubbe, M., Robles-Vidal, C.D., and Maafs-Molina, E. (2008). [Molecular classification of breast cancer]. *Cir Cir* 76, 87-93.

Zhang, X., Gureasko, J., Shen, K., Cole, P.A., and Kuriyan, J. (2006). An allosteric mechanism for activation of the kinase domain of epidermal growth factor receptor. *Cell* 125, 1137-1149.

Zhou, M., and Ghosh, I. (2007). Quantum dots and peptides: a bright future together. *Biopolymers* 88, 325-339.

Zwick, E., Bange, J., and Ullrich, A. (2001). Receptor tyrosine kinase signalling as a target for cancer intervention strategies. *Endocr Relat Cancer* 8, 161-173.